Impact-defined climate targets : estimating ensembles of pathways of compatible anthropogenic drivers through inversion of the cause-effect chain

Thomas Bossy

université PARIS-SACLAY

Impact-defined climate targets: estimating ensembles of pathways of compatible anthropogenic drivers through inversion of the cause-effect chain

Objectifs climatiques définis en termes d'impacts: obtention de faisceaux de trajectoires d'activités anthropiques compatibles par inversion de la chaine causale

Thèse de doctorat de l'université Paris-Saclay

École doctorale n° 129 Sciences de l'environnement d'Île de France (SEIF)
Spécialité de doctorat: Géosciences
Graduate School : Géosciences, climat, environnement et planètes. Référent : Université de Versailles-Saint-Quentin-en-Yvelines

Thèse préparée dans l'unité de recherche **Laboratoire des sciences du climat et de l'environnement (Université Paris-Saclay, CNRS, CEA, UVSQ)** , sous la direction de **Philippe BOUSQUET**, professeur des universités, et la co-direction de **Philippe CIAIS**, directeur de recherche

Thèse soutenue à Nogent-sur-Marne, le 2 Octobre 2023, par

Thomas BOSSY

Composition du jury

Membres du jury avec voix délibérative

Masa KAGEYAMA Directrice de recherche, LSCE	Présidente
Daniel JOHANSSON Professeur, Chalmers Institute of technology	Rapporteur & Examinateur
Benjamin SANDERSON Directeur de reherche, CICERO	Rapporteur & Examinateur
Céline GUIVARCH Directrice de recherche, CIRED	Examinatrice

THESE DE DOCTORAT

NNT : 2023UPASJ022

université PARIS-SACLAY

ÉCOLE DOCTORALE
Sciences de l'Environnement d'Île-de-France (SEIF)

Titre: Objectifs climatiques définis en termes d'impacts: obtention de faisceaux de trajectoires d'activités anthropiques compatibles par inversion de la chaine causale

Mots clés: Modèles climatiques, Accords de Paris, Impacts climatiques, Scénarios d'émissions, Cycle du carbone

Résumé: Cette thèse présente une approche multidisciplinaire de la recherche sur la modélisation du changement climatique. Elle explore les limites du cadre actuel d'élaboration de scénarios prospectifs utilisé par le Groupe d'experts intergouvernemental sur l'évolution du climat (GIEC) et présente de nouvelles approches alternatives et complémentaires pour surmonter ces limites. À l'aide de Pathfinder, un modèle simple axé sur le climat et le cycle du carbone, on investit un espace inexploré par la gamme des modèles climatiques simples existants en incorporant les données les plus récentes et en inversant le processus usuel de génération des scénarios de changement climatique. Des perspectives d'amélioration de notre modèle sont ensuite identifiées en examinant la représentation de l'océan dans Pathfinder, en se concentrant sur le Nexus chaleur-carbone océanique et son rôle critique dans le cycle global du carbone et la réponse du climat aux émissions cumulées de CO2. Une comparaison est faite entre les représentations de l'interface carbone-chaleur océanique dans Pathfinder et les modèles du système terrestre les plus récents, mettant en évidence les divergences significatives et les implications potentielles pour les scénarios de réchauffement à venir. Après avoir présenté Pathfinder en détail, ma recherche examine tout d'abord les réductions d'émissions de CO2 physiquement nécessaires pour atteindre l'objectif de réchauffement global de 1,5C, en soulignant l'importance des émissions de CO2 provenant de l'utilisation des terres et du forçage non lié au CO2. Nous inversons ensuite la chaîne de causalité pour relier les impacts environnementaux aux activités anthropiques, ce qui constitue une approche unique. L'étude cartographie les espaces d'activités anthropiques compatibles avec certaines limites planétaires et introduit un cadre de modélisation qui tient compte du réchauffement climatique, de l'acidification des océans, de l'élévation du niveau de la mer et de la fonte de la banquise arctique. En outre, cette thèse examine le rôle des modèles d'évaluation intégrée dans la compréhension des coûts d'atténuation des émissions associés à ces scénarios climatiques. Elle explore l'impact des choix conceptuels dans ces modèles sur l'identification de scénarios d'atténuation robustes et examine les effets de l'incertitude physique et de l'équité intergénérationnelle. Ce manuscrit se termine par une appréciation des contributions clés de ma recherche doctorale à la modélisation du changement climatique, l'exploration de nouvelles frontières et opportunités dans le domaine, et de mon ressenti personnel sur le domaine de recherche. Dans l'ensemble, cette thèse représente une approche unique et innovante de la modélisation du changement climatique qui, je l'espère, fournira des outils pratiques pour l'évaluation et le développement de stratégies d'atténuation.

université PARIS-SACLAY
ÉCOLE DOCTORALE
Sciences de l'Environnement d'Île-de-France (SEIF)

Title: Impact-defined climate targets: estimating ensembles of pathways of compatible anthropogenic drivers through inversion of the cause-effect chain
Keywords: Climate models, Paris agreement, Climate impacts, Emissions scenarios, Carbon cycle

Abstract: This dissertation presents a multidisciplinary approach to climate change research. It explores the limitations of the current scenario-building framework used by the Intergovernmental Panel on Climate Change (IPCC) and presents new strategies for better understanding climate futures. Using Pathfinder, a simple model focused on climate and the carbon cycle, this research fills a gap in the range of existing simple climate models by incorporating the latest data and providing a backward, temperature-driven examination of climate change scenarios. Prospects for improvement are then identified by discussing the representation of the ocean in Pathfinder, focusing on the Ocean Heat-Carbon Nexus and its critical role in the global carbon cycle and the response of Earth's climate to cumulative CO_2 emissions. A comparison is made between the representations of the Ocean Heat-Carbon Nexus in Pathfinder and state-of-the-art Earth system models, highlighting the significant discrepancies and potential implications for future warming scenarios. After introducing Pathfinder, my research first examines the CO_2 emission reductions physically required to meet the 1.5C global warming target, emphasizing the importance of CO_2 emissions from land use and non-CO_2 forcing. We then reverse the causal chain to link environmental impacts to anthropogenic activities, which is a unique approach. The study maps the spaces of anthropogenic activities compatible with planetary boundaries and introduces a modeling framework that accounts for global warming, ocean acidification, sea level rise, and Arctic sea ice melt. Furthermore, this thesis examines the role of Integrated Assessment Models (IAMs) in understanding the costs associated with these climate scenarios. It explores the impact of conceptual choices in these models on the identification of robust mitigation pathways and examines the effects of physical uncertainty and intergenerational equity. This manuscript concludes with an appreciation of the key contributions of my doctoral research to climate change modeling, exploration of new frontiers and opportunities in the field, and personal insights into the research journey. Overall, this research represents a unique, innovative approach to climate change modeling that will hopefully provide practical tools for assessing and developing mitigation strategies.

4

Contents

Acknowledgments

I would like to express my deepest gratitude to all those who have contributed to the completion of this PhD thesis. Without their support, encouragement, and guidance, this work would not have been possible.

First and foremost, I would like to thank my main advisor, Thomas Gasser. Your expertise, patience, and unwavering commitment to excellence have been instrumental in shaping my research journey. I would also like to thank all the great researchers that co-supervised my work, Philippe Ciais, Franck Lecocq, Katsumasa Tanaka and Philippe Bousquet. Your guidance and insightful feedback have significantly enhanced the quality of this thesis. I am truly grateful for the hours all of you dedicated to mentoring me and for your valuable contributions to my academic and personal growth.

I would like to acknowledge the jury of my PhD with Daniel Johansson and Benjamin Sanderson as reviewers, and Céline Guivarch and Masa Kageyama as examiners. Thank you for the time you spent reading and understanding this manuscript.

I would also like to extend my sincere appreciation to the members of my thesis committee, Roland Séférian and Sonia Seneviratne. Your thoughtful insights, constructive criticism, and valuable suggestions have greatly enriched my research and have played a crucial role in shaping the direction of this work.

I am indebted to the faculty and staff of LSCE, IIASA and CIRED, whose commitment to education and research has created an inspiring academic environment. The stimulating discussions, research seminars, and conferences organized by the department have broadened my horizons and enriched my understanding of my field of study.

My heartfelt thanks go to my fellow researchers and colleagues, both past and present, who have shared their expertise, collaborated with me, and provided invaluable assistance throughout my doctoral journey. Your support, friendship, and intellectual exchanges have made this experience rewarding and memorable.

Lastly, I would like to acknowledge all my friends and family who have stood by me during this challenging period. Your companionship, humor, and unwavering belief in me have provided much-needed respite and motivation during times of stress and self-doubt.

To all those mentioned and those who may have inadvertently been omitted, please accept my heartfelt gratitude. Your contributions, whether big or small, have shaped this thesis and have had a lasting impact on my personal and professional development. I am deeply indebted to each and every one of you.

Publications

The work presented in this thesis is or is to be published in five different publications. I am first author on four of them.
Bossy et al. (2022) has already been published in Geophysical Model Development and forms the main body of Chapter 2
All other work has not yet been submitted, but is far enough along to be presented here.
As an introduction to Chapter 3, we propose Bossy, Gasser, Tanaka and Ciais (2023). It was rejected as a comment in One Earth under the form presented here. However, it was suggested for resubmission as a research paper with a more in-depth version. Because of time constraints, this version is not presented in this thesis
Bossy, Gasser, Ciais, Tanaka, Lecocq and Bousquet (2023) is the main body of Chapter 3 and is to be submitted in Nature.
Bossy, Gasser, Ciais, Tanaka and Lecocq (2023), presented in Chapter 4, is not as far along in the writing process, but is also to be submitted before the defense
Finally, the discussion of Chapter 2 on the representation of the ocean in Pathfinder is adapted from the draft of Séférian et al. (2023), which has also not yet been submitted.

Bibliography

Bossy, T., Gasser, T. and Ciais, P. (2022). Pathfinder v1. 0.1: a bayesian-inferred simple carbon–climate model to explore climate change scenarios, *Geoscientific Model Development* **15**(23): 8831–8868.

Bossy, T., Gasser, T., Ciais, P., Tanaka, K. and Lecocq, F. (2023). Near-optimal and paris-compliant pathways robust to physical uncertainty, economic paradigms, and intergenerational equity, *To be submitted* .

Bossy, T., Gasser, T., Ciais, P., Tanaka, K., Lecocq, F. and Bousquet, P. (2023). Spaces of anthropogenic activities compatible with planetary boundaries, *To be submitted* .

Bossy, T., Gasser, T., Tanaka, K. and Ciais, P. (2023). On the chances of staying below the 1.5°c warming target, *submitted to One Earth* .

Séférian, R., Bossy, T., Gasser, T., Nicholls, Zebedee, a. D. K., Su, X., Tsutsui, J. and Santana-Falcón, Y. (2023). Physical inconsistencies in the representation the ocean heat-carbon nexus in simple climate models, *Submitted to Nature Climate Change* .

Contributions de cette thèse

Le fil conducteur de cette thèse tourne autour de la question que nous posons dans la section 1.5 : Pouvons-nous proposer un cadre méthodologique qui permette de construire des scénarios qui inversent la chaîne de causalité depuis la définition de l'exposition aux impacts jusqu'aux contraintes socio-économiques des scénarios d'atténuation cohérents avec les impacts précédemment définis ?

Dans un premier temps, nous présentons Pathfinder, un nouveau modèle simple qui répond aux principales exigences que nous avons identifiées pour appliquer notre cadre méthodologique. En particulier, Pathfinder est inversible et peut donc être modéliser une inversion de la chaîne causale. Une fois notre outil principal développé et diagnostiqué, la deuxième étape consiste à développer une approche rétrospective qui nous permet de calculer à rebours les émissions de CO_2 à partir des trajectoires ex ante de température et de concentration atmosphérique de CO_2. Grâce à cette approche, nous proposons un nouveau cadre qui permet de trouver un ensemble exhaustif de scénarios d'émissions compatibles avec les objectifs choisis pour les impacts physiques du changement climatique tels que l'élévation du niveau de la mer, le réchauffement planétaire et l'acidification des océans. Enfin, la dernière étape développée dans cette thèse fournit une première évaluation de la robustesse économique des scénarios précédemment définis. Les sous-sections suivantes détaillent la principale contribution de mon travail à ces trois étapes, en soulignant l'inversion de la chaîne causale.

Présentation de Pathfinder

Le chapitre 2 présente le modèle Pathfinder, un modèle climatique global nouveau et innovant représentant le cycle du carbone. Ce modèle a été développé pour concilier simplicité et précision, en mettant l'accent sur la représentation des processus physiques liés au CO_2. Le modèle Pathfinder est calibré par inférence bayésienne de manière à pouvoir intégrer les observations les plus récentes. Sa simplicité facilite le couplage avec des modèles d'évaluation intégrée et l'exploration d'un large éventail de scénarios climatiques. Le modèle est open source et fait l'objet d'une description complète pour la première fois dans ce chapitre, détaillant le processus de calibration et l'estimation des paramètres.

La performance du modèle Pathfinder est évaluée à l'aide de métriques de diagnostic considérées comme clés. Nous montrons que le modèle fonctionne très bien dans la période historique. Nous fournissons également des diagnostics pour des simulations idéalisées qui démontrent l'intérêt de la calibration bayésienne pour fournir des estimations "intermédiaires" entre des modèles complexes et des observations. Enfin, nous validons le modèle par rapport aux scénarios de prévision utilisés dans l'AR6 du GIEC. Les projections de Pathfinder s'accordent très bien avec les scénarios évalués par le GIEC dans l'AR6, en particulier pour les scénarios de faible réchauffement, que nous avons largement explorés dans nos différentes études.

Le modèle Pathfinder comble une lacune dans la littérature en fournissant un modèle simple mais efficace pour les scénarios climatiques. Malgré sa simplicité, le modèle Pathfinder reproduit

fidèlement le comportement et les résultats de modèles plus complexes. Ceci est particulièrement utile pour les modèles d'évaluation intégrée. Nous identifions également des possibilités d'amélioration du modèle, notamment la réduction de la complexité lorsque cela est possible, le développement d'une formulation alternative de la dynamique du carbone océanique, l'intégration de l'usage des terres, l'extension de l'approche bayésienne et l'inclusion potentielle de forçages climatiques autres que le CO_2 dans le modèle Pathfinder. Notre approche de ces améliorations potentielles souligne leur engagement à améliorer l'utilité et l'efficacité du modèle dans la modélisation climatique.

Thomas Gasser avait déjà développé le modèle avant le début de mon doctorat. Personnellement, j'ai participé au développement du module de niveau de la mer, j'ai effectué tous les tests de diagnostic et j'ai fait l'analyse de la représentation de l'océan dans Pathfinder.

Proposer un nouveau cadre pour l'élaboration de scénarios

Comme première application de Pathfinder, nous estimons les chances de limiter le réchauffement à 1,5°C en effectuant une analyse complète des exigences physiques nécessaires pour limiter le réchauffement climatique à 1,5°C, sur la base des données les plus récentes jusqu'en 2022. Nous affirmons qu'une probabilité de 50 % de maintenir le réchauffement climatique en dessous de 1,5 °C au cours de ce siècle nécessite une diminution linéaire des émissions de CO_2 provenant des combustibles fossiles et de l'industrie d'environ 5 % par an, un taux de décarbonisation qui doit être maintenu chaque année. Il est intéressant de noter que ce taux n'est que légèrement inférieur aux réductions sans précédent des émissions à court terme observées pendant la pandémie de COVID-19. Notre étude met également en évidence le rôle critique des émissions de CO_2 supposées provenir de l'utilisation des terres et du forçage non CO_2 dans la détermination de la probabilité de rester en dessous du seuil de réchauffement global de 1,5°C.

Pour faire avancer l'exploration des scénarios, nous avons proposé une nouvelle approche rétrospective qui inclut non seulement l'objectif de température mais aussi des impacts tels que l'acidification des océans et l'élévation du niveau de la mer. Plus précisément, nous examinons des milliers de scénarios dans 1 500 états physiques du monde différents afin de fournir une estimation complète de l'éventail des scénarios possibles, qui restent tous, par construction, en deçà de la limite de réchauffement global de 2 °C. Nous considérons différentes limites planétaires indépendamment et en les combinant les unes avec les autres, et examinons les effets non linéaires de ces combinaisons sur l'espace d'émissions compatible en comparant l'enveloppe de tous les scénarios qui restent dans une limite donnée.

Nous exprimons l'espace compatible en termes de caractéristiques clés des activités anthropiques et les associons à une probabilité que cet espace soit sûr, ce que nous appelons le niveau de sécurité. Nous analysons ces espaces compatibles pour comprendre et quantifier les compromis entre les différentes options et stratégies d'atténuation. Dans l'ensemble, il en résulte un cadre innovant qui détermine ce qui est physiquement possible ou non afin de rester à l'intérieur d'un ensemble de limites planétaires.

Concernant ma contribution personnelle à la création de ce cadre, j'ai joué un rôle actif dans la conceptualisation des deux études. J'ai réalisé l'ensemble des représentations graphiques et des

analyses des données présentées dans les articles.

Évaluer la robustesse économique des scénarios

Dans le chapitre 4, notre travail commence à partir des scénarios générés dans le chapitre 3. Nous nous concentrons uniquement sur la limite des 2°C de réchauffement global et ajoutons une dimension socio-économique pour réduire l'espace compatible physiquement pertinent à un ensemble de trajectoires économiquement robustes. Pour ce faire, nous adoptons une approche basée uniquement sur les coûts d'atténuation.

Notre objectif est de fournir une analyse complète des mécanismes qui déterminent les coûts quasi-optimaux. Les coûts des trajectoires d'émissions de CO_2 calculés par Pathfinder sont estimés et comparés en utilisant une série de choix conceptuels pour le critère de minimisation et la fonction de coût choisie pour estimer les coûts d'atténuation. Les trajectoires parmi les 10% les moins coûteuses sont définies comme quasi-optimales, et nous introduisons le concept de trajectoires robustes pour désigner les trajectoires qui sont communes à toutes les approches conceptuelles que nous examinons. Outre l'incertitude économique découlant des choix conceptuels, nous prenons également en compte l'incertitude physique en calculant les proportions de trajectoires robustes dans chaque état physique du monde. Nous prenons également en compte l'équité intergénérationnelle en essayant de minimiser la différence entre une génération actuelle (2021-2060) et une génération future (2061-2100).

Enfin, nous illustrons des trajectoires économiquement et générationnellement robustes pour différentes configurations et fournissons une représentation visuelle de l'analyse afin d'aider les décideurs politiques à prendre des décisions plus éclairées sur les stratégies d'atténuation du changement climatique. Nous montrons que l'éventail des trajectoires quasi-optimales est réduit lorsque des conditions de robustesse sont ajoutées. Les trajectoires présentant des pics d'émissions tardifs ou nécessitant l'utilisation d'une grande quantité d'émissions négatives ne font pas partie des trajectoires les plus robustes. L'enveloppe la plus restrictive des trajectoires garantit la robustesse générationnelle et économique. Cela suggère que le fait d'atteindre rapidement des émissions nettes nulles en utilisant des émissions négatives dans la seconde moitié du 21e siècle est plus équitable que les trajevtoires économiquement robustes qui visent des émissions nettes nulles à la fin du siècle.

Pour cette partie, j'ai été très actif dans la proposition et la conceptualisation de l'étude. J'ai également réalisé l'ensemble de la représentation et de l'analyse des données.

1 - Introduction

1.1 . A brief history of climate change attribution

Climate change, a pervasive and escalating global concern, is intrinsically tied to the rapid increase in the concentration of greenhouse gases (GHGs) in Earth's atmosphere, primarily resulting from human activities (IPCC; 2021b). These GHGs, including carbon dioxide, methane, and nitrous oxide, play a fundamental role in regulating the planet's temperature through the greenhouse effect - a natural process where GHGs trap the infra-red waves emitted by the Earth, preventing them from escaping back into space, thereby warming the Earth's surface.

The scientific understanding and attribution of global warming to human influence constitute a progressive revelation that has unfolded over two centuries. The genesis of this notion can be traced back to the 19th century when Joseph Fourier postulated the existence of the Earth's natural greenhouse effect (Fourier; 1824), and John Tyndall discovered the heat-absorbing capacity of certain gases (Tyndall; 1861), which set the foundation for our comprehension of greenhouse gases. This was followed by Svante Arrhenius's groundbreaking prediction in 1896 that the combustion of coal could lead to a rise in global temperatures (Arrhenius; 1896).

A significant leap was made in the mid-20th century when Charles David Keeling initiated direct measurements of atmospheric CO_2 levels at the Mauna Loa Observatory in Hawaii, yielding a steady rise in CO_2 concentrations, encapsulated in the Keeling Curve (Keeling; 1960). Subsequent advancements in the latter half of the 20th century involved the development of intricate climate models that indicated the inability of natural factors alone to account for the observed warming trend (Manabe and Wetherald; 1967).

The role of the Intergovernmental Panel on Climate Change (IPCC) has been indispensable in this scientific journey. This institution was established in 1988 by the World Meteorological Organization (WMO) and the United Nations Environment Programme (UNEP). Its role is not to produce any research but only to assess existing research. Beginning with a cautious attribution of some observed warming to human activities in their first assessment report in 1990 (Houghton et al.; 1990), the IPCC has, with increasing certainty, underscored the human fingerprint on climate change in subsequent reports. By their 2001 report, the "likely" association of human activities with the majority of observed warming in the past half-century was proposed (Houghton et al.; 2001). This connection was deemed "very likely" in 2007 (Alley et al.; 2007) and "extremely likely" in 2013 (IPCC; 2013), culminating in the unequivocal assertion of human-induced warming in the 2021 report (IPCC; 2021b).

This gradual understanding over centuries led to affirming the consensus within the scientific community regarding the anthropogenic causes of climate change. However, much research is still needed to understand all the mechanisms of climate change, as well as to explore the need for and solutions to adaptation and mitigation. One task of the IPCC is to collect and summarize current knowledge on all these issues.

1.2 . Studying climate change now requires a multidisciplinary approach

The IPCC operates through three distinct but interconnected Working Groups (WGs), each tasked with addressing specific facets of climate change. Working Group I (WG I) takes on the

responsibility of examining the physical science underpinning climate change, focusing on our current understanding of climatic systems, processes, and the scientific basis of climate change. The activities of WG I are centered around determining how and why the climate is changing, and projecting how it might change in the future (IPCC; 2021a). Working Group II (WG II) delves into the implications of climate change for socio-economic and natural systems. This group appraises both potential risks and opportunities arising from climate change, exploring the concept of vulnerability and how human and natural systems might adapt to climate change (Pörtner et al.; 2022). Working Group III (WG III), on the other hand, investigates the various strategies for mitigating climate change. This entails the exploration of technological, socio-economic, and policy instruments that could potentially limit the magnitude or rate of global warming and its related effects (IPCC; 2022a). Despite each group working within its distinct realm, there exists a profound degree of interaction among them which notably arises in the process of building projections scenarios. This process stands as a quintessential component of the IPCC's function and is intrinsically linked to the collective work of the IPCC's three WGs. These scenarios serve as projections of the future, weaving together elements of societal, economic, and environmental significance to illuminate the potential impacts of climate change and to propose response strategies (IPCC; 2023b). Primarily, the mission of WG I is to understand, explain, and project the relationship between anthropogenic activities and climate change variables such as radiative forcing, temperature, or sea level rise (IPCC; 2021b). Understanding this relationship helps WG III set emissions budgets consistent with a target for radiative forcing or temperature to create scenarios for anthropogenic activities. This group is examining the effectiveness and feasibility of a range of options for reducing greenhouse gas emissions that include changes in energy production and use, changes in land use, and the adoption of new technologies (IPCC; 2022b). These emissions scenarios, based on different levels of radiative forcing for the year 2100, form the essential basis for Earth System Models (ESMs) used by the WG I communities to simulate future climate conditions (IPCC; 2021b). The WG II then uses these projected climate conditions under the form of global warming temperatures to assess their potential impacts and vulnerabilities. The group assesses the impacts of different scenarios on sectors such as agriculture, water resources, ecosystems, and human health. In addition, the group is assessing how socioeconomic variables, including population growth, economic progress, and governance, might affect the vulnerability of societies to projected climate change (IPCC; 2022c). Throughout this intricate procedure to generate scenarios, there exists significant interaction and mutual feedback among the three working groups. The culmination of this process is the RCP-SSP framework that provides a comprehensive suite of scenarios, each presenting a consistent portrayal of potential future climate conditions and responsive strategies (Van Vuuren et al.; 2014; O'Neill et al.; 2020).

1.3 . The RCP-SSP framework

The Representative Concentration Pathways (RCPs) and Shared Socioeconomic Pathways (SSPs) together form an integral framework in contemporary climate change research (Van Vuuren et al.; 2014; O'Neill et al.; 2020), serving to illustrate potential trajectories of climate evolution and societal response. The previous approach (with scenarios A1, A2, B1, B2 in IPCC (2023a)) was defining stories

leading to emissions (WGIII) leading to implications for climate (WGI) and impacts (WGII), on which mitigation was discussed by WGIII only at the end of the process. The RCP-SSP framework starts with the RCPs, allowing to work directly on climate impacts (WGI), and in parallel discusses the conditions under which such a concentration can be achieved following different socioeconomic narratives (WGIII). The RCPs, introduced by the IPCC for its fifth Assessment Report (AR5) in 2014 (Van Vuuren et al.; 2011; IPCC; 2013), encompass four distinct greenhouse gas concentration trajectories. Each RCP signifies a unique radiative forcing scenario - the measure of the change in energy in the Earth's atmosphere due to greenhouse gases - by the year 2100, relative to preindustrial levels. The RCPs—RCP2.6, RCP4.5, RCP6.0, and RCP8.5—encompass a spectrum of future emissions from low to very high levels and were utilized as crucial input for projecting future climatic alterations. In contrast, SSPs, a more recent introduction for the IPCC's sixth Assessment Report (AR6), portray divergent socioeconomic futures in the absence of explicit climate policy interventions, indifferent to specific climatic outcomes (Van Vuuren, Riahi, Moss, Edmonds, Thomson, Nakicenovic, Kram, Berkhout, Swart, Janetos et al.; 2012; O'Neill et al.; 2014). Five SSP narratives—SSP1 through SSP5—offer a wide spectrum of global development possibilities, reflecting a variety of challenges for climate change mitigation and adaptation (Riahi et al.; 2017). The coupling of RCPs and SSPs yields the RCP-SSP framework, providing an inclusive matrix to delve into prospective scenarios (Van Vuuren et al.; 2014). The goals of this framework are well summarized by O'Neill et al. (2020):

• To support climate change-related research globally across research communities and be extendable to other scales, sectors and issue areas;

• To facilitate research that integrates climate and societal futures by providing more detailed socioeconomic and political conditions as inputs to studies of impacts, adaptation and mitigation;

• To foster consideration of uncertainty in future climate and societal conditions by describing a wide range of plausible futures

• To encourage more coherent synthesis in scientific assessments by improving the consistency of climate and societal assumptions in the literature; and

• To support research and analysis to inform policy

Overall, the framework achieved its goal (O'Neill et al.; 2020) and five combinations of SSPs and RCPs were chosen to be representative illustrative pathways in the most recent IPCC report (O'Neill et al.; 2016).

1.4 . Limitations and needs for improvement of WGs cooperation in the scenario-making process

We have quickly explained how the IPCC WGs possess immense potential for fostering a robust, interdisciplinary understanding of climate change (IPCC; 2023b). However, there are inherent needs and limitations in the collaborative approach within and between these WGs. A key requisite involves intensifying cross-disciplinary collaboration, which is crucial given the interdisciplinary nature of climate change, spanning from physical sciences to socio-economic impacts and mitigation strategies. Another aspect to address is the synchronization of report timelines, currently exhibiting variability between the working groups, which can impede the effective integration of their findings (IPCC; 2022c). Streamlining the production of reports could expedite the assimilation

of findings from one group into the work of the others. The integration of the work of the three WGs through an iterative risk management framework (Rawshan Ara Begum et al.; 2022; New et al.; 2022) that combines identifying risks, assessing response options, and monitoring and reviewing the effectiveness of these measures is another approach suggested by WG II (IPCC; 2022c).

The development of shared scenarios across the working groups can ensure consistency and coherence in their assessments. The RCP-SSP scenario framework, while essential, needs improvement to maintain its relevance and applicability (O'Neill et al.; 2020). When refining the scenario framework, a crucial focus is on integrating feedback loops (Calvin and Bond-Lamberty; 2018), expanding the scope to include impacts, adaptation, and vulnerability (IAV) (Wilbanks and Ebi; 2014), biodiversity studies, and downscaling to capture the multiple manifestations of climate change at regional and local scales (O'Neill et al.; 2020). However, these additions come with significant modeling and computational costs. Fully coupling all elements of climate change with their inherent complexity could make the modeling process computationally prohibitive (Van Vuuren, Bayer, Chuwah, Ganzeveld, Hazeleger, van den Hurk, Van Noije, O'Neill and Strengers; 2012; Calvin and Bond-Lamberty; 2018). One challenge is finding the right level of model complexity for the study (Calvin and Bond-Lamberty; 2018).

One solution is to develop emulators capable of reproducing the results of complex models, but at a much lower computational cost (Nicholls et al.; 2020, 2021). Simple carbon climate models are among the most widely developed and used emulators. Such models have found extensive applications as mediators between Working Groups I and III (Guivarch et al.; 2022) to assess the climate impacts of socioeconomic scenarios. Since these models are generally used as assessment tools by economists rather than being integrated into Integrated Assessment Models (IAMs) via extensive feedback loops, there are many opportunities to develop them further. In addition, the development of emulators that facilitate the connection between the climate science and IAV communities is still in its early stages. This is partly because most emulators operate on a global scale and focus primarily on temperature, whereas climate change impacts are local and not necessarily linear with temperature. However, there is a clear need in this area, as ISIMIP studies currently have to wait for ESMs to provide them with scenarios that do not even necessarily meet all of their needs (O'Neill et al.; 2020; Wilbanks and Ebi; 2014; Rosenzweig et al.; 2017). A reverse approach, focusing on simple climate models (SCMs) and using IAMs to assess the feasibility of scenarios, would allow complexity to be favored on the Earth system side to improve the representation of relevant impact variables. Therefore, WGII could more easily create their own scenarios that meet their needs, and it would be easier for WGIII to integrate impacts into their socioeconomic scenarios.

1.5 . Aims and structure of this thesis

This thesis is designed to contribute to the global considerations for improving the existing scenario framework, to promote the integration of different domains of climate change research, and to utilize emulators for more efficient computation. Specifically, the goal of this thesis is to propose a framework that considers different physical impacts of climate change. While most existing scenarios are based only on a temperature target, we want to consider other physical impacts such as sea level rise or ocean acidification. In a second step, we aim to express the impacts

in terms of exposures (on land, population, costs, etc.), with a direct link to physical variables. Based on these impacts, we then intend to map emission scenarios associated with selected exposures. Finally, we aspire for our framework to provide an initial assessment of the socioeconomic costs generated by the proposed scenarios. In summary, the scientific question guiding all the studies presented in this thesis is the proposition of a methodological framework that allows the construction of scenarios, reversing the causal chain from the definition of impact exposure to the socioeconomic constraints of mitigation scenarios compatible with the previously defined impacts.

In the first part of the thesis (Chapter 2), we start with the physical sciences and find that a new, robust SCM is needed that accounts for geophysical uncertainty. The construction of a new model is critical because it is the most important tool we use to understand potential changes in the Earth's climate system due to anthropogenic activities.

In the second part (Chapter 3), we venture into the realm of multiple climate impacts and use them to delineate a compatible space and support the selection of scenarios for detailed study. This process involves mapping a very large ensemble of scenarios that capture the tradeoffs and opportunities constrained by the choice of mitigation strategies and planetary boundaries.

The third part (Chapter 4) integrates socioeconomic considerations and assesses the robustness of some of the impact-based scenarios developed in the previous phase. This section emphasizes the ease with which the scope of the Working Group III can be integrated into our proposed framework. Through this integration, we ensure that the prospective strategies for mitigating climate change are not only scientifically feasible, but can also be economically viable.

In essence, this thesis aims to illustrate through a case study that new methodologies can be developed to contribute to thinking about how the individual threads of climate science, impact assessment, and socioeconomic factors can be woven together to create a more comprehensive and actionable tapestry of climate change scenarios.

Bibliography

Alley, R., Berntsen, T., Bindoff, N. L., Chen, Z., Chidthaisong, A., Friedlingstein, P., Gregory, J., Hegerl, G., Heimann, M., Hewitson, B. et al. (2007). Climate change 2007: The physical science basis, *Contribution of Working Group I to the Fourth Assessment Report of the Intergovernmental Panel on Climate Change. Summary for Policymakers. IPCC Secretariat, Geneva, Switzerland. 21p* .

Arrhenius, S. (1896). ober den einflub des atmospharischen kohlesziuregehars auf die temperatur der erdoberflache (on the influence of carbon dioxide in the atmosphere on the temperature of the earth), *Stockholm (Royal Swedish Science Academy)* .

Calvin, K. and Bond-Lamberty, B. (2018). Integrated human-earth system modeling—state of the science and future directions, *Environmental Research Letters* **13**(6): 063006.

Fourier, J. (1824). Remarques générales sur les températures du globe terrestre et des espaces planétaires, *Annales de Chemie et de Physique*, Vol. 27, pp. 136–167.

Guivarch, C., Kriegler, E., Portugal Pereira, J., Bosetti, V., Edmonds, J., Fischedick, M., Havlik, P., Jaramillo, P., Krey, V., Lecocq, F., Lucena, A., Meinshausen, M., Mirasgedis, S., O'Neill, B., Peters, G.,

Rogelj, J., Rose, S., Saheb, Y., Strbac, G., Stromman, A. H., Van Vuuren, D. P. and Zhou, N. (2022). Annex iii: Scenarios and modelling method, *Climate change 2022: Mitigation of Climate Change. Contribution of Working Group III to the Sixth Assessment Report of the Intergovernmental Panel on Climate Change* .

Houghton, J., Albritton, D., Allen, M., Baede, A., Church, J., Cubasch, U., Xiaosu, D., Yihui, D., Ehhalt, D., Folland, C. et al. (2001). Summary for policymakers., *Climate Change 2001: The Scientific Basis. Contributions of Working Group I to the Third Assessment Report of the Intergovernmental Panel on Climate Change*, Cambridge University Press, pp. 1–20.

Houghton, J. T., Jenkins, G. J. and Ephraums, J. J. (1990). Climate change: the ipcc scientific assessment, *American Scientist;(United States)* **80**(6).

IPCC (2013). Summary for policymakers, *in* T. Stocker, D. Qin, G.-K. Plattner, M. Tignor, S. Allen, J. Boschung, A. Nauels, Y. Xia, V. Bex and P. Midgley (eds), *Climate Change 2013: The Physical Science Basis. Contribution of Working Group I to the Fifth Assessment Report of the Intergovernmental Panel on Climate Change*, Cambridge University Press, Cambridge, United Kingdom and New York, NY, USA, book section SPM, p. 1–30.
URL: *http://www.climatechange2013.org*

IPCC (2021a). *Climate Change 2021: The Physical Science Basis. Contribution of Working Group I to the Sixth Assessment Report of the Intergovernmental Panel on Climate Change*, Cambridge University Press, Cambridge, UK and New York, NY, USA.
URL: *https://report.ipcc.ch/ar6/wg1/IPCC*$_{A}R6_{W}GI_{F}ullReport.pdf$

IPCC (2021b). Summary for policymakers, *in* V. Masson-Delmotte, P. Zhai, A. Pirani, S. L. Connors, C. Péan, S. Berger, N. Caud, Y. Chen, L. Goldfarb, M. I. Gomis, M. Huang, K. Leitzell, E. Lonnoy, J. B. R. Matthews, T. K. Maycock, T. Waterfield, O. Yelekçi, R. Yu and B. Zhou (eds), *Climate Change 2021: The Physical Science Basis. Contribution of Working Group I to the Sixth Assessment Report of the Intergovernmental Panel on Climate Change*, Cambridge University Press, Cambridge, UK and New York, NY, USA.
URL: *https://www.ipcc.ch/report/ar6/wg1/downloads/report/IPCC*$_{A}R6_{W}GI_{S}PM.pdf$

IPCC (2022a). *Climate Change 2022: Mitigation of Climate Change. Contribution of Working Group III to the Sixth Assessment Report of the Intergovernmental Panel on Climate Change*, Cambridge University Press, Cambridge, UK and New York, NY, USA.
URL: *https://www.ipcc.ch/report/ar6/wg3/downloads/report/IPCC*$_{A}R6_{W}GIII_{F}ullReport.pdf$

IPCC (2022b). Summary for policymakers, *in* P. Shukla, J. Skea, R. Slade, A. A. Khourdajie, R. van Diemen, D. McCollum, M. Pathak, S. Some, P. Vyas, R. Fradera, M. Belkacemi, A. Hasija, G. Lisboa, S. Luz and J. Malley (eds), *Climate Change 2022: Mitigation of Climate Change. Contribution of Working Group III to the Sixth Assessment Report of the Intergovernmental Panel on Climate Change*, Cambridge University Press, Cambridge, UK and New York, NY, USA.
URL: *https://www.ipcc.ch/report/ar6/wg3/downloads/report/IPCC*$_{A}R6_{W}GIII_{S}ummaryForPolicymakers.pdf$

IPCC (2022c). Summary for policymakers, *in* H. O. Pörtner, D. C. Roberts, M. Tignor, E. S. Poloczanska, K. Mintenbeck, A. Alegría, M. Craig, S. Langsdorf, S. Löschke, V. Möller, A. Okem and B. Rama (eds), *Climate Change 2022: Impacts, Adaptation and Vulnerability. Contribution of Working Group II to the Sixth Assessment Report of the Intergovernmental Panel on Climate Change*, Cambridge University Press, Cambridge, UK and New York, NY, USA.
URL: *https://www.ipcc.ch/report/ar6/wg2/downloads/report/IPCC*$_{A}R6_{W}GII_{S}ummaryForPolicymakers.pdf$

IPCC (2023a). *Climate Change 2007: Synthesis Report. Contribution of Working Groups I, II and III to the Fourth Assessment Report of the Intergovernmental Panel on Climate Change*.

IPCC (2023b). *Climate Change 2023. A Report of the Intergovernmental Panel on Climate Change. Contribution of Working Groups I, II and III to the Sixth Assessment Report of the Intergovernmental Panel on Climate Change*, Cambridge University Press, Cambridge, UK and New York, NY, USA.

Keeling, C. D. (1960). The concentration and isotopic abundances of carbon dioxide in the atmosphere, *Tellus* **12**(2): 200–203.

Manabe, S. and Wetherald, R. T. (1967). Thermal equilibrium of the atmosphere with a given distribution of relative humidity.

New, M., Reckien, D., Viner, D., Adler, C., Cheong, S.-M., Conde, C., Constable, A., Coughlan de Perez, E., Lammel, A., Mechler, R., Orlove, B. and Solecki, W. (2022). Decision-making options for managing risk, *in* H. O. Pörtner, D. C. Roberts, M. Tignor, E. S. Poloczanska, K. Mintenbeck, A. Alegría, M. Craig, S. Langsdorf, S. Löschke, V. Möller, A. Okem and B. Rama (eds), *Climate Change 2022: Impacts, Adaptation and Vulnerability. Contribution of Working Group II to the Sixth Assessment Report of the Intergovernmental Panel on Climate Change*, Cambridge University Press, Cambridge, UK and New York, NY, USA, book section 17.
URL: *https://www.ipcc.ch/report/ar6/wg2/downloads/report/IPCC*$_{A}R6_{W}GII_{C}hapter17.pdf$

Nicholls, Z., Meinshausen, M., Lewis, J., Corradi, M. R., Dorheim, K., Gasser, T., Gieseke, R., Hope, A. P., Leach, N., McBride, L. A. et al. (2021). Reduced complexity model intercomparison project phase 2: Synthesizing earth system knowledge for probabilistic climate projections, *Earth's Future* **9**(6): e2020EF001900.

Nicholls, Z. R., Meinshausen, M., Lewis, J., Gieseke, R., Dommenget, D., Dorheim, K., Fan, C.-S., Fuglestvedt, J. S., Gasser, T., Golüke, U. et al. (2020). Reduced complexity model intercomparison project phase 1: introduction and evaluation of global-mean temperature response, *Geoscientific Model Development* **13**(11): 5175–5190.

O'Neill, B. C., Tebaldi, C., Van Vuuren, D. P., Eyring, V., Friedlingstein, P., Hurtt, G., Knutti, R., Kriegler, E., Lamarque, J.-F., Lowe, J. et al. (2016). The scenario model intercomparison project (scenariomip) for cmip6, *Geoscientific Model Development* **9**(9): 3461–3482.

O'Neill, B. C., Carter, T. R., Ebi, K., Harrison, P. A., Kemp-Benedict, E., Kok, K., Kriegler, E., Preston, B. L., Riahi, K., Sillmann, J. et al. (2020). Achievements and needs for the climate change scenario framework, *Nature climate change* **10**(12): 1074–1084.

O'Neill, B. C., Kriegler, E., Riahi, K., Ebi, K. L., Hallegatte, S., Carter, T. R., Mathur, R. and Van Vuuren, D. P. (2014). A new scenario framework for climate change research: the concept of shared socioeconomic pathways, *Climatic change* **122**: 387–400.

Pörtner, H.-O., Roberts, D. C., Adams, H., Adler, C., Aldunce, P., Ali, E., Begum, R. A., Betts, R., Kerr, R. B. and Biesbroek, R. (2022). Climate change 2022: Impacts, adaptation and vulnerability, *IPCC Sixth Assessment Report* .

Rawshan Ara Begum, R., Lempert, R., E. Ali, T. B., Bernauer, T., Cramer, W., Cui, X., Mach, K., Nagy, G., Stenseth, N., Sukumar, R. and Wester, P. (2022). Point of departure and key concepts, *in* H. O. Pörtner, D. C. Roberts, M. Tignor, E. S. Poloczanska, K. Mintenbeck, A. Alegría, M. Craig, S. Langsdorf, S. Löschke, V. Möller, A. Okem and B. Rama (eds), *Climate Change 2022: Impacts, Adaptation and Vulnerability. Contribution of Working Group II to the Sixth Assessment Report of the Intergovernmental Panel on Climate Change*, Cambridge University Press, Cambridge, UK and New York, NY, USA, book section 1.
URL: *https://www.ipcc.ch/report/ar6/wg2/downloads/report/IPCC*$_{A}R6_{W}GII_{C}hapter01.pdf$

Riahi, K., van Vuuren, D. P., Kriegler, E., Edmonds, J., O'Neill, B. C., Fujimori, S., Bauer, N., Calvin, K., Dellink, R., Fricko, O., Lutz, W., Popp, A., Cuaresma, J. C., KC, S., Leimbach, M., Jiang, L., Kram, T., Rao, S., Emmerling, J., Ebi, K., Hasegawa, T., Havlik, P., Humpenöder, F., Da Silva, L. A., Smith, S., Stehfest, E., Bosetti, V., Eom, J., Gernaat, D., Masui, T., Rogelj, J., Strefler, J., Drouet, L., Krey, V., Luderer, G., Harmsen, M., Takahashi, K., Baumstark, L., Doelman, J. C., Kainuma, M., Klimont, Z., Marangoni, G., Lotze-Campen, H., Obersteiner, M., Tabeau, A. and Tavoni, M. (2017). The Shared Socioeconomic Pathways and their energy, land use, and greenhouse gas emissions implications: An overview, *Global Environmental Change* **42**: 153–168.

Rosenzweig, C., Arnell, N. W., Ebi, K. L., Lotze-Campen, H., Raes, F., Rapley, C., Smith, M. S., Cramer, W., Frieler, K., Reyer, C. P. et al. (2017). Assessing inter-sectoral climate change risks: the role of isimip, *Environmental Research Letters* **12**(1): 010301.

Tyndall, J. (1861). Xxiii. on the absorption and radiation of heat by gases and vapours, and on the physical connexion of radiation, absorption, and conduction.—the bakerian lecture, *The London, Edinburgh, and Dublin Philosophical Magazine and Journal of Science* **22**(146): 169–194.

Van Vuuren, D. P., Bayer, L. B., Chuwah, C., Ganzeveld, L., Hazeleger, W., van den Hurk, B., Van Noije, T., O'Neill, B. and Strengers, B. J. (2012). A comprehensive view on climate change: coupling of earth system and integrated assessment models, *Environmental research letters* **7**(2): 024012.

Van Vuuren, D. P., Edmonds, J., Kainuma, M., Riahi, K., Thomson, A., Hibbard, K., Hurtt, G. C., Kram, T., Krey, V., Lamarque, J.-F. et al. (2011). The representative concentration pathways: an overview, *Climatic change* **109**(1-2): 5.

Van Vuuren, D. P., Kriegler, E., O'Neill, B. C., Ebi, K. L., Riahi, K., Carter, T. R., Edmonds, J., Hallegatte, S., Kram, T., Mathur, R. et al. (2014). A new scenario framework for climate change research: scenario matrix architecture, *Climatic Change* **122**: 373–386.

Van Vuuren, D. P., Riahi, K., Moss, R., Edmonds, J., Thomson, A., Nakicenovic, N., Kram, T., Berkhout, F., Swart, R., Janetos, A. et al. (2012). A proposal for a new scenario framework to support research and assessment in different climate research communities, *Global Environmental Change* **22**(1): 21–35.

Wilbanks, T. J. and Ebi, K. L. (2014). Ssps from an impact and adaptation perspective, *Climatic change* **122**: 473–479.

2 - Presentation and diagnosis of a simple carbon-climate model

2.1 . Existing climate models

To fully understand the stakes and interests of our approach, it is important to situate the model we use within the global spectrum of climate models. A wide range of numerical models are used in the study of the climate system. These climate models (Figure 2.1) are the main tools for studying the possible future of climate under different scenarios. The most complicated models are called global Earth system models (ESMs). Each ESM has at its core a GCM (General Circulation Model) that simulates the dynamics of the atmosphere and ocean. Regional models and a hierarchy of simpler models are used to complement the ESMs. (Chen et al.; 2021; Hajima et al.; 2014) There are three aspects on which we can play to define a climate model (Claussen et al.; 2002). The first aspect we need to consider is the level of integration of the model. This refers to the number of components of the Earth system that are represented. Since everything in the system is interconnected, adding a component means adding new interactions between the already existing components. Then one can choose the number of processes that describe the climate component that one wants to represent. The third aspect is complexity, which is characterized by the level of detail in which each process is represented. The closer we want to be to the physical reality of a process, the more complex it becomes. It is obvious that improving the representation of any of these three aspects is associated with increasing computational costs. Thus, depending on the intentions of the modeler, some models may be more relevant than others.

2.1.1 . Earth System Models (ESMs)

The Earth System is a complex network of physical, biological, and chemical processes that have global implications. Since conducting experiments on the real Earth System is not feasible, scientists rely on computer simulations to understand its behavior and response to external factors like greenhouse gases. These simulations help improve our understanding of the Earth System, guide further studies, and make projections of future climate change (Flato; 2011).

In the early 20th century, Vilhelm Bjerknes developed the 'primitive equations' of motion and state, which describe the dynamics of weather using principles of physics (Bjerknes; 1910). However, these equations lacked closed-form solutions and numerical techniques were not advanced enough to provide approximate solutions (Edwards; 2011). It was not until the advent of digital computers after World War II that better mathematical methods for numerical modeling emerged. Weather prediction was one of the first applications of digital computers, using Cartesian grids and finite-difference methods (Harper; 2012). This success led to efforts to model the global circulation and simulate climate using General Circulation Models or global climate models (GCMs). GCMs extended the techniques of numerical weather prediction to a larger scale and employed the primitive equations to compute atmospheric motion. GCMs consist of a 'dynamical core' and 'model physics' to simulate large-scale fluid motion and other physical processes (Edwards; 2011; Grassl; 2000). Now, GCMs are especially focused on the dynamics of climate circulation. They are very complete in terms of detail of representation of the process they model but they do not necessarily cover all aspects of climate sciences. They can be integrated altogether to improve their comprehensiveness of the global climate system. They can also be coupled to models that simulate other processes (such as the ice-sheet).

Evaluating and comparing these models has become increasingly important, leading to

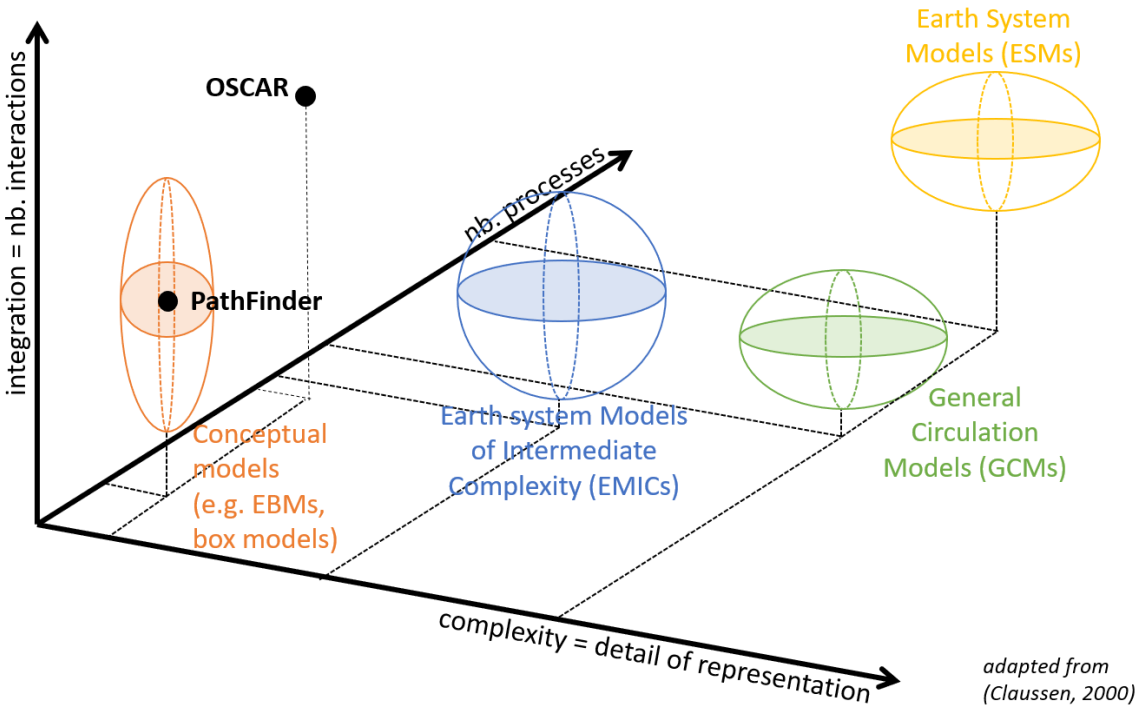

Figure 2.1: Classification of climate models. The OSCAR model that inspired our model is looking to have as much interactions and processes as possible while keeping a low detail of representation to reduce computational costs. Our model (PathFinder) focuses on the carbon cycle and some impacts emulation. Thanks to this simplicity, it can be counted among the conceptual models.

collaborative projects and intercomparison studies. These simulations have revealed important findings, such as the ocean's capacity to absorb heat and the cooling effects of sulfate aerosols (Flato; 2011).

However, comprehensive Earth System Models (ESMs) that incorporate feedbacks between the physical climate and biogeochemical cycles are necessary for a more holistic understanding of climate change (Flato; 2011). Different institutes have developed their own ESMs by combining various component models, such as the dynamic global vegetation model and carbon cycle model, to study the impact of biogeochemical and biophysical processes on climate (Kawamiya et al.; 2020). The structure of ESMs includes atmospheric-ocean coupled climate models, terrestrial ecosystem models, ocean ecosystem models, land surface models, and aerosol transport models. They are based on fundamental physical principles (such as the Navier-Stokes or Clausius–Clapeyron equations) or on empirical relationships derived from observations, and, to the extent that is practical, they are bound by such principles (such as the conservation of mass and energy) (Chen et al.; 2021). The Coupled Climate-Carbon Cycle Model Intercomparison Project (C4MIP) has explored climate-carbon cycle feedback in ESMs and highlighted the importance of incorporating the carbon cycle into climate change projections (Friedlingstein et al.; 2006). The CMIP (Coupled Model Intercomparison Project) has played a critical role in contributing to IPCC reports by including experiments using ESMs with carbon cycle components (Arora et al.; 2013, 2020).

However, their global approach make them very demanding in term of computational cost. High-performance computers are used to numerically calculate the evolution of climate-relevant variables on three-dimensional discrete grids (Staniforth and Thuburn; 2012; André et al.; 2014; Balaji et al.; 2017). Which processes can be openly resolved or require parameterization depends on the horizontal and vertical spatial (and temporal) resolution of these grids (Chen et al.; 2021).

2.1.2 . EMICs

Earth System Models of Intermediate Complexity (EMICs), another class of models described in Claussen et al. (2000), occupy a unique position in climate modeling. Though they encapsulate many of the processes seen in more comprehensive models, they do so in a simpler, more parameterized form. EMICs are capable of explicitly simulating the interactions among various components of the climate system, including biogeochemical cycles. On the other hand, an EMIC is simple enough to support long-term climate simulations spanning tens of thousands of years, even up to the timescales of glacial cycles. One key distinction of EMICs lies in their degrees of freedom. Like comprehensive models, but unlike conceptual models, an EMIC's degrees of freedom significantly outnumber its adjustable parameters, often by several orders of magnitude.

EMICs can be classified into a spectrum of climate system models based on their level of detail and integration of components (see Figure 2.1). Models in this spectrum can include a variety of atmospheric modules such as statistical-dynamical models, energy-moisture balance models, quasi-geostrophic models, and primitive equation models (Hajima et al.; 2014). They may also include ocean modules, which may be three-dimensional or zonally averaged, and sea ice modules, which may be purely thermodynamic or include advection and dynamics. Biospheric modules in these models generally account for terrestrial carbon pools, marine and terrestrial carbon pools,

and global vegetation dynamics. The dimensionality of a model, whether 2D, 2.5D, or 3D, represents its spatial resolution and the number of critical processes it explicitly describes. EMICs are typically classified as simplified comprehensive models, integration-focused models, or models with unique characteristics, determined by their module combination and intended research focus. This model spectrum also includes comprehensive models that differ in their level of detail and component variety (Claussen et al.; 2002).

2.1.3 . SCMs and emulators

The study by Chen et al. (2021) provides an in-depth explanation of the terms 'physical emulators' and 'simple climate models'. These denote a vast category of heavily parameterized models designed to reproduce the responses of the more complex, process-based models, and provide rapid translation of emissions into probabilistic forecasts of physical climate system changes, factoring in concentrations and radiative forcing. Emulators primarily extrapolate findings from ESMs and observational data to cover a wider range of emissions scenarios (see Cross-Chapter Box 7.1 of Forster et al. (2021)). Due to their computational efficiency, they present novel analytical opportunities, especially considering the extensive computational resources required for ESM simulations. However, the practicality and value of emulation methods are bound by their skill in reproducing the global mean climate responses generated by ESMs. This is largely limited to global mean or hemispheric land/ocean temperatures and their capacity to skillfully extrapolate beyond the calibrated range. The terms 'emulator' and 'simple climate model' (SCM) are often used interchangeably, but they are distinct. SCM pertains to a class of models with fewer dimensions that simulate elements like the energy balance, radiative transfer, and the carbon cycle, or combinations thereof. SCMs can also be calibrated to replicate the climate-mean variables of a particular ESM, provided they have the structural flexibility to encapsulate both parametric and structural uncertainties inherent in process-oriented ESM responses. In such a configuration, they are referred to as emulators.

Different sorts of SCMs

Various SCMs have been developed to emulate and simulate climate processes, each with its own level of complexity and representation of physical phenomena and of climate components. At the simplest end, we find the generic impulse response model (AR5-IR) outlined in Myhre et al. (2013) that provides a parametric representation of climate forcers' impacts on the energy budget with annual-mean values. Models similar to AR5-IR are called two-layer models (Held et al.; 2010; Rohrschneider et al.; 2019; Nicholls et al.; 2020), they simulate the exchange of heat between upper and deep ocean layers, reflecting the ocean heat uptake and its effect on surface warming. In the cross-chapter box 7.1 from Forster et al. (2021), the two-layer emulator is defined as equivalent to a two-timescale impulse-response model (Geoffroy et al.; 2013). In that case, the emulator is an extension of the energy budget equation (Forster et al.; 2021) and allows for heat exchange between the upper- and deep-ocean layers, mimicking the ocean heat uptake that reduces the rate of surface warming under radiative forcing. SCMs also count higher-complexity approaches that include upwelling, diffusion and entrainment in the ocean component (e.g., MAGICC (Meinshausen et al.; 2011); OSCAR (Gasser et al.; 2017); CICERO SCM (Skeie et al.; 2017); FaIR (Smith et al.; 2018; Leach et al.;

Model (acronym used in figures)	Spatial resolution	Climate response to radiative forcing	Key references
ACC2 (ACC2-v4-2)	Global land/ocean	1D ocean heat diffusion (DOECLIM)	Tanaka and O'Neill (2018); Tanaka et al. (2007) (also Hooss et al., 2001; Bruckner et al., 2003; Kriegler, 2005)
AR5IR (ar5ir-2box, ar5ir-3box)	Global	Impulse response	Myhre et al. (2013)
CICERO-SCM (CICERO-SCM)	Hemispheric	Energy balance/upwelling–diffusion ocean	Skeie et al. (2017) (also Schlesinger et al., 1992; Joos et al., 1996; Etminan et al., 2016; Skeie et al., 2018)
EMGC (EMGC)	Global	Multiple linear regression model (temperature regressed against radiative forcing and natural variability indices)	Canty et al. (2013); Hope et al. (2017)
ESCIMO (ESCIMO)	Global	Conserved flows of carbon, heat, albedo, permafrost, biome and biomass change – driven by GHG emissions; the rest is endogenous	Randers et al. (2016)
FaIR (FaIR-v1-5)	Global	Modified impulse response	Smith et al. (2018a); Etminan et al. (2016)
GIR (GIR)	Global	Modified impulse response	Leach et al. (2020)
GREB (GREB-v1-0-1)	96 × 48 grid	Energy balance model with atmospheric transport of heat and moisture, surface and subsurface ocean layers	Dommenget et al. (2019)
Hector (hector)	Global	1D ocean heat diffusion (DOECLIM)	Hartin et al. (2015); Dorheim et al. (2020); Vega-Westhoff et al. (2019) (see also Kriegler, 2005; Tanaka et al., 2007)
Held et. al two-layer model (held-two-layer-uom)	Global	Energy balance with two-layer ocean and state-dependent climate feedback factor	Rohrschneider et al. (2019); Held et al. (2010)
MAGICC (MAGICC-v7-1-0-beta)	Hemispheric land/ocean	Atmospheric energy balance model with 50-layer upwelling–diffusion–entrainment ocean	Meinshausen et al. (2011, 2020) (see also Schneider von Deimling et al., 2012; Nauels et al., 2017)
MCE (MCE-v1-1)	Global	Impulse response	Tsutsui (2017, 2020) (see also Joos et al., 1996; Hooss et al., 2001)
OSCAR (OSCAR-v3-0)	Global, with regionalised land carbon cycle	Impulse response	Gasser et al. (2017)
WASP (WASP-v2)	Global	Energy balance using time-evolving climate feedback, with conservation of heat	Goodwin (2018); Goodwin et al. (2019) (see also Goodwin et al., 2014; Goodwin, 2016)

Figure 2.2: Ensemble of SCMs assessed by RCMIP (Nicholls et al.; 2020, 2021)

2020)). More comprehensive models like MAGICC (Meinshausen et al.; 2011) encompass a multitude of components, including representations of greenhouse gas cycles, aerosol emissions, hemispheric and regional differentiations, and multiple ocean layers, operating on a monthly time step internally but reporting annual mean values. Some models adopt a hybrid approach, enhancing complexity in specific domains while maintaining simplicity elsewhere. For instance, OSCAR (Gasser et al.; 2017) incorporates a regionalized land carbon cycle, and EMGC (Hope et al.; 2017) captures natural variability in its representation. Finally, a range of statistical approaches (Schwarber et al.; 2019; Beusch et al.; 2020; Cummins et al.; 2020; Quilcaille et al.; 2022) can be used to emulate some processes too complex to be represented in SCMs such as regional downscaling (Jalota et al.; 2018; Beusch et al.; 2020), natural variability (Cummins et al.; 2020; Hope et al.; 2017) or extreme temperatures (Quilcaille et al.; 2022).

Different use of SCMs

The development of different SCMs is driven by various purposes and objectives (Chen et al.; 2021). Some models aim to be as simple as possible for teaching purposes, such as the two-layer energy balance model (Myhre et al.; 2013; Held et al.; 2010). Others strive for comprehensiveness to capture

uncertainties across multiple Earth system domains, as exemplified by models like MAGICC (Meinshausen et al.; 2011). There are also models like OSCAR that focus on higher-complexity representations of specific domains (Gasser et al.; 2017).

A common motivation underlying many models is the improvement of parameterizations to reflect the latest understanding of complex Earth system interactions. These models aim to emulate the global mean temperature response. Simple models that incorporate rudimentary representations of spatial heterogeneity, like four-box simple climate models, also seek to better represent heterogeneous forcers such as black carbon, refine the forcing-feedback framework, explore new parameterizations of ocean heat uptake, and enhance representations of volcanic aerosol-induced cooling (Chen et al.; 2021). Simple models also play a crucial role in understanding climate feedback and sensitivity by enabling investigations into the climate response to changes in the Earth's energy balance (Rohrschneider et al.; 2019).

Emulators or SCMs have been extensively utilized in recent IPCC reports (IPCC; 2021, 2022). The cross-chapter box 7.1 of Forster et al. (2021) enumerates all the different use of SCMs and emulators. In the WGI Report (IPCC; 2021), emulation is primarily employed to estimate the change in global surface air temperature (GSAT) resulting from effective radiative forcing (ERF) or concentration changes. Multiple versions of a two-layer energy budget emulator are employed, albeit with different calibrations in various sections, to maintain independent lines of evidence. Fox-Kemper et al. (2021) also incorporates projections of ocean heat content from the two-layer emulator of Forster et al. (2021) to estimate the thermostatic component of future sea level rise.

Emissions-driven emulators are another type of emulator used in the report. They are employed in Lee et al. (2021) to emulate GSAT beyond 2100, as the long-term response has been deemed suitable for representing the behavior of Earth System Models (ESMs). In Canadell et al. (2021), emissions-driven emulators are used to explore the non-CO_2 GSAT contribution in emissions scenarios. Szopa et al. (2021) and Forster et al. (2021) utilize two-layer model configurations calibrated to match the probabilistic GSAT responses of emissions-driven emulators.

In the WGIII report (IPCC; 2022), emissions-driven emulators are used to communicate the outcomes of the physical climate science assessment and quantify temperature outcomes associated with different emissions scenarios. These emulators provide computational efficiency, enabling analysis of numerous multi-gas emissions scenarios with various characteristics, such as the year of peak temperature or 2030 emissions levels, in line with the goal of limiting global warming to below 1.5°C or 2.0°C. The emulators' probabilistic distributions are calibrated based on WGI-assessed ranges of Equilibrium Climate Sensitivity (ECS), Transient Climate Response (TCR), historical GSAT change, ERF, carbon cycle metrics, and future warming projections under the concentration-driven Shared Socioeconomic Pathway (SSP) scenarios. They are then utilized by WGIII for a GSAT-based classification of mitigation scenarios consistent with the physical understanding assessed in WGI.

Validation and future development of SCMs

Given the broad usage and significant implications of SCMs and emulators, it is of paramount importance to continually evaluate and update these models. An important part of this process is the Reduced Complexity Model Intercomparison Project (RCMIP), which enables the systematic,

standardized, and comprehensive evaluation of SCMs.

In their evaluation in Nicholls et al. (2021), they have observed that the best-performing SCMs can effectively match their proxy assessment across various climate metrics. However, it is important to note that no SCM was able to match the proxy assessment across all metrics they evaluate. Even among models with similar levels of agreement with the proxy assessment, some divergence in future projections was evident. This divergence can be attributed to the different model structures employed in simple climate models.

RCMIP ensures that these models effectively integrate the latest scientific understanding (Nicholls et al.; 2020, 2021). The integration of this understanding within an internally consistent SCM framework, accounting for implicit cross-correlations, represents the best existing approach to inform decision-making processes and other scientific domains.

For this reason, the development and improvement of SCMs to broaden their scope is critical to integrate more and more aspects of climate change research. In the next section, we introduce Pathfinder, an SCM designed to address some of the limitations identified in existing SCMs.

Bibliography

André, J.-C., Aloisio, G., Biercamp, J., Budich, R., Joussaume, S., Lawrence, B. and Valcke, S. (2014). High-performance computing for climate modeling, *Bulletin of the American Meteorological Society* **95**(5): ES97–ES100.

Arora, V. K., Boer, G. J., Friedlingstein, P., Eby, M., Jones, C. D., Christian, J. R., Bonan, G., Bopp, L., Brovkin, V., Cadule, P., Hajima, T., Ilyina, T., Lindsay, K., Tjiputra, J. F. and Wu, T. (2013). Carbon–concentration and carbon–climate feedbacks in cmip5 earth system models, *Journal of Climate* **26**(15): 5289–5314.
URL: *http://journals.ametsoc.org/doi/abs/10.1175/JCLI-D-12-00494.1*

Arora, V. K., Katavouta, A., Williams, R. G., Jones, C. D., Brovkin, V., Friedlingstein, P., Schwinger, J., Bopp, L., Boucher, O., Cadule, P. et al. (2020). Carbon–concentration and carbon–climate feedbacks in cmip6 models and their comparison to cmip5 models, *Biogeosciences* **17**(16): 4173–4222.

Balaji, V., Maisonnave, E., Zadeh, N., Lawrence, B. N., Biercamp, J., Fladrich, U., Aloisio, G., Benson, R., Caubel, A., Durachta, J. et al. (2017). Cpmip: measurements of real computational performance of earth system models in cmip6, *Geoscientific Model Development* **10**(1): 19–34.

Beusch, L., Gudmundsson, L. and Seneviratne, S. I. (2020). Emulating earth system model temperatures with mesmer: from global mean temperature trajectories to grid-point-level realizations on land, *Earth System Dynamics* **11**(1): 139–159.

Bjerknes, V. (1910). *Dynamic Meteorology and Hydrography: Part [1]-2,[and atlas of plates]*, number 88, Carnegie Institution of Washington.

Canadell, J. G., Monteiro, P. M. S., Costa, M. H., Cotrim da Cunha, L., Cox, P. M., Eliseev, A. V., Henson, S., Ishii, M., Jaccard, S., Koven, C., Lohila, A., Patra, P. K., Piao, S., Rogelj, J., Syampungani, S., Zaehle,

S. and Zickfeld, K. (2021). Global carbon and other biogeochemical cycles and feedbacks, *Climate Change 2021: The Physical Science Basis. Contribution of Working Group I to the Sixth Assessment Report of the Intergovernmental Panel on Climate Change* .

Chen, D., Rojas, M., Samset, B., Cobb, K., Diongue Niang, A., Edwards, P., Emori, S., Faria, S., Hawkins, E., Hope, P., Huybrechts, P., Meinshausen, M., Mustafa, S., Plattner, G.-K. and Tréguier, A.-M. (2021). Framing, context, and methods, *in* V. Masson-Delmotte, P. Zhai, A. Pirani, S. L. Connors, C. Péan, S. Berger, N. Caud, Y. Chen, L. Goldfarb, M. I. Gomis, M. Huang, K. Leitzell, E. Lonnoy, J. B. R. Matthews, T. K. Maycock, T. Waterfield, O. Yelekçi, R. Yu and B. Zhou (eds), *Climate Change 2021: The Physical Science Basis. Contribution of Working Group I to the Sixth Assessment Report of the Intergovernmental Panel on Climate Change*, Cambridge University Press, Cambridge, UK and New York, NY, USA, book section 1.
URL: *https://www.ipcc.ch/report/ar6/wg1/downloads/report/IPCC*$_A R6_W GI_C hapter01.pdf$

Claussen, M., Ganopolski, A., Schellnhuber, J. and Cramer, W. (2000). Earth system models of intermediate complexity, *IGPB Newsletter* **41**: 4–6.

Claussen, M., Mysak, L., Weaver, A., Crucifix, M., Fichefet, T., Loutre, M.-F., Weber, S., Alcamo, J., Alexeev, V., Berger, A. et al. (2002). Earth system models of intermediate complexity: closing the gap in the spectrum of climate system models, *Climate dynamics* **18**: 579–586.

Cummins, D. P., Stephenson, D. B. and Stott, P. A. (2020). Optimal estimation of stochastic energy balance model parameters, *Journal of Climate* **33**(18): 7909–7926.
URL: *https://journals.ametsoc.org/view/journals/clim/33/18/jcliD190589.xml*

Edwards, P. N. (2011). History of climate modeling, *Wiley Interdisciplinary Reviews: Climate Change* **2**(1): 128–139.

Flato, G. M. (2011). Earth system models: an overview, *Wiley Interdisciplinary Reviews: Climate Change* **2**(6): 783–800.

Forster, P., Storelvmo, T., Armour, K., Collins, T., Dufresne, J. L., Frame, D., Lunt, D. J., Mauritsen, T., Palmer, M. D., Watanabe, M., Wild, M. and Zhang, H. (2021). *The Earth's Energy Budget, Climate Feedbacks, and Climate Sensitivity*, Cambridge, United Kingdom, book section 7, pp. 923–1054.

Fox-Kemper, B., Hewitt, H. T., Xiao, C., Aðalgeirsdóttir, G., Drijfhout, S. S., Edwards, T. L., Golledge, N. R., Hemer, M., Kopp, R. E., Krinner, G., Mix, A., Notz, D., Nowicki, S., Nurhati, I. S., Ruiz, L., Sallée, J.-B., A.Slangen, A. B. and Yu, Y. (2021). *Ocean, Cryosphere and Sea Level Change*.

Friedlingstein, P., Cox, P., Betts, R., Bopp, L., von Bloh, W., Brovkin, V., Cadule, P., Doney, S., Eby, M., Fung, I. et al. (2006). Climate–carbon cycle feedback analysis: results from the c4mip model intercomparison, *Journal of climate* **19**(14): 3337–3353.

Gasser, T., Ciais, P., Boucher, O., Quilcaille, Y., Tortora, M., Bopp, L. and Hauglustaine, D. (2017). The compact Earth system model OSCAR v2.2: Description and first results, *Geoscientific Model Development* **10**(1): 271–319.

Geoffroy, O., Saint-Martin, D., Bellon, G., Voldoire, A., Olivié, D. J. and Tytéca, S. (2013). Transient climate response in a two-layer energy-balance model. Part II: Representation of the efficacy of deep-ocean heat uptake and validation for CMIP5 AOGCMs, *Journal of Climate* **26**(6): 1859–1876.

Grassl, H. (2000). Status and improvements of coupled general circulation models, *Science* **288**(5473): 1991–1997.

Hajima, T., Kawamiya, M., Watanabe, M., Kato, E., Tachiiri, K., Sugiyama, M., Watanabe, S., Okajima, H. and Ito, A. (2014). Modeling in earth system science up to and beyond ipcc ar5, *Progress in Earth and Planetary Science* **1**(1): 1–25.

Harper, K. C. (2012). *Weather by the numbers: the genesis of modern meteorology*, MIT Press.

Held, I. M., Winton, M., Takahashi, K., Delworth, T., Zeng, F. and Vallis, G. K. (2010). Probing the fast and slow components of global warming by returning abruptly to preindustrial forcing, *Journal of Climate* **23**(9): 2418–2427.

Hope, A. P., Canty, T. P., Salawitch, R. J., Tribett, W. R. and Bennett, B. F. (2017). Forecasting global warming, *Paris climate agreement: Beacon of hope* pp. 51–114.

IPCC (2021). *Climate Change 2021: The Physical Science Basis. Contribution of Working Group I to the Sixth Assessment Report of the Intergovernmental Panel on Climate Change*, Cambridge University Press, Cambridge, UK and New York, NY, USA.
URL: *https://report.ipcc.ch/ar6/wg1/IPCC*$_A R6_W GI_F ullReport.pdf$

IPCC (2022). *Climate Change 2022: Mitigation of Climate Change. Contribution of Working Group III to the Sixth Assessment Report of the Intergovernmental Panel on Climate Change*, Cambridge University Press, Cambridge, UK and New York, NY, USA.
URL: *https://www.ipcc.ch/report/ar6/wg3/downloads/report/IPCC*$_A R6_W GIII_F ullReport.pdf$

Jalota, S., Vashisht, B., Sharma, S. and Kaur, S. (2018). Chapter 2 - climate change projections, *in* S. Jalota, B. Vashisht, S. Sharma and S. Kaur (eds), *Understanding Climate Change Impacts on Crop Productivity and Water Balance*, Academic Press, pp. 55 – 86.
URL: *http://www.sciencedirect.com/science/article/pii/B9780128095201000021*

Kawamiya, M., Hajima, T., Tachiiri, K., Watanabe, S. and Yokohata, T. (2020). Two decades of earth system modeling with an emphasis on model for interdisciplinary research on climate (miroc), *Progress in Earth and Planetary Science* **7**: 1–13.

Leach, N. J., Nicholls, Z., Jenkins, S., Smith, C. J., Lynch, J., Cain, M., Wu, B., Tsutsui, J. and Allen, M. R. (2020). Gir v1. 0.0: a generalised impulse-response model for climate uncertainty and future scenario exploration, *Geoscientific Model Development Discussions* pp. 1–29.

Lee, J. Y., Marotzke, J., Bala, G., Cao, L., Corti, S., Dunne, J. P., Engelbrecht, F., Fischer, E., Fyfe, J. C., Jones, C., Maycock, A., Mutemi, J., Ndiaye, O., Panickal, S. and Zhou, T. (2021). Future global climate: Scenario-based projections and near-term informations, *Climate Change 2021: The Physical Science*

Basis. Contribution of Working Group I to the Sixth Assessment Report of the Intergovernmental Panel on Climate Change .

Meinshausen, M., Raper, S. C. and Wigley, T. M. (2011). Emulating coupled atmosphere-ocean and carbon cycle models with a simpler model, magicc6–part 1: Model description and calibration, *Atmospheric Chemistry and Physics* **11**(4): 1417–1456.

Myhre, G., Shindell, D., Bréon, F.-M., Collins, W., Fuglestvedt, J., Huang, J., Koch, D., Lamarque, J.-F., Lee, D., Mendoza, B., Nakajima, T., Robock, A., Stephens, G., Takemura, T. and Zhang, H. (2013). AR5 - Working Group 1, Chapter 8 : Anthropogenic and Natural Radiative Forcing - Contribution of Working Group I, *Cambridge University Press* **23**: 56.

Nicholls, Z., Meinshausen, M., Lewis, J., Corradi, M. R., Dorheim, K., Gasser, T., Gieseke, R., Hope, A. P., Leach, N., McBride, L. A. et al. (2021). Reduced complexity model intercomparison project phase 2: Synthesizing earth system knowledge for probabilistic climate projections, *Earth's Future* **9**(6): e2020EF001900.

Nicholls, Z. R., Meinshausen, M., Lewis, J., Gieseke, R., Dommenget, D., Dorheim, K., Fan, C.-S., Fuglestvedt, J. S., Gasser, T., Golüke, U. et al. (2020). Reduced complexity model intercomparison project phase 1: introduction and evaluation of global-mean temperature response, *Geoscientific Model Development* **13**(11): 5175–5190.

Quilcaille, Y., Gudmundsson, L., Beusch, L., Hauser, M. and Seneviratne, S. I. (2022). Showcasing mesmer-x: Spatially resolved emulation of annual maximum temperatures of earth system models, *Geophysical Research Letters* **49**(17): e2022GL099012.

Rohrschneider, T., Stevens, B. and Mauritsen, T. (2019). On simple representations of the climate response to external radiative forcing, *Climate Dynamics* **53**: 3131–3145.

Schwarber, A. K., Smith, S. J., Hartin, C. A., Vega-Westhoff, B. A. and Sriver, R. (2019). Evaluating climate emulation: fundamental impulse testing of simple climate models, *Earth System Dynamics* **10**(4): 729–739.

Skeie, R. B., Fuglestvedt, J., Berntsen, T., Peters, G. P., Andrew, R., Allen, M. and Kallbekken, S. (2017). Perspective has a strong effect on the calculation of historical contributions to global warming, *Environmental Research Letters* **12**(2): 024022.

Smith, C. J., Forster, P. M., Allen, M., Leach, N., Millar, R. J., Passerello, G. A. and Regayre, L. A. (2018). Fair v1. 3: a simple emissions-based impulse response and carbon cycle model, *Geoscientific Model Development* **11**(6): 2273–2297.

Staniforth, A. and Thuburn, J. (2012). Horizontal grids for global weather and climate prediction models: a review, *Quarterly Journal of the Royal Meteorological Society* **138**(662): 1–26.

Szopa, S., Naik, V., Adhikary, B., Artaxo, P., Berntsen, T., Collins, W., Fuzzi, S., Gallardo, L., Kiendler-Scharr, A., Klimont, Z., Liao, H., Unger, N. and Zanis, P. (2021). Short-lived climate forcers, *in*

V. Masson-Delmotte, P. Zhai, A. Pirani, S. L. Connors, C. Péan, S. Berger, N. Caud, Y. Chen, L. Goldfarb, M. I. Gomis, M. Huang, K. Leitzell, E. Lonnoy, J. B. R. Matthews, T. K. Maycock, T. Waterfield, O. Yelekçi, R. Yu and B. Zhou (eds), *Climate Change 2021: The Physical Science Basis. Contribution of Working Group I to the Sixth Assessment Report of the Intergovernmental Panel on Climate Change*, Cambridge University Press, Cambridge, UK and New York, NY, USA, book section 6.
URL: *https://www.ipcc.ch/report/ar6/wg1/downloads/report/IPCC*$_A R6_W G I_C hapter 06.pdf$

2.2 . Pathfinder v1.0.1: a Bayesian-inferred simple carbon–climate model to explore climate change scenarios

Abstract: The Pathfinder model was developed to fill a perceived gap within the range of existing simple climate models. Pathfinder is a compilation of existing formulations describing the climate and carbon cycle systems, chosen for their balance between mathematical simplicity and physical accuracy. The resulting model is simple enough to be used with Bayesian inference algorithms for calibration, which enables assimilation of the latest data from complex Earth system models and the IPCC 6th assessment report, as well as a yearly update based on observations of global temperature and atmospheric CO2. The model's simplicity also enables coupling with integrated assessment models and their optimization algorithms, or running the model in a backward temperature-driven fashion. In spite of this simplicity, the model accurately reproduces behaviours and results from complex models – including several uncertainty ranges – when run following standardized diagnostic experiments. Pathfinder is open-source, and this is its first comprehensive description.

Pathfinder v1.0.1: a Bayesian-inferred simple carbon-climate model to explore climate change scenarios

Thomas Bossy[1,2,*], Thomas Gasser[1,*], and Philippe Ciais[2]

[1]International Institute for Applied Systems Analysis (IIASA), Laxenburg, Austria
[2]Laboratoire des Sciences du Climat et de l'Environnement (LSCE), Gif-sur-Yvette, France
[*]These authors contributed equally to this work.

Correspondence: Thomas Gasser (gasser@iiasa.ac.at)

1 Introduction

Simple climate models (SCMs) typically simulate global mean temperature change caused by either atmospheric concentration changes or anthropogenic emissions, of CO2 and other climatically active species. They are most often composed of ad hoc parametric laws that emulate the behaviour of more complex Earth system models (ESMs). The emulation allows simulating large ensembles of experiments that would be too costly to compute with ESMs. However, the SCM denomination refers to a fairly broad range of models whose complexity can go from a couple of boxes that only emulate one part of the climate system (e.g. a global temperature impulse response function; Geoffroy et al., 2013b) to hundreds of state variables representing the different cycles of greenhouse gases and their effect on climate change (e.g. the compact Earth system model OSCAR; Gasser et al., 2017). Simpler models are easier and faster to solve, but they may not be adequate for all usages. Therefore, finding the "simplest but not simpler" model depends on a study's precise goals.

In our recent research, we have perceived a deficiency within the existing offer of SCMs, in spite of their large and growing number (Nicholls et al., 2020). We have therefore developed the Pathfinder model to fill this gap: it is a parsimonious CO2-only model that carefully balances simplicity and accuracy of representation of physical processes. Pathfinder was designed to fulfil three key requirements: 1. the capacity to be calibrated using Bayesian inference, 2. the capacity to be coupled with integrated assessment models (IAMs), and 3. the capacity to explore a very large number of climate scenarios to narrow down those compatible with limiting climate impacts. The latter motivated the model's name.

While these three requirements clearly call for the simplest model possible, as they all need a fast solving model, they also imply a certain degree of complexity. The Bayesian calibration requires an explicit representation of the processes (i.e. the variables) that are used to constrain the model. Coupling with IAMs requires accurately embedding the latest advances of climate sciences to be policy relevant (National Academies of Sciences and Medicine, 2017). And exploring future climate impacts requires the flexibility to link additional (and potentially regional) impact variables to the core carbon-climate equations.

The Pathfinder model is essentially an integration of existing formulations, adapted to our modelling framework and goals. It is calibrated on Earth system models that contributed to the Coupled Model Intercomparison Project phase 6 (CMIP6), on additional data from the 6th assessment report of the IPCC (AR6), and on observations of global Earth properties up to the year

2021. The calibration philosophy of Pathfinder is to use complex models as prior information, and only real-world observations and assessments combining many lines of evidence as constraints.

Compared to other SCMs (Nicholls et al., 2020), Pathfinder is much simpler than models like MAGICC (Meinshausen et al., 2011), OSCAR (Gasser et al., 2017) or even HECTOR (Hartin et al., 2015). It is comparable in complexity to FaIR (Smith et al., 2018) or BernSCM (Strassmann and Joos, 2018), although it is closer to the latter as it trades off an explicit representation of non-CO2 species for one of the carbon cycle's main components. This choice was made to help calibration, keep the model invertible, and be compatible with IAMs such as DICE (Nordhaus, 2017). While most SCMs are calibrated using procedures that resemble Bayesian inference (Nicholls et al., 2021), Pathfinder relies on an established algorithm whose implementation is fully tractable, and that allows for an annual update as observations of atmospheric CO2 and global temperature become available.

Here, we present the first public release of Pathfinder and its source code. We first provide a detailed description of the model's equations. We then describe the Bayesian setup used for calibration, the sources of prior information for it, and the resulting posterior configuration. We end with a validation of the model using standard diagnostic simulations and quantitative metrics for the climate system and carbon cycle.

2 Equations

An overview of Pathfinder is presented in Figure 1. The model is composed of a climate module, of three separate modules for the carbon cycle (ocean, land without land use and land permafrost), and of two additional modules describing global impacts: sea level rise (SLR), and surface ocean acidification. We do not emulate cycles of other non-CO_2 gases. Mathematically, the model is driven by prescribing time series of any combination of two of four variables: global mean surface temperature (GMST) anomaly (noted T), global atmospheric CO2 concentration (C), global non-CO2 effective radiative forcing (R_x), and global anthropogenic emissions of CO2 (E_{CO2}). The model can therefore be run in the traditional emission-driven and concentration-driven modes, but also in a temperature-driven mode (in terms of code, implemented as separate versions of the model). This is notably important for the calibration, during which it is driven by observations of GMST and atmospheric CO2.

The following presents all equations of the models. Variables are noted using Roman letters, and compiled in Tables B1 and B2. With a few exceptions, parameters are noted using Greek letters, and summarized in Tables B3 and B4. The model has 21 state variables that follow a first-order differential equations in time. The time variable is noted t and kept implicit unless required.

2.1 Climate

The GMST change (T) induced by effective radiative forcing (ERF; R) is represented using a widely used two-box energy balance model with deep ocean heat uptake efficacy (Geoffroy et al., 2013a; Armour, 2017). The first box represents the Earth surface's temperature (including atmosphere, land and surface ocean), and the other one is the deep ocean's temperature (T_d).

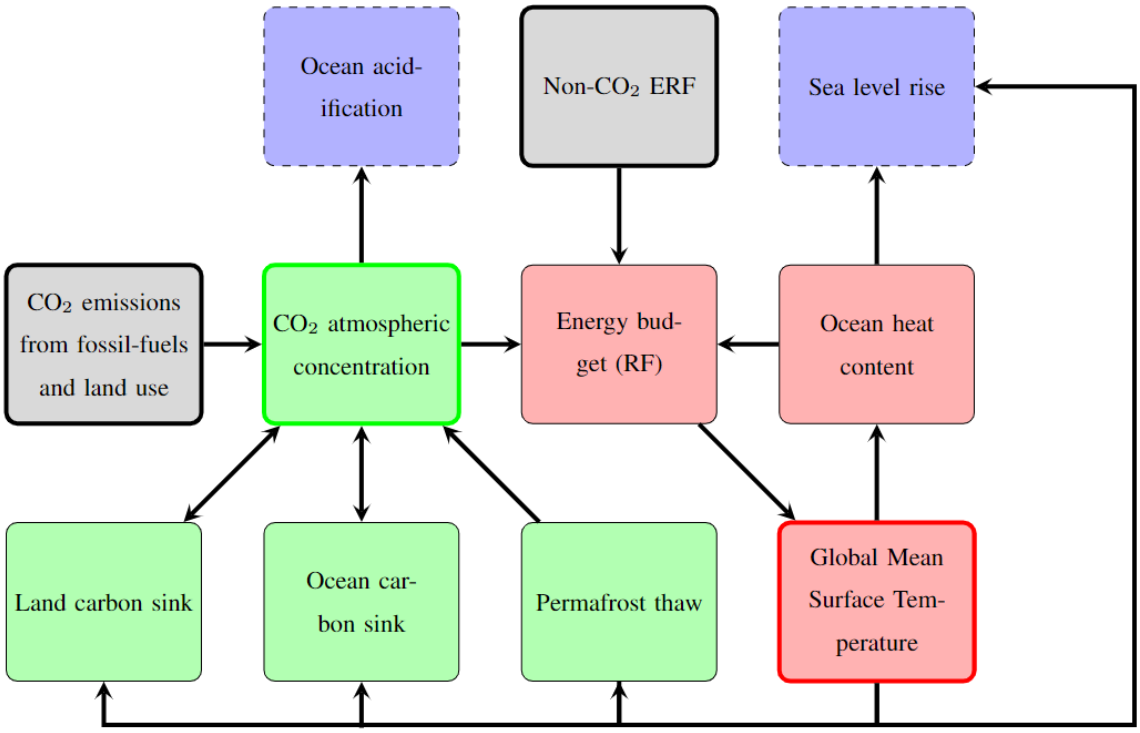

Figure 1. Pathfinder in a nutshell: Green blocks represent the carbon cycle, and red blocks the climate response. Blue blocks with dotted arrows are impacts that can be derived with the model. Grey blocks are variables that are directly related to anthropogenic activity. Possible inputs of the model are distinguishable through the bold contours of the blocks. In this scheme, arrows correspond to a forward mode where inputs would be E_{CO2} and R_x

Their time-differential equations are:

$$\Theta_s \frac{\mathrm{d}T}{\mathrm{d}t} = R - \frac{\phi \ln(2)}{T_{2\times}} T - \epsilon_{\mathrm{heat}}\, \theta\, (T - T_d) \tag{1}$$

and

$$\Theta_d \frac{\mathrm{d}T_d}{\mathrm{d}t} = \theta\, (T - T_d) \tag{2}$$

where ϕ is the radiative parameter of CO2, $T_{2\times}$ is the equilibrium climate sensitivity (ECS) at CO2 doubling, Θ_s is the heat capacity of the surface, Θ_d is the heat capacity of the deep ocean, θ is the heat exchange coefficient, and ϵ_{heat} is the deep ocean heat uptake efficacy.

The global ERF is simply the sum of the CO2 contribution (R_{CO2}), expressed using the IPCC AR5 formula (Myhre et al., 2013), and that of non-CO2 climate forcers (R_x):

$$R = R_{\mathrm{CO2}} + R_x \tag{3}$$

with

$$R_{\mathrm{CO2}} = \phi \ln\left(\frac{C}{C_{\mathrm{pi}}}\right) \tag{4}$$

where C_{pi} is the preindustrial atmospheric CO2 concentration.

The above energy balance model naturally provides the ocean heat content (OHC; U_{ohc}) as:

$$U_{\mathrm{ohc}} = \alpha_{\mathrm{ohc}} \left(\Theta_s \, T + \Theta_d \, T_d\right) \tag{5}$$

and the ocean heat uptake (OHU) as:

$$\frac{\mathrm{d}U_{\mathrm{ohc}}}{\mathrm{d}t} = \alpha_{\mathrm{ohc}} \left(\Theta_s \, \frac{\mathrm{d}T}{\mathrm{d}t} + \Theta_d \, \frac{\mathrm{d}T_d}{\mathrm{d}t}\right) \tag{6}$$

where α_{ohc} is the fraction of energy used to warm the ocean (i.e. excluding the energy needed to heat up the atmosphere and land, and to melt ice).

2.2 Sea level rise

Global SLR has been implemented in Pathfinder as a variable of interest to model climate change impacts. In this version, it is firstly a proof of concept, modelled in a simple yet sensible manner. The total sea level rise (H_{tot}) is the sum of contributions from thermal expansion (H_{thx}), Greenland ice sheet (GIS; H_{gis}), Antarctica ice sheet (AIS; H_{ais}), and glaciers (H_{gla}):

$$H_{\mathrm{tot}} = H_{\mathrm{thx}} + H_{\mathrm{gis}} + H_{\mathrm{ais}} + H_{\mathrm{gla}} \tag{7}$$

The thermal expansion contribution scales linearly with the OHC (Goodwin et al., 2017; Fox-Kemper et al., 2021):

$$H_{\mathrm{thx}} = \Lambda_{\mathrm{thx}} \, U_{\mathrm{ohc}} \tag{8}$$

where Λ_{thx} is the scaling factor of the thermosteric contribution to SLR. Note, however, that the thermal capacity of the climate module does not match that of the real-world ocean (Geoffroy et al., 2013b), and so this equation cannot describe equilibrium SLR over millennial timescales.

To model contributions from ice sheets and glaciers, we followed the general approach of Mengel et al. (2016). The SLR caused by GIS follows a first-order differential equation with its specific timescale, and the equilibrium SLR from GIS is assumed to be a cubic function of GMST:

$$\frac{\mathrm{d}H_{\mathrm{gis}}}{\mathrm{d}t} = \lambda_{\mathrm{gis}} + \frac{1}{\tau_{\mathrm{gis}}} \left(\Lambda_{\mathrm{gis1}} \, T + \Lambda_{\mathrm{gis3}} \, T^3 - H_{\mathrm{gis}}\right) \tag{9}$$

where λ_{gis} is an offset parameter introduced because GIS was not in a steady state at the end of the preindustrial era, Λ_{gis1} is the linear term of equilibrium of GIS SLR, Λ_{gis3} is the cubic term of equilibrium of GIS SLR, and τ_{gis} is the timescale of the GIS contribution. The motivation for replacing the quadratic term of Mengel et al. (2016) by a cubic one is the oddness of the cubic function that leads to negative (and not positive) SLR for negative T (which happens during the earlier years of the calibration run).

The contribution from glaciers is also a first-order differential equation with an equilibrium inspired by Mengel et al. (2016). We expanded it with a cubic term to account for the fact that we aggregate all glaciers together and allow more skewness in the curve describing the equilibrium SLR as a function of T. In addition, we added an exponential sensitivity to speed up the convergence to equilibrium under warmer climate:

$$\frac{\mathrm{d}H_{\mathrm{gla}}}{\mathrm{d}t} = \lambda_{\mathrm{gla}} + \frac{\exp(\gamma_{\mathrm{gla}}\,T)}{\tau_{\mathrm{gla}}}\,\left(\Lambda_{\mathrm{gla}}\,\left(1-\exp\left(-\Gamma_{\mathrm{gla1}}\,T-\Gamma_{\mathrm{gla3}}\,T^3\right)\right)-H_{\mathrm{gla}}\right) \tag{10}$$

where λ_{gla} is an offset parameter accounting for the lack of initial steady-state, Λ_{gla} is the SLR potential if all glaciers melted, Γ_{gla1} is the linear sensitivity of glaciers' equilibrium to climate change, Γ_{gla3} is the cubic sensitivity of glaciers' equilibrium to climate change, τ_{gla} is the timescale of the glaciers contribution, and γ_{gla} is the sensitivity of glaciers' timescale to climate change.

Following Mengel et al. (2016), the contribution from AIS is further divided in two terms, one for surface mass balance (SMB; $H_{\mathrm{ais,smb}}$) and one for solid ice discharge (SID; $H_{\mathrm{ais,sid}}$), so that $H_{\mathrm{ais}} = H_{\mathrm{ais,smb}} + H_{\mathrm{ais,sid}}$. It is expected that precipitation will increase over Antarctica under higher GMST, leading to increase in SMB and to a negative sea level rise contribution modeled as:

$$\frac{\mathrm{d}H_{\mathrm{ais,smb}}}{\mathrm{d}t} = -\Lambda_{\mathrm{ais,smb}}\,T \tag{11}$$

where $\Lambda_{\mathrm{ais,smb}}$ is the AIS SMB sensitivity to climate change (expressed in sea level equivalent). At the same time, increasing surface ocean temperatures will cause more SID through basal melting, which we model using a first-order differential equation assumed to be independent of the SMB effect, and with a term that speeds up the effect the more SID happened:

$$\frac{\mathrm{d}H_{\mathrm{ais,sid}}}{\mathrm{d}t} = \lambda_{\mathrm{ais}} + \frac{1+\alpha_{\mathrm{ais}}\,H_{\mathrm{ais,sid}}}{\tau_{\mathrm{ais}}}\,\left(\Lambda_{\mathrm{ais}}\,T - H_{\mathrm{ais,sid}}\right) \tag{12}$$

where λ_{ais} is an offset parameter accounting for the lack of initial steady-state, Λ_{ais} is the SLR equilibrium of AIS SID, τ_{ais} is the timescale of the AIS SID contribution, and α_{ais} is the sensitivity of the timescale to past SID. In the model's code, however, we directly solve for the total AIS contribution as:

$$\frac{\mathrm{d}H_{\mathrm{ais}}}{\mathrm{d}t} = -\Lambda_{\mathrm{ais,smb}}\,T + \lambda_{\mathrm{ais}} + \frac{1+\alpha_{\mathrm{ais}}\,(H_{\mathrm{ais}}-H_{\mathrm{ais,smb}})}{\tau_{\mathrm{ais}}}\,\left(\Lambda_{\mathrm{ais}}\,T - (H_{\mathrm{ais}}-H_{\mathrm{ais,smb}})\right) \tag{13}$$

2.3 Ocean carbon

To calculate the ocean carbon sink, we use the classic mixed-layer impulse response function model from Joos et al. (1996), updated to the equivalent box-model formulation of Strassmann and Joos (2018), and extended in places to introduce parameter adjustments for calibration. In the model, the mixed layer is split into 5 boxes (subscript j), as represented in Figure 4, so that the total carbon in the mixed layer pool (C_o) is:

$$C_o = \sum_j C_{o,j} \tag{14}$$

This total carbon mass is converted into a molar concentration of dissolved inorganic carbon (DIC; c_{dic}) following:

$$c_{\mathrm{dic}} = \frac{\alpha_{\mathrm{dic}}}{\beta_{\mathrm{dic}}}\,C_o \tag{15}$$

where α_{dic} is a fixed conversion factor, and β_{dic} is a scaling factor for the conversion. (The latter can be seen as a factor multiplying the mixed layer depth: it is 1 if the depth is unchanged from the original Strassmann and Joos (2018) model.)

The non-linear carbonate chemistry in the mixed layer is emulated in two steps. First, the model's original polynomial function is used to determine the partial pressure of CO2 affected by changes in DIC only (p_{dic}):

$$\begin{aligned} p_{\mathrm{dic}} = {} & (1.5568 - 0.013993\,T_o)\,c_{\mathrm{dic}} \\ & + (7.4706 - 0.20207\,T_o)\,10^{-3}\,{c_{\mathrm{dic}}}^2 \\ & - (1.2748 - 0.12015\,T_o)\,10^{-5}\,{c_{\mathrm{dic}}}^3 \\ & + (2.4491 - 0.12639\,T_o)\,10^{-7}\,{c_{\mathrm{dic}}}^4 \\ & - (1.5768 - 0.15326\,T_o)\,10^{-10}\,{c_{\mathrm{dic}}}^5 \end{aligned} \tag{16}$$

where T_o is the preindustrial surface ocean temperature. Second, the actual partial pressure of CO2 (p_{CO2}) is calculated using an exponential climate sensitivity (Takahashi et al., 1993; Joos et al., 2001):

$$p_{\mathrm{CO2}} = (p_{\mathrm{dic}} + C_{\mathrm{pi}})\,\exp(\gamma_{\mathrm{dic}}\,T) \tag{17}$$

where γ_{dic} is the sensitivity of p_{CO2} to climate change.

The flux of carbon between the atmosphere and the ocean (F_{ocean}, defined positively if it is a carbon sink) is caused by the difference in partial pressure of CO2 in the atmosphere and at the oceanic surface, following an exchange rate that varies linearly with GMST, that is here used as a proxy for wind changes:

$$F_{\mathrm{ocean}} = \nu_{\mathrm{gx}}\,(1 + \gamma_{\mathrm{gx}}\,T)\,(C - p_{\mathrm{CO2}}) \tag{18}$$

where ν_{gx} is the preindustrial gas-exchange rate, and γ_{gx} is its sensitivity to climate change.

This flux of carbon entering the ocean is split between the mixed layer carbon subpools, and this added carbon is subsequently transported towards the deep ocean at a rate specific to each subpool. This leads to the following differential equations:

$$\frac{\mathrm{d}C_{o,j}}{\mathrm{d}t} = -\frac{C_{o,j}}{\kappa_{\tau_o}\,\tau_{o,j}} + \alpha_{o,j}\,F_{\mathrm{ocean}}, \quad \forall j \tag{19}$$

where $\alpha_{o,j}$ are the subpools' splitting shares (with $\sum_j \alpha_{o,j} = 1$), $\tau_{o,j}$ are the subpools' timescales for transport to the deep ocean, and κ_{τ_o} is a scaling factor applied to all subpools. Finally, the deep ocean carbon pool (C_d) is obtained through mass balance:

$$\frac{\mathrm{d}C_d}{\mathrm{d}t} = \sum_j \frac{C_{o,j}}{\kappa_{\tau_o}\,\tau_{o,j}} \tag{20}$$

2.4 Ocean acidification

While in the real world, ocean acidification is directly related to the carbonate chemistry and the ocean uptake of anthropogenic carbon, we do not have a simple formulation at our disposal that could link it to our ocean carbon cycle module. We therefore

use a readily available emulation of the surface ocean acidification (pH) that links it directly to the atmospheric concentration of CO2 (Bernie et al., 2010) with the following polynomial approximation:

$$\mathrm{pH} = \kappa_{\mathrm{pH}} \left(8.5541 - 0.00173\, C + 1.3264\, 10^{-6}\, C^2 - 4.4943\, 10^{-10}\, C^3\right) \tag{21}$$

where κ_{pH} is a scaling factor (that defaults to 1). We note that this approach is reasonable for the surface ocean, as it quickly equilibrates with the atmosphere (but it would not work for the deep ocean).

2.5 Land carbon

The land carbon module of Pathfinder is a simplified version of the one in OSCAR (Gasser et al., 2017, 2020). It is shrunk down to four global carbon pools: vegetation, litter, active and passive soil (see Figure 2). All terrestrial biomes are lumped together, and there is therefore no accounting of the impact of land use change on the land carbon cycle in this version of Pathfinder. This is an extreme assumption – although very common in SCMs – motivated by simplicity, and it implies that CO2 emissions from fossil fuel burning and land use change are assumed to behave in the exact same way, in spite of their not doing so in reality (Gitz and Ciais, 2003; Gasser and Ciais, 2013).

The vegetation carbon pool (C_v) results from the balance between net primary productivity (NPP; F_{npp}), emission from wildfires (E_{fire}), emission from harvest and grazing (E_{harv}), and loss of carbon from biomass mortality (F_{mort}):

$$\frac{\mathrm{d}C_v}{\mathrm{d}t} = F_{\mathrm{npp}} - E_{\mathrm{fire}} - E_{\mathrm{harv}} - F_{\mathrm{mort}} \tag{22}$$

NPP is expressed as its own preindustrial value multiplied by a function of CO2 and of GMST (r_{npp}). This function thus embeds the so-called CO2-fertilisation effect, whereby NPP increases with atmospheric CO2, described using a generalised logarithmic functional form:

$$F_{\mathrm{npp}} = F_{\mathrm{npp0}}\, r_{\mathrm{npp}} \tag{23}$$

with

$$r_{\mathrm{npp}} = \left(1 + \frac{\beta_{\mathrm{npp}}}{\alpha_{\mathrm{npp}}} \left(1 - \left(\frac{C}{C_{\mathrm{pi}}}\right)^{-\alpha_{\mathrm{npp}}}\right)\right)(1 + \gamma_{\mathrm{npp}}\, T) \tag{24}$$

where F_{npp0} is the preindustrial NPP, β_{npp} is the CO2-fertilisation sensitivity, α_{npp} is the CO2-fertilisation shape parameter for saturation, and γ_{npp} is the sensitivity of NPP to climate change (that can be positive or negative). The generalised logarithmic functional form implies that: $r_{\mathrm{npp}} \to (1 + \beta_{\mathrm{npp}} \ln(C/C_{\mathrm{pi}}))(1 + \gamma_{\mathrm{npp}} T)$ as $\alpha_{\mathrm{npp}} \to 0^+$.

Harvesting and mortality fluxes are taken proportional to the carbon pool itself even though in reality the mortality fluxes are climate dependent. For simplicity we assume a constant mortality following the equations in OSCAR (Gasser et al., 2017):

$$E_{\mathrm{harv}} = \nu_{\mathrm{harv}}\, C_v \tag{25}$$

and

$$F_{\mathrm{mort}} = \nu_{\mathrm{mort}}\, C_v \tag{26}$$

where ν_{harv} is the harvesting/grazing rate, and ν_{mort} is the mortality rate.

Wildfires emissions are also assumed proportional to the vegetation carbon pool, but with an additional linear dependency of the emission rate on CO2 (as a proxy of changes in leaf area index and evapotranspiration) and GMST (r_{fire}):

$$E_{\mathrm{fire}} = \nu_{\mathrm{fire}}\, r_{\mathrm{fire}}\, C_v \tag{27}$$

with

$$r_{\mathrm{fire}} = \left(1 + \beta_{\mathrm{fire}} \left(\frac{C}{C_{\mathrm{pi}}} - 1\right)\right) (1 + \gamma_{\mathrm{fire}}\, T) \tag{28}$$

where ν_{fire} is the wildfires rate, β_{fire} is the sensitivity of wildfires to CO2, and γ_{fire} is their sensitivity to climate change.

Soil carbon is divided into three pools. The litter carbon pool (C_{s1}) receives the mortality flux as sole input, it emits part of its carbon through heterotrophic respiration (E_{rh1}), and it transfers another part to the next pool through stabilization (F_{stab}):

$$\frac{\mathrm{d}C_{s1}}{\mathrm{d}t} = F_{\mathrm{mort}} - F_{\mathrm{stab}} - E_{\mathrm{rh1}} \tag{29}$$

Similarly, the active soil carbon pool (C_{s2}) receives the stabilization flux, is respired (E_{rh2}), and transfers carbon to the last pool through passivization (F_{pass}):

$$\frac{\mathrm{d}C_{s2}}{\mathrm{d}t} = F_{\mathrm{stab}} - F_{\mathrm{pass}} - E_{\mathrm{rh2}} \tag{30}$$

The passive carbon pool (C_{s3}) receives this final input flux and is respired (E_{rh3}):

$$\frac{\mathrm{d}C_{s3}}{\mathrm{d}t} = F_{\mathrm{pass}} - E_{\mathrm{rh3}} \tag{31}$$

Although information pertaining to this fourth pool is not commonly provided by ESMs, it was introduced in Pathfinder to adjust the complex models' turnover time of soil carbon to better match isotopic data (He et al., 2016). For completeness, we note that the total heterotrophic respiration is $E_{\mathrm{rh}} = E_{\mathrm{rh1}} + E_{\mathrm{rh2}} + E_{\mathrm{rh3}}$, and the total soil carbon pool is $C_s = C_{s1} + C_{s2} + C_{s3}$.

All soil-originating fluxes are taken proportional to their pool of origin, and multiplied by a function (r_{rh}) explained hereafter. For the litter pool, this gives:

$$E_{\mathrm{rh1}} = \nu_{\mathrm{rh1}}\, r_{\mathrm{rh}}\, C_{s1} \tag{32}$$

and

$$F_{\mathrm{stab}} = \nu_{\mathrm{stab}}\, r_{\mathrm{rh}}\, C_{s1} \tag{33}$$

where ν_{rh1} is the litter respiration rate, and ν_{stab} is the stabilization rate. For the active soil pool, we have:

$$E_{\mathrm{rh2}} = \frac{\nu_{\mathrm{rh23}} - \nu_{\mathrm{rh3}}\, \alpha_{\mathrm{pass}}}{1 - \alpha_{\mathrm{pass}}}\, r_{\mathrm{rh}}\, C_{s2} \tag{34}$$

and

$$F_{\mathrm{pass}} = \nu_{\mathrm{rh3}} \frac{\alpha_{\mathrm{pass}}}{1-\alpha_{\mathrm{pass}}} r_{\mathrm{rh}} C_{s2} \tag{35}$$

and for the passive soil pool:

$$E_{\mathrm{rh3}} = \nu_{\mathrm{rh3}} r_{\mathrm{rh}} C_{s3} \tag{36}$$

where ν_{rh23} is the soil respiration rate (averaged over active and passive pools), ν_{rh3} is the passive soil respiration rate, and α_{pass} is the fraction of passive carbon (over active+passive soil carbon). This slightly convoluted formulation is motivated by the lack of information regarding the active/passive split in ESMs, which we alleviate using additional data during calibration.

In addition, the function r_{rh}, describing the dependency of respiration (and related fluxes) on temperature and on the availability of fresh organic matter to be decomposed, is defined as:

$$r_{\mathrm{rh}} = \frac{\underbrace{\left(1+\beta_{\mathrm{rh}}\left(\frac{C_{s1}}{C_{s1}+C_{s2}+C_{s3}}\left(1+\frac{\nu_{\mathrm{stab}}}{\nu_{\mathrm{rh23}}}\right)-1\right)\right)}}{\left(1+\beta_{\mathrm{rh}}\left(\frac{C_{s1}}{C_s}\frac{C_s(t_0)}{C_{s1}(t_0)}-1\right)\right)} \exp(\gamma_{\mathrm{rh}}\, T) \tag{37}$$

where β_{rh} is the sensitivity of the respiration to fresh organic matter availability (expressed here as the relative change in the C_{s1}/C_s ratio with regard to preindustrial times), and γ_{rh} is its sensitivity to climate change (equivalent to a "Q_{10}" formulation with $Q_{10} = \exp(10\,\gamma_{\mathrm{rh}})$).

Finally, the net carbon flux from the atmosphere to the land (F_{land}, defined positively if it is a carbon sink) is obtained as the net budget of all pools combined:

$$F_{\mathrm{land}} = F_{\mathrm{npp}} - E_{\mathrm{fire}} - E_{\mathrm{harv}} - E_{\mathrm{rh}} \tag{38}$$

and this system of equations leads to the following preindustrial steady-state:

$$\begin{cases} C_v(t_0) = \frac{F_{\mathrm{npp0}}}{\nu_{\mathrm{fire}}+\nu_{\mathrm{harv}}+\nu_{\mathrm{mort}}} \\ C_{s1}(t_0) = C_v(t_0)\frac{\nu_{\mathrm{mort}}}{\nu_{\mathrm{rh1}}+\nu_{\mathrm{stab}}} \\ C_{s2}(t_0) = C_{s1}(t_0)\frac{\nu_{\mathrm{stab}}}{\nu_{\mathrm{rh23}}}(1-\alpha_{\mathrm{pass}}) \\ C_{s3}(t_0) = C_{s1}(t_0)\frac{\nu_{\mathrm{stab}}}{\nu_{\mathrm{rh23}}}\alpha_{\mathrm{pass}} \end{cases} \tag{39}$$

2.6 Permafrost carbon

As the land carbon cycle described in the previous section does not account for permafrost carbon, we implemented this feedback using the emulator developed by Gasser et al. (2018) but aggregated into a unique global region. Figure 3 gives a representation of the permafrost module as described in the following. The emulation starts with a theoretical thawed fraction ($\bar{a}$) that represents the fraction of thawed carbon under steady-state for a certain level of local warming. It is formulated with a

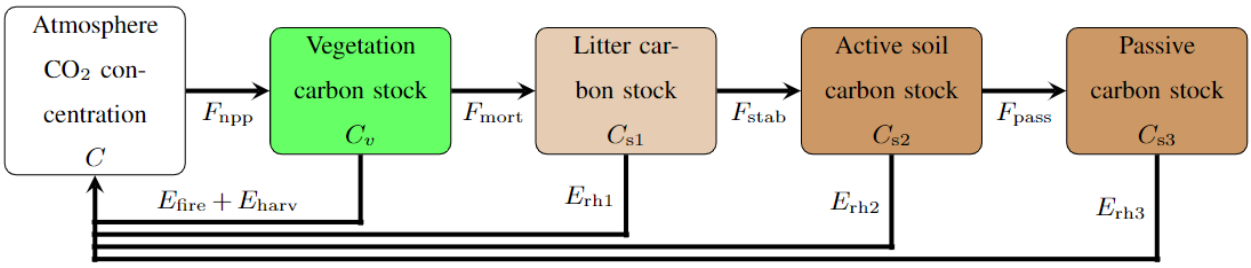

Figure 2. The land sink model in Pathfinder is derived from OSCAR (Gasser et al., 2017) and represents the biosphere as a set of four carbon pools: vegetation, litter , active soil and passive soil. These pools exchange carbon through fluxes whose direction is given by the arrows.

sigmoid function (that equals 0 at preindustrial and 1 under very high GMST):

$$\bar{a} = -a_{\min} + \frac{(1 + a_{\min})}{\left(1 + \left(\left(1 + \frac{1}{a_{\min}}\right)^{\kappa_a} - 1\right) \exp(-\gamma_a \, \kappa_a \, \alpha_{\mathrm{lst}} \, T)\right)^{\frac{1}{\kappa_a}}} \tag{40}$$

where $-a_{\min}$ is the minimum thawed fraction (corresponding to 100% frozen soil carbon), κ_a is a shape parameter determining the asymmetry of the function, γ_a is the sensitivity of the theoretical thawed fraction to local climate change, and α_{lst} is the proportionality factor between local and global climate change.

The actual thawed fraction (a) then moves towards its theoretical value at a speed that depends on whether it is thawing (i.e. $a < \bar{a}$) or freezing (i.e. $a > \bar{a}$). This is written as a non-linear differential equation:

$$\frac{\mathrm{d}a}{\mathrm{d}t} = 0.5 \, (\nu_{\mathrm{thaw}} + \nu_{\mathrm{froz}}) \, (\bar{a} - a) + 0.5 \, |(\nu_{\mathrm{thaw}} - \nu_{\mathrm{froz}}) \, (\bar{a} - a)| \tag{41}$$

where ν_{thaw} is the rate of thawing, and ν_{froz} is the rate of freezing. Because $\nu_{\mathrm{thaw}} > \nu_{\mathrm{froz}}$, the absolute value in the equation leads to the right-hand side being $\nu_{\mathrm{thaw}}(\bar{a} - a)$ if $a < \bar{a}$, or $\nu_{\mathrm{froz}}(\bar{a} - a)$ if $a > \bar{a}$. The change in the pool of frozen carbon (C_{fr}) naturally follows:

$$\frac{\mathrm{d}C_{\mathrm{fr}}}{\mathrm{d}t} = -\frac{\mathrm{d}a}{\mathrm{d}t} \, C_{\mathrm{fr0}} \tag{42}$$

where C_{fr0} is the amount of frozen carbon at preindustrial times.

Thawed carbon is not directly emitted to the atmosphere: it is split into three thawed carbon subpools ($C_{\mathrm{th},j}$) that have their own decay time, but are all affected by an additional function (r_{rt}). This leads to the following budget equations:

$$\frac{\mathrm{d}C_{\mathrm{th},j}}{\mathrm{d}t} = -\alpha_{\mathrm{th},j} \, \frac{\mathrm{d}C_{\mathrm{fr}}}{\mathrm{d}t} - \frac{C_{\mathrm{th},j}}{\kappa_{\tau_{\mathrm{th}}} \, \tau_{\mathrm{th},j}} \, r_{\mathrm{rt}}, \quad \forall j \tag{43}$$

where $\alpha_{\mathrm{th},j}$ are the subpools' splitting shares (with $\sum_j \alpha_{\mathrm{th},j} = 1$), $\tau_{\mathrm{th},j}$ are the subpools' decay times, and $\kappa_{\tau_{\mathrm{th}}}$ is a scaling factor applied to all subpools. The additional r_{rt} function describes the sensitivity of heterotrophic respiration to climate change in boreal regions, using a Gaussian formula:

$$r_{\mathrm{rt}} = \exp\left(\kappa_{\mathrm{rt}} \, \gamma_{\mathrm{rt1}} \, \alpha_{\mathrm{lst}} \, T - \kappa_{\mathrm{rt}} \, \gamma_{\mathrm{rt2}} \, (\alpha_{\mathrm{lst}} \, T)^2\right) \tag{44}$$

where κ_{rt} is a factor scaling the sensitivity of thawed carbon against that of regular soil carbon, γ_{rt1} is the sensitivity to local temperature change (i.e. a Q10), and γ_{rt2} is the quadratic term in the latter sensitivity that represents a saturation effect. Noting that all the emitted carbon is assumed to be CO2, the global emission from permafrost (E_{pf}) is thus:

$$E_{\mathrm{pf}} = \sum_j \frac{C_{\mathrm{th},j}}{\kappa_{\tau_{\mathrm{th}}}\, \tau_{\mathrm{th},j}}\, r_{\mathrm{rt}} \tag{45}$$

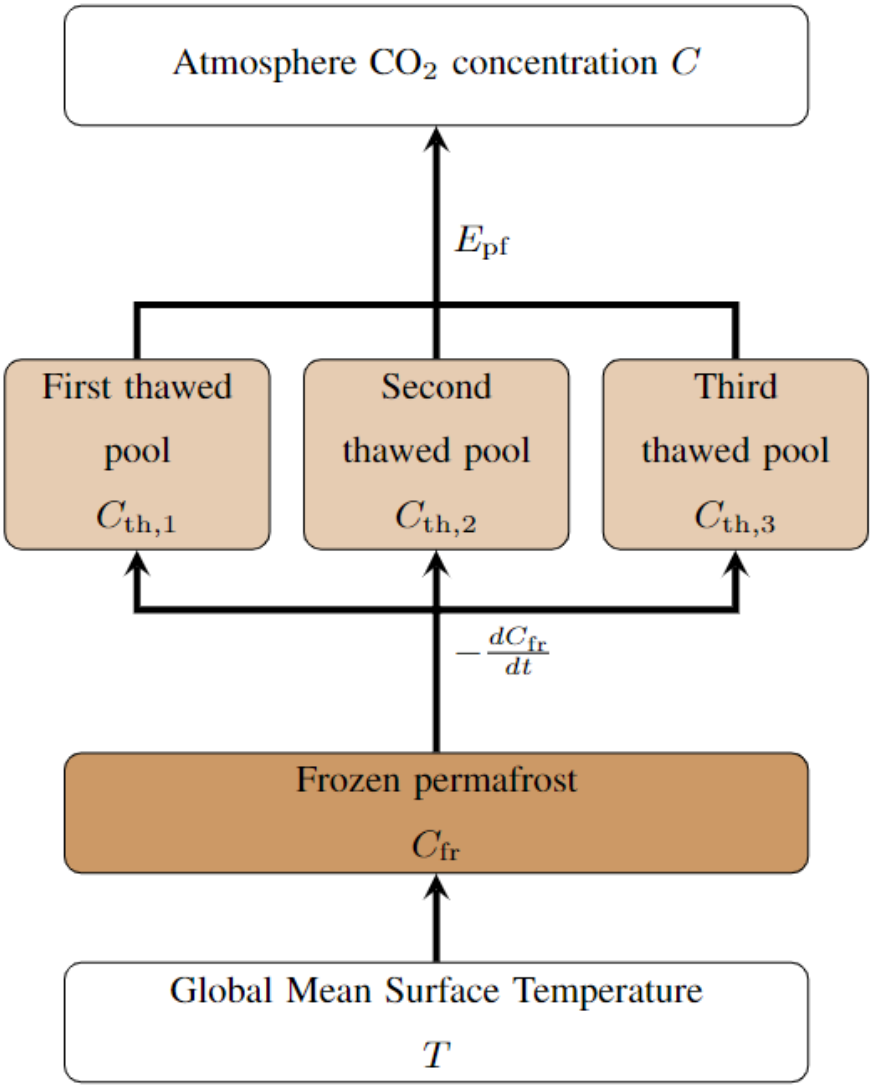

Figure 3. The permafrost carbon model in Pathfinder is taken from Gasser et al. (2018). The frozen pool dynamic lags behind a theoretical value that is determined by the temperature anomaly. Thawed carbon is then split between three pools that are emitted to the atmosphere at different rates.

2.7 Atmospheric CO2

The change in atmospheric concentration of CO2 is the budget of all carbon cycle fluxes to which we add the exogenous anthropogenic emissions (E_{CO2}):

$$\alpha_C \frac{\mathrm{d}C}{\mathrm{d}t} = E_{\mathrm{CO2}} + E_{\mathrm{pf}} - F_{\mathrm{land}} - F_{\mathrm{ocean}} \tag{46}$$

where α_C is the conversion factor from volume fraction to mass for CO2.

3 Bayesian calibration

3.1 Principle

Bayesian inference is a powerful tool for assimilating observational data into reduced-complexity models such as Pathfinder (Ricciuto et al., 2008). The approach consists in deducing probability distributions of parameters from a priori knowledge on those distributions and on distributions of observations of some of the model's variables, using Bayes' theorem (Bayes, 1763).Summarily, the Bayesian calibration updates the joint distribution of parameters to make it as compatible with the constraints as possible given their prior estimates, which increases internal coherence of Pathfinder by excluding combination of parameters that are unlikely.

Such a Bayesian calibration is vulnerable to the possibility that the priors draw on the same information as the constraints. However, given that Pathfinder is a patchwork of emulators whose parameters are obtained independently from one another and following differing experimental setups, we expect that the coherence of information contained within the priors and the constraints is very low. Our choice of using only complex models as prior information and only observations and assessments as constraints also aims at limiting this vulnerability.

Concretely, the posterior probability $\mathcal{P}_{\mathrm{post}}$ of a sample k from the joint parameters distribution $\boldsymbol{\xi}_k$, conditional to a set of observations $\boldsymbol{x}$, is proportional (symbol $\propto$) to its own prior probability $\mathcal{P}_{\mathrm{pre}}$ and to the likelihood $\mathcal{L}$ of the model simulating $\boldsymbol{x}$ given $\boldsymbol{\xi}_k$:

$$\mathcal{P}_{\mathrm{post}}(\boldsymbol{\xi}_k|\boldsymbol{x}) \propto \mathcal{L}(\boldsymbol{x}|\boldsymbol{\xi}_k)\,\mathcal{P}_{\mathrm{pre}}(\boldsymbol{\xi}_k) \tag{47}$$

Here, we assume all observations are independently and identically distributed following a normal distribution (with mean values $\boldsymbol{\mu_x}$, and standard deviations $\boldsymbol{\sigma_x}$ expressed in real physical units), which leads to the following likelihood:

$$\mathcal{L}(\boldsymbol{x}|\boldsymbol{\xi}_k) = \prod_{i=1}^{n_x} \frac{1}{\sigma_{x,i}\sqrt{2\pi}} \exp\left(-\frac{(\mathcal{F}_i(\boldsymbol{\xi}_k) - \mu_{x,i})^2}{2\,\sigma_{x,i}^2}\right) \tag{48}$$

where $\mathcal{F}_i(\boldsymbol{\xi}_k)$ is the model's output for the i-th observable (out of n_x) with input parameters $\boldsymbol{\xi}_k$.

3.2 Implementation

The Pathfinder model is a set of differential equations with a number of input parameters, of which n_ξ are calibrated through Bayesian inference, and an additional two input variables provided as time series (i.e. one value per time step required). While the two input time series can be any combination of two out of four variables (anthropogenic CO2 emissions, non-CO2 ERF, atmospheric CO2 concentration, or GMST), for calibration we use the two most well constrained variables that are direct physical observations of the global Earth system: atmospheric CO2 and GMST. These input time series cover the historical

period from 1751 to 2020. Therefore, the $\boldsymbol{\xi}_k$ vector is:

$$\boldsymbol{\xi}_k = \left\{ \{\xi_j\}_{j=1}^{n_\xi}, \{C(t)\}_{t=1751}^{2021}, \{T(t)\}_{t=1751}^{2021} \right\}_k \tag{49}$$

However, to ease the computation by reducing the dimension of the system, we do not use annual time series of observations as inputs, but we assume that each input time series (for variable X being C or T) follows:

$$X(t) = X_\mu(t) + \tilde{\sigma}_X \, X_\sigma(t) + \epsilon_X \, \mathrm{AR1}(t; \rho_X) \tag{50}$$

where X_μ and X_σ are fixed exogenous annual time series (i.e. structural parameters), $\tilde{\sigma}_X$ is the relative standard deviation of the time series (without noise), ϵ_X is the noise intensity, and $\mathrm{AR1}$ is an autoregressive process of order 1 and autocorrelation parameter ρ_X. This assumption leads to the final expression of the $\boldsymbol{\xi}_k$ vector:

$$\boldsymbol{\xi}_k = \left\{ \{\xi_j\}_{j=1}^{n_\xi}, \tilde{\sigma}_C, \epsilon_C, \rho_C, \tilde{\sigma}_T, \epsilon_T, \rho_T, \right\}_k \tag{51}$$

During this Bayesian assimilation, the Pathfinder model is run solely over the historical period (from 1750 to 2021), as the constraints concern only preindustrial or historical years. For the computation, thetime-differential system of Pathfinder is solved using an implicit-explicit numerical scheme (also called IMEX), with a time step of one quarter of a year. This solving scheme relies on: first, writing the differential equations of all state variables X as:

$$\frac{\mathrm{d}X}{\mathrm{d}t} = -\nu \, X + \mathcal{R} \tag{52}$$

where ν is the constant speed of the linear part of the differential equation, and $\mathcal{R}$ is its non-linear part; second, discretizing these equations as:

$$\frac{X(t+\delta t) - X(t)}{\delta t} = -\nu \, X(t+\delta t) + \mathcal{R}(t) \tag{53}$$

where δt is the solving time step (which is $\frac{1}{n_t}$ times the annual time step of the model's inputs and outputs, here $n_t = 4$); and third, explicitly solving for all $X(t+\delta t)$. We note this is also the default solving scheme for regular simulations with the model, although the value of n_t can be altered and alternative schemes are available.

The Bayesian procedure itself is implemented using the Python computer language, and specifically the PyMC3 package (Salvatier et al., 2016). The solving of equation 47 and its normalization are done using the package's full-rank Automatic Differentiation Variational Inference (ADVI) algorithm (Kucukelbir et al., 2017), with 100,000 iterations (and default algorithm options). The choice of variational inference instead of Markov chain Monte Carlo is motivated by the significant size our model (Blei et al., 2017) and the speed of ADVI. An additional strength of the full-rank version of the ADVI algorithm is its ability to generate correlated posterior distributions even if the prior ones are uncorrelated. Convergence of the algorithm was controlled through convergence of the ELBO metric (Kucukelbir et al., 2017). All results presented hereafter are obtained through drawing 2000 sets of parameters – that we call configurations – from the posterior or prior distributions.

3.3 Constraints

We use a set of 19 constraints related to all aspects of the model that correspond to the set of observations $\boldsymbol{x}$ in the Bayesian calibration. Many of the constraints are observations, but some are ranges assessed by expert panels such as the Global Carbon Project or the IPCC. They cover either a recent point in time or an assumed preindustrial equilibrium, and they are typically taken over a period of at least a few years to reduce the effect of natural variability.

Table 1 summarises these constraints, the periods over which they are considered, and their distributions. The following subsections provide further details on the constraints, and the constraints distributions are shown in Figure 6.

3.3.1 Climate system

To constrain the temperature response, we use the same five data sets of observed GMST as in Section 3.4.8, to derive average and standard deviation of two constraints: the average GMST change, and the average GMST yearly trend obtained through second-order accuracy gradient (Fornberg, 1988), both over the latest 20 years of data (2002–2021). Because this data is already used as input to the Bayesian setup, albeit in a different way, it does not provide much of a constraint, and is used mostly to ensure the $\tilde{\sigma}_T$ and ϵ_T parameters remain within sensible range.

To further constrain the climate system, we use the mean OHU assessed by the IPCC AR6 over 2006–2018 (Gulev et al., 2021, Table 2.7), and the non-CO2 ERF (averaged over 2010-2019) also estimated for the AR6. The central value of the latter is taken from Dentener et al. (2021, Table AIII.3, and corresponding GitHub repository), and its uncertainty is constructed using data from Forster et al. (2021, Table 7.8) and assuming the ERF of all species are normally distributed and uncorrelated, but fully correlated in time for each separate species (which likely overestimates the uncertainty).

To better align with the IPCC AR6, we also constrain the ECS of our model (i.e. the $T_{2\times}$ parameters). To do so, because the distribution of ECS cannot be assumed normal, we follow the framework of Roe and Baker (2007) who define the climate feedback factor ff so that $T_{2\times} = T^*_{2\times}/(1-\mathrm{ff})$, where $T^*_{2\times}$ is the minimal ECS value (roughly corresponding to the Planck feedback). We assume this feedback factor follows a logit-normal distribution, which implies $\mathrm{logit}(\mathrm{ff}) = \ln(\mathrm{ff}/(1-\mathrm{ff})) = \ln(T_{2\times}/T^*_{2\times} - 1)$ follows a normal distribution. We therefore constrain $\mathrm{logit}(\mathrm{ff})$, using distribution parameters and a value of $T^*_{2\times}$ calibrated to fit the probabilistic ranges of ECS provided by the AR6. This fit of the ECS distribution is illustrated in Figure B9.

3.3.2 Carbon cycle

Similarly to what is done with GMST, we constrain the atmospheric CO2 level over the latest 10 years of data (2012-2021) using the NOAA/ESRL data (Tans and Keeling, 2010). The rest of the global CO2 budget is constrained using the 2021 Global Carbon Budget (GCB; Friedlingstein et al., 2022). We use namely the net atmospheric CO2 growth and total anthropogenic emissions (fossil and land use) over the last 10 years, and the ocean and land carbon sinks accumulated since the beginning of the instrumental measurement period (1960-2020). Note that our definition of the land carbon sink ignoring land use change is consistent with that of the GCB.

Given its number of parameters and their inconsistent sources, we further constrain the land carbon module by considering present-day (mean over 1998-2002) NPP (Ciais et al., 2013; Zhao et al., 2005), and preindustrial vegetation and soil carbon pools. These preindustrial pools are taken from the AR6 for the central value (Canadell et al., 2021, Figure 5.12), but their relative uncertainty is taken from the AR5 (Ciais et al., 2013, Figure 6.1) since it is lacking in the AR6. In addition, the soil carbon pool constraint is corrected downward by estimates of peatland carbon (Yu et al., 2010, Table 1), since it is an ecosystem missing in TRENDY models (and in ours) but not in the IPCC assessments.

3.3.3 Sea level rise

To constrain the separate SLR contributions from thermal expansion, GIS, AIS and glaciers, we use the model-based SLR speed estimates over the recent past (averaged over 2006–2018) reported in the AR6 (Fox-Kemper et al., 2021, Table 9.5). To constrain the total contribution, we also use the historical (1901–1990) sea level rise inferred from tide gauges from the same source, although the value is corrected upward for the missed impact of uncharted glaciers (Parkes and Marzeion, 2018).

Contrarily to all other modules, the SLR module is not assumed to start at steady-state in 1750, which is represented through the λ_{ice} ($\mathrm{ice} \in [\mathrm{gla}, \mathrm{gis}, \mathrm{ais}]$) parameters. We assume this is entirely due to the so-called little ice age (LIA) relaxation, which we assume can be simply modeled in Pathfinder through exponential decay of our three ice-related contributions since $t_0 = 1750$. This gives a net LIA contribution of $H_{\mathrm{lia}} = \sum_{\mathrm{ice}} \lambda_{\mathrm{ice}}\, \tau_{\mathrm{ice}}\, \exp\left(-\frac{t-t_0}{\tau_{\mathrm{ice}}}\right)$. We constrain this diagnostic variable using the global SLR reported by Slangen et al. (2016) over 1900–2005 for their control experiment.

3.4 Parameters (prior distributions)

Out of the model's 77 parameters, 33 are assumed to be fixed (i.e. they are structural parameters), and the remaining n_ξ = 44 parameters are estimated through Bayesian inference. Prior distributions of the ξ_j parameters are assumed log-normal if the physical parameter must be defined positive, logit-normal if it must be between 0 and 1, and normal otherwise. To avoid extreme parameter values that could make the model diverge during calibration, the posterior distributions are bound to $\mu_{\xi,j} \pm 5\sigma_{\xi,j}$, where $\mu_{\xi,j}$ and $\sigma_{\xi,j}$ are the mean and standard deviation of the j-th parameter's prior distribution. These two values are taken from the literature, deduced from multi-model ensembles, or in a few instances arbitrarily set, as described in the following subsections. Note that when parameters are deduced from multi-model ensembles, there are effectively two rounds of calibration: first, a calibration on individual models using ordinary least square regressions to obtain prior distributions, and second, the Bayesian calibration itself that leads to the posterior distributions. In addition, the prior distributions of $\tilde{\sigma}_X$, ϵ_X and ρ_X are assumed normal, half-normal and uniform, respectively. All prior distributions are assumed independent, so that the prior joint distribution $\boldsymbol{\xi}$ does not exhibit any covariance.

All parameters are summarised in Tables B5 and B6 along with their properties and values. The following subsections further explain how the prior distributions of the parameters are established, and these distributions are shown in Figure 5

3.4.1 Climate

All the parameters of the climate module are calibrated. The prior distribution of the radiative parameter ϕ is taken from the AR5 (Myhre et al., 2013, Table 8.SM.1). All other prior distributions of the parameters of the climate module (i.e. $T_{2\times}$, Θ_s, Θ_d, θ and ϵ_{heat}) are taken from 35 CMIP6 models whose climate responses were derived for the AR6 using the *abrupt-4xCO2* experiment (Smith et al., 2021, Section 7.SM.2.1, and corresponding GitHub repository). Here, $T_{2\times}$ is simply assumed to be half the reported equilibrium temperature at quadrupled CO2. In addition, the prior distribution of the ocean warming fraction α_{ohc} is taken from the AR6 (Forster et al., 2021, Table 7.1).

3.4.2 Sea level rise

Some parameters from the SLR module are structural: the maximum SLR contribution from glaciers (Λ_{gla}) is taken from Fox-Kemper et al. (2021, Section 9.6.3.2), the equilibrium AIS SLR (Λ_{ais}) is from (Church et al., 2013, Figure 13.14), and the τ_{gis}, τ_{gla} and τ_{ais} timescales are the mean values from Mengel et al. (2016, Table S1) (assuming they provide the 90%-range of a log-normal distribution). All other parameters are calibrated. The prior distribution of the thermosteric parameter Λ_{thx} is taken from the AR6 (Fox-Kemper et al., 2021, Section 9.2.4.1), as are the prior distributions of the preindustrial offset parameters λ_{gis}, λ_{gla} and λ_{ais} (Fox-Kemper et al., 2021, earliest period of Table 9.5). For the remaining parameters, we derive prior distributions using SLR projections compiled by Edwards et al. (2021) for a number of ice sheets and glaciers models, over various RCP and SSP scenarios. Using the models' outputs, we apply equation 9 to estimate the Λ_{gis1} and Λ_{gis3} parameters, equation 10 for the Γ_{gla1}, Γ_{gla3} and γ_{gla} parameters, and equation 12 for the $\Lambda_{\mathrm{ais,smb}}$ and α_{ais} parameters. During these fits, all other parameters are assumed to take their default value if structural, and their best-guess value otherwise. Results of this calibration on the individual models compiled by Edwards et al. (2021) are shown for each SLR contribution in Figures B6, B7 and B8.

3.4.3 Ocean carbon

The ocean carbon cycle module has a number of structural parameters: α_{dic}, all $\alpha_{o,j}$ and all $\tau_{o,j}$ are taken from Strassmann and Joos (2018, Tables A2 and A3, based on the Princeton model). The prior distribution of the adjustment factor κ_{τ_o} is arbitrarily taken to apply a 20% uncertainty on the oceanic transport timescales. All other prior distributions for this module's parameters are derived from 12 CMIP6 models with interactive carbon cycle that contributed to C4MIP (Arora et al., 2020). T_o is taken on average over the *piControl* simulation. ν_{gx} and γ_{gx} are calibrated by applying equation 18 to the models' outputs for the *1pctCO2*, *1pctCO2-rad* and *1pctCO2-bgc* experiments, while β_{dic} and γ_{dic} are calibrated by applying equations 14-17 and 19. Results of this calibration on the individual CMIP6 models is shown in Figures B1 and B2.

3.4.4 Ocean acidification

In this version of Pathfinder, κ_{pH} is a structural parameter set to 1.

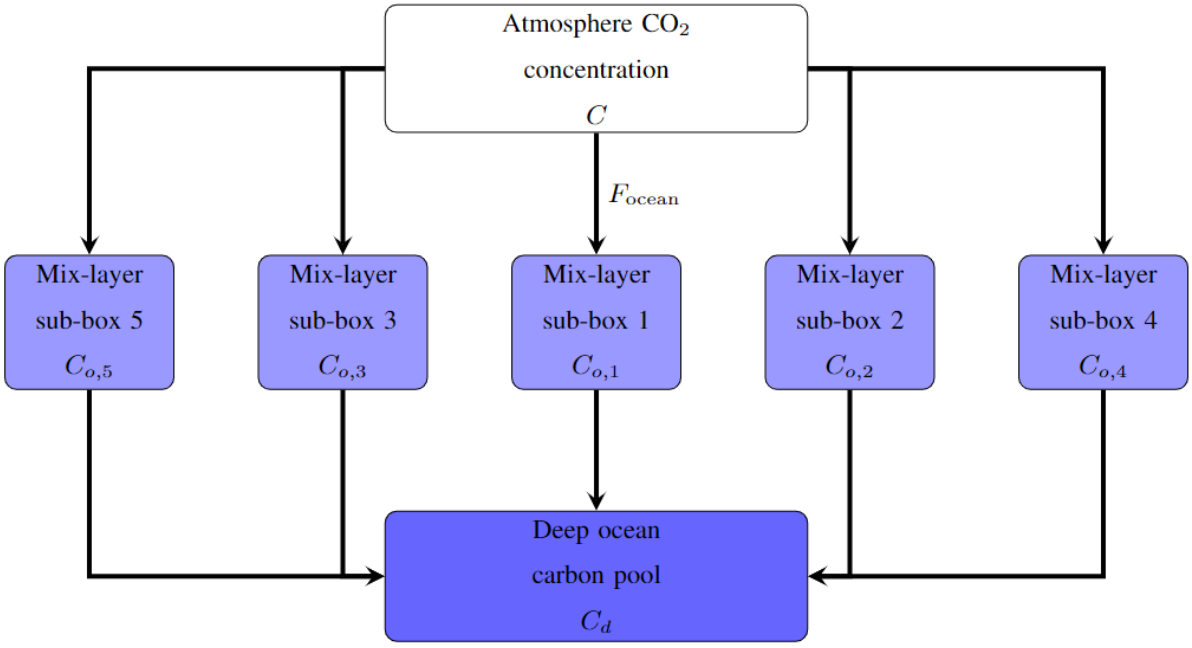

Figure 4. The ocean sink model in Pathfinder follows the structure of the mixed-layer pulse response function introduced by Joos et al. (1996). The mix-layer is represented through five subpools which each has a different timescale for transport to the deep ocean carbon pool

3.4.5 Land carbon

Parameters related to the passive soil carbon pool are taken from He et al. (2016, Table S5): ν_{rh3} is structural, while α_{pass} is not. All the prior distribution of the parameters related to the preindustrial steady-state of the land carbon (i.e. F_{npp0}, ν_{fire}, ν_{harv}, ν_{mort}, ν_{stab}, ν_{rh1} and ν_{cs}) are derived from 11 TRENDYv7 models (Sitch et al., 2015; Le Quéré et al., 2018), exactly as for OSCAR v3.1 (Gasser et al., 2020) except that all biomes and regions are lumped together. The prior distribution of the remaining parameters are derived from 12 CMIP6 models that contributed to C4MIP (Arora et al., 2020). Using the models' outputs for the *1pctCO2*, *1pctCO2-rad* and *1pctCO2-bgc* experiments, we calibrated β_{npp}, α_{npp} and γ_{npp} through equation 24, β_{fire} and γ_{fire} through equation 28, and β_{rh} and γ_{rh} through equation 37. Results of this calibration on the individual CMIP6 models is shown in Figure B3, B4 and B5.

3.4.6 Permafrost carbon

The permafrost module's parameters are recalibrated using the same algorithm as used by Gasser et al. (2018), but adapted to the global formulation of Pathfinder. First, the algorithm is run once to obtain a set of parameters reproducing the behavior of the global average of five permafrost models (with data from UVic (MacDougall, 2021) added to the four original models). This gives the values of the structural parameters (i.e. α_{lst}, γ_{rt1}, γ_{rt2}, κ_{rt}, a_{min}, all $\alpha_{\text{th},j}$, all $\tau_{\text{th},j}$, ν_{thaw} and ν_{froz}). Second,

the algorithm is run five additional times, for each of the five permafrost models separately, with the structural parameters established in the first step, to obtain prior distributions of the remaining parameters (i.e. $C_{\mathrm{fr}0}$, κ_a, γ_a and $\kappa_{\tau_{\mathrm{th}}}$).

3.4.7 Atmospheric CO2

The conversion factor α_C is a structural parameter whose value is taken from the latest GCBs (e.g. Le Quéré et al., 2018). The prior distribution of preindustrial CO2 concentration (C_{pi}) is taken from the AR6 (Gulev et al., 2021, Section 2.2.3.2.1), assuming the difference between minimum and maximum over the 0–1850 period is representative of the 90% uncertainty range.

3.4.8 Historical CO2 and GMST

The structural X_μ and X_σ time series are taken from the latest observations, as follows. T_μ and T_σ are taken as the average and standard deviation of 5 observational GMST data sets: HadCRUT5 (Morice et al., 2021), Berkeley Earth (Rohde et al., 2013; Rohde, 2013), GISTEMP (Hansen et al., 2010), NOAAGlobalTemp (Huang et al., 2020), and JMA. We use the 1850–1900 period to define our preindustrial baseline, and GMST change is assumed to be zero before the earliest date available in each data set. Regarding atmospheric CO2, C_μ is taken as the global value reported by NOAA/ESRL (Tans and Keeling, 2010) and C_σ as a constant ± 1 ppm uncertainty, for 1980 onward (this uncertainty is arbitrarily taken higher than the actual uncertainty estimated through instrumental measures to increase freedom in the calibration). Before that period, C_μ comes from the IPCC AR6 (Dentener et al., 2021, Table AIII.1a), and C_σ is linearly interpolated backwards from the instrumental uncertainty in 1980 to the preindustrial one (Gulev et al., 2021) in 1750. Finally, the prior distribution of ρ_X is set to Uniform over $[0, 1]$, that of $\tilde{\sigma}_X$ is a unit Normal distribution, and that of ϵ_X is set arbitrarily to a Half-Normal of parameter 0.05 K for GMST and 0.5 ppm for CO2.

3.5 Results (posterior distributions)

The following subsections discuss the adjustments between the prior and posterior parameters that are the results of the Bayesian calibration, as well as the matching of the constraints.These sections constantly refer to Figure 5 that shows the prior and posterior distributions of the model's parameters, Figure 6 that shows those of the constrained variables, and Figure 7 that displays the correlation matrix of the posterior parameters. (There is no correlation among the prior parameters.) Prior and posterior values of the parameters can also be retrieved from Table B6.

3.5.1 Climate system

Our climate-related constraints lead to adjusting all the parameters of the climate module. As explained in Section 3.4.8, the constraints for present-day GMST change and its derivative are met by construction.

The ECS ($T_{2\times}$) is the parameter with the strongest adjustment, since it is directly constrained. Its precise value is discussed hereafter in Section 4.2, but we note that it is unsurprisingly decreased, as the CMIP6 model ensemble tends to overestimate the

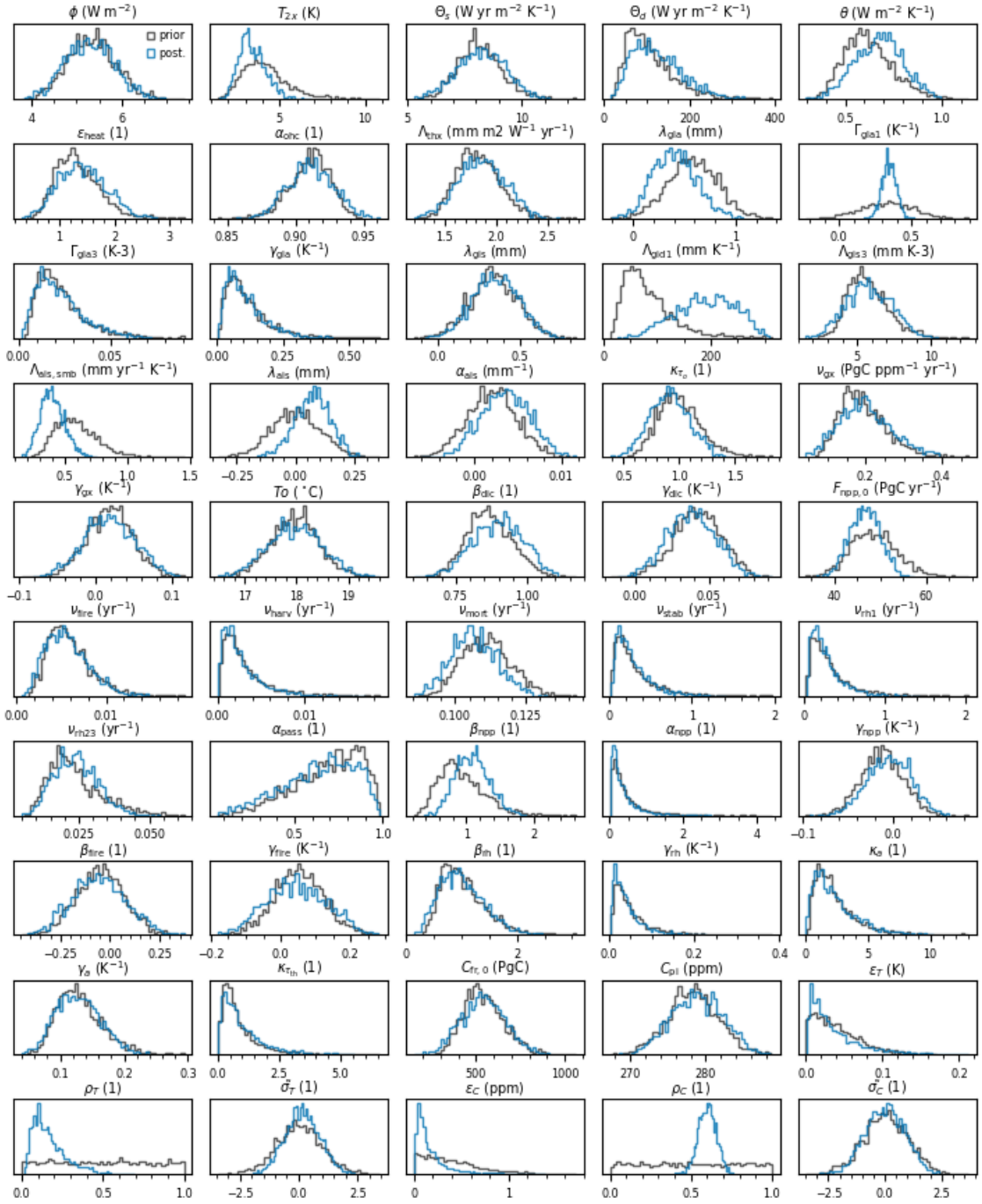

Figure 5. Parameters distributions before (black lines) and after (blue lines) the Bayesian calibration. Parameters are noted under their text notation, and Tables B3 and B4 provide the corresponding notation in code.

ECS compared to the IPCC assessed value. Consequently, our posterior $\mathrm{logit}(\mathrm{ff})$ matches well the constraint. The adjustment of the ECS significantly reduces the gap between our posterior distribution of the non-CO2 ERF and its constraint, although the posterior central value remains 41% lower (but well within uncertainty range).

Among the dynamic parameters that are adjusted, we note that the deep ocean heat capacity Θ_d is somewhat increased compared to the prior, and the heat exchange coefficient θ is also increased. These dynamic parameters are likely adjusted through our OHU constraint that is corrected in the posterior so the difference in the central values is lowered from 22% to 14%, which remains well within the uncertainty range.

In addition, a number of weak but physically meaningful correlations across the climate module's parameters are found, such as a positive correlation between $T_{2\times}$ and ϵ_{heat} (see e.g. Geoffroy et al., 2013a), a positive correlation between $T_{2\times}$ and Θ_d (that tends to exclude configuration that would warm fast and high), and a negative correlation between $T_{2\times}$ and ϕ (to match the GMST and ERF constraints together).

3.5.2 Carbon cycle

Similarly to GMST, the posterior distribution of atmospheric CO2 concentration matches the constraint by construction. Its derivative, however, is (slightly overly) corrected to match the GCB estimate. Global anthropogenic CO2 emissions are significantly increased to get closer to the GCB constraint, but their central value remains 9% too low. Since these emissions are determined through mass balance and the atmospheric CO2 matches observations, this implies that the total carbon sinks (i.e. F_{land} + F_{ocean}) must be weaker.

This is confirmed for the ocean sink, as the posterior central value of F_{ocean} is 8% lower than the constraint, but still noticeably corrected if compared to the prior. This correction is explained by small adjustments in some parameters of the ocean carbon module. The mixed layer depth is slightly increased through β_{dic}. All other parameters remain mostly unaffected by the calibration, and only minor correlations are found. These results, along with the fact that our prior distribution spans only about half of the constraint's distribution, suggest that there is a structural limitation in our ocean carbon module that warrants further investigation.

It is also confirmed that the posterior land sink is weaker than the constraint, by 15% for the central value, which is nevertheless a significant reduction of the prior gap of 34%. To explain this adjustment, we observe that the CO2-fertilization sensitivities (β_{npp} and γ_{npp}) are adjusted upwards. However our constraint on present-day NPP prevents these adjustments from being too important, as the posterior distribution of this variable is similar to the prior and its central value remains 8–9% higher than its constraint. An increased preindustrial NPP mechanically leads to an increase in preindustrial carbon pools, but these require further adjustments of the land carbon turnover rates, and most notably the mortality rate ν_{mort} and the passive carbon fraction α_{pass}, to better match their constraints (of which the one on total soil carbon is perfectly met).

The land carbon module exhibits significant correlations among posterior parameters. This is likely a consequence of all the constraints combined as they dictate both the preindustrial steady-state of the module and it's transient response over the historical period. Eliminated configurations are those, for instance, that would show high initial carbon pools that are very

Variable	Period	Method	Prior	Posterior	Constraints	Unit
E_{CO2}	2011-2020	Mean	9.1 ± 1.3	10.0 ± 0.7	11.0 ± 0.9	PgC yr^{-1}
$\frac{dC}{ct}$	2011-2020	Mean	2.41 ± 0.06	2.40 ± 0.01	2.40 ± 0.01	ppm yr^{-1}
F_{land}	1960-2020	Sum	95 ± 52	123 ± 26	145 ± 35	PgC
F_{ocean}	1960-2020	Sum	89± 12	97 ± 13	105 ± 20	PgC
C_v	1750	Mean	407 ± 54	407 ± 37	450 ± 50	PgC
C_s	1750	Mean	1181 ± 735	1086 ± 284	1088 ± 249	PgC
F_{NPP}	1998-2002	Mean	60.0 ± 7.9	59.5 ± 3.9	55.0 ± 5.0	PgC yr^{-1}
C	2012-2021	Mean	403.6 ± 0.3	403.6 ± 0.1	401.2 ± 0.1	ppm
R_x	2010-2019	Mean	0.01 ± 0.47	0.33 ± 0.37	0.56± 0.53	W m^{-2}
T	2001-2020	Mean	0.96 ± 0.08	0.97 ± 0.06	1.00 ± 0.07	K
$\frac{dT}{dt}$	2000-2019	Mean	0.028 ± 0.003	0.028 ± 0.002	0.029 ± 0.002	K yr^{-1}
$\frac{dU_{\mathrm{ohc}}}{dt}$	2006-2018	Mean	0.56 ± 0.10	0.62 ± 0.09	0.72 ± 0.17	W m^{-2}
$\frac{dH_{\mathrm{thx}}}{dt}$	2006-2018	Mean	1.02 ± 0.22	1.14 ± 0.21	1.39 ± 0.40	mm yr^{-1}
$\frac{dH_{\mathrm{gla}}}{dt}$	2006-2018	Mean	0.63 ± 0.24	0.62 ± 0.04	0.62 ± 0.03	mm yr^{-1}
$\frac{dH_{\mathrm{ais}}}{dt}$	2006-2018	Mean	-0.02 ± 0.23	0.30 ± 0.10	0.37 ± 0.08	mm yr^{-1}
$\frac{dH_{\mathrm{gis}}}{dt}$	2006-2018	Mean	0.36 ± 0.12	0.57 ± 0.10	0.63 ± 0.07	mm yr^{-1}
H_{tot}	1901-1990	Difference	72 ± 17	83 ± 10	89 ± 32	mm
H_{lia}	1750	Mean	45 ± 17	45 ± 11	30 ± 13	mm
$\mathrm{logit(ff)}$	1750	Mean	1.69 ± 0.38	1.47 ± 0.28	1.38 ± 0.37	1

Table 1. Constrained variables in Pathfinder, with values before and after calibration. Variables are noted under their text notation, and Tables B1 and B2 provide the corresponding notation in code. The uncertainty correspond to the 1 σ uncertainty range.

sensitive to climate change (as these would lead to a very weak land sink), or that would exhibit a weak CO2-fertilization effect associated with a fast turnover time (that would also lead to a weak sink).

3.5.3 Sea level rise

The prior parameters of the SLR module are the least informed of our Bayesian setup. The model initially underestimates the thermal expansion, as well as the GIS and AIS SLR rates. The calibration brings the posterior distributions closer to their respective constraints but it always remain in the lower end of the uncertainty range. The correction is done by adjusting many of the module's parameters (most notably Λ_{gis1}, $\Lambda_{\mathrm{ais,smb}}$, λ_{ais} or λ_{gla}), and by finding strong correlations among them (thus excluding physically unrealistic combinations).

The historical SLR is markedly corrected by the constraint: from a 19% gap between the central values of the constraint and the prior estimate, to only 7% after calibration. Here, we also note that the sum of individual contributions to historical SLR reported in AR6 do not match that total SLR (Fox-Kemper et al., 2021, Table 9.5), which likely has some impact on

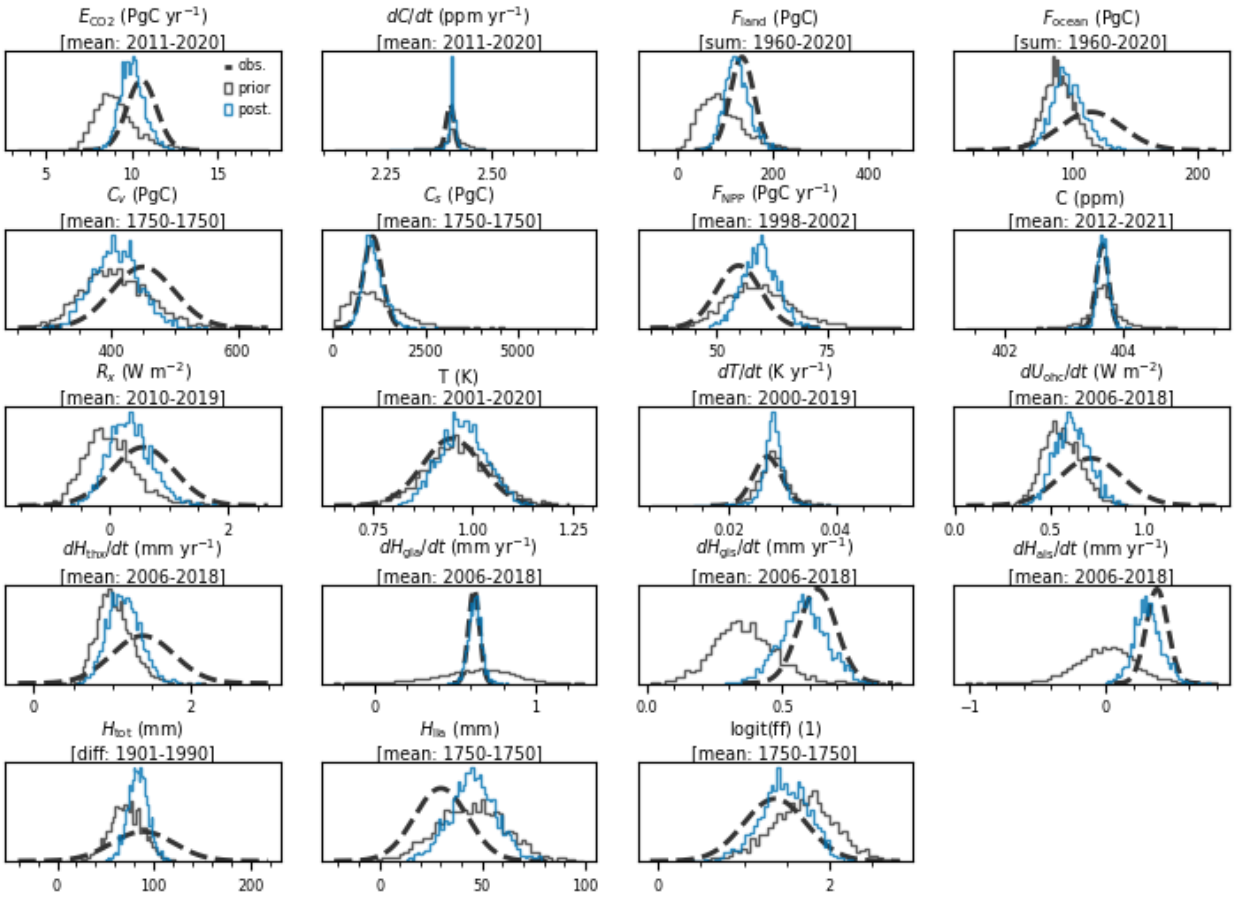

Figure 6. Distributions of the constrained variables. Dashed lines give the distributions used to constrain. Black lines give the distribution before calibration while blue lines give the distribution posterior to calibration. Under a variable's name, we give the period over which the constraint is estimated, and the data processing method: mean over the period, difference between last and first year, or sum of all the years over the period. (1750 is the preindustrial.) Variables are noted under their text notation, and Tables B1 and B2 provide the corresponding notation in code.

the consistency between our constraints. Finally, although the LIA relaxation contribution is not altered by the calibration, as its central value remains 50% too high, it is the likely source of the strong correlations found among the parameters of this module, because it straightforwardly links the individual SLR contributions together.

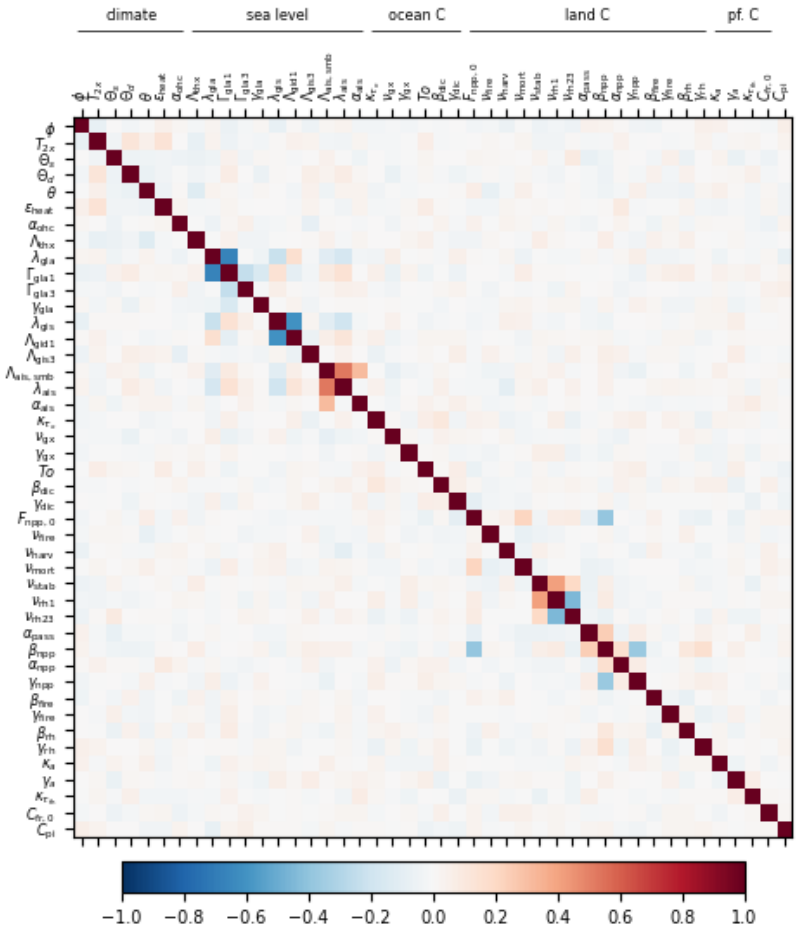

Figure 7. Correlation matrix of Pathfinder's parameters after the Bayesian calibration. Parameters are classified according to the equations they are related to: climate system, sea level, ocean carbon, land carbon and permafrost carbon. Parameters are noted under their text notation, and Tables B3 and B4 provide the corresponding notation in code.

4 Model diagnosis

4.1 Historical period

Because in the Bayesian setup we do not use annual time series of observations as constraints, the posterior distributions given in Figure 6 do not inform on the whole dynamic of the model over the historical period. To further diagnose the model's behavior, Figure 8 gives the time series from 1900 to 2021 of six key variables. GMST and atmospheric CO2 match very well the historical observations, by construction of these input time series. The non-CO_2 ERF exhibits a very high variability, owing to our temperature-driven setup and the natural variability in the GMST input. Beyond that, the ERF time series is consistent with the AR6 estimates (Smith et al., 2021), albeit somewhat lower on average in the recent past, as seen with the posterior distribution. Consistently with the interpretation of carbon cycle variables in the calibration results, anthropogenic CO2 emissions, and the ocean and land carbon sinks are slightly underestimated compared to the GCB estimates (Friedlingstein et al., 2022). Several reasons could explain this discrepancy, from the lack of land use change in Pathfinder to the inconsistency of the GCB figures (that do not close the budget, while ours do). Nevertheless, the interest of the calibration is clearly illustrated, as the posterior uncertainty range covers observations much better than the prior one.

4.2 Idealized simulations

To complete the diagnosis of our model with common metrics used with climate and carbon models, we ran a set of standard idealized experiments, corresponding to the CMIP6 *abrupt-2xCO2*, *1pctCO2*, *1pctCO2-bgc* and *1pctCO2-rad*. A summary of these metrics' values is given in Table 2, and the resulting time series are shown in Figure 9.

The *abrupt-2xCO2* experiment sees an abrupt doubling of atmospheric CO2, and it is used to diagnose the model's ECS that is defined as the equilibrium temperature for a doubling of the preindustrial atmospheric concentration of CO2 (we acknowledge that it is superfluous with this version of Pathfinder since it is also a parameter). Using the GMST anomaly at the end of 1500 years of this experiment leads to an unconstrained estimate of ECS of 4.1 ± 1.3 K and a constrained estimate of 3.3 ± 0.7 K. Consistently, the latter value is between the ECS value extracted from CMIP6 models (Meehl et al., 2020) that is higher (3.7 ± 1.1 K) and the final value assessed in the AR6 that is lower (3.0 K, with a 67% confidence interval between 2.5 and 4.0 K).

Using the *1pctCO2* experiment that sees a 1% yearly increase in atmospheric CO2, we can estimate the model's transient climate response (TCR) that is defined as the GMST change after 70 years, when atmospheric concentration CO2 has just doubled. The CMIP6 models have a TCR of 2.0 ± 0.4 K (Meehl et al., 2020). Pathfinder's unconstrained value is higher, at 2.2 ± 0.5 K, while the constrained one goes down to 1.9 ± 0.3 K. If we divide the TCR by the cumulative anthropogenic CO2 emissions compatible with the atmospheric CO2 increase in this experiment, we obtain an estimate of the transient climate response to emissions (TCRE). Similarly to the TCR, it is higher in the unconstrained ensemble and lower in the constrained one, when compared to CMIP6 models (Arora et al., 2020). Both downward adjustments of the TCR and TCRE are consistent with that of ECS, with the posterior TCRE matching very well the AR6 assessed range (Canadell et al., 2021).

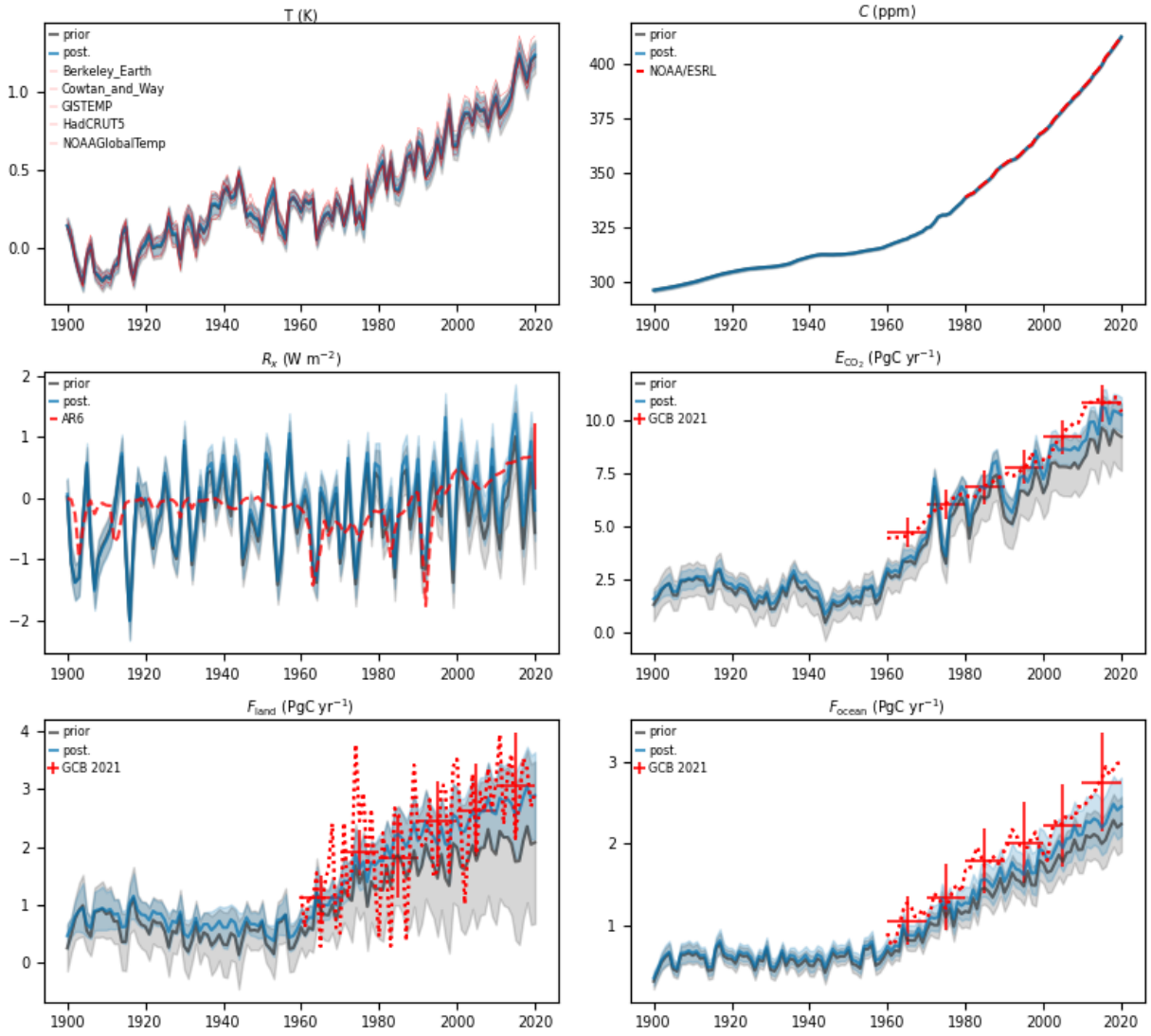

Figure 8. Historical time series of key variables from Pathfinder. Red lines are observations, black lines are the model's outputs before calibration, and blue lines are the same after calibration. Shaded areas and vertical bars correspond to the 1σ uncertainty range. Temperature observations are taken from HadCRUT5 (Morice et al., 2021), Cowtan and Way (2014), Berkeley Earth (Rohde et al., 2013; Rohde, 2013), GISTEMP (Hansen et al., 2010), and NOAA/MLOST (Vose et al., 2012). Other sources are NOAA/ESRL (Tans and Keeling, 2010), GCB 2021 (Friedlingstein et al., 2022), and AR6 (Smith et al., 2021).

To look more closely at the carbon cycle, we perform two variants of the latter experiment: in *1pctCO2-rad*, atmospheric CO2 only has a radiative effect, as it is kept at preindustrial level for the carbon cycle; whereas in *1pctCO2-bgc*, atmospheric CO2 only has a biogeochemical effect, as the climate system sees only preindustrial level. These three experiments are used to calculate the carbon-concentration (β) and carbon-climate (γ) feedback metrics that measure the carbon sinks' sensitivities to changes in atmospheric CO2 and GMST, respectively. We apply the same method as Arora et al. (2020) to calculate these, which leads to metrics at the time of CO2 doubling that are in line with CMIP6 models (Arora et al., 2020). As both carbon sinks were adjusted upwards by the Bayesian calibration, the constraints logically increased both β_{ocean} and β_{land}, to values fairly close to those of the complex models. The γ_{ocean} is not affected by the calibration, and remains 45% too low, which again suggests a structural limitation in our formulation of the ocean sink. This is however compensated during calibration by the γ_{land} being 26% higher than in complex models.

$2\times$ CO_2	Pathfinder unconstrained	Pathfinder constrained	CMIP6	AR6
ECS (K)	4.1 ± 1.3	3.3 ± 0.7	3.7 ± 1.1	3.0 (2.0, 4.5)
TCR (K)	2.2 ± 0.5	1.9 ± 0.3	2.0 ± 0.4	1.8 (1.4, 2.2)
TCRE (K EgC^{-1})	2.20 ± 0.63	1.65 ± 0.32	1.77 ± 0.37	1.65 (1.0, 2.3)
β_{ocean} (PgC ppm^{-1})	0.81 ± 0.10	0.87 ± 0.11	0.91 ± 0.09	
γ_{ocean} (PgC K^{-1})	-12.9 ± 5.4	-12.5 ± 6.0	-8.6 ± 2.9	
β_{land} (PgC ppm^{-1})	1.05 ± 0.5	1.26 ± 0.30	1.22 ± 0.40	
γ_{land} (PgC K^{-1})	-33.2 ± 26.6	-25.3 ± 24.2	-34.1 ± 38.4	

Table 2. Diagnostics of climate and carbon-cycle responses in Pathfinder before and after Bayesian calibration. Comparison with AR6 (Forster et al., 2021; Canadell et al., 2021) and CMIP6 data (Arora et al., 2020; Meehl et al., 2020) is shown. For AR6 data we give the median and the 90% confidence interval while for every other values we give the mean $\pm$ 1 σ

4.3 Scenarios

To further validate Pathfinder, we run the five SSP scenarios (Riahi et al., 2017) for which climate and carbon cycle projections were reported by a large-enough number of models in the AR6 (namely, *ssp119*, *ssp126*, *ssp245*, *ssp370* and *ssp585*). These simulations are run with prescribed CO2 concentration and non-CO2 ERF (the latter is taken from Smith et al. (2021)). Time series of GMST and cumulative land and ocean sinks are shown on Figure 9. Table 3 shows a comparison of the projected changes in GMST to the CMIP6 estimates (Lee et al., 2021, Table 4.2), and of carbon pools to Liddicoat et al. (2021) (since this was not directly reported in the AR6).

Be it on short-, mid- or long-term, Pathfinder's projections of GMST are very much in line with the one assessed by the IPCC in the AR6 based on multiple lines of evidence (Lee et al., 2021, Table 4.5). The only significant difference is a smaller uncertainty range in our projections for the longer-term periods. Although this is the result of the efficiency of the Bayesian

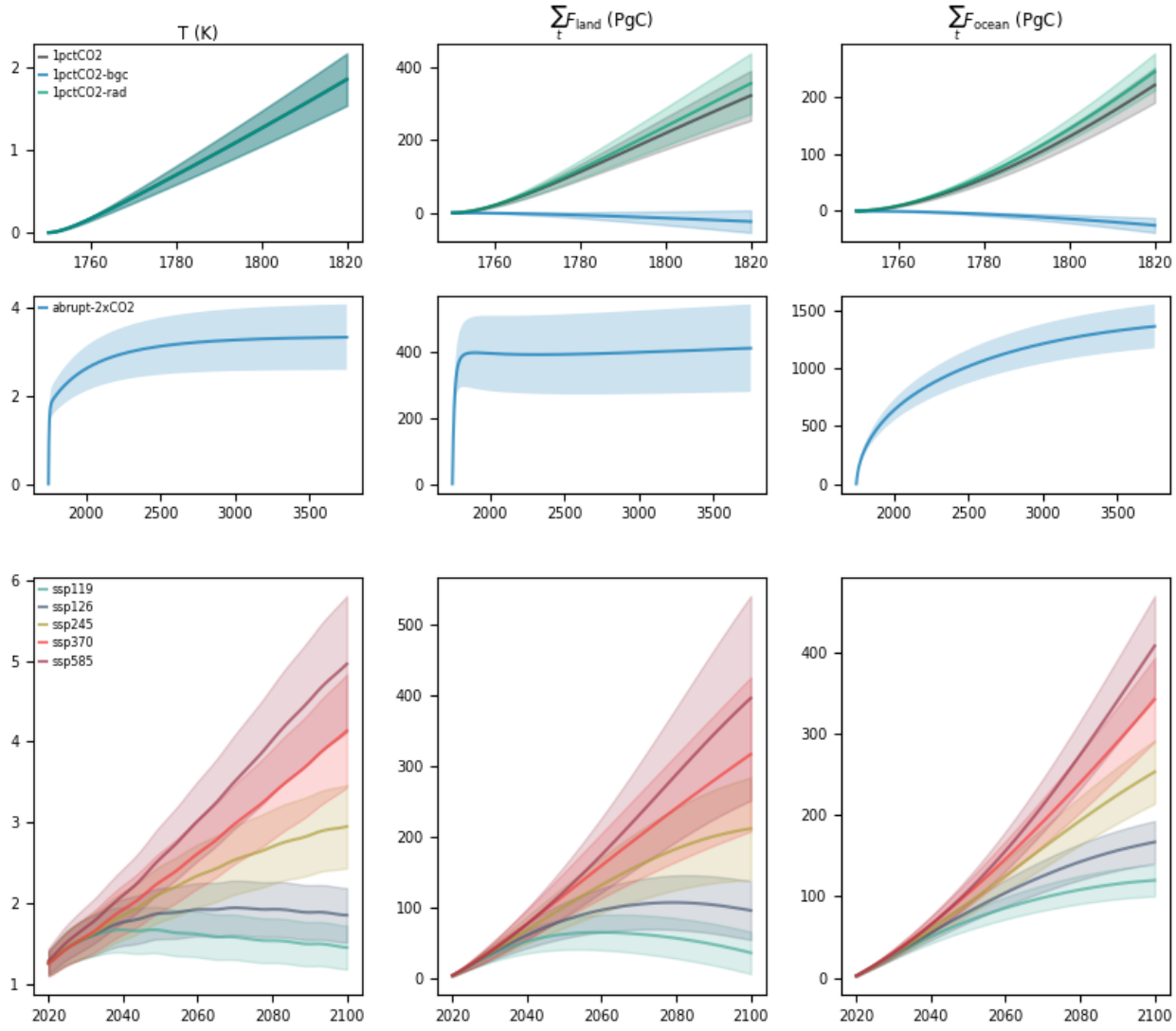

Figure 9. Time series of GMST change, integrated land carbon uptake and integrated ocean carbon uptake for idealized experiments (*abrupt-2xCO2*, *1pctCO2*, *1pctCO2-bgc* and *1pctCO2-rad*), and projections according to SSP scenarios in Pathfinder. Shaded areas give the 1σ uncertainty range.

calibration, one might wonder whether the climate module is over-constrained (or equivalently, too limited in its number of parameters).

The ocean carbon storage appears overestimated by 5% to 20% by Pathfinder across SSP scenarios. This is consistent with the upward adjustment of the ocean carbon sink stemming from our Bayesian calibration. To compare the land carbon storage with CMIP6 models, because our land carbon module does not include land use change processes, we correct the value reported by complex models by the cumulative land use change emissions of each scenario (Riahi et al., 2017; Gidden et al., 2019). While the land carbon storage of Pathfinder is well in line under *ssp126* (a scenario consistent with the 2 °C target), it is underestimated in *ssp119* (consistent with the 1.5 °C target), and increasingly overestimated in higher warming scenarios. A likely explanation is that the climate-carbon feedback on land is underestimated in Pathfinder, as suggested by the γ metric seen in Section 4.2. Alternatively (or concurrently), the absence of loss of sink capacity caused by land cover change (Gasser and Ciais, 2013; Gasser et al., 2020) can explain the overestimation of the land sink under high CO2. The Pathfinder model's estimates of both sinks remain nonetheless well within the CMIP6 models' uncertainty ranges.

Our SLR emulator gives estimates (Table 4) that are always on the lower of the range reported in the AR6 (Fox-Kemper et al., 2021, Table 9.9). This can be explained by the fact that our individual SLR rate estimates are on the lower end of their respective constraints (see Section 3.5.3). This discrepancy also highlights potential structural limitations in the SLR module (e.g. too few separate contributions), and the difficulty of calibrating the module given the short time period of data available, both from complex models (that cover the 21st century only) and observations, compared to the long time scale of the SLR processes. Nevertheless, our estimates remain within uncertainty range of the IPCC assessment, especially as we do not account for contribution from land water storage that causes an additional 0.03 [0.01, 0.04] m of SLR in all scenarios in 2100 (Fox-Kemper et al., 2021).

5 Concluding remarks

In this paper, we have presented the Pathfinder model: a simple global carbon-climate model with selected impact variables, carefully designed to balance accuracy of representation and simplicity of formulation, and calibrated through Bayesian inference on the latest data from Earth system models and observations. Pathfinder has been shown to perform very well in comparison to complex models, although there remains room for further improvement of the model and its calibration setup. We identify four main avenues to improve the model.

First, some parts of the model may well lean too much on the complexity side of the simplicity–accuracy balance we aimed to strike, owing to the creation process of Pathfinder that mostly compiled existing formulations. Future development should therefore strive to reduce complexity wherever possible. The ocean carbon sub-pools and perhaps the land carbon pools are potential leads in this respect.

Second, the ocean carbon module alone appears to be limited by its structure inherited from a 25-year-old (yet seminal) article (Joos et al., 1996). Although it is undoubtedly a significant undertaking, developing an alternative formulation of the

Experiment	Model	GMST (K)	GMST (K)	GMST (K)	Ocean Carbon Storage (PgC)	Land Carbon Storage (PgC)
		2021–2040	2041–2060	2081–2100	2015–2100	2015–2100
ssp119	Pathfinder	1.5 (1.3, 1.8)	1.6 (1.4, 1.9)	1.5 (1.2, 1.7)	132 ± 21	49 ± 33
ssp119	AR6 or CMIP6	1.5 (1.2, 1.7)	1.6 (1.2, 2.0)	1.4 (1.0, 1.8)	111 ± 11	73 ± 33
ssp126	Pathfinder	1.5 (1.3, 1.8)	1.8 (1.6, 2.1)	1.9 (1.6, 2.2)	179 ± 28	109 ± 45
ssp126	AR6 or CMIP6	1.5 (1.2, 1.8)	1.7 (1.3, 2.2)	1.8 (1.3, 2.4)	162 ± 8	120 ± 50
ssp245	Pathfinder	1.6 (1.4, 1.8)	2.1 (1.8, 2.4)	2.8 (2.4, 3.3)	265 ± 41	225 ± 76
ssp245	AR6 or CMIP6	1.5 (1.2, 1.8)	2.0 (1.6, 2.5)	2.7 (2.1, 3.5)	252 ± 11	178 ± 76
ssp370	Pathfinder	1.6 (1.4, 1.8)	2.2 (1.9, 2.6)	3.7 (3.2, 4.3)	354 ± 53	330 ± 112
ssp370	AR6 or CMIP6	1.5 (1.2, 1.8)	2.1 (1.7, 2.6)	3.6 (2.8, 4.6)	338 ± 15	269 ± 124
ssp585	Pathfinder	1.7 (1.5, 1.9)	2.5 (2.2, 2.9)	4.4 (3.8, 5.2)	420 ± 63	409 ± 148
ssp585	AR6 or CMIP6	1.6 (1.3, 1.9)	2.4 (1.9, 3.0)	4.4 (3.3, 5.7)	398 ± 17	311 ± 162

Table 3. Comparison of SSP scenarios for GMST change projections (w.r.t. 1850–1900) to AR6 (Lee et al., 2021, Table 4.5), and for ocean and land carbon storage projections to CMIP6 (Liddicoat et al., 2021). Land carbon storage projections were corrected using the land use change emissions data from SSPs (Riahi et al., 2017; Gidden et al., 2019). For GMST data we give the median and the 90% confidence interval while for every other values we give the mean $\pm$ 1 σ

ocean carbon dynamic, calibrated on state-of-the-art ocean models and properly connected to ocean pH and the ocean of the climate module, would benefit more than just the SCM community.

Third, integration of land use and land cover change in such a model appears warranted, despite the difficulty of doing so in a physically sensible yet simple manner. Given our expertise with the OSCAR model and its bookkeeping module (Gasser et al., 2020), we are confident that this can be done, although it will demand extra care to keep the model compatible with the IAMs it is also meant to be linked to.

Fourth, the Bayesian setup can be extended, notably by including more time periods for the existing constraints, but also by introducing and constraining entirely new variables such as isotopic ratios (Hellevang and Aagaard, 2015) or inter-hemispheric gradients (Ciais et al., 2019); although a balance must be struck with respect to the calibration's computation time. Here, we caution against including complex models' results as constraints in the Bayesian calibration, as was done for the IPCC AR6 (Smith et al., 2021; Nicholls et al., 2021), as it goes against the philosophy of Pathfinder to use complex models' results as prior information only.

Experiment	Model	SLR (m) 2050	SLR (m) 2100	SLR rate (mm yr^{-1}) 2040–2060	SLR rate (mm yr^{-1}) 2080–2100
ssp119	Pathfinder	0.15 (0.13, 0.18)	0.30 (0.25, 0.36)	3.5 (2.9, 4.2)	2.7 (2.2, 3.4)
ssp119	AR6	0.18 (0.15, 0.23)	0.38 (0.28, 0.55)	4.1 (2.8, 6.0)	4.2 (2.4, 6.6)
ssp126	Pathfinder	0.16 (0.14, 0.19)	0.35 (0.30, 0.43)	4.1 (3.5, 5.0)	3.6 (2.9, 4.5)
ssp126	AR6	0.19 (0.16, 0.25)	0.44 (0.32, 0.62)	4.8 (3.5, 6.8)	5.2 (3.2, 8.0)
ssp245	Pathfinder	0.17 (0.15, 0.20)	0.46 (0.39, 0.56)	5.0 (4.2, 6.0)	6.2 (5.1, 8.0)
ssp245	AR6	0.20 (0.17, 0.26)	0.56 (0.44, 0.76)	5.8 (4.4, 8.0)	7.7 (5.2, 11.6)
ssp370	Pathfinder	0.18 (0.15, 0.21)	0.56 (0.47, 0.69)	5.5 (4.7, 6.7)	9.1 (7.4, 11.7)
ssp370	AR6	0.22 (0.18, 0.27)	0.68 (0.55, 0.90)	6.4 (5.0, 8.7)	10.4 (7.4, 14.8)
ssp585	Pathfinder	0.19 (0.17, 0.23)	0.67 (0.56, 0.82)	6.4 (5.4, 7.8)	11.4 (9.1, 15.0)
ssp585	AR6	0.23 (0.20, 0.29)	0.77 (0.63, 1.01)	7.2 (5.6, 9.7)	12.1 (8.6, 17.6)

Table 4. Comparison of SSP scenarios between Pathfinder and AR6 for SLR (w.r.t. 1995–2014) and SLR speed projections (Fox-Kemper et al., 2021, Table 9.9). We give the median value and the 90% confidence interval in parentheses

Fifth, although our model is restricted to CO2 by design because of how IAMs like DICE (Nordhaus, 2017) are also limited to CO2 emissions, we can imagine many reasons why one would want to add non-CO2 climate forcers into Pathfinder. We would suggest doing so by following the model's philosophy: that is, by taking existing reduced-complexity formulations such as something between FaIR (Leach et al., 2020) and OSCAR (Gasser et al., 2017), and adding the new parameters into the Bayesian setup with the relevant observational constraints.

In spite of these few shortcomings and potential development leads, Pathfinder v1.0.1 is a powerful tool that fits perfectly the niche it has been created for. We will further demonstrate the strengths and flexibility of Pathfinder in other publications. Meanwhile, we invite the community to seize this open source model, and use it in any study that could benefit from a simple, fast and accurate carbon-climate model, aligned with the latest climate science.

References

Japan Meteorological Agency, Global Average Surface Temperature Anomalies, https://ds.data.jma.go.jp/tcc/tcc/products/gwp/temp/ann_wld.html, accessed: 2022-07-28.

Armour, K. C.: Energy budget constraints on climate sensitivity in light of inconstant climate feedbacks, Nature Climate Change, 7, 331–335, 2017.

Arora, V. K., Katavouta, A., Williams, R. G., Jones, C. D., Brovkin, V., Friedlingstein, P., Schwinger, J., Bopp, L., Boucher, O., Cadule, P., et al.: Carbon–concentration and carbon–climate feedbacks in CMIP6 models and their comparison to CMIP5 models, Biogeosciences, 17, 4173–4222, 2020.

Bayes, T.: LII. An essay towards solving a problem in the doctrine of chances. By the late Rev. Mr. Bayes, FRS communicated by Mr. Price, in a letter to John Canton, AMFR S, Philosophical transactions of the Royal Society of London, pp. 370–418, 1763.

Bernie, D., Lowe, J., Tyrrell, T., and Legge, O.: Influence of mitigation policy on ocean acidification, Geophysical Research Letters, 37, 1–5, https://doi.org/10.1029/2010GL043181, 2010.

Blei, D. M., Kucukelbir, A., and McAuliffe, J. D.: Variational inference: A review for statisticians, Journal of the American statistical Association, 112, 859–877, 2017.

Bossy, T., Gasser, T., and Ciais, P.: Pathfinder v1. 0: a Bayesian-inferred simple carbon-climate model to explore climate change scenarios, EGUsphere, pp. 1–52, 2022.

Canadell, J. G., Monteiro, P. M. S., Costa, M. H., Cotrim da Cunha, L., Cox, P. M., Eliseev, A. V., Henson, S., Ishii, M., Jaccard, S., Koven, C., Lohila, A., Patra, P. K., Piao, S., Rogelj, J., Syampungani, S., Zaehle, S., and Zickfeld, K.: Global Carbon and other Biogeochemical Cycles and Feedbacks, Climate Change 2021: The Physical Science Basis. Contribution of Working Group I to the Sixth Assessment Report of the Intergovernmental Panel on Climate Change, 2021.

Church, J. A., Clark, P. U., Cazenave, A., Gregory, J. M., Jevrejeva, S., Levermann, A., Merrifield, M. A., Milne, G. A., Nerem, R. S., Nunn, P. D., et al.: Sea level change, Tech. rep., PM Cambridge University Press, 2013.

Ciais, P., Sabine, C., Bala, G., Bopp, L., Brovkin, V., Canadell, J., Chhabra, A., DeFries, R., Galloway, J., Heimann, M., Jones, C., Le Quéré, C., Myneni, R., Piao, S., and Thornton, P.: AR5-Working Group 1, Chapter 6: Carbon and Other Biogeochemical Cycles 6 - Contribution of Working Group I, Climate Change 2013: The Physical Science Basis. Contribution of Working Group I to the Fifth Assessment Report of the Intergovernmental Panel on Climate Change, 2013.

Ciais, P., Tan, J., Wang, X., Roedenbeck, C., Chevallier, F., Piao, S.-L., Moriarty, R., Broquet, G., Le Quéré, C., Canadell, J., et al.: Five decades of northern land carbon uptake revealed by the interhemispheric CO2 gradient, Nature, 568, 221–225, 2019.

Cowtan, K. and Way, R. G.: Coverage bias in the HadCRUT4 temperature series and its impact on recent temperature trends, Quarterly Journal of the Royal Meteorological Society, 140, 1935–1944, 2014.

Dentener, F. J., Hall, B., and Smith, C.: Annex III: Tables of historical and projected well-mixed greenhouse gas mixing ratios and effective radiative forcing of all climate forcers, Climate Change 2021: The Physical Science Basis. Contribution of Working Group I to the Sixth Assessment Report of the Intergovernmental Panel on Climate Change, 2021.

Edwards, T. L., Nowicki, S., Marzeion, B., Hock, R., Goelzer, H., Seroussi, H., Jourdain, N. C., Slater, D. A., Turner, F. E., Smith, C. J., et al.: Projected land ice contributions to twenty-first-century sea level rise, Nature, 593, 74–82, 2021.

Fornberg, B.: Generation of finite difference formulas on arbitrarily spaced grids, Mathematics of computation, 51, 699–706, 1988.

Forster, P., Storelvmo, T., Armour, K., Collins, T., Dufresne, J. L., Frame, D., Lunt, D. J., Mauritsen, T., Palmer, M. D., Watanabe, M., Wild, M., and Zhang, H.: The Earth's Energy Budget, Climate Feedbacks, and Climate Sensitivity, Climate Change 2021: The Physical Science Basis. Contribution of Working Group I to the Sixth Assessment Report of the Intergovernmental Panel on Climate Change, 2021.

Fox-Kemper, B., Hewitt, H. T., Xiao, C., Aðalgeirsdóttir, G., Drijfhout, S. S., , Edwards, T. L., Golledge, N. R., Hemer, M., Kopp, R. E., Krinner, S. S., Mix, A., Notz, D., Nowicki, S., Nurhati, I. S., Ruiz, L., Sallée, J.-B., and Slangen, A. B. A., a. Y. Y.: Ocean, Cryosphere and Sea Level Change, Climate Change 2021: The Physical Science Basis. Contribution of Working Group I to the Sixth Assessment Report of the Intergovernmental Panel on Climate Change, 2021.

Friedlingstein, P., Jones, M. W., O'Sullivan, M., Andrew, R. M., Bakker, D. C., Hauck, J., Le Quéré, C., Peters, G. P., Peters, W., Pongratz, J., et al.: Global carbon budget 2021, Earth System Science Data, 14, 1917–2005, 2022.

Gasser, T.: tgasser/Pathfinder: v1.0, https://doi.org/10.5281/zenodo.7003849, 2022.

Gasser, T. and Ciais, P.: A theoretical framework for the net land-to-atmosphere CO2 flux and its implications in the definition of "emissions from land-use change", Earth System Dynamics, 4, 171–186, https://doi.org/10.5194/esd-4-171-2013, 2013.

Gasser, T., Ciais, P., Boucher, O., Quilcaille, Y., Tortora, M., Bopp, L., and Hauglustaine, D.: The compact Earth system model OSCAR v2.2: Description and first results, Geoscientific Model Development, 10, 271–319, https://doi.org/10.5194/gmd-10-271-2017, 2017.

Gasser, T., Kechiar, M., Ciais, P., Burke, E. J., Kleinen, T., Zhu, D., Huang, Y., Ekici, A., and Obersteiner, M.: Path-dependent reductions in CO 2 emission budgets caused by permafrost carbon release, Nature Geoscience, 11, 830–835, https://doi.org/10.1038/s41561-018-0227-0, 2018.

Gasser, T., Crepin, L., Quilcaille, Y., Houghton, R. A., Ciais, P., and Obersteiner, M.: Historical CO 2 emissions from land use and land cover change and their uncertainty, Biogeosciences, 17, 4075–4101, 2020.

Geoffroy, O., Saint-Martin, D., Bellon, G., Voldoire, A., Olivié, D. J., and Tytéca, S.: Transient climate response in a two-layer energy-balance model. Part II: Representation of the efficacy of deep-ocean heat uptake and validation for CMIP5 AOGCMs, Journal of Climate, 26, 1859–1876, https://doi.org/10.1175/JCLI-D-12-00196.1, 2013a.

Geoffroy, O., Saint-Martin, D., Olivié, D. J. L., Voldoire, A., Bellon, G., and Tytéca, S.: Transient Climate Response in a Two-Layer Energy-Balance Model. Part I: Analytical Solution and Parameter Calibration Using CMIP5 AOGCM Experiments, Journal of Climate, 26, 1841–1857, https://doi.org/10.1175/JCLI-D-12-00195.1, 2013b.

Gidden, M. J., Riahi, K., Smith, S. J., Fujimori, S., Luderer, G., Kriegler, E., Van Vuuren, D. P., Van Den Berg, M., Feng, L., Klein, D., Calvin, K., Doelman, J. C., Frank, S., Fricko, O., Harmsen, M., Hasegawa, T., Havlik, P., Hilaire, J., Hoesly, R., Horing, J., Popp, A., Stehfest, E., and Takahashi, K.: Global emissions pathways under different socioeconomic scenarios for use in CMIP6: A dataset of harmonized emissions trajectories through the end of the century, Geoscientific Model Development, 12, 1443–1475, https://doi.org/10.5194/gmd-12-1443-2019, 2019.

Gitz, V. and Ciais, P.: Amplifying effects of land-use change on future atmospheric CO2 levels, Global Biogeochemical Cycles, 17, 2003.

Goodwin, P., Haigh, I. D., Rohling, E. J., and Slangen, A.: A new approach to projecting 21st century sea-level changes and extremes, Earth's Future, 5, 240–253, https://doi.org/10.1002/2016EF000508, 2017.

Gulev, S. K., Thorne, P. W., Ahn, J., Dentener, F. J., Domingues, C. M., Gerland, S., Gong, D., Kaufman, D. S., Nnamchi, H. C., Quaas, J., Rivera, J. A., Sathyendranath, S., Smith, S. L., Trewin, B., von Shuckmann, K., and Vose, R.: Changing State of the Climate System, Climate Change 2021: The Physical Science Basis. Contribution of Working Group I to the Sixth Assessment Report of the Intergovernmental Panel on Climate Change, 2021.

Hansen, J., Ruedy, R., Sato, M., and Lo, K.: Global Surface Temperature Change, Review of Geophysics, 5, 1–29, https://doi.org/10.1029/2010RG000345.1.INTRODUCTION, 2010.

Harris, C. R., Millman, K. J., Van Der Walt, S. J., Gommers, R., Virtanen, P., Cournapeau, D., Wieser, E., Taylor, J., Berg, S., Smith, N. J., et al.: Array programming with NumPy, Nature, 585, 357–362, 2020.

Hartin, C. A., Patel, P., Schwarber, A., Link, R. P., and Bond-Lamberty, B.: A simple object-oriented and open-source model for scientific and policy analyses of the global climate system–Hector v1. 0, Geoscientific Model Development, 8, 939–955, 2015.

He, Y., Trumbore, S. E., Torn, M. S., Harden, J. W., Vaughn, L. J., Allison, S. D., and Randerson, J. T.: Radiocarbon constraints imply reduced carbon uptake by soils during the 21st century, Science, 353, 1419–1424, 2016.

Hellevang, H. and Aagaard, P.: Constraints on natural global atmospheric CO2 fluxes from 1860 to 2010 using a simplified explicit forward model, Scientific reports, 5, 1–12, 2015.

Hoyer, S. and Hamman, J.: xarray: N-D labeled arrays and datasets in Python, Journal of Open Research Software, 5, https://doi.org/10.5334/jors.148, 2017.

Huang, B., Menne, M. J., Boyer, T., Freeman, E., Gleason, B. E., Lawrimore, J. H., Liu, C., Rennie, J. J., Schreck III, C. J., Sun, F., et al.: Uncertainty estimates for sea surface temperature and land surface air temperature in NOAAGlobalTemp version 5, Journal of Climate, 33, 1351–1379, 2020.

Joos, F., Bruno, M., Fink, R., Siegenthaler, U., Stocker, T. F., Le Quéré, C., and Sarmiento, J. L.: An Efficient and accurate representation of complex oceanic and biospheric models of anthropogenic carbon uptake, 1996.

Joos, F., Prentice, I. C., Sitch, S., Meyer, R., Hooss, G., Plattner, G.-K., Gerber, S., and Hasselmann, K.: Global warming feedbacks on terrestrial carbon uptake under the Intergovernmental Panel on Climate Change (IPCC) emission scenarios, Global Biogeochemical Cycles, 15, 891–907, 2001.

Kucukelbir, A., Tran, D., Ranganath, R., Gelman, A., and Blei, D. M.: Automatic differentiation variational inference, Journal of machine learning research, 2017.

Le Quéré, C., Andrew, R. M., Friedlingstein, P., Sitch, S., Hauck, J., Pongratz, J., Pickers, P. A., Korsbakken, J. I., Peters, G. P., Canadell, J. G., Arneth, A., Arora, V. K., Barbero, L., Bastos, A., Bopp, L., and Zheng, B.: Global Carbon Budget 2018, Earth System Science Data, pp. 2141–2194, https://doi.org/10.5194/essd-8-605-2016, 2018.

Leach, N. J., Nicholls, Z., Jenkins, S., Smith, C. J., Lynch, J., Cain, M., Wu, B., Tsutsui, J., and Allen, M. R.: GIR v1. 0.0: a generalised impulse-response model for climate uncertainty and future scenario exploration, Geoscientific Model Development Discussions, pp. 1–29, 2020.

Lee, J. Y., Marotzke, J., Bala, G., Cao, L., Corti, S., Dunne, J. P., Engelbrecht, F., Fischer, E., Fyfe, J. C., Jones, C., Maycock, A., Mutemi, J., Ndiaye, O., Panickal, S., and Zhou, T.: Future Global Climate: Scenario-Based Projections and Near-Term Informations, Climate Change 2021: The Physical Science Basis. Contribution of Working Group I to the Sixth Assessment Report of the Intergovernmental Panel on Climate Change, 2021.

Liddicoat, S. K., Wiltshire, A. J., Jones, C. D., Arora, V. K., Brovkin, V., Cadule, P., Hajima, T., Lawrence, D. M., Pongratz, J., Schwinger, J., et al.: Compatible Fossil Fuel CO 2 Emissions in the CMIP6 Earth System Models' Historical and Shared Socioeconomic Pathway Experiments of the Twenty-First Century, Journal of Climate, 34, 2853–2875, 2021.

MacDougall, A. H.: Estimated effect of the permafrost carbon feedback on the zero emissions commitment to climate change, Biogeosciences, 18, 4937–4952, 2021.

Meehl, G. A., Senior, C. A., Eyring, V., Flato, G., Lamarque, J.-F., Stouffer, R. J., Taylor, K. E., and Schlund, M.: Context for interpreting equilibrium climate sensitivity and transient climate response from the CMIP6 Earth system models, Science Advances, 6, eaba1981, 2020.

Meinshausen, M., Raper, S. C., and Wigley, T. M.: Emulating coupled atmosphere-ocean and carbon cycle models with a simpler model, MAGICC6–Part 1: Model description and calibration, Atmospheric Chemistry and Physics, 11, 1417–1456, 2011.

Mengel, M., Levermann, A., Frieler, K., Robinson, A., Marzeion, B., and Winkelmann, R.: Future sea level rise constrained by observations and long-term commitment, Proceedings of the National Academy of Sciences, 113, 2597–2602, 2016.

Morice, C. P., Kennedy, J. J., Rayner, N. A., Winn, J., Hogan, E., Killick, R., Dunn, R., Osborn, T., Jones, P., and Simpson, I.: An updated assessment of near-surface temperature change from 1850: The HadCRUT5 data set, Journal of Geophysical Research: Atmospheres, 126, e2019JD032 361, 2021.

Myhre, G., Shindell, D., Bréon, F.-M., Collins, W., Fuglestvedt, J., Huang, J., Koch, D., Lamarque, J.-F., Lee, D., Mendoza, B., Nakajima, T., Robock, A., Stephens, G., Takemura, T., and Zhang, H.: AR5 - Working Group 1, Chapter 8 : Anthropogenic and Natural Radiative Forcing - Contribution of Working Group I, Cambridge University Press, 23, 56, 2013.

National Academies of Sciences, E. and Medicine: Valuing climate damages: updating estimation of the social cost of carbon dioxide, National Academies Press, 2017.

Nicholls, Z., Meinshausen, M., Lewis, J., Corradi, M. R., Dorheim, K., Gasser, T., Gieseke, R., Hope, A. P., Leach, N., McBride, L. A., et al.: Reduced complexity Model Intercomparison Project Phase 2: Synthesizing Earth system knowledge for probabilistic climate projections, Earth's Future, 9, e2020EF001 900, 2021.

Nicholls, Z. R., Meinshausen, M., Lewis, J., Gieseke, R., Dommenget, D., Dorheim, K., Fan, C.-S., Fuglestvedt, J. S., Gasser, T., Golüke, U., et al.: Reduced Complexity Model Intercomparison Project Phase 1: introduction and evaluation of global-mean temperature response, Geoscientific Model Development, 13, 5175–5190, 2020.

Nordhaus, W. D.: Revisiting the social cost of carbon, Proceedings of the National Academy of Sciences, 114, 1518–1523, https://doi.org/10.1073/pnas.1609244114, 2017.

Parkes, D. and Marzeion, B.: Twentieth-century contribution to sea-level rise from uncharted glaciers, Nature, 563, 551–554, 2018.

Pérez, F. and Granger, B. E.: IPython: a System for Interactive Scientific Computing, Computing in Science and Engineering, 9, 21–29, https://doi.org/10.1109/MCSE.2007.53, 2007.

Riahi, K., van Vuuren, D. P., Kriegler, E., Edmonds, J., O'Neill, B. C., Fujimori, S., Bauer, N., Calvin, K., Dellink, R., Fricko, O., Lutz, W., Popp, A., Cuaresma, J. C., KC, S., Leimbach, M., Jiang, L., Kram, T., Rao, S., Emmerling, J., Ebi, K., Hasegawa, T., Havlik, P., Humpenöder, F., Da Silva, L. A., Smith, S., Stehfest, E., Bosetti, V., Eom, J., Gernaat, D., Masui, T., Rogelj, J., Strefler, J., Drouet, L., Krey, V., Luderer, G., Harmsen, M., Takahashi, K., Baumstark, L., Doelman, J. C., Kainuma, M., Klimont, Z., Marangoni, G., Lotze-Campen, H., Obersteiner, M., Tabeau, A., and Tavoni, M.: The Shared Socioeconomic Pathways and their energy, land use, and greenhouse gas emissions implications: An overview, Global Environmental Change, 42, 153–168, https://doi.org/10.1016/j.gloenvcha.2016.05.009, 2017.

Ricciuto, D. M., Davis, K. J., and Keller, K.: A Bayesian calibration of a simple carbon cycle model: The role of observations in estimating and reducing uncertainty, Global biogeochemical cycles, 22, 2008.

Roe, G. H. and Baker, M. B.: Why is climate sensitivity so unpredictable?, Science, 318, 629–632, 2007.

Rohde, R.: Comparison of Berkeley Earth, NASA GISS, and Hadley CRU averaging techniques on ideal synthetic data, Berkeley Earth Memo, January, 2, 013, 2013.

Rohde, R., Muller, R., Jacobsen, R., Perlmutter, S., Rosenfeld, A., Wurtele, J., Curry, J., Wickham, C., and Mosher, S.: Berkeley Earth temperature averaging process, Geoinformatics & Geostatistics: An Overview, 1, 1–13, 2013.

Salvatier, J., Wiecki, T. V., and Fonnesbeck, C.: Probabilistic programming in Python using PyMC3, PeerJ Computer Science, 2, e55, 2016.

Sitch, S., Friedlingstein, P., Gruber, N., Jones, S. D., Murray-Tortarolo, G., Ahlström, A., Doney, S. C., Graven, H., Heinze, C., Huntingford, C., et al.: Recent trends and drivers of regional sources and sinks of carbon dioxide, Biogeosciences, 12, 653–679, 2015.

Slangen, A., Church, J. A., Agosta, C., Fettweis, X., Marzeion, B., and Richter, K.: Anthropogenic forcing dominates global mean sea-level rise since 1970, Nature Climate Change, 6, 701–705, 2016.

Smith, C., Nicholls, Z. R. J., Armour, K., Collins, W., Forster, P., M. M., Palmer, M. D., and Watanabe, M.: The Earth's Energy Budget, Climate Feedbacks, and Climate Sensitivity Supplementary Material, Climate Change 2021: The Physical Science Basis. Contribution of Working Group I to the Sixth Assessment Report of the Intergovernmental Panel on Climate Change, 2021.

Smith, C. J., Forster, P. M., Allen, M., Leach, N., Millar, R. J., Passerello, G. A., and Regayre, L. A.: FAIR v1. 3: a simple emissions-based impulse response and carbon cycle model, Geoscientific Model Development, 11, 2273–2297, 2018.

Strassmann, K. M. and Joos, F.: The Bern Simple Climate Model (BernSCM) v1.0: An extensible and fully documented open-source re-implementation of the Bern reduced-form model for global carbon cycle-climate simulations, Geoscientific Model Development, 11, 1887–1908, https://doi.org/10.5194/gmd-11-1887-2018, 2018.

Takahashi, T., Olafsson, J., Goddard, J. G., Chipman, D. W., and Sutherland, S.: Seasonal variation of CO2 and nutrients in the high-latitude surface oceans: A comparative study, Global Biogeochemical Cycles, 7, 843–878, 1993.

Tans, P. and Keeling, R.: NOAA, ESRL (www. esrl. noaa. gov/gmd/ccgg/trends/), 2010.

Theano Development Team: Theano: A Python framework for fast computation of mathematical expressions, arXiv e-prints, abs/1605.02688, http://arxiv.org/abs/1605.02688, 2016.

Van Rossum, G. and Drake, F. L.: Python 3 Reference Manual, CreateSpace, Scotts Valley, CA, 2009.

Virtanen, P., Gommers, R., Oliphant, T. E., Haberland, M., Reddy, T., Cournapeau, D., Burovski, E., Peterson, P., Weckesser, W., Bright, J., van der Walt, S. J., Brett, M., Wilson, J., Millman, K. J., Mayorov, N., Nelson, A. R. J., Jones, E., Kern, R., Larson, E., Carey, C. J., Polat, İ., Feng, Y., Moore, E. W., VanderPlas, J., Laxalde, D., Perktold, J., Cimrman, R., Henriksen, I., Quintero, E. A., Harris, C. R., Archibald, A. M., Ribeiro, A. H., Pedregosa, F., van Mulbregt, P., and SciPy 1.0 Contributors: SciPy 1.0: Fundamental Algorithms for Scientific Computing in Python, Nature Methods, 17, 261–272, https://doi.org/10.1038/s41592-019-0686-2, 2020.

Vose, R. S., Arndt, D., Banzon, V. F., Easterling, D. R., Gleason, B., Huang, B., Kearns, E., Lawrimore, J. H., Menne, M. J., Peterson, T. C., et al.: NOAA's merged land–ocean surface temperature analysis, Bulletin of the American Meteorological Society, 93, 1677–1685, 2012.

Yu, Z., Loisel, J., Brosseau, D. P., Beilman, D. W., and Hunt, S. J.: Global peatland dynamics since the Last Glacial Maximum, Geophysical research letters, 37, 2010.

Zhao, M., Heinsch, F. A., Nemani, R. R., and Running, S. W.: Improvements of the MODIS terrestrial gross and net primary production global data set, Remote sensing of Environment, 95, 164–176, 2005.

Code and data availability. The source code of Pathfinder is openly available at: https://github.com/tgasser/Pathfinder. A frozen version of the code and data as developed in the paper can be found on Zenodo: https://doi.org/10.5281/zenodo.7003848 (Gasser, 2022).

Author contributions. TG developed the model, with contributions from TB on sea level rise and PC on land carbon cycle. TG coded the model and its calibration. TB ran the diagnostic simulations and made the final figures. TB and TG wrote the manuscript with input from PC.

Competing interests. The authors declare they have no competing interests.

Acknowledgements. Development of Pathfinder was supported by the European Union's Horizon 2020 research and innovation programme under grant agreement #820829 (CONSTRAIN project), and by the Austrian Science Fund (FWF) under grant agreement P31796-N29 (ERM project). We thank A. H. MacDougall for sharing permafrost simulations made with UVic.

2.3 . Representation of the ocean in Pathfinder

In the concluding segment of our paper referenced in section 2.2, we proposed potential advancements through an alternative representation of the ocean in Pathfinder. In this section, we delve deeper into the limitations currently present in Pathfinder's representation of the oceans. This discussion draws on Séférian et al., 2023, to which I am a co-author.

2.3.1 . Ocean Heat-Carbon nexus

The pivotal role of the oceans in decelerating atmospheric CO_2 accumulation and global warming is well recognized. Observational data confirms that they absorb more than a quarter of annual human-induced CO_2 emissions. This characteristic equips the oceans with a substantial influence on atmospheric CO_2 levels. Additionally, the oceans sequester the majority of the supplementary heat generated by radiative forcing from greenhouse gas accumulation in the atmosphere. By moderating both CO_2 and heat uptake, the oceans establish a critical link between Earth's climate and carbon cycle responses to cumulative CO_2 emissions, collectively known as the "Ocean Heat-Carbon Nexus" (Canadell et al.; 2021)

The mechanisms leading to the Ocean Heat-Carbon Nexus are multi-faceted, yet well understood. The primary drivers are the exchanges of heat and carbon across the sea-air interface, which direct the partitioning of anthropogenic CO_2 emissions and additional heat (MacDougall; 2017; Frölicher et al.; 2015). These processes are typically parameterized into well-established expressions that link the flux to wind stress and the gradient of heat or CO_2 across the sea-to-air interface (Garbe et al.; 2014). The other driver of the Ocean Heat-Carbon Nexus arises from the suite of processes controlling the capacity of the oceans to store heat and CO_2, respectively governed by the important heat capacity and the CO_2 buffering capacity of seawater.

2.3.2 . Regime Shift in the Ocean Heat-Carbon Nexus

Under rising atmospheric CO_2 and associated climate change, both theory and complex models suggest that the Ocean Heat-Carbon Nexus may display a regime shift (Figure 2.3). This regime shift arises from a combination of three factors. First, both models and theory show that there is no physical limitation that would reduce the ability of surface ocean temperature to equilibrate with the atmospheric temperature. This implies that there is no mechanism that would limit the capacity of the oceans to absorb the additional heat from the atmosphere. Second, and in contrast, the capacity of the oceans to store CO_2 differs from its capacity to store heat because the carbon buffering capacity decreases as soon as the oceans absorbs anthropogenic CO_2 and stores it as dissolved inorganic carbon (Egleston et al.; 2010). Third, the accumulation of heat tends to simultaneously exacerbate this phenomenon by reinforcing the stratification of the surface ocean, preventing the water masses in contact with the atmosphere from mixing with the subsurface ocean. It reinforces the regime shift of the ocean heat-carbon nexus in a future warmer climate where each Joules taken up by the oceans drive a stronger saturation of the ocean carbon uptake.

2.3.3 . Comparison of key geophysical properties between ESMs and Pathfinder

Virtually all climate models are assumed to capture the key features of the Ocean Heat-Carbon Nexus. In particular, because all models do simulate a near proportional relationship between

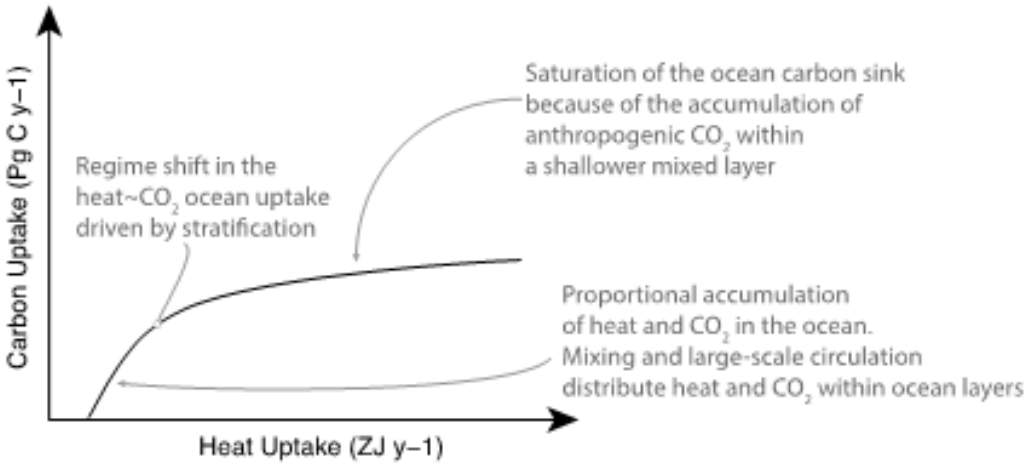

Figure 2.3: Depiction of the expected regime shift in the ocean heat-carbon nexus (from Seferian et al.). The ocean heat-carbon nexus emerges from the relationship between the ocean heat uptake (x axis) and the ocean carbon uptake (y axis).

cumulative emissions of CO_2 and change in global mean temperature (the so-called transient climate response to cumulative CO_2 emissions) that mainly arises from the interplay between the heat and carbon uptake by the oceans (MacDougall and Friedlingstein; 2015; Williams et al.; 2016; MacDougall; 2017). However, the question of how far the representation of the ocean heat-carbon nexus is comparable and physically consistent across these different modelling platforms has never been investigated. Here we take a closer look at the representation of the ocean heat-carbon nexus in Pathfinder and compare it with the representation in the ESMs.

The modelling paradigm of ESMs primarily arise from the process understanding of the flow of energy, moisture and chemicals through the atmosphere, ocean and land surface, governing Earth's climate. These processes are either explicitly resolved or parameterized in ESMs. On the other hand, SCMs like Pathfinder are much simpler models than ESMs. They are parametric models designed to be CPU-efficient, flexible and easily tunable in order to emulate the response of complex ESMs within a certain domain of validity. Although based on a suite of assumptions and simplification, Pathfinder is fitted to reproduce key global features of the modern climate, as shown in section 2.2.

If the performances of Pathfinder on replicating historical observations are very satisfying, its response when used in an idealistic simulation framework where atmospheric CO_2 rises by 1% per year exhibits a much different picture (Figure 2.4). Although the change in global mean surface temperature is consistent with the model behavior as documented in published climate sensitivity assessment (Forster et al.; 2021), the response of the ocean heat and carbon uptake as simulated by Pathfinder does not display the saturation of the ocean carbon uptake observed in the ESMs on Figure 2.4 and confirmed by theory.

Interestingly, the response of Pathfinder and ESMs is almost indistinguishable, with the uptake of heat and carbon mirroring historical periods in magnitude. This divergence between historical period consistency and theoretical inconsistency in idealistic simulations can be attributed to two key factors. Firstly, the available historical observations do not provide a sufficient constraint on the

calibrated SCMs when projecting SCMs in a warmer range. Sherwood et al. (2020) also showed the limitations of the historical record to constrain climate sensitivity.

Secondly, Pathfinder poorly captures the regime shift in the ocean heat-carbon nexus. When tracking the timing of the regime shift in the ocean heat-carbon nexus as simulated by both modelling platform, we show a change in the heat-carbon uptake relationship in Pathfinder in year 1900 for a simulation starting in 1850. This is similar to what can be found in ESMs, with a timing of the regime shift in year 1896±10. However, with pronounced heat and carbon uptake, differences are clear. While ESMs show saturation in carbon uptake around 5 PgC yr^{-1}, Pathfinder only shows a progressive diminution of the slope without saturating at 6 PgC yr^{-1}. The perturbed parameter ensemble (Figure A.1) suggests that this feature is robust across a wide range of parameters and hence demonstrated that the representation of the ocean heat carbon nexus arises prominently from the structural properties of Pathfinder.

2.3.4 . Inconsistent physical representation of the key driving mechanisms of the ocean heat-carbon nexus

Our study identifies several limitations in the Pathfinder model's representation of the ocean heat-carbon nexus. Pathfinder uses certain assumptions and simplifications which lead to inconsistencies when compared to Earth System Models (ESMs). An analysis of the model's properties shows that the modelling framework of Pathfinder do treat in two distinct modules the thermal response of the ocean to radiative forcing and that of the ocean carbon cycle. Therefore, Pathfinder may rely on physically inconsistent structures and parameters – such as mixed-layer depths (MLD) and relaxation time-scales – to simulate the ocean Heat-Carbon nexus, because of essentially modelling two different oceans. In contrast, ESMs do resolve the suite of processes governing the uptake of heat and carbon by the ocean consistently.

Compared to ESMs which consistently process the uptake of heat and carbon by the ocean, our analysis reveals that Pathfinder overlooks or simplifies certain processes. It utilizes a pure-diffusion scheme for vertical heat and carbon exchange with the atmosphere, and indirect interactions for the coupling between ocean physics and the carbon cycle (see section 2.2). The MLD is a notable example of such a simplification. In Pathfinder, the MLD is fixed in time and calculated from the model parameters, producing inconsistent depths in the climate and carbon modules. Indeed, the MLD is estimated at 86 +- 11 m in the climate module while it is 45 +- 4 m in the carbon module. Both those values of MLD fall outside the observation range, suggesting that this parameter has been underlooked. However, ESMs resolve the MLD and allow it to respond to anthropogenic forcing. These structural and parametric oversights in the Pathfinder model could contribute to an inaccurate representation of the ocean heat-carbon nexus explaining the failure in reproducing the saturation of the ocean carbon sink.

2.3.5 . Consequences on projections

When the Pathfinder model is used for projections, its limitations have implications, as illustrated in Figures 2.4 and 2.6. To address these, we introduced a new constraint using data from ESMs, tying the ocean heat uptake and the ocean carbon uptake at 2xCO_2 (year 70 of the 1pctCO_2 simulation). The distribution of this model-based constraint is assumed normal, and taken from the CMIP6 ESMs' average and standard deviation (4.58 ± 0.38 ZJ PgC^{-1}). We integrate this novel

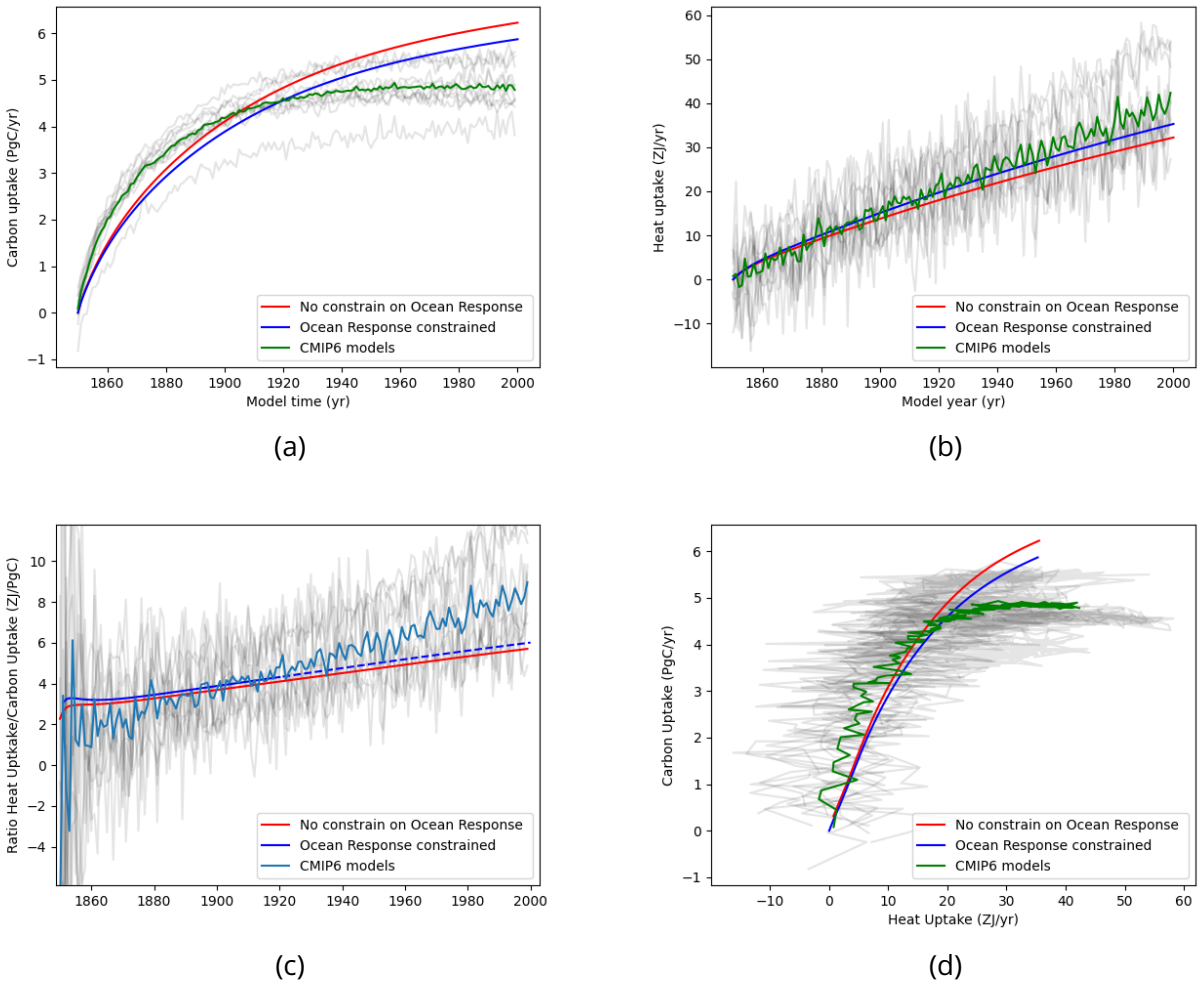

Figure 2.4: Comparison of projected warming and ocean heat carbon nexus between ESMs and SCMs under an idealized set-up. Panels a), b) and c) shows the temporal evolution of the projected ocean heat uptake, ocean carbon uptake and the of the heat uptake on the carbon uptake as simulated by both ESMs and Pathfinder. Panel d) display the representation of the ocean heat carbon nexus between ESMs and SCMs. Pathfinder projections with and without the constraint on the ocean response are given in colored solid lines, individual ESMs in thin grey lines and ESM multi-model mean in green lines.

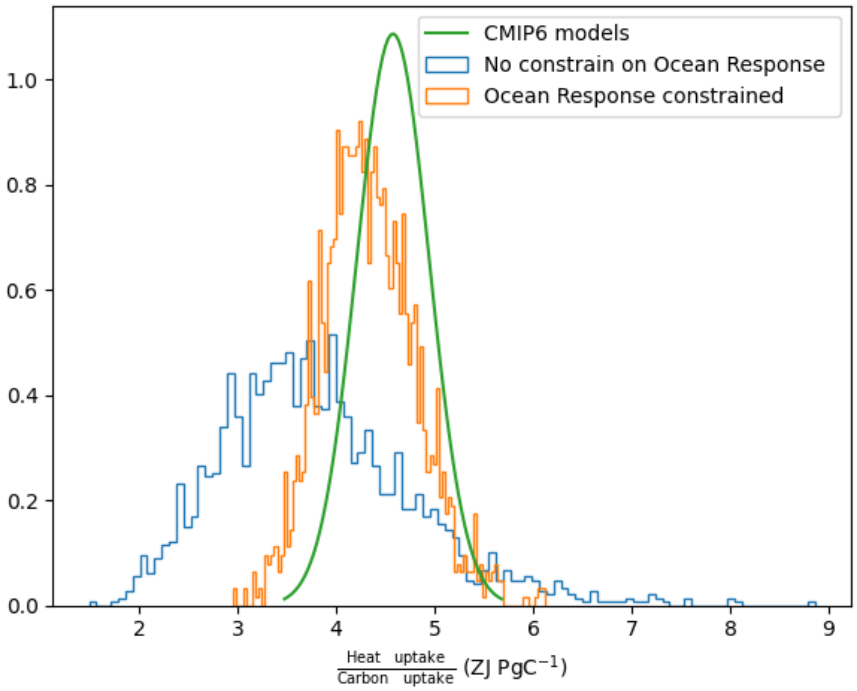

Figure 2.5: Distribution of the ratio between the ocean heat uptake and carbon uptake. Green line gives the distribution in ESMs CMIP6 models used to constrain. Blue line gives the distribution posterior to the calibration without the constraint on the ratio. Orange line gives the distribution posterior to the calibration considering the constraint on the ratio

constraint to the 19 others already used during the Bayesian calibration of Pathfinder and show its effect on the ratio's distribution in Figure 2.5. The main effect is to generate a correlation between the parameter reflecting the depth of the mixed layer and the parameters of the climate module. We also observe a small effect on idealistic projections in Figure 2.4 with a slightly earlier regime shift and a diminution of the maximum carbon uptake. However, there is still no clear saturation of the carbon uptake.

Before applying the constraint, when focusing on the two high-mitigation/low overshoot scenarios (ssp119 and ssp126), we find at peak warming ranges from 0.91°C to 2.98°C with a mean estimate of 1.66°C for ssp119, and from1.03°C to 3.57°C with a mean estimate of 1.94°C for ssp126. The high overshoot scenario (ssp534-over) displays a range of peak warming between 1.42°C and 4.76°C with a mean estimate of 2.60°C. The application of the geophysical constraint in the ocean heat-carbon nexus reinforced the simulated warming by about +0.1°C for both high-mitigation/low overshoot scenarios and up to 0.2°C for the high-overshoot scenario. The constraint also results in a slightly smaller spread in projected warming (about 5-8% with respect to the reference simulations). Pathfinder simulates a mean warming of 1.75°C at peak warming with a range of 0.99–2.91°C in ssp119 and 2.06°C with a range of 1.14–3.52°C for ssp126. Under the high-overshoot scenario the peak warming ranges between 1.57°C

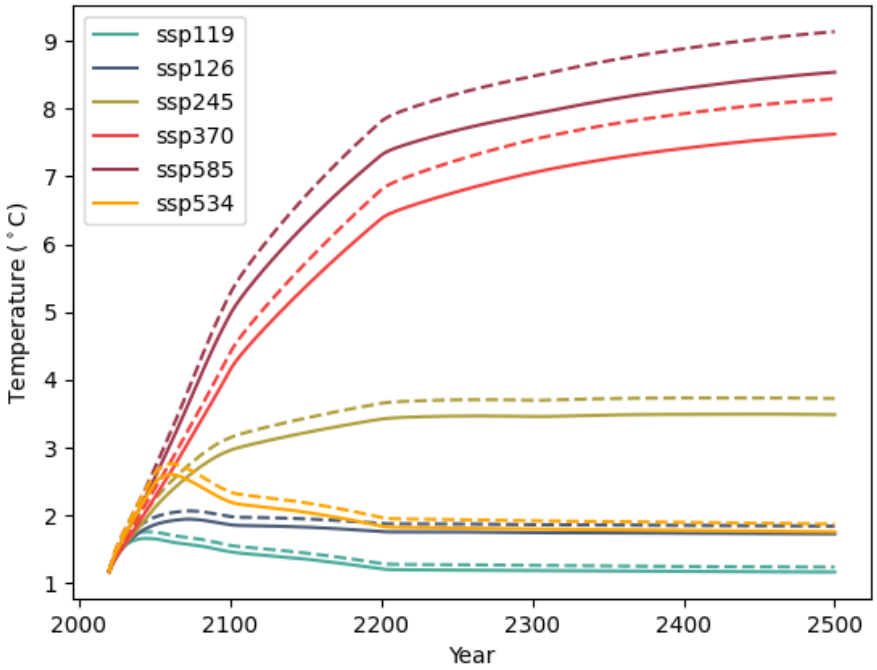

Figure 2.6: Temperature projections of six SSPs scenarios without constraining the ratio between the ocean heat uptake and the ocean carbon uptake at 2xCO_2 (plain lines) and with constraining the ratio (dashed lines). We only show the median value across 2000 Pathfinder's configurations.

and 4.72°C with a mean estimate of 2.76°C. While seemingly low, this 0.1°C difference is consequential in the case of ambitious low-warming scenarios. With an older version of the MAGICC simple climate models (Meinshausen et al.; 2011) with the 600-probabilistic parameters samples, it was assessed that +0.1°C at peak warming reduces the likelihood of the ssp126 scenario to stay below 2°C from 66% to 54% and from 10% to 6%. A similar difference of 0.1°C in MAGICC temperature outcomes was also found in Nicholls et al. (2022) when comparing the IPCC SR15 (Rogelj et al.; 2018) and AR6 (Riahi et al.; 2022) due to the increase in assessed historical warming between SR1.5 and AR6, and an improved (i.e., weaker) response to emissions.

As stated in this work, such difference is enough to cause all the "1.5°C no overshoot" scenarios to be reclassified as "1.5°C low overshoot" scenarios. Here, our finding has a stronger implication has it concerns a geophysical feature commonly misrepresented in all SCMs, potentially inducing in systematic biases in the projected warming. The implication for the recent categorization of scenarios (Schleussner et al.; 2022) might be stronger as the additional warming could result in emptying the C1 category that limits warming to 1.5°C in 2100 with a greater than 50% chance.

2.3.6 . Improving Pathfinder

The limitations of the Pathfinder model and their implications necessitate improvements. Despite the corrections made by adding a constraint on ocean response, the existing structure of

the Pathfinder model, based on a quarter-century-old article (Joos et al.; 1996), prevents significant changes in its behavior. For this reason, we decided not to include this constraint in Pathfinder for all other studies published in this thesis. A thorough revision is needed to develop an alternative formulation of ocean carbon dynamics based on modern ocean models and properly linked to the climate module. This would not only help improve the ocean carbon dynamics in Pathfinder, but also the ocean pH estimates. Given the implications of these results for categorizing scenarios and achieving low warming targets, addressing these limitations should be a priority for future research.

Bibliography

Canadell, J. G., Monteiro, P. M. S., Costa, M. H., Cotrim da Cunha, L., Cox, P. M., Eliseev, A. V., Henson, S., Ishii, M., Jaccard, S., Koven, C., Lohila, A., Patra, P. K., Piao, S., Rogelj, J., Syampungani, S., Zaehle, S. and Zickfeld, K. (2021). Global carbon and other biogeochemical cycles and feedbacks, *Climate Change 2021: The Physical Science Basis. Contribution of Working Group I to the Sixth Assessment Report of the Intergovernmental Panel on Climate Change* .

Egleston, E. S., Sabine, C. L. and Morel, F. M. (2010). Revelle revisited: Buffer factors that quantify the response of ocean chemistry to changes in dic and alkalinity, *Global Biogeochemical Cycles* **24**(1).

Forster, P., Storelvmo, T., Armour, K., Collins, T., Dufresne, J. L., Frame, D., Lunt, D. J., Mauritsen, T., Palmer, M. D., Watanabe, M., Wild, M. and Zhang, H. (2021). *The Earth's Energy Budget, Climate Feedbacks, and Climate Sensitivity*, Cambridge, United Kingdom, book section 7, pp. 923–1054.

Frölicher, T. L., Sarmiento, J. L., Paynter, D. J., Dunne, J. P., Krasting, J. P. and Winton, M. (2015). Dominance of the southern ocean in anthropogenic carbon and heat uptake in cmip5 models, *Journal of Climate* **28**(2): 862–886.

Garbe, C. S., Rutgersson, A., Boutin, J., de Leeuw, G., Delille, B., Fairall, C. W., Gruber, N., Hare, J., Ho, D. T., Johnson, M. T. et al. (2014). Transfer across the air-sea interface, *Ocean-atmosphere interactions of gases and particles* pp. 55–112.

Joos, F., Bruno, M., Fink, R., Siegenthaler, U., Stocker, T. F., Le Quéré, C. and Sarmiento, J. L. (1996). An Efficient and accurate representation of complex oceanic and biospheric models of anthropogenic carbon uptake.

MacDougall, A. H. (2017). The oceanic origin of path-independent carbon budgets, *Scientific Reports* **7**(1): 10373.

MacDougall, A. H. and Friedlingstein, P. (2015). The origin and limits of the near proportionality between climate warming and cumulative co2 emissions, *Journal of Climate* **28**(10): 4217–4230.

Meinshausen, M., Raper, S. C. and Wigley, T. M. (2011). Emulating coupled atmosphere-ocean and carbon cycle models with a simpler model, magicc6–part 1: Model description and calibration, *Atmospheric Chemistry and Physics* **11**(4): 1417–1456.

Nicholls, Z., Meinshausen, M., Lewis, J., Smith, C. J., Forster, P., Fuglestvedt, J. S., Rogelj, J., Kikstra, J., Riahi, K. and Byers, E. (2022). Changes in ipcc scenario assessment emulators between sr1. 5 and ar6 unraveled, *Geophysical Research Letters* **49**(20): e2022GL099788.

Riahi, K., Schaeffer, R., Arango, J., Calvin, K., Guivarch, C., Hasegawa, T., Jiang, K., Kriegler, E., Matthews, R. and Peters, G. (2022). Mitigation pathways compatible with long-term goals, *Climate change* .

Rogelj, J., Popp, A., Calvin, K. V., Luderer, G., Emmerling, J., Gernaat, D., Fujimori, S., Strefler, J., Hasegawa, T., Marangoni, G., Krey, V., Kriegler, E., Riahi, K., van Vuuren, D. P., Doelman, J., Drouet, L., Edmonds, J., Fricko, O., Harmsen, M., Havlík, P., HumpenÃ¶der, F., Stehfest, E. and Tavoni, M. (2018). Scenarios towards limiting global mean temperature increase below 1.5 °c, *Nature Climate Change* **8**(4): 325–332.

Schleussner, C.-F., Ganti, G., Rogelj, J. and Gidden, M. J. (2022). An emission pathway classification reflecting the paris agreement climate objectives, *Communications Earth & Environment* **3**(1): 135.

Sherwood, S., Webb, M. J., Annan, J. D., Armour, K. C., Forster, P. M., Hargreaves, J. C., Hegerl, G., Klein, S. A., Marvel, K. D. and Rohling, E. J. (2020). An assessment of earth's climate sensitivity using multiple lines of evidence, *Reviews of Geophysics* **58**(4): e2019RG000678.

Williams, R. G., Goodwin, P., Roussenov, V. M. and Bopp, L. (2016). A framework to understand the transient climate response to emissions, *Environmental Research Letters* **11**(1): 015003.

3 - Using Pathfinder to explore CO2 emission scenarios

In chapter 2, the need for a new SCM is justified. In the same chapter, we respond to this need by proposing Pathfinder, which we describe and diagnose, highlighting its strengths but also its opportunities for improvement. In this chapter, we use Pathfinder to explore new mitigation scenarios. First, we use the most recent data in a very classical way to estimate the chances that climate change will stay below 1.5°C, for 54 different idealized but meaningful scenarios (section 3.1). We then propose an innovative approach to map the range of pathways compatible with different planetary boundaries to climate change (section 3.3).

3.1 . On the chances of staying below the 1.5°C warming target

Abstract: The 2022 rebound in fossil fuel CO2 emissions to pre-COVID19 level and the insufficient mitigation pledges at recent COPs question the feasibility of "keeping the 1.5°C target alive." Here, we calculate the CO2 emissions reduction physically required to stay below 1.5°C, using the latest available data up to 2022. For a 50% chance of staying below 1.5°C during this century, fossil fuel and industry CO2 emissions need to decrease linearly by about 5% per year. This level of decarbonization would need to occur every year. Such an annual mitigation rate is only slightly less than the short-term unprecedented emissions reduction caused by the COVID19 pandemic. We further show that the chances of staying below 1.5°C of global warming critically hinge on the assumed land-use CO2 emissions and non-CO2 forcing.

On the chances of staying below the 1.5°C warming target

Thomas Bossy[1,2], Thomas Gasser[2], Katsumasa Tanaka[1,3], Philippe Ciais[1]

[1]*Laboratoire des sciences du climat et de l'environnement (LSCE), IPSL, CEA/CNRS/UVSQ, Université Paris-Saclay, Gif-sur-Yvette, France*

[2]*International Institute for Applied System Analysis (IIASA), Laxenburg, Austria*

[3]*Earth System Division, National Institute for Environmental Studies (NIES), Tsukuba, Japan*

Main

At COP27 in Sharm El Sheikh, the Parties reaffirmed their ambition to limit climate change to a temperature target of 1.5°C above pre-industrial levels[1]. Given the world's emissions trajectory in recent years[2-4], meeting this target without overshoot seems very ambitious at best, and virtually impossible at worst. Global warming has already reached 1.09°C above pre-industrial levels over the 2010-2019 period[5]. The latest IPCC 6th Assessment Report (AR6)[6] gave an estimate of the remaining carbon budget (RCB; that is, the total amount of allowable anthropogenic CO_2 emissions) of 500 $GtCO_2$ from January 2020 for a 50% chance of staying below 1.5°C. This was recently updated[2] to 380 $GtCO_2$ from January 2023, given current annual emissions of ~40 $GtCO_2$ per year[2]. Another study using an updated methodology[7] gave an estimate of 300 $GtCO_2$ from January 2022, which is 260 $GtCO_2$ from January 2023. One of the sources of uncertainty in the RCB is the assumed level of non-CO_2 emissions. An aggressive and early abatement of methane and black carbon emissions would advance the timing of peak warming and reduce its magnitude[8]. On the other hand, reductions in sulphate aerosol and NOx emissions would cause additional warming in the short term[9]. Here, we combine the latest available data on temperature[10], CO_2 concentration[11], fossil fuel CO_2 emissions (including industrial processes), land use change (LUC) emissions[2], and non-CO_2 radiative forcing (RF)[12] with the Pathfinder model to calculate what it takes to remain below 1.5°C. Pathfinder is a reduced-complexity climate and carbon-cycle model, calibrated on observations and climate projections from AR6[13]. By differentiating between fossil fuel and LUC emissions, and by exploring non-CO_2 RF scenarios corresponding to the range of ambitious mitigation scenarios in AR6, we shed light on the likelihood of staying below the 1.5°C target and the effect of LUC and non-CO_2 on this likelihood.

To estimate the level of effort needed to remain below 1.5°C, we created stylized mitigation scenarios (Supplementary Figure 1). We consider fossil fuel and LUC CO_2 emissions separately, as they have different dynamics and drivers. For fossil fuel CO_2 emissions, we assume a linear rate of decrease starting from 2022 and reaching zero in 6 different years (every 5 years from 2035 to 2060). For LUC emissions, we apply three interpretations of the Glasgow pledge on deforestation[14]: a pessimistic one with constant emissions until 2050, a mid-range one with a linear decrease of LUC emissions down to zero in 2050, and an optimistic one that leads to a peak of negative CO_2 emissions in 2035; all interpretations then go back to zero in 2100. We also use three contrasted scenarios of non-CO_2 RF within the most ambitious category of scenarios assessed in the latest IPCC report[15,16] (C1 category). Finally, we simulate global temperature change until 2100, a commonly accepted time frame of the Paris Agreement, and further until 2300 to analyse longer-term dynamics.

Figure 1 shows that staying below 1.5°C is not fully guaranteed in any of our mitigation scenarios. Even a very high decarbonization rate (fossil fuel) of 7.7% yr^{-1} with the most optimistic assumptions on non-CO_2 and LUC gives only up to an 83% chance. If we take a scenario with intermediate assumptions on

non-CO_2 and LUC, a decarbonization rate of 5.6% yr^{-1} (i.e. net-zero fossil fuel CO_2 emissions in 2040) is required to maintain a 53% chance of staying below 1.5°C. This represents a reduction of the same order as the temporary 6.3% reduction observed in 2020 during the COVID19 pandemic[17], when human activities were severely constrained; however, this level of decarbonization would need to occur each single year. Our results further show that the choice of non-CO_2 scenario has a larger impact on the exceedance probability than the LUC scenario, with a maximal spread of 48 and 22 percentage points respectively (Figure 1). This finding is consistent with the large uncertainty in future warming due to non-CO_2 reported earlier[18].

The RCB shown in the latest IPCC report is based on a large number of scenarios and many models with different assumptions. Our approach selectively presents scenarios under an internally consistent set of model assumptions. Despite this conceptual difference, a comparison between the decarbonization rates in our scenarios and the ones implied by the standard IPCC RCB is still informative. Our middle-of-the-road scenario combined with a decarbonization rate of 7.7% yr^{-1} leads to 65% chance of staying below 1.5°C, while the same decarbonization rate gives 50% chance with the latest estimate from the IPCC[7] (after subtracting the central CO_2 LUC emissions). The reference milestone of the Emissions Gap report[19] of 33 $GtCO_2$ yr^{-1} emissions in 2030 is comparable to a decarbonization rate of 2.6% yr^{-1} combined with the high LUC scenario. This scenario of the Gap report is estimated to have a 33% chance of staying below 1.5°C, while our comparable scenario with a mid-range non-CO_2 scenario gives only an 11% chance. We are therefore more pessimistic than the Gap report and more optimistic than the IPCC approach.

However, if we extend the time horizon to 2300 assuming constant non-CO_2 RF after 2100, the chance of staying below 1.5°C with a 7.7% yr^{-1} decarbonization rate drops to 37% (compared to 65%). The lower chance for staying below 1.5°C over the longer time horizon is caused by the long-term dynamics of the carbon sinks and permafrost carbon, which altogether release CO_2 after reaching zero emissions. This implies that even if we make the tremendous mitigation efforts needed to stay below 1.5°C until 2100, some net negative emissions will be needed later on, although such long-term CO_2 emission pathways beyond this century are highly model-dependent[3,20] and require further analysis using multiple models.

We have shown that the chances of exceeding the 1.5 °C warming level are high under a wide range of assumptions. But when will we know that we have actually crossed the 1.5 °C threshold? If we keep emitting CO_2 at the current rate, there is about a 50% chance of exceeding the 1.5°C level in 2033 (Supplementary Figure 2). If we further consider the natural variability in global temperature (see Methods), the same likelihood occurs four years earlier (in 2029). This estimate is slightly more optimistic than the estimate from the Met Office (that is, a 48% chance of exceeding 1.5°C before 2026). However, those are estimates for a one-year exceedance whereas the Paris Agreement goal is to limit long-term warming levels, which are typically taken over a 10- or 20-year interval[5].

The 1.5°C target plays a central role in climate negotiations. Today, the mitigation efforts required to keep a mere fifty-fifty chance of meeting the 1.5°C target are comparable to sustaining a CO_2 emissions reduction with a magnitude similar to the drop caused by COVID19. This would need to happen every year until 2040, and to be followed by net negative emissions to avoid any rebound effect. While additional efforts to stop deforestation and to reduce emissions of warming non-CO_2 species such as methane and black carbon would lower the challenge on the fossil fuel CO_2 side, nothing less than a

linear decarbonization rate of 3% yr^{-1} can preserve these odds. Over the past five years, the trend of fossil fuel CO_2 emissions has remained positive at 0.3% yr^{-1}. Even if emissions have actually started to plateau, we argue that staying below 1.5°C is all but out of reach. We believe it is time the scientific community acknowledged this fact. While it is likely that we will exceed the 1.5°C threshold, it does not change the fundamental challenge: we have to anticipate and adapt to climate impacts, and we have to pursue mitigation efforts, because every fraction of a degree matters.

Lead contact

The lead contact is Thomas Bossy: thomas.bossy@lsce.ipsl.fr

Data and code availability

The source code of Pathfinder is openly available at https://github.com/tgasser/Pathfinder (last access: 13 March 2023). A frozen version of the code as developed in the paper can be found on Zenodo at https://doi.org/10.5281/zenodo.7003848. Additional data available upon request.

Experimental procedures

We used Pathfinder v1.0.1[13], a reduced-complexity carbon-climate model. The climate subcomponent that links global mean surface temperature to effective RF follows a widely used 2-box model with deep ocean heat uptake[21]. The ocean carbon cycle follows the structure of the Bern Simple Climate Model[22]. The land carbon cycle was adapted from the compact Earth system model OSCAR[23]. CO_2 emissions from permafrost thaw are globally calculated with the emulator developed by *Gasser et al.*[24]. The 77 model parameters are based on CMIP6 models, and 44 of them are calibrated through Bayesian inference[25] using observations and assessed values from the latest IPCC report[13]. In particular, we used observations until 2021 to constrain the temperature[10], the non-CO_2 RF[12], the CO_2 concentration[11], CO_2 emissions[2] as well as the ocean and land carbon sinks[2]. To account for physical uncertainty, the model is run under 534 different configurations in which the 44 parameters are drawn from the posterior probability distributions obtained after the Bayesian calibration. The configurations were chosen so the historical non-CO_2 RF and the anthropogenic CO_2 emissions remain within the uncertainty range of the most recent estimates. Those estimates were taken in 2022 for CO_2 emissions[2] (36.7 ± 1.8 $GtCO_2$ yr^{-1} for fossil fuel and 4.0 ± 2.2 $GtCO_2$ yr^{-1} for LUC) and 2019 for non-CO_2 RF[11] (1.16 ± 0.13 W m^{-2}). To have the historical starting point of our simulations in 2022, we used the trend on the last 10 years available for non-CO_2 RF to infer the 2020, 2021 and 2022 values (while CO_2 emissions were taken from the latest Global Carbon Budget[2]). To model inter-annual temperature variability, we added *ex-post* a red noise on the RF and a white noise on the temperature in the climate module[26], using the same parameter distributions as in FaIR v2.1 that is calibrated on CMIP6 models[27].

As historical pathways are different in every configuration of the model due to physical uncertainty, the starting point of our future scenarios differs depending on the configuration (Supplementary Figure 1). For fossil-fuel emissions, we apply a stochastic approach to introduce uncertainty to the historical values consistent with the global carbon budget. The historical values of LUC emissions and their uncertainty are inferred by computing the difference between global anthropogenic total CO_2 emissions obtained from the Pathfinder historical simulations and those from fossil-fuel emissions. Similarly, we decompose non-CO_2 RF into a component of non-CO_2 greenhouse gases (GHGs) and another component of all other non-CO_2 RF (including aerosols). We apply a similar stochastic approach to non-CO_2 GHGs to incorporate uncertainty using assessments from the AR6[9]. By subtracting the RF of non-CO_2 GHGs from the overall non-CO_2 RF, we derive the associated uncertainty on other non-CO_2 RF.

In total we explore 54 scenarios reaching net-zero CO_2. We have 6 possible dates for net-zero fossil fuel emissions (including industrial processes) in 2035, 2040, 2045, 2050, 2055 and 2060. Those emissions are assumed to decrease linearly to zero at the chosen date and to remain zero afterwards. To each fossil fuel emission scenario we associate 3 LUC scenarios and 3 non-CO_2 RF scenarios. Low LUC emission scenario is equivalent to the "end gross forest loss" interpretation of the Glasgow pledge on deforestation[12]. Medium LUC is the "end net forest loss" scenario. High LUC is the "end tree cover loss" scenario. For non-CO_2 RF, we choose 3 scenarios from the C1 category in the latest IPCC report[15,16]. One in the upper range of this set, one mid-rand and one in the lower range (see Supplementary Figure 1). To be consistent with historical values in every configuration of the model, we rescale non-CO_2 RF due to GHGs and other non-CO_2 RF separately.

For Supplementary Figure 2, we needed to explore a business as usual scenario, so we took a mid-range scenario (IMAGE 3.2 - SSP2_SPA2_45I_LIRE) among the C6-C7 ensemble. Both fossil fuel and LUC CO_2 emissions remain at 2022 level until 2050.

Author contributions Methodology, T.B. and T.G.; writing – original draft, T.B.; visualization, T.B.; conceptualization – writing – review & editing – all authors.

Acknowledgements We thank Chris Smith for sharing the red noise equations and calibration data. K.T. benefited from State assistance managed by the National Research Agency in France under the Programme d'Investissements d'Avenir under the reference ANR-19-MPGA-0008. T.G. acknowledges support from the European Union's Horizon 2020 research and innovation programme under grant agreements #820829 (CONSTRAIN project) and #101003536 (ESM2025 project).

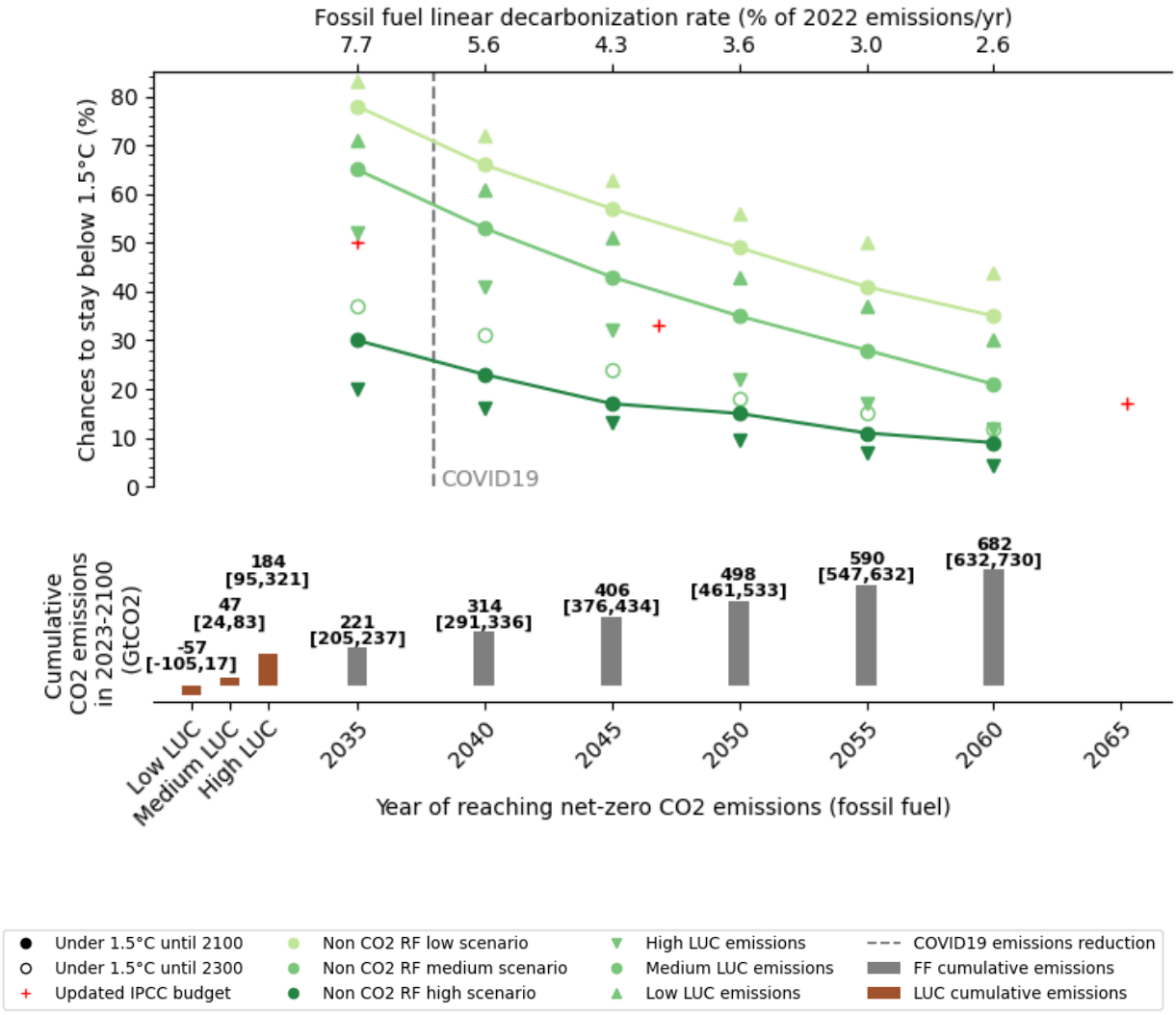

Figure 1 Chances of staying below 1.5°C following various mitigation scenarios for fossil fuel and LUC CO_2 emissions and non-CO_2 RF. Fossil fuel CO_2 emissions are assumed to decrease linearly to zero in 2035, 2040, 2045, 2050, 2055 or 2060. The colors distinguish the scenarios for non-CO_2 RF, marker shapes differentiate scenarios for CO_2 LUC emissions while filled and open markers differentiate the time horizon considered for the 1.5°C target (respectively 2100 and 2300). To keep the figure readable, the open circle for the 2300 likelihood is only given for the central case (medium LUC and RF) and the low LUC /high non-CO_2 and high LUC /low non-CO_2 combinations are not shown. The red crosses are the updated IPCC budgets estimated by Lamboll et al.[7] to which our central LUC CO_2 emissions was subtracted. The dashed line indicates the level of the short-term drop in fossil fuel CO_2 emissions caused by the COVID pandemic[17]. Bar plots show the associated budget for fossil fuel emissions (grey bars) and the LUC emissions scenarios (brown bars). The 90% uncertainty range is shown in the brackets.

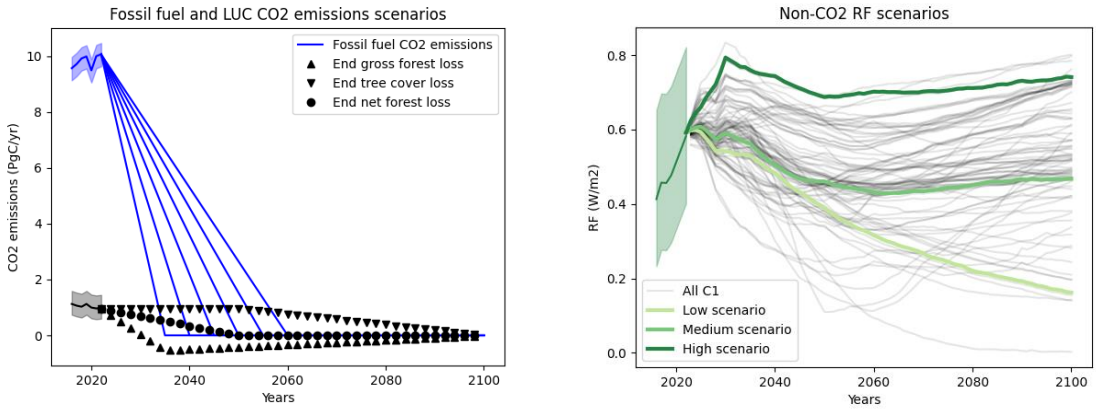

Supplementary Figure 1 CO_2 emissions and non-CO_2 RF scenarios used in this study. Shaded areas around historical pathways indicate the 1-sigma uncertainty range. As historical pathways are different in every configuration of the model due to physical uncertainty, the starting point of our projection scenarios differs depending on the configuration. Here, plain lines for both historical and projections show the median value given by Pathfinder.

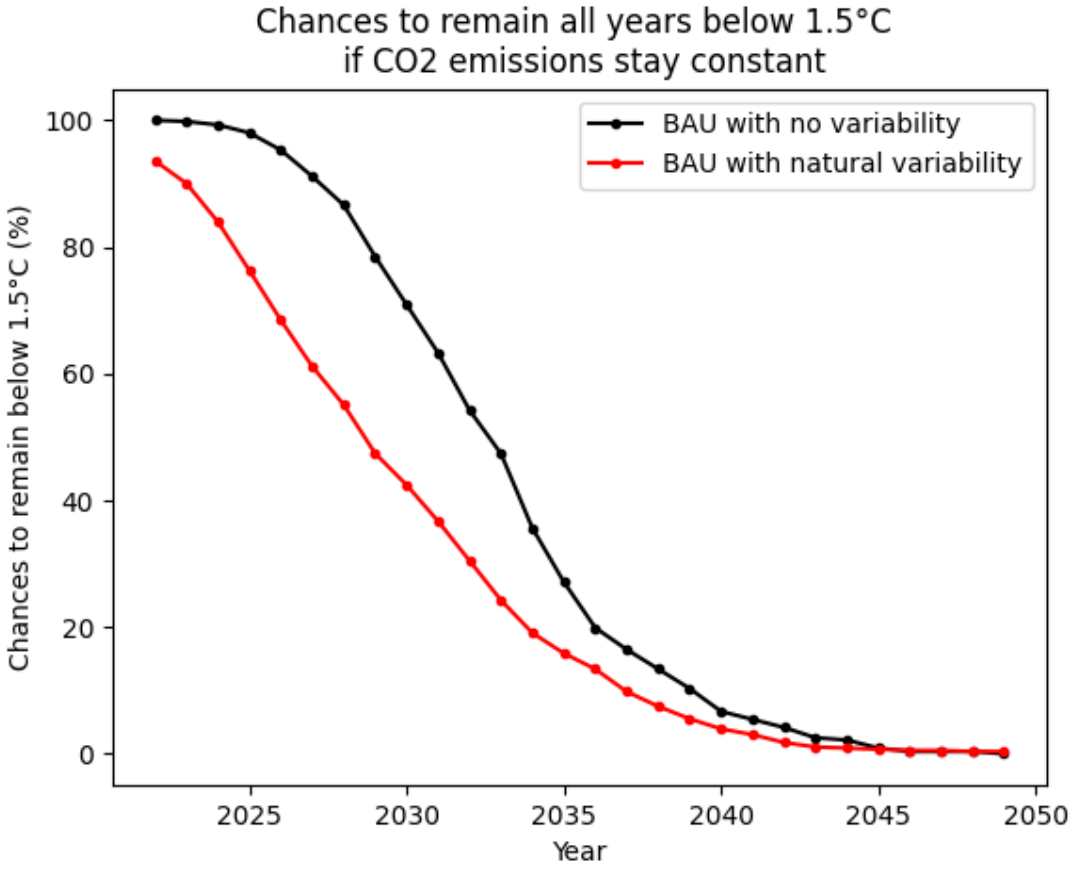

Supplementary Figure 2 Chances of remaining below 1.5°C if CO_2 emissions remain at current 2022 levels and if non-CO_2 RF follows a scenario in the middle range of the C6-C7 ensemble[16] from AR6 (corresponding to a combination of current policies and moderate actions). Black line indicates the results obtained without considering natural variability. Red line shows those including natural variability.

1 UNFCC. (ed UNFCC) (2022).
2 Friedlingstein, P. *et al.* Global carbon budget 2022. *Earth System Science Data* **14**, 4811-4900 (2022).
3 Tanaka, K. & O'Neill, B. C. The Paris Agreement zero-emissions goal is not always consistent with the 1.5 C and 2 C temperature targets. *Nature Climate Change* **8**, 319-324 (2018).
4 Boucher, O. *et al.* In the wake of Paris Agreement, scientists must embrace new directions for climate change research. *Proceedings of the National Academy of Sciences* **113**, 7287-7290 (2016).
5 Gulev, S. K., and Thorne, P. W., and Ahn, J., and Dentener, F. J., and Domingues, C. M., and Gerland, S., and Gong, D., and Kaufman, D. S., and Nnamchi, H. C., and Quaas, J., and Rivera, J. A., and Sathyendranath, S., and Smith, S. L., and Trewin, B., and von Shuckmann, K., and Vose, R.J. in *Climate Change 2021: The Physical Science Basis. Contribution of Working Group I to the Sixth Assessment Report of the Intergovernmental Panel on Climate Change* (ed Cambridge University Press) (2021).
6 Canadell, J. G., Monteiro, P. M. S., Costa, M. H., Cotrim da Cunha, L., Cox, P. M., Eliseev, A. V., Henson, S., Ishii, M., Jaccard, S., Koven, C., Lohila, A., Patra, P. K., Piao, S., Rogelj, J., Syampungani, S., Zaehle, S., and Zickfeld, K. in *Climate Change 2021: The Physical Science Basis, Contribution of Working Group I to the Sixth Assessment Report of the Intergovernmental Panel on Climate Change* (2021).
7 Lamboll, R. *et al.* Assessing the size and uncertainty of remaining carbon budgets. (2022).
8 Ou, Y. *et al.* Role of non-CO2 greenhouse gas emissions in limiting global warming. *One Earth* **5**, 1312-1315 (2022).
9 Forster, P., and Storelvmo, T., and Armour, K., and Collins, T., and Dufresne, J. L., and Frame, D., and Lunt, D. J., and Mauritsen, T., and Palmer, M. D., and Watanabe, M., and Wild, M., and Zhang, H. in *Climate Change 2021: The Physical Science Basis. Contribution of Working Group I to the Sixth Assessment Report of the Intergovernmental Panel on Climate Change* (ed Cambridge University Press) Ch. 7, 923-1054 (2021).
10 Morice, C. P. *et al.* An updated assessment of near-surface temperature change from 1850: the HadCRUT5 data set. *Journal of Geophysical Research: Atmospheres* **126**, e2019JD032361 (2021).
11 Tans, P. & Keeling, R. NOAA. *ESRL (www. esrl. noaa. gov/gmd/ccgg/trends/)* (2010).
12 Smith, C., Nicholls, Z. R. J., Armour, K., Collins, W., Forster, P., M. M., Palmer, M. D., and Watanabe, M. in *Climate Change 2021: The Physical Science Basis, Contribution of Working Group I to the Sixth Assessment Report of the Intergovernmental Panel on Climate Change* (2021).
13 Bossy, T., Gasser, T. & Ciais, P. Pathfinder v1. 0.1: a Bayesian-inferred simple carbon–climate model to explore climate change scenarios. *Geoscientific Model Development* **15**, 8831-8868 (2022).
14 Gasser, T., Ciais, P. & Lewis, S. L. How the Glasgow Declaration on Forests can help keep alive the 1.5° C target. *Proceedings of the National Academy of Sciences* **119**, e2200519119 (2022).
15 Riahi, K. *et al.* Mitigation pathways compatible with long-term goals. *Climate change* (2022).
16 Byers, E. *et al.* (International Institute for Applied Systems Analysis, 2022).
17 Liu, Z. *et al.* Global patterns of daily CO2 emissions reductions in the first year of COVID-19. *Nature Geoscience* **15**, 615-620 (2022).
18 Watson-Parris, D. & Smith, C. J. Large uncertainty in future warming due to aerosol forcing. *Nature Climate Change*, 1-3 (2022).
19 Programme, U. N. E. Emissions Gap Report 2022. (United Nations Environment Programme, 2022).
20 Wigley, T. The Paris warming targets: emissions requirements and sea level consequences. *Climatic Change* **147**, 31-45 (2018).

21 Geoffroy, O. *et al.* Transient Climate Response in a Two-Layer Energy-Balance Model. Part II: Representation of the Efficacy of Deep-Ocean Heat Uptake and Validation for CMIP5 AOGCMs. *Journal of Climate* **26**, 1859-1876, doi:10.1175/JCLI-D-12-00196.1 (2013).
22 Strassmann, K. M. & Joos, F. The Bern Simple Climate Model (BernSCM) v1. 0: an extensible and fully documented open-source re-implementation of the Bern reduced-form model for global carbon cycle–climate simulations. *Geoscientific Model Development* **11**, 1887-1908 (2018).
23 Gasser, T. *et al.* The compact Earth system model OSCAR v2. 2: description and first results. *Geoscientific Model Development* **10**, 271-319 (2017).
24 Gasser, T. *et al.* Path-dependent reductions in CO 2 emission budgets caused by permafrost carbon release. *Nature Geoscience* **11**, 830-835 (2018).
25 Ricciuto, D. M., Davis, K. J. & Keller, K. A Bayesian calibration of a simple carbon cycle model: The role of observations in estimating and reducing uncertainty. *Global biogeochemical cycles* **22** (2008).
26 Cummins, D. P., Stephenson, D. B. & Stott, P. A. Optimal Estimation of Stochastic Energy Balance Model Parameters. *Journal of Climate* **33**, 7909-7926, doi:10.1175/jcli-d-19-0589.1 (2020).
27 Leach, N. J. *et al.* FaIRv2. 0.0: a generalized impulse response model for climate uncertainty and future scenario exploration. *Geoscientific Model Development* **14**, 3007-3036 (2021).

3.2 . Inversion of the causal chain

In Chapter 2 we presented Pathfinder and demonstrated its robustness and reliability. Therefore, we could use it to assess the chances of staying below 1.5°C for a series of idealistic scenarios presented in the previous section. This small study follows the traditional causal chain which is also followed by the IPCC to create its reference scenarios. As we reflected on the limitations of this approach, we came up with the idea of using the features of Pathfinder to propose an entirely new framework for creating and analyzing innovative emissions scenarios.

The conventional method adheres to the natural causation of the Earth system, resulting in a limited number of scenarios. This limitation arises from the inflexibility and the complexity of the models, leading to a limited number of scenarios being analyzed in each IPCC cycle. Furthermore, these scenarios, built on socio-economic storylines, have little constraint on their potential future impact levels, which leads to a weak sampling of potential climatic impacts. Indeed, the future state of the climate system and its impacts are often overly simplified to a single physical variable: the average change in global surface temperature. While this simplification aids communication, it provides a vague and abstract understanding that masks the myriad of potential mitigation options and various climatic impacts (Hansen et al.; 2012; Riahi et al.; 2017; Seneviratne et al.; 2018).

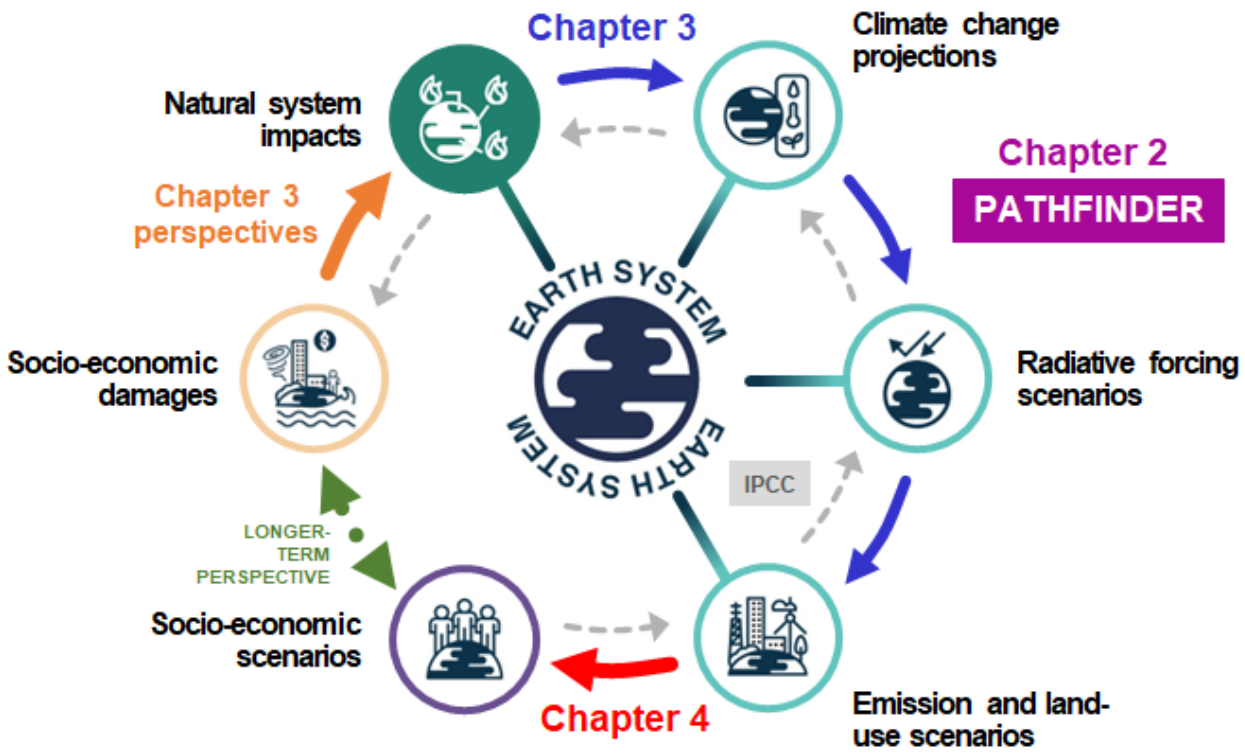

Figure 3.1: Synthesis of our approach to inverse the IPCC's natural causal chain

Here, we aim to introduce a more innovative and holistic approach, thereby addressing the limitations in the current method. By flipping the causal chain, we propose to explore future

climates from a fresh perspective. This innovative approach anchors itself on the physical modeling of the Earth system, essentially reversing the natural causality of the system (Figure 3.1). Climate objectives are defined in terms of system's physical variables. These set of trajectories are then numerically inverted to derive compatible anthropogenic emission trajectories. We want to further emphasize the importance of formulating climate targets in terms of impacts. These impacts are global (global temperature change, ocean acidification, sea level rise), but our approach is devoted to be enlarged to regional, or even socio-economic impacts (see section 3.4). The approach pays particular attention to potential incompatibilities and synergies between objectives that we define in terms of planetary boundaries in the next section.

The following chapters of this thesis will further elaborate on this innovative approach. Chapter 3 delves into the inverse approach from physical impacts to CO_2 emissions, and Chapter 4 will assess the cost of these CO_2 emissions. This approach aims to reflect on some limitations of the current IPCC approach, offering a comprehensive, flexible, and impact-focused methodology that can better inform climate change research and scenario makers.

Bibliography

Hansen, J., Sato, M. and Ruedy, R. (2012). Perception of climate change, *Proceedings of the National Academy of Sciences* **109**(37): E2415–E2423.

Riahi, K., van Vuuren, D. P., Kriegler, E., Edmonds, J., O'Neill, B. C., Fujimori, S., Bauer, N., Calvin, K., Dellink, R., Fricko, O., Lutz, W., Popp, A., Cuaresma, J. C., KC, S., Leimbach, M., Jiang, L., Kram, T., Rao, S., Emmerling, J., Ebi, K., Hasegawa, T., Havlik, P., Humpenöder, F., Da Silva, L. A., Smith, S., Stehfest, E., Bosetti, V., Eom, J., Gernaat, D., Masui, T., Rogelj, J., Strefler, J., Drouet, L., Krey, V., Luderer, G., Harmsen, M., Takahashi, K., Baumstark, L., Doelman, J. C., Kainuma, M., Klimont, Z., Marangoni, G., Lotze-Campen, H., Obersteiner, M., Tabeau, A. and Tavoni, M. (2017). The Shared Socioeconomic Pathways and their energy, land use, and greenhouse gas emissions implications: An overview, *Global Environmental Change* **42**: 153–168.

Seneviratne, S. I., Rogelj, J., Séférian, R., Wartenburger, R., Allen, M. R., Cain, M., Millar, R. J., Ebi, K. L., Ellis, N., Hoegh-Guldberg, O. et al. (2018). The many possible climates from the paris agreement's aim of 1.5 c warming, *Nature* **558**(7708): 41–49.

3.3 . Spaces of anthropogenic activities compatible with planetary boundaries

Abstract: The concept of planetary boundaries delineates the Earth system's limits within which humanity can sustainably prosper. While these boundaries are expressed in terms of maximum environmental impacts, translating them into actionable policies requires linking them to anthropogenic activities. Some boundaries are expressed directly in terms of anthropogenic activities, and the climate change boundary on temperature can be translated into a carbon budget. However, other boundaries such as ocean acidification have not been translated into anthropogenic activities and the effect of combining boundaries has not yet been addressed. Here, we introduce a new modelling framework to translate four 'planetary boundaries': two of the nine original boundaries (global warming, ocean acidification), and two new relevant ones for climate impacts (sea level rise and Arctic sea ice melt). Using a reduced-form carbon-climate model, we map a wide range of anthropogenic CO2 emissions and removals pathways compatible with these boundaries, accounting or not for solar radiation management (SRM) actions that would reduce warming. To account for uncertainties, our framework estimates 'safety levels' as probabilities that ensure adherence to these boundaries. For each combination of planetary boundaries, we either set the safety level and determine limits of the compatible spaces for emissions or we impose conditions on key characteristics to estimate an associated safety level. With CO2 emission peaking in 2030, achieving net-zero CO2 in 2100 would still require up to 10 PgC yr-1 of CDR but no SRM to ensure a safety level of the global warming boundary of 66%. This probability drops to 50% for when the sea level rise or the Arctic sea ice boundary cannot be surpassed. Considering the ocean acidification boundary further reduces the safety level to only 26%. Notably, the combination of all four boundaries results in a safety level of 12%, highlighting a non-linear relationship where the safety level is lower for all boundaries together rather than for any individual. These non-linear limits on compatible emissions when adding multiple boundaries emphasize the need to include multiple impact targets in future scenarios. Our framework offers insights for exploring and designing such new scenarios, aiding in the development of sustainable and resilient strategies for the future.

Spaces of anthropogenic CO_2 emissions compatible with planetary boundaries

Thomas Bossy, Thomas Gasser, Philippe Ciais, Katsumasa Tanaka, Franck Lecocq, and Philippe Bousquet

Abstract

The concept of planetary boundaries delineates the Earth system's limits within which humanity can sustainably prosper.

Here we introduce a new modeling framework to translate four "planetary boundaries": global warming, ocean acidification, sea level rise, and Arctic sea ice melt. Using a reduced-form carbon- climate model, we map a range of anthropogenic CO2 emissions and removals pathways consistent with these boundaries, accounting or not for solar radiation management (SRM) measures that would reduce warming. Our framework also estimates 'safety levels' as probabilities to stay within these boundaries, considering the uncertainties about the carbon cycle and climate physics.

Setting the CO2 emissions peak in 2030, net-zero CO2 in 2100, CDR deployment capacity of up to 10 PgC per year, and not allowing SRM ensure a safety level of 66% to remain within the global warming boundary. This probability drops to 50% for staying within the sea level rise or the Arctic sea ice boundary under the same conditions. When the ocean acidification boundary is considered, the safety level drops further to 26%. When all four boundaries are considered together, the safety level drops to only 12%, indicating a complex interplay of planetary boundaries in determining the safety level.

Our results suggest a need to assess planetary boundaries holistically to develop sustainable future strategies.

Introduction

Planetary boundaries define a safe operating space within which humanity can continue to develop and prosper[1,2]. Staying within physical boundaries implies limiting the level of anthropogenic interference to the earth system. Therefore, there is a space of CO_2 emissions compatible with every planetary boundary and with their combinations[3]. This compatible emission space (henceforth 'compatible space') has so far been explored for individual planetary boundaries, for instance limiting phosphorus or nitrogen fertilizers inputs[4-6], or for the global warming boundary of 2°C[7-9]. There is however no systematic exploration of the compatible space for multiple boundaries combined.

Here, we introduce a modeling framework to systematically explore the compatible space for four critical Earth system boundaries: global warming, ocean acidification, sea level rise (SLR) and Arctic sea ice melt. While global warming and ocean acidification are original boundaries of Rockstrom et al.[1], the other two give complementary insight on climate-related impacts. We estimate how the compatible space is shaped by different boundaries, individually or as a constellation.

The remaining carbon budget[7], the total amount of CO_2 that can be emitted before reaching a given global warming level, is an indicator used to summarize the space compatible with the global warming boundary. This concept is based on the near-linear relationship[10] between cumulative anthropogenic CO_2 emissions and global warming. However, the carbon budget is insufficient to summarize spaces compatible with other planetary boundaries, as there is no near-linear relationship between emissions and pH[11] or SLR[12].

To summarize compatible spaces of emissions under multiple boundaries, we focus on four indicators derived from the emission timeseries defining the space: the maximum annual amount of Carbon Dioxide Removal (CDR), the year of net-zero CO_2 emissions, the year of peak CO_2 emissions, and the maximum annual amount of Solar Radiation Management (SRM) in case this option is considered.

Possible emissions constrained by planetary boundaries

To derive the compatible space of emissions without ex-ante socioeconomic constraints, we propose a backward (or inverse) approach using the Pathfinder carbon climate model. Pathfinder is a reduced-complexity model calibrated through Bayesian inference on state-of-the-art complex Earth system models and constrained using observational and IPCC AR6 data[13]. Ex-ante atmospheric CO_2 concentration and global temperature timeseries were generated randomly with analytical expressions as input to Pathfinder until year 2500 (Methods). The model is then used to back-calculate compatible CO_2 emissions through mass balance, given its simulation of the land and ocean carbon sinks, including permafrost emissions. The non-CO_2 radiative forcing was obtained by inversion of the energy balance equations of the climate module. We estimated CDR and SRM as subcomponents of CO_2 emissions and non-CO_2 radiative forcing, respectively. To do so, we took the most mitigation-intensive trajectories, without the use of negative emission technologies, from the AR6 scenarios database[14] (Methods) as a mitigation floor[15]. If a Pathfinder emission pathway was lower than this floor, we attributed the gap to CDR or SRM. Pathfinder emulates physical variables related to our planetary boundaries: pH at the oceanic surface, SLR, and Arctic sea ice (Methods). To account for the Earth system's physical uncertainty, the model is run under 1500 different configurations in which parameters are drawn from the posterior probability distribution obtained after the Bayesian calibration and represent equally likely physical states of the world (Methods). The combination of these configurations with the thousands of ex-ante pathways gives us several million possible futures that we use to map the space of emissions compatible with staying within planetary boundaries.

The temperature pathways that we generate all stay below +2°C and asymptotically reach +1.5°C, which by construction makes them remain within the global warming planetary boundary[1,16]. We introduce three additional boundaries, as explained above: i) avoiding a collapse of the Arctic sea ice in summer, which is equivalent to not exceeding 1.7 ± 0.2°C of global warming[17], ii) avoiding ocean acidification with a pH decrease limited to -0.2 unit compared to the pre-industrial level, a threshold beyond which oceanic biodiversity integrity may be threatened[18-20], and iii) remaining below 5 cm of SLR per decade, a precautionary threshold consistent with previous studies[18,19].

Because our framework accounts for uncertainty about the carbon cycle and physical climate (see Box and Figure 1), we can define the concept of safety level as the percentage of physical configurations finding at least one emissions pathway compatible with one or more planetary boundaries in a space of emissions bounded by constraints on the key characteristics. To map a compatible space, we determine the limit value of a pathway characteristics beyond which a planetary boundary is breached for a given safety level. For instance, 2037 is the limit on the peak date of CO_2 emissions for the global warming boundary with a 67% safety level if there is at least one pathway staying below 2°C with a peak CO_2 emissions date greater than or equal to 2037 in 67% of the model equiprobable physical configurations. When we use the concept of safety level, safe pathways are not necessarily the same in the different physical configurations. The safety level is then different from the IPCC's definition of confidence level[21,22] that is the probabilistic assessment across different physical configurations of the compatibility of a given emission pathway with one or several planetary boundaries. The limits of a compatible space can be explored for one or multiple planetary boundaries. However, in a safe configuration, other pathways with the same characteristic as the limits of the compatible space do not necessarily adhere to the planetary boundary. For "safer limits", we investigated alternative definitions of the compatible space in Methods.

Box: Method to determine compatible spaces

Figure 1 illustrates, step by step, our backward approach. First, we generate around 15,000 trajectories of global mean surface temperature and atmospheric CO_2 concentration that follow historical data and asymptotically reach 1.5°C with an overshoot up to the 2°C warming level (see Methods). Those trajectories are used as inputs to Pathfinder (step 1). To account for physical uncertainties, we run the model (step 2) with 1500 sets of parameters that can be seen as 1500 possible states of the world with their own physics, all independent and calibrated on historical observations.

All pathways stay below the +2°C global warming boundary by construction, and we define conditions on CO_2 anthropogenic emissions and non-CO_2 radiative forcing that we consider realistic: in step 3, we exclude pathways rising too quickly (quicker than the most pessimistic pathway from AR6 scenarios) or using too much CDR (more than 10 PgC yr^{-1}). We use the envelope of all the pathways that stay within a given boundary to illustrate the compatible space. We compare the envelope of the default space compatible with the global warming boundary (black envelope) with envelopes obtained for other planetary boundaries, either independently (green envelope for ocean acidification in Figure 1, step 3) or combined (purple envelope). As explained in main text, respecting more boundaries leads to narrower envelopes.

The next steps are illustrated with the ocean acidification boundary only. To express the compatible space in terms of key characteristics, we search for limit values of the characteristics for which there remains one last pathway in the compatible space. In Step 4 we extract three of those final pathways that show that delaying the CO_2 emissions peak requires to deploy more CDR.

In step 5, we represent the compatible space of CDR deployment and CO_2 emission peak associated with the ocean acidification boundary. Inside this compatible space, the model always finds at least one pathway compatible with the given boundary (here, ocean acidification). The limit of the domain gives the trade-off between the two pathway characteristics that are represented assuming conditions on other key characteristics remain unchanged.

These successive steps are illustrated for one Pathfinder configuration only but were repeated for all 1500 configurations. Therefore, for a given set of conditions on pathway characteristics and planetary boundaries, we assess the existence of at least one compatible pathway in all individual physical states of world (i.e. configurations). We define the safety level (in %) as the percentage of configurations that find at least one emissions pathway compatible with one or more planetary boundaries.

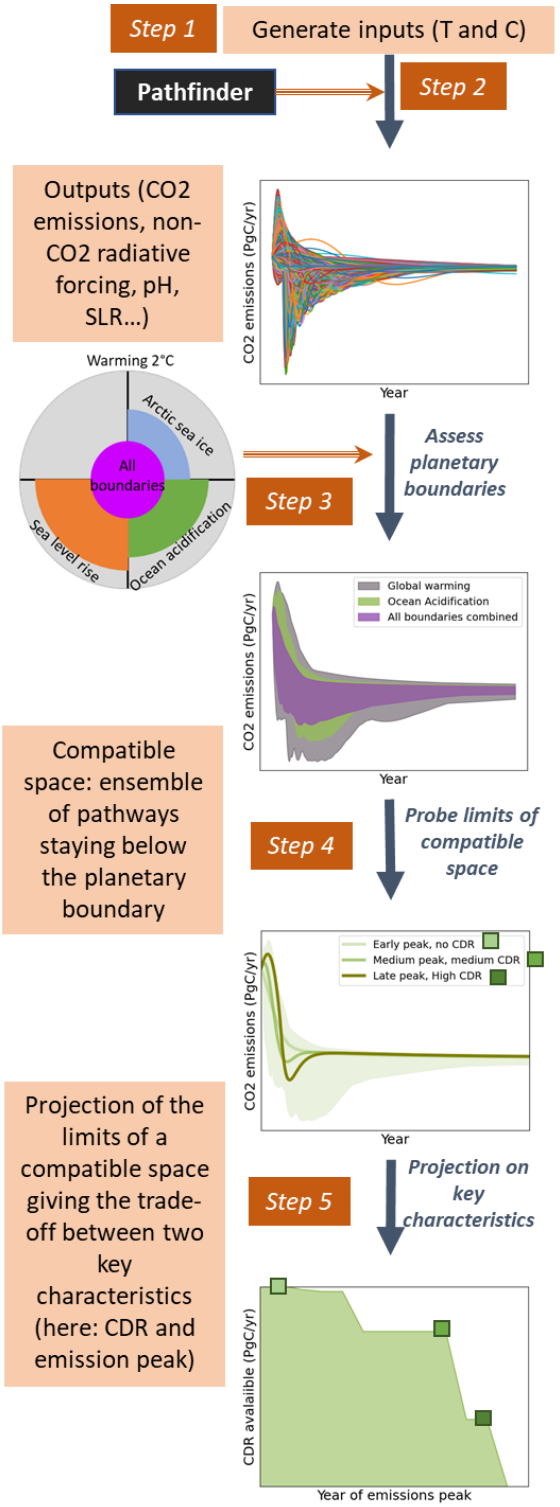

Figure 1: Overview of the interpretative framework applied in this study on one of the 1500 configurations of Pathfinder. We reiterate this process on all configurations to take physical uncertainty into account. We define the safety level (in %) as the percentage of configurations that find at least one emissions pathway compatible with one or more planetary boundaries for a given set of conditions on pathway characteristics. See Box text for a detailed step-by-step walkthrough.

Results

Implications of planetary boundaries for emissions peak, CDR, and net-zero

First, we verified that our ensemble of emission trajectories encompasses all IPCC AR6 scenarios[14] that keep temperature below 2°C (the so-called C1, C2 and C3 categories) (Figure S1). We found that without any CDR, it is possible to respect the global warming boundary with a safety level of only 20%, even if CO_2 emissions peak in 2025. With a peak in 2025, safety levels for no-CDR scenarios are kept at 20% for the SLR boundary, reduce to 19% for the ocean acidification boundary, 15% for the arctic sea ice boundary, and also 15% for all four boundaries combined. In contrast, if large amounts of CDR are assumed (up to 10 PgC yr^{-1}), the global warming boundary safety level is at 86% even with a later peak in 2035, and decreases to 83% for the SLR boundary, 64% for the arctic sea ice boundary, 53% for the ocean acidification boundary and only 28% for all boundaries combined (Figure 2). The results indicate that the restriction of the compatible space is non-linear when combining boundaries. The gap in safety levels between no-CDR scenarios with early peak emissions and CDR scenarios with with late peak emissions highlight the fact that CDR 'buys some time' by delaying the peak of emissions.

Figure 3 (see also Figure S2) showcases the trade-offs between the year of peak emission and the amount of assumed CDR at a 67% safety level for each planetary boundary and their combination. The slope of the frontier in Figure 3a quantifies the deployment of (maximum annual) CDR required to compensate a delay in the peak date. For example, peaking in 2023 requires less than 2 PgC yr^{-1} of CDR, while peaking in 2030 requires at least 5 PgC yr^{-1} of CDR to stay under the global warming boundary. Over a range of peak dates going from 2023 to 2030, the SLR and acidification boundaries are met with the same safety level if the global warming boundary is also met. The arctic sea ice boundary, however, requires a stricter compatible space and necessitates an additional 1 PgC yr^{-1} of CDR. Finally, remaining below all the boundaries with peak emissions later than 2030 increases the requirements for CDR, up to the assumed maximum value of 10 PgC yr^{-1}. Even for this maximum level of CDR, the ultimate dates for emissions to peak is 2033 to remain below all boundaries, 2034 for the arctic sea ice and acidification boundaries, 2036 for the SLR boundary, and 2037 for the global warming boundary alone.

While delaying the peak of CO_2 emissions can be compensated to a certain extent by the deployment of CDR, the deployment of CDR does not need to happen in the short term. Even for the ambitious target of keeping within all boundaries with a 67% safety level, CDR does not appear at significant levels (>0.5 PgC yr^{-1}) before 2080 (Figure S3). To respect the global warming boundary alone, CDR does not need to be significantly deployed before 2100, as long as CO_2 emissions peak before 2030. In contrast, IPCC's AR6 trajectories usually deploy CDR in the second half of the 21st century to remain within a Paris-compliant global warming boundary[8,23]. We explain this difference to our results by our longer timeframe extended until 2500, the absence of a technical learning curve for CDR constraining Pathfinder, and our assumption that CDR arrives only after emissions have reached a mitigation-intensive floor, while AR6 models deploy CDR simultaneously to mitigation efforts[24].

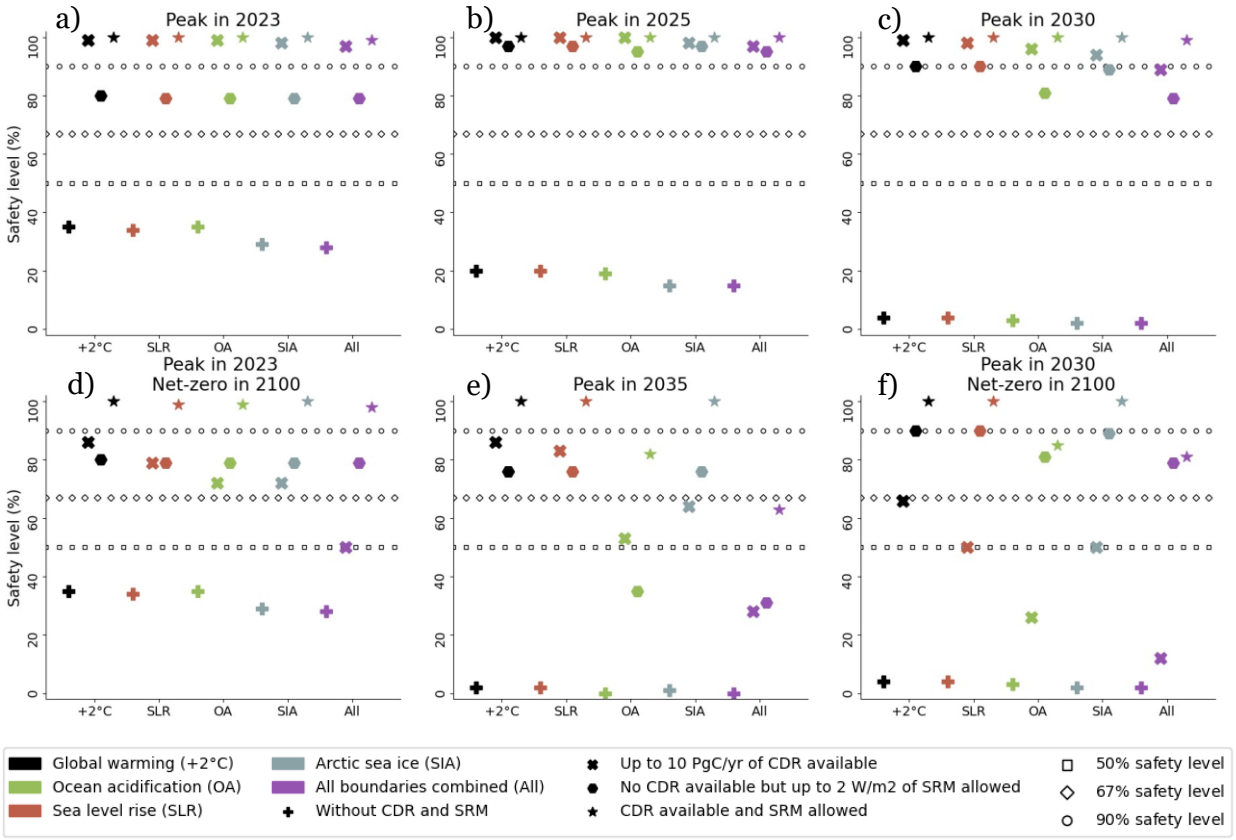

Figure 2: Safety levels of compatible spaces defined by various combinations of conditions on pathway characteristics. Panels a) to f) distinguish conditions on the date of CO_2 emissions peak and of net-zero. *Net-zero in 2100* means that CO_2 net-zero is reached in 2100 or later. No information on net-zero means that this pathways characteristic is not constrained. *Peak in 2023, 2025, 2030 and 2035* means that the compatible CO_2 pathways reaches their peak in 2023, 2025, 2030, or 2035. Markers distinguish conditions on speculative technologies, *Up to 10 PgC yr^{-1} of CDR* assumes that SRM will never be available while CDR will be available, possibly up to 10 PgC yr^{-1}. *No technologies* assumes that neither SRM nor CDR will be available. *CDR available and SRM allowed* assumes SRM being possibly used up to 2 W m^{-2} in addition to CDR. Finally, the *SRM replaces CDR* case assumes that CDR will never be available but SRM can be used up to 2 W m^{-2}. Marker lines show the 90% safety level, 67% safety level and 50% safety level.

We found that reaching net-zero CO_2 emissions in the 21st century is not absolutely required to remain within planetary boundaries. Figure 2 shows that achieving net-zero later than 2100 is mainly a threat to planetary boundaries in the case of a late emission peak. For instance, staying within the acidification boundary with a CO_2 emission peak in 2023 and up to 10 PgC yr^{-1} of CDR has a 99% safety level if net zero must be reached before 2100, which drops to 72% if net-zero is reached later than 2100. Similar drops are observed for the global warming boundary (99% to 86%), the Arctic sea ice boundary (98% to 72%), the SLR boundary (99% to 79%) or all boundaries (97% to 50%), giving another illustration of the non-linear effect of combined boundaries. The same values but with a peak in 2030 results in a drop of from 96% to 26% for the acidification boundary, from 99% to 66% for the global warming boundary,

from 94% to 50% for the Arctic sea ice boundary, from 98% to 50% for the SLR boundary, and from 89% to 12% for all boundaries. Altogether, the drop in the safety level due to a late net zero is significantly larger for a peak in 2030 than for a peak in 2023. It demonstrates that reaching net-zero earlier mainly helps to offset a late peak in emissions.

Figure 3b quantifies the trade-off between net-zero and peak emissions for all boundaries at the 67% safety level. With a peak in 2023, net-zero does not have to be reached before 2100 to remain within any single planetary boundary as also shown in Figure 2. However, remaining within all boundaries together requires net-zero to occur no later than 2075. Delaying the peak of emissions requires net-zero CO_2 emissions to occur earlier in the second half of the 21st century. A late peak means more emissions to compensate for and fewer time to compensate them, to remain below 2°C. For the SLR boundary, we find pathways that peak in 2037 if net-zero is reached in 2075 whereas if net-zero is reached in 2100, emissions must peak by 2025 at the latest. This example shows a stronger effect of short term-action on reducing emissions: delaying the peak by 12 years requires to bring net-zero (i.e. long-term action) forward by 25 years.

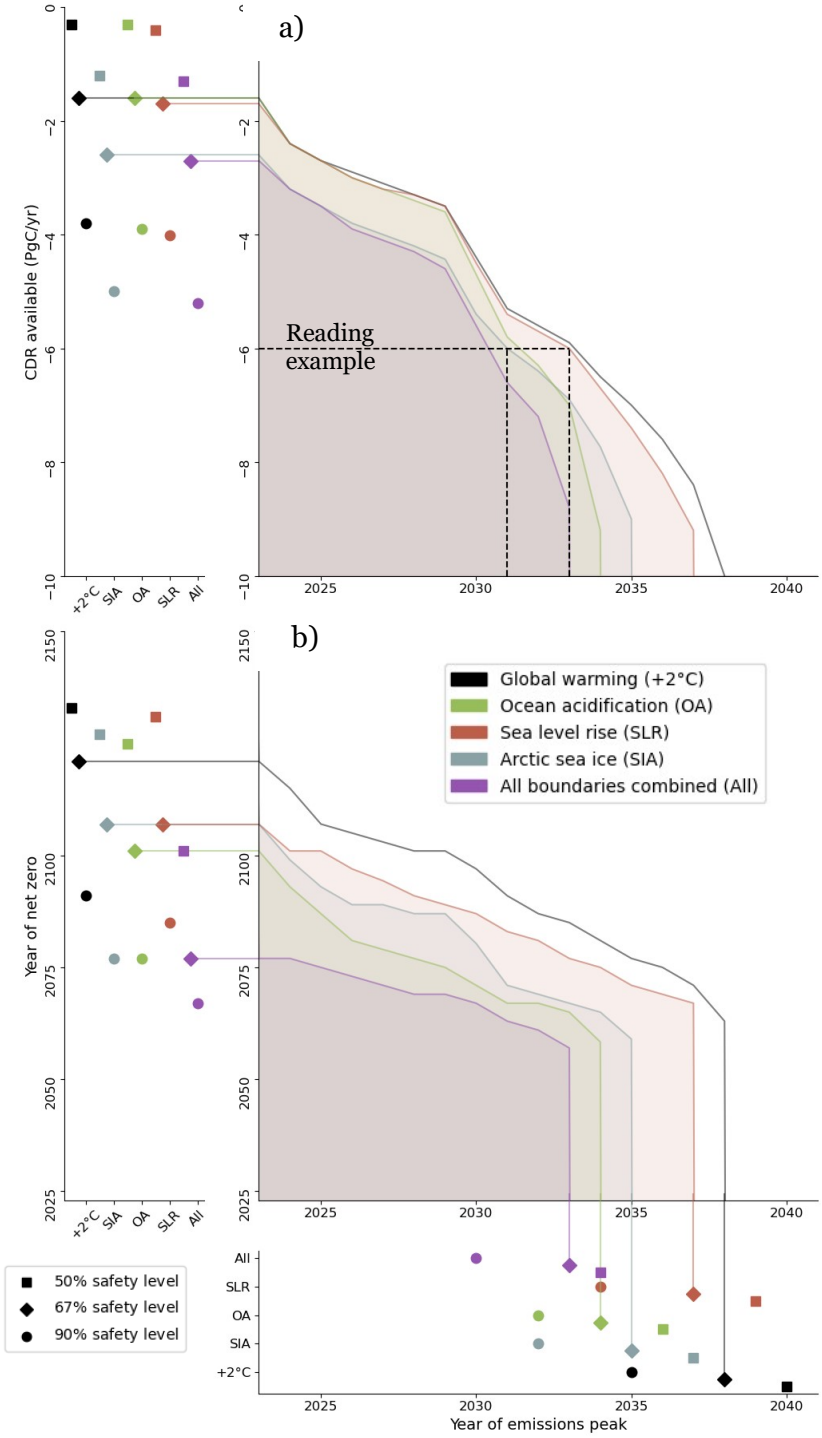

Figure 3: Trade-offs between pathway characteristics for 67% safety level. Panel a) gives compatible spaces depending on CDR availability (PgC yr^{-1}) and the year of CO_2 emissions peak. Panel b) gives compatible spaces depending on the years of CO_2 emissions net-zero and peak. Shaded areas represent the spaces compatible with planetary boundaries and their combination. Plain lines give the frontier of the compatible space: at the right or above these lines, it is not geophysically possible to stay below the boundary. Markers plots show the limit of the compatible space if the other pathway characteristic is not constrained and for three safety levels: 50% (squares), 67% (diamonds) and 90% (circles). Black is

for the global warming boundary, green for the ocean acidification boundary, red for the SLR boundary, blue for the Arctic sea ice boundary, and purple for the combination all boundaries.

Reading example with black dashed lines on panel a): If up to 6 PgC yr^{-1} of CDR are available, all boundaries can be respected with a peak in 2030, the Arctic sea ice and acidification boundaries with a peak in 2031 and the SLR and global warming boundaries with a peak in 2033.

Adding solar geoengineering to the compatible space

Considering solar geoengineering to mitigate climate change raises ethical questions as this technology has potential unexpected consequences[24]. We nevertheless investigated whether SRM could help extend the compatible space of emissions. Indeed, some Pathfinder's ex-ante pathways exhibit a non-CO_2 radiative forcing lower than the most ambitious AR6 scenario in reducing short-lived climate forcers. We explain these pathways with low non-CO_2 radiative forcing by the deployment of SRM (see above and Methods). Allowing the use of SRM in addition to CDR improves the safety level of the compatible spaces for a late peak in CO_2 emissions. With SRM, the safety level is of 65% for an emission peak in 2035 when respecting all boundaries, compared to 30% without SRM (Figure 2). Specifically, there is a trade-off between postponing the year of peak CO_2 emissions and implementing SRM (Figure 4) for all boundaries excepted acidification. We see that allowing up to 2W m^{-2} of SRM only allows to delay peak emissions by 3 years (2037 instead of 2034) to keep within the acidification boundary with a safety level of 67%. This lack of beneficial impact of SRM is because acidification depends on increased atmospheric concentration of CO_2, which is only marginally impacted by global temperature change under our model assumptions.

Our approach also allows to quantify SRM as a substitute for CDR in the case of a late peak in emissions, when CDR is significant. If the peak is later than 2030, SRM could work as a substitute for CDR: at a 67% safety level, there is a substitution of ≈ 1 PgC yr^{-1} of CDR for 0.2 W m^{-2} of SRM allowed, to stay within any individual or combined boundary (Figure S4). This trade-off is also valid for the ocean acidification boundary as, in this study, CDR is mainly used for net negative CO_2 emissions that cause a decrease in atmospheric CO_2 concentration. Therefore, trading CDR for SRM does not necessarily imply an increase in atmospheric CO_2 concentration and does not increase the probability of crossing the pH threshold relative to the acidification boundary.

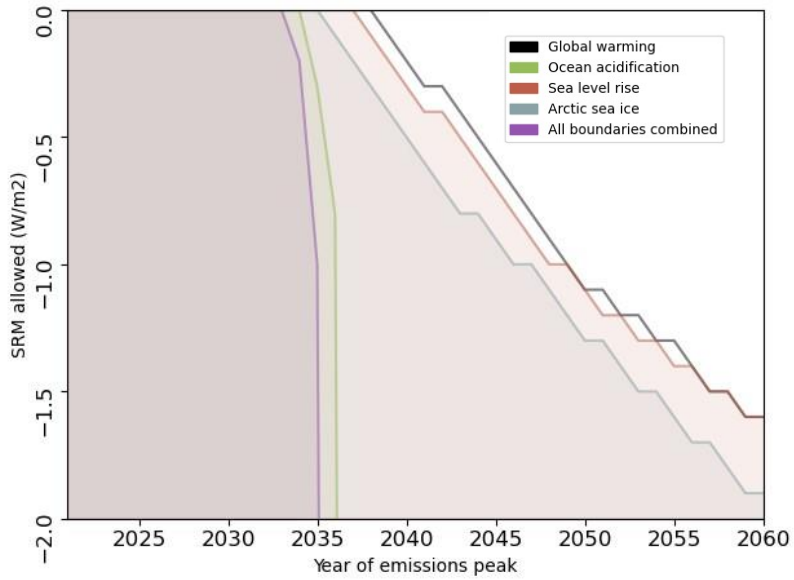

Figure 4: Trade-offs between the year of CO_2 emissions peak and the amount of SRM (W m^{-2}) allowed for a 67% safety level. Shaded areas represent the spaces compatible with one planetary boundary. Plain lines give the frontier of the compatible space. Black is for the global warming boundary, green for the ocean acidification boundary, red for the SLR boundary, blue for the Arctic sea ice boundary, and purple for the combination all boundaries

Discussion

Despite nonlinear safety level reductions when planetary boundaries are combined, this study shows that there is a low probability of meeting climate-related planetary boundaries without CDR if CO_2 emissions peak before 2025. Significant CDR implementation may allow for a later emissions peak but the trade-off is limited and peaking later than 2030 seriously jeopardizes the chances to remain within planetary boundaries. Other relevant results suggest that ambitious CDR need not be deployed before the late 21st century and that early net-zero emissions (between 2050 and 2075) can offset later peaks. In addition, the inclusion of SRM can improve the safety level, but the impact on acidification is limited due to the dominant role of atmospheric CO_2 concentration on this specific impact.

Our results show that assumptions about the level of future CDR and SRM have a significant impact on the space of anthropogenic activities compatible with planetary boundaries, in line with previous results[15,25-27]. Our backward approach only infers compatible global CO_2 emissions or non-CO_2 effective radiative forcing. That is why we define CDR and SRM as additional mitigation solution when a floor of positive emissions is reached (see Method). This floor being the lower bound of the AR6 scenarios envelope[14] without these technologies, we assume that all possible mitigation efforts have been made before resorting to CDR or SRM.

It is generally accepted that global warming primarily depends on the cumulative CO_2 emissions budget, rather than the magnitude or timing of emissions peaks[28]. As a result, long-term mitigation strategies often prioritize achieving a net-zero CO_2 emissions target[29]. However, the diversification of boundaries diminishes the relevance of carbon budget as a unique indicator to define compatible spaces of emissions[7]. Our study highlights the importance of considering additional key mitigation characteristics to comprehensively map the space of compatible future CO_2 emissions. In particular, the timing of peak CO_2 emissions emerges as a key factor in trade-off mechanisms. We have quantified how an earlier emissions peak can enable a shift in the net-zero CO_2 date, reduce the need for CDR measures, and even eliminate the need for SRM techniques. This concept extends the notion of a "closing door" introduced by Stocker[30], who examined the relationship between the starting date of mitigation efforts, the mitigation rate, and the attainment of a specific temperature target. In addition, considering different planetary boundaries independently changes the compatible space, and combining them further narrows it. The four planetary boundaries could be supplemented by additional boundaries arising from physical or anthropogenic impacts of climate change. The selected thresholds are also subject to debate due to the inherent uncertainties and judgement values associated with quantifying planetary boundaries[2,31]

The trade-off between peak emissions and negative emissions has already been highlighted in the results of IAM-based projections, but the current AR6 scenario's framework[14] explored a narrower range of pathways than our study, often with strong negative emissions in the second half of the 21st century[25,32], without inclusion of SRM, and limited to the 2100 horizon. Here, we produced ex-ante a large ensemble of pathways, ignoring socioeconomic and technological constraints, which allows us to search for original scenarios consistent with the Paris Agreement that were not analyzed by IAMs. Figure S1 illustrates that Pathfinder covers a wider range of possible pathways than was explored by the IAMs. Although the IAMs propose scenarios that respect all planetary boundaries, they are based primarily on the global warming boundary and do not explore all alternatives.

The non-linearity of boundary combinations argues for diversification of climate impact indicators to be considered ex-ante by scenario developers. It is instructive and complementary to IAMs to expand the scope of emissions compatible with these boundaries. Even if these pathways turn out not to be economically optimal, it is critical to first draw what is physically possible and then decide what is socioeconomically feasible. To assess the relevance of a pathway in the socioeconomic dimension, coupling of Pathfinder with an IAM or simple impact models seems a natural next step in our work, as it would allow the exploration of compatible spaces that are also constrained in the socioeconomic and technological dimensions.

In summary, the framework developed in this study can contribute to enhancing dialogue among the Earth system, impacts, and integrated assessment modeling (IAM) communities and encourage scenario narratives that explore a wider range of possible futures in an integrated manner.

Methods

Description of Pathfinder

The Pathfinder model. It is a compilation of existing formulations that describe parts of the Earth system, chosen for their good balance between mathematical simplicity and physical accuracy, and brought together to form a consistent carbon-climate model of reduced complexity. Here, the global temperature anomaly (T) and global atmospheric CO_2 concentration (C) are given as independent inputs to the model. The model has 73 parameters. 29 of them are fixed and the other 44 parameters constrained through a Bayesian calibration[33] based on observations and AR6 assessments, as detailed in a previous paper[13]. The drivers (T and C) have been updated with the latest observations available until 2021. However, the model is not designed to provide insights for 2022, the first year of the simulation, due to the functional form used to generate scenarios. We thus show and discuss the results only from 2023 onward.

A comprehensive description of Pathfinder is provided in Bossy et al. [34], and briefly summarized here. The climate subcomponent that links T to effective radiative forcing (R) follows a widely used 2-box model with deep ocean heat uptake efficacy[35]. The total R is caused by atmospheric CO_2 (following the IPCC AR5 logarithmic formula[36]) and an aggregate of non-CO_2 species. Anthropogenic CO_2 emissions are determined by the balance between atmospheric CO_2, ocean and land carbon sinks, and permafrost carbon emissions. The ocean carbon cycle follows the structure of the Bern Simple Climate Model[37]. The land carbon cycle follows the formulation of the compact Earth system model OSCAR[38], although it is aggregated into one global biome, land cover change is ignored, and it accounts for the so-called passive soil carbon that is ignored in most complex models[39]. It leads to a total of four land carbon pools. Emissions from permafrost thaw are calculated with the emulator developed by Gasser et al.[40], but aggregated into one unique region. Sea level rise is split into thermosteric, glaciers, Greenland and Antarctica effects that each follows a first-order differential equation[12,41]. Additionally, ocean surface acidification follows a polynomial fit on C[42].

The use of Bayesian inference allows for the integration of observational data into simplified models like Pathfinder[33]. This approach involves deriving joint probability distributions of parameters based on prior knowledge of those distributions and the distributions of observed variables in the model. The posterior probability of a sample from the joint parameter distribution, given a set of observations, is proportional to the likelihood of the model simulating the observations and the prior probability of the parameters. The 44 Pathfinder parameters estimated using Bayesian inference are constrained using a set of 18 observations pertaining to most aspects of the global Earth System[13]: : T (present-day value and derivative across five datasets[43-47]), ocean heat content[48], non-CO_2 radiative forcing[36], recent global carbon budget[49] (for land, ocean, and atmosphere), preindustrial carbon pools[50] (land and atmosphere), and satellite-derived sea level rise speeds[51]. The prior distributions of the parameters are determined based on literature values and multi-model ensembles. To estimate the posterior distributions, a full-rank Automatic Differentiation Variational Inference (ADVI) algorithm is used[52], and the Pathfinder model is solved using an explicit Eulerian exponential integrator scheme. The paper by Bossy et al.[13],

provides detailed information on the parameter and observational constraints, as well as diagnostic tests to validate the model.

Input trajectories

We randomly and independently draw temperature and atmospheric CO_2 concentration trajectories using 4 different approaches grouped into "series" (Figure S5 and S6 for illustration). Series 1, 2 and 3 correspond to different analytical expressions while series 4 is derived from AR6 scenarios[14]. All series are divided in sub-series that have common constraints: (1) $T, \frac{d}{dt}T$ and C are defined and differentiable; (2) We impose an upper boundary so that $T \leq 2^{\circ}C$; (3) We also impose $\lim_{t\to\infty} T = 1.5^{\circ}C$; (4) We randomly choose an asymptotic value for C which is determined by the share $k_{x,final}$ of non-CO_2 components in the global radiative forcing. $k_{x,final}$ is uniformly drawn from one of three equiprobable ensembles: $k_{x,final} \in]-1;-0.1[$; $k_{x,final} \in [-0.1;0.1]$; $k_{x,final} \in]0.1;0.66[$

In Series 1, for X being T or C, we choose X of the form $X(t) = X_0 + (X_{lim} - X_0) \cdot \omega(t - t_0) + \alpha \cdot t \cdot (1 - \omega(t - t_0))$, with $X_0 = X(t{=}t_0)$ the initial value of X given by the historical calibration, with t_0=2021, and X_{lim} the asymptotic value. We determine α so that $\left.\frac{dX}{dt}\right|_{t=t_0} = \left.\frac{dX}{dt}\right|_0$, where $\left.\frac{dX}{dt}\right|_0$ is the differentiated variable given by the historical calibration in 2021.

$\omega(t)$ is the function we use to distinguish the sub-series. This function must tend towards 0 for t = 0 and towards 1 for $t \to \infty$. To keep the continuity and differentiability for X and $\frac{dX}{dt}$, ω must be continuously differentiable at least once. In series 1a, $\omega(t) = 1 - e^{-\mu_0 t - \mu_1^2 t^2}$ [53], in series 1b, $\omega(t) = \frac{t}{\mathrm{t} + \mu_1 e^{-\mu_0 t}}$, and in series 1c, $\omega(t) = \frac{\mu_0 t^2 + \mu_1 t}{1 + \mu_0 t^2}$. Parameter distributions are given in Table S1.

Series 2 follows the probability density function of a Kumaraswamy distribution[54] until it peaks (i.e. for $t < t_{peak}$), $\mathrm{X}(t < t_{peak}) = \mathrm{X}_0 + [X_{peak} - \mathrm{X}_0] \cdot [1 - (1 - (\tau_o / (\tau_o - t_{peak}))^{\alpha})^{-\beta} \cdot (1 - ((\tau_o - t) / (\tau_o - t_{peak}))^{\alpha})^{\beta}]$. Peaking dates ($t_{peak}$) and peaking values ($X_{peak}$) are chosen randomly in ensembles that are compatible with our constraints and for which we can maintain continuity and differentiability of X and $\frac{dX}{dt}$. τ_o is defined such as $f(\tau_o) = -t_{peak}$ with $f(t) = -t \cdot ((1 - \frac{t_{peak}}{t})^{\alpha} - 1) - \alpha \cdot \beta \cdot \frac{X_{peak} - \mathrm{X}_0}{\left.\frac{dX}{dt}\right|_0}$. Sub-series have different functional forms after the peak ($t > t_{peak}$) to converge to the asymptotic value X_{lim}. Series 2a follows the probability density function of a normal distribution such as $\mathrm{X}(t \geq t_{peak}) = X_{lim} + (X_{peak} - X_{lim}) \cdot e^{-\frac{(t - t_{peak})^2}{\tau^2}}$. With $\tau = \frac{\sqrt{X_{peak} - X_{lim}}}{\sqrt{X_{peak} - X_0}} \cdot (t_{peak} - \tau_o) \cdot \left(1 - \left(-\frac{\tau_o}{t_{peak} - \tau_o}\right)^{\alpha}\right)^{\beta/2} \cdot \sqrt{\frac{2}{\alpha^2 \cdot \beta \cdot (\beta - 1)}}$. Series 2b follows the probability function of a log-normal distribution so $\mathrm{X}(t \geq t_{peak}) = X_{lim} + (X_{peak} - X_{lim}) \cdot e^{-0.5\frac{log(t/t_{peak})^2}{\sigma^2}}$. With $\sigma = \frac{\sqrt{X_{peak} - X_{lim}}}{\sqrt{X_{peak} - X_0}} \cdot \left(1 - \frac{\tau_o}{t_{peak}}\right) \cdot \left(1 - \left(-\frac{\tau_o}{t_{peak} - \tau_o}\right)^{\alpha}\right)^{\beta/2} \cdot \sqrt{\frac{2}{\alpha^2 \cdot \beta \cdot (\beta - 1)}}$. Series 2c follows the probability function of a Gompertz distribution[55]: $\mathrm{X}(t \geq t_{peak}) = X_{lim} + (X_{peak} - X_{lim}) \cdot \eta^{1 - t/t_{peak}\ e^{1 - \eta^{1 - t/t_{peak}}}}$. With $\eta = exp\left(\frac{\sqrt{X_{peak} - X_{lim}}}{\sqrt{X_{peak} - X_0}} \cdot \left(1 - \frac{\tau_o}{t_{peak}}\right) \cdot \left(1 - \left(-\frac{\tau_o}{t_{peak} - \tau_o}\right)^{\alpha}\right)^{-\beta/2} \cdot$

$\sqrt{\frac{2}{\alpha^2 \cdot \beta \cdot (\beta-1)}}\Big)$. We apply all three sub-series to the temperature but only series 2a and 2c to the atmospheric CO_2 concentration. Parameter distributions are given in Table S1.

Series 3 follows the solution of a damped harmonic oscillator differential system with non-zero initial positions and velocities. Depending on sub-series, it is either in a critical regime (series 3a) under the form $X(t) = X_{lim} + (\mathrm{X}_0 - X_{lim} + (\kappa \cdot (\mathrm{X}_0 - X_{lim}) + \frac{dX}{dt}\Big|_0) \cdot t) \cdot e^{-\kappa t}$, or in an over-critical regime (aperiodic) for series 3b, $X(t) = X_{lim} + [(\mathrm{X}_0 - X_{lim}) \cdot cosh(\sqrt{\kappa^2 - \Omega^2} \cdot t) + \frac{\kappa \cdot (\mathrm{X}_0 - X_{lim}) + \frac{dX}{dt}\Big|_0}{\sqrt{\kappa^2 - \Omega^2}} \cdot sinh(\sqrt{\kappa^2 - \Omega^2} \cdot t)] \cdot e^{-\kappa t}$. Parameter distributions are given in Table S1.

Series 4 is derived from the AR6 scenarios. Initially, we simulate all AR6 scenarios[14] using Pathfinder (as detailed in the subsequent section), and select only those scenarios where the maximum temperature remains below 2°C. To these T and C time series, we introduce noise generated through an AR(1) process[56]. We then apply an 11-year moving average to smoothen the trajectories affected by noise. We infer the lost 11 values by following the trend observed in the original T or C time series. To ensure the generated pathways are continuously differentiable, we fit the resulting trajectories with spline functions. These functions are defined piecewise by polynomials and allow for differentiation. Similar to other series, we impose constraints on the initial values of *X* and $\frac{dX}{dt}$ to maintain continuity with the historical trajectory. Additionally, to prevent splines with excessively steep or rapid trends at 2100, we also constrain the derivative at that point with the original value of the AR6 scenario before the noise.

Since Series 4 are derived from AR6 scenarios, the processed trajectories are limited to the year 2100. However, for our purposes, we require pathways that span up to 2500. To address this, we employ the analytical form of Series 3a to extend the trajectories from 2100 to 2500, ensuring continuity and differentiability are maintained throughout the extended period.

Series	Parameters	Values	Distribution
1a	μ_0	[-0.05, 0, 0.10]	Triangular
	μ_1	[0, 0.05, 0.10]	Triangular
1b	μ_0	[0.001, 0.01, 0.10]	Triangular
	μ_1	[1,100,1000]	Triangular
1c	μ_0	[2.5E-5, 3E-5, 1E-1]	Triangular
	μ_1	0	
2	α	[1.001, 1.0015, 20]	Triangular
	β	2	
	t_{peak}	[10, 70, 120]	Triangular
3a - 3b	κ	[0, 0.05, 0.15]	Triangular
3b	Ω	[0, κ]	Uniform

Table S1 Characteristics of the parameters for the T and CO_2 time series. Values for triangular distributions give the minimum, the peak and the maximum of the distribution. Values for uniform distribution give the minimum and the maximum.

Implementation of AR6 scenarios in Pathfinder

The AR6 database[14] hosts the result of all scenarios explored by different IAM for the working group 3 of the IPCC. However, these projections are inconsistent with the historical values of Pathfinder, making it infeasible to directly incorporate the raw data into our model.

In the AR6 database, the drivers are CO_2 emissions and non-CO_2 radiative forcing (R_x). To utilize CO_2 emissions and R_x as inputs in the forward mode of Pathfinder, we perform linear interpolation to convert the decadal data into annual data. Subsequently, we rescale both drivers to align with the historical trajectories of Pathfinder. Due to the inherent natural variability present in Pathfinder's historical runs, it is not possible to directly utilize the year 2021 as a reference for rescaling. Instead, we compute the mean value of the historical Pathfinder's pathways between 2011 and 2021. For observed CO_2 emissions, we employ the most recent estimates available until 2022[57] , while for R_x, we utilize estimates from 2019[58]. To establish the starting point of our simulations in 2021, we rely on the available trend for R_x over the last 10 years to infer the values for 2020 and 2021. (while CO_2 emissions were taken from the latest Global Carbon Budget[57]).

To rescale CO_2 emissions, we extend the mean values calculated in Pathfinder for 2016 by incorporating the trend in observational values until 2021. This approach ensures consistency with Pathfinder's configurations, as the 2016 value is specific to each configuration, while also aligning with the most recently observed trend. The rescaling factor is determined by comparing the reconstructed value for 2021 with the corresponding value in the AR6 scenario.

Similarly, for R_x, we reconstruct the historical value in 2021 by extending the mean value calculated in Pathfinder for 2016 and incorporating the trend in observational values until 2021. However, the treatment of R_x differs from that of CO_2 emissions due to its nature as a radiative forcing resulting from a combination of various GHGs (positive) and aerosols (mostly negative). Consequently, depending on the model's parameterization, the reconstructed historical R_x value in 2021 can be either negative or positive. Rescaling R_x without accounting for this decomposition could potentially lead to an artificial reversal of the sign of R_x in the scenarios. To address this, we first decompose R_x and rescale each component separately: $R_x^{AR6} = R_{x,ghgs}^{AR6} + R_{x,aerosols}^{AR6}$, where R_x^{AR6} is the radiative forcing due to non-CO_2 forcers in AR6 scenarios, $R_{x,ghgs}^{AR6}$ is the radiative forcing due to a combination of different GHGs in AR6 scenarios, and $\mathrm{R}_{\mathrm{x,aerosols}}^{\mathrm{AR6}}$ is the radiative forcing due to aerosols in AR6 scenarios. As Pathfinder lacks such a decomposition, we use the IPCC AR6 extrapolated value of $R_{x,ghgs}^{hist} = 1.18 \pm 0.14\, W\, m^{-2}$ in 2021[58]. Assuming a normal distribution we randomly draw one value of the GHG component of R_x for each configuration of Pathfinder. Finally, the rescaling factor for GHGs is $\frac{R_{x,ghgs}^{hist}}{R_{x,ghgs}^{AR6,2021}}$, and the rescaling factor for aerosols is $\frac{R_x^{hist} - R_{x,ghgs}^{hist}}{R_{x,aerosols}^{AR6,2021}}$, where R_x^{hist} is the reconstructed historical value in Pathfinder in 2021 and $R_{x,aerosols}^{AR6,2021}$.and $R_{x,ghgs}^{AR6,2021}$ are the respective AR6 radiative forcing due to a combination of aerosols and different GHGs in 2021.

Definition of SRM and CDR variables

Carbon Dioxide Removal (CDR) Because of our inverse modelling approach, we do not know the CDR contribution to the net anthropogenic CO_2 emission pathways (E_{CO2}) we estimate. To do so, we

define a time-dependent floor (CDR_{floor}) below which we consider that CDR is needed (Figure S7). This CDR_{floor} follows the lower bound of the CO_2 emission pathways envelope from the AR6 scenarios[14], excluding afforestation and bio-energy with carbon capture and storage ($E^{AR6}_{CO2,min}$). In addition, the AR6 scenarios were rescaled to be consistent with both Pathfinder historical values and latest observed trends. Because, in that case, we want CDR to be 0 in 2021, we must rescale $E^{AR6}_{CO2,min}$. This gives:

$$CDR = \begin{cases} E_{CO2} - CDR_{floor} \; if \; E_{CO2} < CDR_{floor} \\ 0 \; otherwise \end{cases}$$

with

$$CDR_{floor} = \frac{E_{CO2,2021}}{E^{AR6}_{CO2,min,2021}} E^{AR6}_{CO2,min},$$

where $E_{CO2,2021}$ is the Pathfinder's anthropogenic CO_2 emissions in 2021 and $E^{AR6}_{CO2,min,2021}$ is the lower bound of the CO_2 emission pathways envelope from the AR6 scenarios in 2021.

Solar Radiation Management (SRM) AR6 scenarios do not include SRM or any removal technology for GHGs other than CO_2. Thus, we directly extract the R_x variable from the AR6 scenarios implemented in Pathfinder, and we select the lower bound of the pathway's envelope (Figure S7). Because, it is not regularly decreasing, we smooth it out by taking its minimum value over a rolling period of 5 years ($R^{AR6}_{x,min}$). Finally, we offset this already rescaled floor by Pathfinder's 2021 value ($R_{x,2021}$). That is:

$$SRM = \begin{cases} R_x - SRM_{floor} \; if \; R_x < SRM_{floor} \\ 0 \; otherwise \end{cases}$$

with

$$SRM_{floor} = R_{x,2021} - R^{AR6}_{x,min,2021} + R^{AR6}_{x,min},$$

where $R^{AR6}_{x,min,2021}$is the lower bound of the R_x pathways envelope from the AR6 scenarios in 2021.

Planetary boundaries

The first planetary boundary we investigate is global warming, whose quantitative boundary is defined as an increase of +2°C in global mean surface temperature compared to preindustrial times (late Holocene)[1,10,59]. Inspired by previous studies[18,19,30,60,61], we decided to define boundaries focused on three key physical impacts: ocean acidification, sea level rise and Arctic sea ice collapse in summer. As a baseline for pre-industrial level, we take the starting date of Pathfinder's historical simulations in 1750.

Ocean acidification

Acidification, combined with deoxygenation and sea surface temperature, will severely damage ocean ecosystems[62]. One of the main effects of acidification appears on organisms producing calcium carbonate shells and skeletons[63]. Effects of acidification depend on other factor than just pH and can vary regionally[62]. carbonate shells and skeletons[63]. Effects of acidification depend on other factor than just pH and can vary regionally[62]. Because it is delicate to identify one global threshold, however, we decided to apply a precautionary principle to preserve the oceanic biosphere integrity. Based on the

literature[18-20,61,64,65] oceanic biosphere integrity. Based on the literature[18-20,61,64,65] we propose that global pH should not lose 0.2 points compared to pre-industrial level.

Rate of sea level rise

Sea level rise can have direct impacts on coastal population[66]. Some countries (such as small island states) are directly threatened with submersion. However, the main impacts of SLR will be coastal inundations due to extreme sea levels[67]. Other impacts can occur like the salinization of freshwater lens[68] or negative impacts on ecosystems like coral reefs[68,69] or mangroves[66]. SLR is a phenomenon with a significant inertia that makes it inevitable to a certain degree in the coming century, even if global warming stopped immediately[66,70]. That is why the stakes are mainly about the rate of SLR to let time to society to adapt[66]. SLR impacts and adaptation capacity vary greatly depending on the coastal geography[67,71], making it delicate to define a global threshold. As for acidification we impose a precautionary threshold of 5 cm per decade that was also used elsewhere[18,19].Sea level rise can have direct impacts on coastal population[66]. Some countries (such as small island states) are directly threatened with submersion. However, the main impacts of SLR will be coastal inundations due to extreme sea levels[67]. Other impacts can occur like the salinization of freshwater lens[68] or negative impacts on ecosystems like coral reefs[68,69] or mangroves[66]. SLR is a phenomenon with a significant inertia that makes it inevitable to a certain degree in the coming century, even if global warming stopped immediately[66,70]. That is why the stakes are mainly about the rate of SLR to let time to society to adapt[66]. SLR impacts and adaptation capacity vary greatly depending on the coastal geography[67,71], making it delicate to define a global threshold. As for acidification we impose a precautionary threshold of 5 cm per decade that was also used elsewhere[18,19].

Arctic sea ice collapse in summer

The entire Arctic ecosystem, including polar bears, marine mammals, fish, and the local population, will suffer adverse consequences due to the reduction of Arctic sea ice during the summer[66]. Recent papers highlighted also a role of the decline of Arctic sea ice on the weakening of the Atlantic meridian overturning circulation (AMOC)[72], and even a potential domino effect for a whole range of tipping points[73]. The commonly used threshold to consider the Arctic sea-ice free is when the sea ice area reaches below 1 million km^2. This sea ice coverage in summer can be directly linked to the temperature The entire Arctic ecosystem, including polar bears, marine mammals, fish, and the local population, will suffer adverse consequences due to the reduction of Arctic sea ice during the summer[66]. Recent papers highlighted also a role of the decline of Arctic sea ice on the weakening of the Atlantic meridian overturning circulation (AMOC)[72], and even a potential domino effect for a whole range of tipping points[73]. The commonly used threshold to consider the Arctic sea-ice free is when the sea ice area reaches below 1 million km^2. This sea ice coverage in summer can be directly linked to the temperature anomaly, with a threshold on temperature anomaly of $1.7\pm 0.2^{\circ}C$ (for a 95% likelihood interval) that covers the ranges proposed by key existing studies[17,74-76]. The uncertainty in the boundary itself is included in Pathfinder's probabilistic assessment and chosen safety levels. We assume a normal distribution of the threshold and randomly draw a value for every of the 1500 states of the world we

explore. Hence, every configuration of the model has only one threshold value above which the Arctic sea ice is collapsing in summer.

Our four planetary boundaries could be supplemented by additional boundaries arising from physical or anthropogenic impacts of climate change.

Alternative definitions of the compatible space

It is crucial to emphasize that since we are mapping out the limits of the compatible space, even though at least one pathway remains with key characteristics equal to the investigated limit, for example with a peak date of 2037, other pathways with the same characteristic do not necessarily adhere to the planetary boundary. This is because they may fail to comply with the limits of the compatible space for other key characteristics. In our example, 2037 is therefore the last year before the remaining envelope disappears entirely.

In the context where defining a safety level based on the presence of "at least one trajectory" is deemed excessively risky, it becomes possible to introduce a precautionary threshold by imposing a minimal size for the remaining envelope. This approach leads to more stringent constraints on the compatible space, as demonstrated in Figure S8. To evaluate the size of the remaining envelope, we estimate its area and compare it to a reference area. As depicted in Figure 1, the reference area is determined by the envelope of pathways that adhere to the global warming boundary, allowing up to 10 PgC yr^{-1} of CDR, prohibiting SRM, and without restrictions on the year of achieving net-zero CO_2 emissions or the peak of CO_2 emissions. We refer to the ratio of the area of the remaining envelope to the reference area as the "area ratio," which quantifies the magnitude of the window allowing to remain within a given boundary. This definition implies that when only one pathway remains, the envelope area becomes null, and consequently, the area ratio becomes null as well. Figure S9 demonstrates that for the global warming boundary, the size of the remaining envelope is three times larger when CO_2 emissions peak in 2028 compared to when they peak in 2035. In this context, the year 2037 represents the last feasible date before the envelope completely disappears. In Figure S8, we introduce a threshold of 1% for the area ratio and compare the resulting safety level values with the values obtained in Figure 2 using the "at least one pathway" definition of the compatible space. The analysis reveals that the safety level is primarily influenced by the threshold definition when approaching the limit of the compatible space. Typically, under the default conditions of a CO_2 emissions peak -in 2023 and without imposing restrictions on the year of achieving net-zero CO_2 emissions, we observe that the change in safety level due to the alteration of the threshold definition is visible only when CDR and SRM are prohibited. Even in such cases, the change in safety level is not substantial, ranging from -3 to -7 points of percentage. Conversely, if a peak in CO_2 emissions is enforced in 2035, we demonstrate that the impact of the threshold definition on the safety levels is both strong and significant, except when the safety levels were already very low. This outcome implies that even under the most extreme conditions regarding key characteristics (late peak, no SRM, few CDR available), the most optimistic states of the world (i.e. configurations) in Pathfinder can identify multiple pathways compatible with a given planetary boundary.

1 Rockström, J. *et al.* Planetary boundaries: exploring the safe operating space for humanity. *Ecology and society* **14** (2009).

2 Steffen, W. *et al.* Planetary boundaries: Guiding human development on a changing planet. *Science* **347**, 1259855 (2015).

3 Lade, S. J. *et al.* Human impacts on planetary boundaries amplified by Earth system interactions. *Nature sustainability* **3**, 119-128 (2020).

4 Schulte-Uebbing, L., Beusen, A., Bouwman, A. & De Vries, W. From planetary to regional boundaries for agricultural nitrogen pollution. *Nature* **610**, 507-512 (2022).

5 Bouwman, L. *et al.* Exploring global changes in nitrogen and phosphorus cycles in agriculture induced by livestock production over the 1900–2050 period. *Proceedings of the National Academy of Sciences* **110**, 20882-20887 (2013).

6 Mekonnen, M. M. & Hoekstra, A. Y. Global anthropogenic phosphorus loads to freshwater and associated grey water footprints and water pollution levels: A high-resolution global study. *Water resources research* **54**, 345-358 (2018).

7 Lamboll, R. *et al.* Assessing the size and uncertainty of remaining carbon budgets. (2022).

8 Rogelj, J. *et al.* in *Global Warming of 1.5°C. An IPCC Special Report on the impacts of global warming of 1.5°C above pre-industrial levels and related global greenhouse gas emission pathways, in the context of strengthening the global response to the threat of climate change, sustainable development, and efforts to eradicate poverty* Ch. 2, (2018).

9 Rogelj, J. *et al.* A new scenario logic for the Paris Agreement long-term temperature goal. *Nature* **573**, 357-363 (2019).

10 Masson-Delmotte, V. *et al.* Climate change 2021: the physical science basis. *Contribution of working group I to the sixth assessment report of the intergovernmental panel on climate change* **2** (2021).

11 Bernie, D., Lowe, J., Tyrrell, T. & Legge, O. Influence of mitigation policy on ocean acidification. *Geophysical Research Letters* **37** (2010).

12 Mengel, M. *et al.* Future sea level rise constrained by observations and long-term commitment. *Proceedings of the National Academy of Sciences* **113**, 2597-2602, doi:10.1073/pnas.1500515113 (2016).

13 Bossy, T., Gasser, T. & Ciais, P. Pathfinder v1. 0.1: a Bayesian-inferred simple carbon–climate model to explore climate change scenarios. *Geoscientific Model Development* **15**, 8831-8868 (2022).

14 Byers, E. *et al.* (International Institute for Applied Systems Analysis, 2022).

15 Gasser, T., Guivarch, C., Tachiiri, K., Jones, C. & Ciais, P. Negative emissions physically needed to keep global warming below 2 C. *Nature communications* **6**, 1-7 (2015).

16 Hoegh-Guldberg, O. *et al.* Impacts of 1.5 C global warming on natural and human systems. . *Global warming of 1.5° C. An IPCC Special Report on the impacts of global warming of 1.5°C above pre-industrial levels and related global greenhouse has emission pathways, in the context of strengthening the global response to the threat of climate change, sustainable development, and efforts to eradicate poverty*, 175-312, doi:10.1017/9781009157940.005 (2018).

17 Niederdrenk, A. L. & Notz, D. Arctic sea ice in a 1.5 C warmer world. *Geophysical Research Letters* **45**, 1963-1971 (2018).

18 Schubert, R. *et al.* The Future Oceans: warming up, rising high, turning sour. (2006).

19 Kvale, K. *et al.* Carbon dioxide emission pathways avoiding dangerous ocean impacts. *Weather, Climate, and Society* **4**, 212-229 (2012).

20 Gattuso, J.-P. *et al.* Contrasting futures for ocean and society from different anthropogenic CO2 emissions scenarios. *Science* **349** (2015).

21 Mastrandrea, M. D. *et al.* Guidance note for lead authors of the IPCC fifth assessment report on consistent treatment of uncertainties. (2010).

22 Mastrandrea, M. D. *et al.* The IPCC AR5 guidance note on consistent treatment of uncertainties: a common approach across the working groups. *Climatic Change* **108**, 675-691 (2011).

23 Shukla, P.-R. *et al.* Mitigation of Climate Change. Contribution of Working Group III to the Sixth Assessment Report of the Intergovernmental Panel on Climate Change. *IPCC Sixth Assessment Report*, doi:10.1017/9781009157926.001 (2022).

24 Babiker, M. *et al.* in *Climate change 2022: Mitigation of Climate Change. Contribution of Working Group III to the Sixth Assessment Report of the Intergovernmental Panel on Climate Change* (ed 2022 IPCC) Ch. 12, (Cambridge University Press, 2022).

25 Obersteiner, M. *et al.* How to spend a dwindling greenhouse gas budget. *Nature Climate Change* **8**, 7-10 (2018).

26 Aengenheyster, M., Feng, Q. Y., Van Der Ploeg, F. & Dijkstra, H. A. The point of no return for climate action: effects of climate uncertainty and risk tolerance. *Earth System Dynamics* **9**, 1085-1095 (2018).

27 Tokarska, K. B. & Zickfeld, K. The effectiveness of net negative carbon dioxide emissions in reversing anthropogenic climate change. *Environmental Research Letters* **10**, 094013 (2015).

28 Allen, M. R. *et al.* Warming caused by cumulative carbon emissions towards the trillionth tonne. *Nature* **458**, 1163-1166 (2009).

29 van Soest, H. L., den Elzen, M. G. & van Vuuren, D. P. Net-zero emission targets for major emitting countries consistent with the Paris Agreement. *Nature communications* **12**, 1-9 (2021).

30 Stocker, T. F. The closing door of climate targets. *Science* **339**, 280-282 (2013).

31 Rockström, J. *et al.* Safe and just Earth system boundaries. *Nature*, 1-10 (2023).

32 Riahi, K. *et al.* The Shared Socioeconomic Pathways and their energy, land use, and greenhouse gas emissions implications: An overview. *Global environmental change* **42**, 153-168 (2017).

33 Ricciuto, D. M., Davis, K. J. & Keller, K. A Bayesian calibration of a simple carbon cycle model: The role of observations in estimating and reducing uncertainty. *Global biogeochemical cycles* **22** (2008).

34 Bossy, T., Gasser, T. & Ciais, P. Pathfinder v1. 0: a Bayesian-inferred simple carbon-climate model to explore climate change scenarios. *EGUsphere*, 1-52 (2022).

35 Geoffroy, O. *et al.* Transient Climate Response in a Two-Layer Energy-Balance Model. Part II: Representation of the Efficacy of Deep-Ocean Heat Uptake and Validation for CMIP5 AOGCMs. *Journal of Climate* **26**, 1859-1876, doi:10.1175/JCLI-D-12-00196.1 (2013).

36 Myhre, G. *et al.* in *Climate Change 2013: The Physical Science Basis. Contribution of Working Group I to the Fifth Assessment Report of the Intergovernmental Panel on Climate Change* (eds T.F. Stocker *et al.*) Ch. 8, 659–740 (Cambridge University Press, 2013).

37 Strassmann, K. M. & Joos, F. The Bern Simple Climate Model (BernSCM) v1.0: an extensible and fully documented open-source re-implementation of the Bern reduced-form model for global carbon cycle–climate simulations. *Geosci. Model Dev.* **11**, 1887-1908, doi:10.5194/gmd-11-1887-2018 (2018).

38 Gasser, T. *et al.* The compact Earth system model OSCAR v2.2: description and first results. *Geosci. Model Dev.* **10**, 271-319, doi:10.5194/gmd-10-271-2017 (2017).

39 He, Y. *et al.* Radiocarbon constraints imply reduced carbon uptake by soils during the 21st century. *Science* **353**, 1419-1424, doi:10.1126/science.aad4273 (2016).

40 Gasser, T. *et al.* Path-dependent reductions in CO2 emission budgets caused by permafrost carbon release. *Nature Geoscience* **11**, 830-835, doi:10.1038/s41561-018-0227-0 (2018).

41 Goodwin, P. *et al.* Pathways to 1.5 °C and 2 °C warming based on observational and geological constraints. *Nature Geoscience* **11**, 102-107, doi:10.1038/s41561-017-0054-8 (2018).

42 Bernie, D., Lowe, J., Tyrrell, T. & Legge, O. Influence of mitigation policy on ocean acidification. *Geophysical Research Letters* **37**, L15704, doi:10.1029/2010GL043181 (2010).

43 Cowtan, K. & Way, R. G. Coverage bias in the HadCRUT4 temperature series and its impact on recent temperature trends. *Quarterly Journal of the Royal Meteorological Society* **140**, 1935-1944, doi:10.1002/qj.2297 (2013).

44 Morice, C. P., Kennedy, J. J., Rayner, N. A. & Jones, P. D. Quantifying uncertainties in global and regional temperature change using an ensemble of observational estimates: The HadCRUT4 data set. *Journal of Geophysical Research: Atmospheres* **117**, doi:10.1029/2011JD017187 (2012).

45 Rohde, R. *et al.* Berkeley Earth Temperature Averaging Process. *Geoinformatics & Geostatistics: An Overview* **1**, doi:10.4172/gigs.1000103 (2013).

46 Hansen, J., Ruedy, R., Sato, M. & Lo, K. GLOBAL SURFACE TEMPERATURE CHANGE. *Reviews of Geophysics* **48**, doi:10.1029/2010RG000345 (2010).

47 Smith, T. M., Reynolds, R. W., Peterson, T. C. & Lawrimore, J. Improvements to NOAA's Historical Merged Land–Ocean Surface Temperature Analysis (1880–2006). *Journal of Climate* **21**, 2283-2296, doi:10.1175/2007JCLI2100.1 (2008).

48 Bindoff, N. L. *et al.* in *Climate Change 2013: The Physical Science Basis. Contribution of Working Group I to the Fifth Assessment Report of the Intergovernmental Panel on Climate Change* (eds T.F. Stocker *et al.*) Ch. 10, 867–952 (Cambridge University Press, 2013).

49 Friedlingstein, P. *et al.* Global Carbon Budget 2019. *Earth Syst. Sci. Data* **11**, 1783-1838, doi:10.5194/essd-11-1783-2019 (2019).

50 Ciais, P. *et al.* in *Climate Change 2013: The Physical Science Basis. Contribution of Working Group I to the Fifth Assessment Report of the Intergovernmental Panel on Climate Change* (eds T.F. Stocker *et al.*) Ch. 6, 465–570 (Cambridge University Press, 2013).

51 Church, J. A. *et al.* in *Climate Change 2013: The Physical Science Basis. Contribution of Working Group I to the Fifth Assessment Report of the Intergovernmental Panel on Climate Change* (eds T.F. Stocker *et al.*) Ch. 13, 1137–1216 (Cambridge University Press, 2013).

52 Kucukelbir, A., Tran, D., Ranganath, R., Gelman, A. & Blei, D. M. Automatic Differentiation Variational Inference. *Journal of Machine Learning Research* **18**, 1-45 (2017).

53 Huntingford, C. *et al.* Flexible parameter-sparse global temperature time profiles that stabilise at 1.5 and 2.0° C. *Earth System Dynamics* **8**, 617-626 (2017).

54 Kumaraswamy, P. A generalized probability density function for double-bounded random processes. *Journal of hydrology* **46**, 79-88 (1980).

55 Gompertz, B. XXIV. On the nature of the function expressive of the law of human mortality, and on a new mode of determining the value of life contingencies. In a letter to Francis Baily, Esq. FRS &c. *Philosophical transactions of the Royal Society of London*, 513-583 (1825).

56 Salvatier, J., Wiecki, T. V. & Fonnesbeck, C. Probabilistic programming in Python using PyMC3. *PeerJ Computer Science* **2**, e55 (2016).

57 Friedlingstein, P. *et al.* Global carbon budget 2022. *Earth System Science Data* **14**, 4811-4900 (2022).

58 Smith, C., Nicholls, Z. R. J., Armour, K., Collins, W., Forster, P., M. M., Palmer, M. D., and Watanabe, M. in *Climate Change 2021: The Physical Science Basis, Contribution of Working Group I to the Sixth Assessment Report of the Intergovernmental Panel on Climate Change* (2021).

59 Agreement, P. in *Report of the Conference of the Parties to the United Nations Framework Convention on Climate Change (21st Session, 2015: Paris). Retrived December.* 2017 (HeinOnline).

60 Zickfeld, K. & Bruckner, T. Reducing the risk of Atlantic thermohaline circulation collapse: sensitivity analysis of emissions corridors. *Climatic Change* **91**, 291-315 (2008).

61 Steinacher, M., Joos, F. & Stocker, T. F. Allowable carbon emissions lowered by multiple climate targets. *Nature* **499**, 197-201 (2013).

62 Heinze, C. *et al.* The quiet crossing of ocean tipping points. *Proceedings of the National Academy of Sciences* **118** (2021).

63 Gattuso, J.-P. & Hansson, L. Ocean acidification: background and history. *Ocean acidification*, 1-20 (2011).

64 Nakicenovic, N. World in Transition: Governing the Marine Heritage. Summary [Welt im Wandel: Menschheitserbe Meer. Zusammenfassung]. (2013).

65 Nakicenovic, N. *Human progress within planetary guardrails: a contribution to the SDG debate*. (2014).

66 Bindoff, N. L. *et al.* Changing ocean, marine ecosystems, and dependent communities. *IPCC special report on the ocean and cryosphere in a changing climate*, 477-587 (2019).

67 Kulp, S. A. & Strauss, B. H. New elevation data triple estimates of global vulnerability to sea-level rise and coastal flooding. *Nature communications* **10**, 1-12 (2019).

68 Duvat, V. K. *et al.* Risks to future atoll habitability from climate-driven environmental changes. *Wiley Interdisciplinary Reviews: Climate Change* **12**, e700 (2021).

69 Storlazzi, C. D. *et al.* Most atolls will be uninhabitable by the mid-21st century because of sea-level rise exacerbating wave-driven flooding. *Science Advances* **4**, eaap9741 (2018).

70 Field, C. B. & Barros, V. R. *Climate change 2014–Impacts, adaptation and vulnerability: Regional aspects*. (Cambridge University Press, 2014).

71 Rasmussen, D., Kopp, R. E., Kulp, S. A., Oppenheimer, M. & Strauss, B. in *AGU Fall Meeting Abstracts*. NH042-004.

72 Sévellec, F., Fedorov, A. V. & Liu, W. Arctic sea-ice decline weakens the Atlantic meridional overturning circulation. *Nature Climate Change* **7**, 604-610 (2017).

73 Lenton, T. M. *et al.* Tipping elements in the Earth's climate system. *Proceedings of the national Academy of Sciences* **105**, 1786-1793 (2008).

74 Notz, D. & Community, S. Arctic sea ice in CMIP6. *Geophysical Research Letters* **47**, e2019GL086749 (2020).

75 Notz, D. & Stroeve, J. The trajectory towards a seasonally ice-free Arctic Ocean. *Current Climate Change Reports* **4**, 407-416 (2018).

76 Jahn, A. Reduced probability of ice-free summers for 1.5 C compared to 2 C warming. *Nature Climate Change* **8**, 409-413 (2018).

3.4 . Possible addition of impacts in relation with human activities

In section 3.3, we propose to reverse the natural causality of the system. We define the planetary boundaries and look for the anthropogenic activities that make it possible to stay within these boundaries. However, these limits are physical variables and cannot be directly converted into exposure. A natural improvement to this framework would be to define climate targets locally in terms of the exposure of land or population in each country. To this end, Pathfinder could be coupled with the spatially resolved emulator MESMER, which can emulate local annual temperatures (Beusch et al.; 2020), extreme temperatures (Quilcaille et al.; 2022), and even local precipitation (Schöngart et al.; 2023) from global temperature projections. This coupling would allow local variables to be used to emulate local impacts.

For starters, we could use existing crop yield emulators. The AgMIP emulator (Franke et al.; 2020) was used to calibrate a very simple model linking crop yields to atmospheric CO_2 concentration, temperature anomaly, precipitation perturbation and applied nitrogen via a polynomial model of order 3. In another study (Abramoff et al.; 2023), machine learning methods were used to predict yields of four crop species (maize, rice, wheat, soybeans) based on spatial coordinates, the average local area-weighted temperature in degrees Celsius measured around 2000, the average local area-weighted annual precipitation in mm around the year 2000, the projected global temperature change from a base period (2000-2010), the projected annual site-specific precipitation change from the base period, and the mean CO_2 concentration in parts per million to emulate. Coupling one of these emulators with Pathfinder and MESMER, and then crossing the maps with population projections, would allow estimation of human exposure to changes in crop yields.

Another relatively simple improvement to add more human impacts would be to link the global SLR to local extreme sea levels that cause coastal flooding. To this end, an emulator has been developed that projects local sea level based on global sea level rise and tide gauge data to project local sea level (Kopp et al.; 2014). Based on this local sea level, using the GEV distribution, it is possible to estimate the evolution of the return period of local extreme sea levels (Buchanan et al.; 2017). Assuming that cities are currently adapted to a 1 in 100 year return period, their model yields the new return period of such events as a function of global SLR. By comparing these data with population projections, it is possible to estimate the change in the number of people exposed to extreme sea levels.

These two impacts are of particular interest because they are not linearly dependent on temperature. Therefore, we expect nonlinear combination effects similar to those we observed in the previous section. We have not found similarly simple emulators for other impacts. However, the ISIMIP dataset provides a framework for defining functions that allow population or land exposure to a range of country-level impacts to be linked to global temperature change (Rosenzweig et al.; 2017). Previous work has created such an emulator for a range of impacts: Wildfires, tropical cyclones, river floods, heat waves, or droughts (Lange et al.; 2020). Using more recent data (ISIMIP3b, `www.isimip.org`), the Climate Solutions Explorer (`www.climate-solutions-explorer.eu`) maps and presents information on mitigation pathways, avoided climate impacts, vulnerabilities, and risks arising from development and climate change (Werning et al.; 2023). We can use this type of data to reverse the approach and show the temperature associated with an acceptable threshold for exposure. For illustration, we set this threshold at 5% of the currently unexposed population. Then, for a given impact, here medium water stress assessed by the water stress index (WSI), we can indicate the temperature at which this

acceptable threshold is exceeded (see Figure 3.2). To prevent more than 5% of the world's population, who are not currently at risk, from being exposed to medium water stress, it is necessary to stay below 1.9C. Therefore, this type of inverted map may be interesting for setting temperature targets at the international or regional level. Overall, these three examples show that Pathfinder can be used to estimate an ensemble of anthropogenic emission pathways that are consistent with climate targets defined by impacts. This can be very interesting for scenario development in collaboration with policy makers, as climate change impacts are more concrete in terms of affected populations than a global temperature target.

Bibliography

Abramoff, R. Z., Ciais, P., Zhu, P., Hasegawa, T., Wakatsuki, H. and Makowski, D. (2023). Adaptation strategies strongly reduce the future impacts of climate change on simulated crop yields, *Earth's Future* **11**(4): e2022EF003190.

Beusch, L., Gudmundsson, L. and Seneviratne, S. I. (2020). Emulating earth system model temperatures with mesmer: from global mean temperature trajectories to grid-point-level realizations on land, *Earth System Dynamics* **11**(1): 139–159.

Buchanan, M. K., Oppenheimer, M. and Kopp, R. E. (2017). Amplification of flood frequencies with local sea level rise and emerging flood regimes, *Environmental Research Letters* **12**(6): 064009.

Franke, J. A., Müller, C., Elliott, J., Ruane, A. C., Jägermeyr, J., Snyder, A., Dury, M., Falloon, P. D., Folberth, C., François, L. et al. (2020). The ggcmi phase 2 emulators: global gridded crop model responses to changes in co 2, temperature, water, and nitrogen (version 1.0), *Geoscientific Model Development* **13**(9): 3995–4018.

Kopp, R. E., Horton, R. M., Little, C. M., Mitrovica, J. X., Oppenheimer, M., Rasmussen, D., Strauss, B. H. and Tebaldi, C. (2014). Probabilistic 21st and 22nd century sea-level projections at a global network of tide-gauge sites, *Earth's future* **2**(8): 383–406.

Lange, S., Volkholz, J., Geiger, T., Zhao, F., Vega, I., Veldkamp, T., Reyer, C. P., Warszawski, L., Huber, V., Jägermeyr, J. et al. (2020). Projecting exposure to extreme climate impact events across six event categories and three spatial scales, *Earth's Future* **8**(12): e2020EF001616.

Quilcaille, Y., Gudmundsson, L., Beusch, L., Hauser, M. and Seneviratne, S. I. (2022). Showcasing mesmer-x: Spatially resolved emulation of annual maximum temperatures of earth system models, *Geophysical Research Letters* **49**(17): e2022GL099012.

Rosenzweig, C., Arnell, N. W., Ebi, K. L., Lotze-Campen, H., Raes, F., Rapley, C., Smith, M. S., Cramer, W., Frieler, K., Reyer, C. P. et al. (2017). Assessing inter-sectoral climate change risks: the role of isimip, *Environmental Research Letters* **12**(1): 010301.

Schöngart, S., Lejeune, Q., Gudmundsson, L., Nath, S., Seneviratne, S. and Schleußner, C.-F. (2023). Extending mesmer-m to jointly emulate earth system model temperature and precipitation realizations, *Technical report*, Copernicus Meetings.

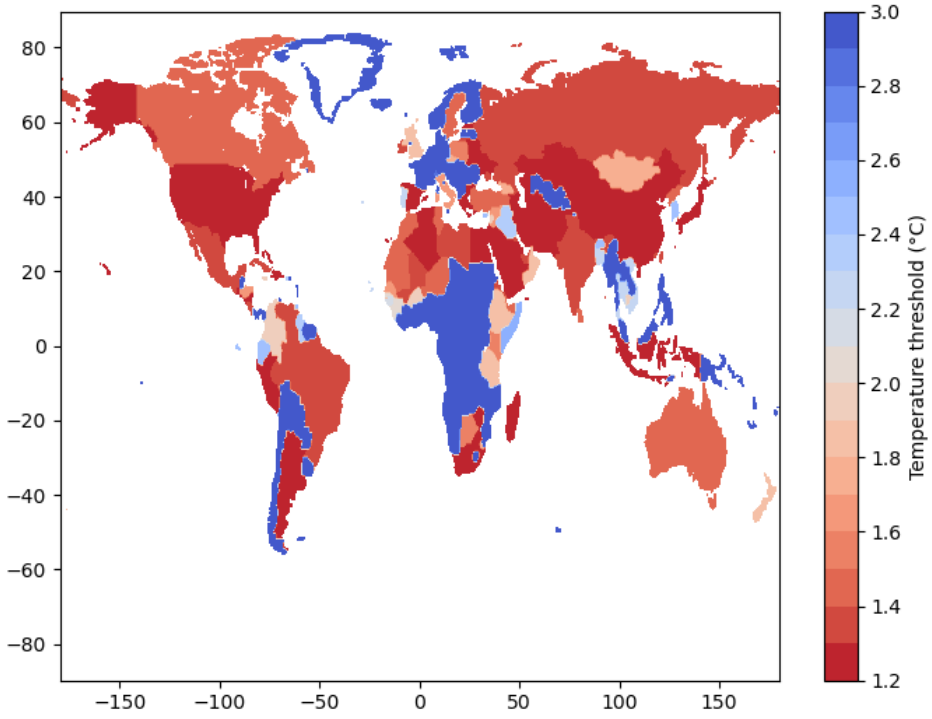

Figure 3.2: Map of temperature threshold per country above which more than 5% of the currently unexposed population will face medium water stress (Werning et al.; 2023). This map is based on the mean results of several climate and hydrological models from ISIMIP3b at 5 global warming levels (1.2°C, 1.5°C, 2°C, 2.5°C, 3°C). To obtain thresholds every 0.1°C, we performed linear interpolation. 3°C is the highest temperature for which the WSI was calculated, i.e., the temperature target set for all countries that do not exceed the threshold. The exposure is calculated using a population projection to the year 2100 (with a time step of 10 years). The final temperature target is the lowest of all population projections.

Werning, M., Frank, S., Nguyen, B., Rafaj, P., Satoh, Y., Krey, V., Riahi, K., van Ruijven, B. and Byers, E. (2023). Climate Solutions Explorer - hazard, impacts and exposure data.
URL: *https://doi.org/10.5281/zenodo.7971430*

4 - Estimating costs

4.1 . Different sorts of IAMs

Preamble

For the introduction of this chapter I want to give some context of the socio-economic modelling of mitigation pathways. Such dissertation subject is not new and a lot of literature has already done a very good job. In particular, an entire annex of AR6 WGIII report is dedicated to describe the different modelling tools. Hence, this section is greatly inspired from this annex (Guivarch et al.; 2022).

4.1.1 . Economic Modelling Frameworks

Economic modelling frameworks form a diverse spectrum, distinguished by several critical characteristics, following the classifications proposed by various authors (Hardt and O'Neill; 2017; Capellán-Pérez et al.; 2020). The literature typically categorizes models across three dimensions: level of detail and heterogeneity, mathematical algorithm concepts, and temporal and spatial system boundaries (Krey; 2014).

Climate mitigation models, for instance, are commonly distinguished as bottom-up or top-down, based on their degree of detail (Van Vuuren et al.; 2009). Bottom-up models offer intricate technical detail on a limited set of mitigation strategies for a specific sector or sub-sector. However, they often overlook the relations and interactions within the broader system. Conversely, top-down models provide a comprehensive, albeit less detailed, analysis, focusing on systemic interactions like market dynamics and policy instrument interactions within the global economy. Significantly, IAMs are generally top-down, with a focus on modeling sectoral mitigation strategies. Nonetheless, the dichotomy between bottom-up and top-down models has blurred since the IPCC's Fifth Assessment Report (AR5), with models now incorporating elements from both.

A further characteristic that models are classified on is their mathematical algorithm concept. Simulation models observe the dynamic behavior of a system and require comprehensive knowledge to make choices among alternatives (Lund et al.; 2017). On the other hand, optimisation models aim to maximize or minimize an objective function within set constraints (Iqbal et al.; 2014).

Moreover, modelling tools differ in their approach to temporal considerations. Some models utilize an intertemporal optimization approach with perfect foresight, where decisions are based on complete information about the system's future states (Keppo and Strubegger; 2010). In contrast, recursive-dynamic models make decisions sequentially, without foreknowledge of future states (Nerini et al.; 2017).

4.1.2 . Classification Integrated Assessment Models (IAMs)

IAMs are simplified simulacra of the complex interplay between economy, society, and the environment (Weyant; 2017). They depict the interconnected energy-economy-land-climate system to varying degrees. Significant differences among IAMs include geographical, sectoral, spatial and time resolution, socio-economic assumptions, technological representation, and assumptions of equilibrium. IAMs differ in the extent to which they endogenize all emissions and their sources, processes, and activities. However, they can be classified in two broad categories.

Cost-benefit IAMs were conceived to evaluate the optimal strategies of climate policy, considering both the economic expenses of mitigation and the financial repercussions of climate change. In these models, the problem of climate change mitigation is addressed through a

cost-benefit framework, making a direct comparison between the economic costs of mitigation and the economic benefits of lessened impacts (Weyant; 2017). This perspective results in a focus on issues like the social cost of carbon or optimal trade-offs over time between mitigation and impacts (Metcalf and Stock; 2017). Despite considerable uncertainties, these models generate a specific output path, with the damage function contributing to over 50% of this uncertainty (van der Wijst et al.; 2021). The oldest cost-benefit IAM is DICE, which was developed based on the work of Nordhaus (Nordhaus; 1992). The DICE model was initially employed to examine the integration of human and natural Earth systems within a cost-benefit framework. Soon, a multiregional version called the Regional Dynamic Integrated model of Climate and the Economy (RICE) was developed (Nordhaus and Yang; 1996). Further models have been developed along the same lines, such as PAGE (Hope; 2013)), and FUND (Tol; 1997). Typically, these models comprise three parts: emissions and mitigation, atmosphere and climate, and climate impacts. The costs associated with mitigation and the damages from climate change are generally monetized, allowing a comparison between mitigation and impacts on a common basis. Detailed descriptions of the energy or land-use systems that generate emissions are usually absent, and likewise, detailed descriptions of the physical process links between climate change and emissions are generally beyond their scope. Instead, these models utilize emission mitigation supply schedules and climate damage functions, allowing cost-benefit IAMs to explicitly weigh costs and benefits, albeit without the ability to provide insight into the actual processes that lead to these costs and benefits. Challenges for these models include assigning value to human life loss and non market damages, as well as determining the relative value of impacts over different periods of time.

Process-based IAMs share a similar developmental timeframe with cost benefit IAMs but were crafted along different lines to serve distinct purposes. These models were created to offer detailed information about human and natural Earth system processes and their interactions. Their initial focus was on determining anthropogenic carbon emissions, prompting the development of detailed representations of long-term energy production, transformation, and land-use processes (Riahi et al.; 2017). Over time, these models have evolved in complexity, incorporating increasing detail in their representations of the energy system and economy, while also broadening their scope to include natural Earth system processes such as the carbon cycle. Current iterations of process-based IAMs typically contain representations of agriculture, land use, land cover, and terrestrial carbon cycle processes, in addition to atmosphere and climate processes. Each process-based IAM was developed independently, resulting in models that emphasize different features of the climate change problem. Some models, for instance, accentuate the development of detailed atmosphere and climate system models. Others focus on the comprehensive representation of technology, while some highlight regional differences in emission patterns and energy systems data. These process-based IAMs require an interdisciplinary approach, given their complex nature, involving research and modeling teams across various fields.

4.1.3 . Policy relevance of IAMs

IAMs provide crucial knowledge to guide future climate action strategies. They offer potential climate change and action pathways under varying assumptions about socio-economic, institutional, and technological developments. IAMs aid policymakers, the private sector, and civil society by

outlining possible approaches towards a multitude of long-term climate outcomes, while simultaneously presenting potential conflicts between various pathways. The IAM literature has examined numerous trade-offs, such as mitigation levels (Riahi et al.; 2017), timing of action(Luderer et al.; 2018), global vs regionally and sectorally fragmented actions (Bauer et al.; 2020), supply-side vs demand-side measures (Grubler et al.; 2018), technology deployment preferences (Krey; 2014), and varying socio-economic futures (Riahi et al.; 2017), amongst others. Policy analysis with IAMs generally involves comparison of a baseline scenario with policy intervention scenarios. Uncertainties in baseline projections are addressed using SSPs that represent a spectrum of possible future developments. The baseline scenario can be defined as a no-policy scenario, or it can include GHG emissions policies such as the Nationally Determined Contributions (NDCs, Roelfsema et al. (2020)), and other preexisting policies like energy subsidies and taxes. It can be augmented by additional sector policies, such as technology support, aimed at helping the long-term climate goals to be reached. Another key paramater for the policy relevance of IAMs is the discounting that is used to compare economic flows through time. For instance, in cost-benefit analysis (CBA), the choice of discount rate is critical for balancing mitigation costs against the cost of avoided climate damages in the future. A lower discount rate encourages more significant abatement efforts and lesser global temperature increases. In cost-effective analysis (CEA), the discount rate influences the timing of emission reductions to limit warming to a specific temperature level. A lower discount rate here promotes more immediate emission reductions and the use of currently available mitigation options. CBA and CEA both use a social discount rate to compare costs and benefits over time. Discounting is also used for ex-post comparison of mitigation cost pathways across models and scenarios, with typically applied discount rates of 2-5% (Admiraal et al.; 2016). Overall, understanding and appropriately using discount rates is crucial for policy decisions relating to climate change mitigation, adaptation, and inter-generational equity. IAMs allow for sensitivity analysis, helping to assess the importance of strategically developing new technologies and options for mitigation. They can identify sticking points in climate policy frameworks, providing guidance on policy prioritization by identifying crucial levers for achieving long-term climate mitigation targets.

4.1.4 . Limitations of IAMs

Aggregated IAMs, while useful for exploring a wide range of scenarios, have limited accuracy and are more suited to qualitative than quantitative insights (Heal; 2017). Critics have targeted optimization modelling, which assumes perfect foresight of future costs, and focuses on a cost-optimal path . The heavy dependence of these paths on the discount rate has also been criticized. The cost functions in IAMs, including damage functions and others, are seen as highly uncertain, leading to a degree of scepticism (Keppo et al.; 2021; Trutnevyte; 2016; Pindyck; 2017). Moreover, IAMs have faced criticism for potentially omitting important dynamics related to climate damages, economic benefits of mitigation (Stern; 2016), bioenergy, land degradation and management (Creutzig et al.; 2015), carbon dioxide removal (Smith et al.; 2016), technological progress (Creutzig et al.; 2017), actor heterogeneity, and the distributional impacts of climate change and policy. Other concerns include the perceived lack of transparency in IAMs and their inability to account for underlying socio-cultural transitions and extreme or discontinuous outcomes (Weyant;

2017). Critics argue that IAMs tend to focus on only a subset of relevant futures, potentially steering society in certain directions without sufficient scrutiny (Beck and Mahony; 2017).

Despite these criticisms, the IAMs community has made continuous improvements in model design and scenario creation. These include better representations of energy demand, renewable energy, carbon dioxide removal technologies, and land management. Increased efforts have also been made to enhance transparency and better contextualise results for users. The research community is also addressing the limitations related to transformative change, engaging with social scientists to provide a more complete picture of high-impact climate change scenarios and deep transformation pathways. An iterative approach between researchers and societal actors is being adopted to continuously refine research questions and IAM applications.

4.1.5 . Potential of inverting the IAM-SCM approach

The conventional approach of employing Simple Climate Models (SCMs) has largely seen them serve as assessment tools for IAMs to foster integration between the WGI and WGIII sections of the IPCC reports. This framework operates as a pipeline, comprising three key stages: harmonization of emission scenarios, infilling of missing data, and climate model emulation, all aimed at ensuring a comprehensive, consistent, and comparable evaluation of climate responses across different emission scenarios. The harmonization stage, which aligns emission scenarios with a common source of historical emissions, ensures that climate futures arising from different scenarios reflect unique future emission evolutions, not disparate historical starting points (Nicholls et al.; 2020; Gidden et al.; 2019). The infilling process complements the harmonization step by ensuring that all relevant anthropogenic emissions are accounted for, minimizing the risk of a skewed climate assessment. This step is necessary due to variations in reporting by different IAMs (Lamboll et al.; 2020). Lastly, the pipeline utilizes WGI-calibrated climate model emulators, selected based on expert judgment, to provide a scientifically robust assessment of climate responses (Forster et al.; 2021). These emulators are calibrated to match a range of key climate metrics assessed by WGI. The outcome is a robust climate assessment process that effectively integrates WGI's physical climate understanding and WGIII's socio-economic climate strategies, providing a comprehensive overview of climate change trajectories and related implications. This perspective and usage have significantly shaped the interpretation and application of such models in understanding climate change scenarios. However, in an endeavour to overcome limitations and address critical viewpoints, it may be beneficial to consider inverting this conventional approach by using Pathfinder described in Chapter 2 as a starting point. This new framework would not replace the conventional approach, but would complement it and help identify in advance what types of scenarios should be explored in detail.

An innovative way of contemplating this is to let physics, particularly climate and impact models, delineate a set of scenarios compatible with desired climate targets. These scenarios, generated by physical models and impact assessments, inherently factor in a broad spectrum of climate variables and associated impacts, thereby ensuring a wide-ranging consideration of possible climate futures. The approach described in chapter 3 makes it possible to generate such scenarios. Then an economic module can be employed to assess the cost implications of each scenario. This appraisal allows for the ranking of these climate pathways based on economic feasibility, subsequently guiding decision-

makers in choosing the most cost-effective strategy. This is the subject of this chapter.
This reversed approach could address one of the main critiques levelled against IAMs, namely, their perceived lack of focus on the full spectrum of possible outcomes. With this inversion, we propose exploring the entire realm of possibilities initially and then narrowing down to a more relevant subset that can be further scrutinized using complex IAMs.

Bibliography

Admiraal, A. K., Hof, A. F., Den Elzen, M. G. and van Vuuren, D. P. (2016). Costs and benefits of differences in the timing of greenhouse gas emission reductions, *Mitigation and Adaptation Strategies for Global Change* **21**: 1165–1179.

Bauer, N., Bertram, C., Schultes, A., Klein, D., Luderer, G., Kriegler, E., Popp, A. and Edenhofer, O. (2020). Quantification of an efficiency–sovereignty trade-off in climate policy, *Nature* **588**(7837): 261–266.

Beck, S. and Mahony, M. (2017). The ipcc and the politics of anticipation, *Nature Climate Change* **7**(5): 311–313.

Capellán-Pérez, I., de Blas, I., Nieto, J., de Castro, C., Miguel, L. J., Carpintero, O., Mediavilla, M., Lobejón, L. F., Ferreras-Alonso, N., Rodrigo, P. et al. (2020). Medeas: A new modeling framework integrating global biophysical and socioeconomic constraints, *Energy & environmental science* **13**(3): 986–1017.

Creutzig, F., Agoston, P., Goldschmidt, J. C., Luderer, G., Nemet, G. and Pietzcker, R. C. (2017). The underestimated potential of solar energy to mitigate climate change, *Nature Energy* **2**(9): 1–9.

Creutzig, F., Ravindranath, N. H., Berndes, G., Bolwig, S., Bright, R., Cherubini, F., Chum, H., Corbera, E., Delucchi, M., Faaij, A. et al. (2015). Bioenergy and climate change mitigation: an assessment, *Gcb Bioenergy* **7**(5): 916–944.

Forster, P., Storelvmo, T., Armour, K., Collins, T., Dufresne, J. L., Frame, D., Lunt, D. J., Mauritsen, T., Palmer, M. D., Watanabe, M., Wild, M. and Zhang, H. (2021). *The Earth's Energy Budget, Climate Feedbacks, and Climate Sensitivity*, Cambridge, United Kingdom, book section 7, pp. 923–1054.

Gidden, M. J., Riahi, K., Smith, S. J., Fujimori, S., Luderer, G., Kriegler, E., Van Vuuren, D. P., Van Den Berg, M., Feng, L., Klein, D., Calvin, K., Doelman, J. C., Frank, S., Fricko, O., Harmsen, M., Hasegawa, T., Havlik, P., Hilaire, J., Hoesly, R., Horing, J., Popp, A., Stehfest, E. and Takahashi, K. (2019). Global emissions pathways under different socioeconomic scenarios for use in CMIP6: A dataset of harmonized emissions trajectories through the end of the century, *Geoscientific Model Development* **12**(4): 1443–1475.

Grubler, A., Wilson, C., Bento, N., Boza-Kiss, B., Krey, V., McCollum, D. L., Rao, N. D., Riahi, K., Rogelj, J., De Stercke, S. et al. (2018). A low energy demand scenario for meeting the 1.5 c target and sustainable development goals without negative emission technologies, *Nature energy* **3**(6): 515–527.

Guivarch, C., Kriegler, E., Portugal Pereira, J., Bosetti, V., Edmonds, J., Fischedick, M., Havlik, P., Jaramillo, P., Krey, V., Lecocq, F., Lucena, A., Meinshausen, M., Mirasgedis, S., O'Neill, B., Peters, G., Rogelj, J., Rose, S., Saheb, Y., Strbac, G., Stromman, A. H., Van Vuuren, D. P. and Zhou, N. (2022). Annex iii: Scenarios and modelling method, *Climate change 2022: Mitigation of Climate Change. Contribution of Working Group III to the Sixth Assessment Report of the Intergovernmental Panel on Climate Change* .

Hardt, L. and O'Neill, D. W. (2017). Ecological macroeconomic models: assessing current developments, *Ecological economics* **134**: 198–211.

Heal, G. (2017). The economics of the climate, *Journal of Economic Literature* **55**(3): 1046–1063.

Hope, C. (2013). Critical issues for the calculation of the social cost of co 2: why the estimates from page09 are higher than those from page2002, *Climatic Change* **117**: 531–543.

Iqbal, M., Azam, M., Naeem, M., Khwaja, A. and Anpalagan, A. (2014). Optimization classification, algorithms and tools for renewable energy: A review, *Renewable and sustainable energy reviews* **39**: 640–654.

Keppo, I., Butnar, I., Bauer, N., Caspani, M., Edelenbosch, O., Emmerling, J., Fragkos, P., Guivarch, C., Harmsen, M. and Lefevre, J. (2021). Exploring the possibility space: taking stock of the diverse capabilities and gaps in integrated assessment models, *Environmental Research Letters* **16**(5): 053006.

Keppo, I. and Strubegger, M. (2010). Short term decisions for long term problems–the effect of foresight on model based energy systems analysis, *Energy* **35**(5): 2033–2042.

Krey, V. (2014). Global energy-climate scenarios and models: a review, *Wiley Interdisciplinary Reviews: Energy and Environment* **3**(4): 363–383.

Lamboll, R. D., Nicholls, Z. R., Kikstra, J. S., Meinshausen, M. and Rogelj, J. (2020). Silicone v1. 0.0: an open-source python package for inferring missing emissions data for climate change research.

Luderer, G., Vrontisi, Z., Bertram, C., Edelenbosch, O. Y., Pietzcker, R. C., Rogelj, J., De Boer, H. S., Drouet, L., Emmerling, J., Fricko, O. et al. (2018). Residual fossil co2 emissions in 1.5–2 c pathways, *Nature Climate Change* **8**(7): 626–633.

Lund, H., Arler, F., Østergaard, P. A., Hvelplund, F., Connolly, D., Mathiesen, B. V. and Karnøe, P. (2017). Simulation versus optimisation: theoretical positions in energy system modelling, *Energies* **10**(7): 840.

Metcalf, G. E. and Stock, J. H. (2017). Integrated assessment models and the social cost of carbon: a review and assessment of us experience, *Review of Environmental Economics and Policy* .

Nerini, F. F., Keppo, I. and Strachan, N. (2017). Myopic decision making in energy system decarbonisation pathways. a uk case study, *Energy strategy reviews* **17**: 19–26.

Nicholls, Z. R., Meinshausen, M., Lewis, J., Gieseke, R., Dommenget, D., Dorheim, K., Fan, C.-S., Fuglestvedt, J. S., Gasser, T., Golüke, U. et al. (2020). Reduced complexity model intercomparison project phase 1: introduction and evaluation of global-mean temperature response, *Geoscientific Model Development* **13**(11): 5175–5190.

Nordhaus, W. D. (1992). The 'dice'model: background and structure of a dynamic integrated climate-economy model of the economics of global warming.

Nordhaus, W. D. and Yang, Z. (1996). A regional dynamic general-equilibrium model of alternative climate-change strategies, *The American Economic Review* pp. 741–765.

Pindyck, R. S. (2017). The use and misuse of models for climate policy, *Review of Environmental Economics and Policy* .

Riahi, K., van Vuuren, D. P., Kriegler, E., Edmonds, J., O'Neill, B. C., Fujimori, S., Bauer, N., Calvin, K., Dellink, R., Fricko, O., Lutz, W., Popp, A., Cuaresma, J. C., KC, S., Leimbach, M., Jiang, L., Kram, T., Rao, S., Emmerling, J., Ebi, K., Hasegawa, T., Havlik, P., Humpenöder, F., Da Silva, L. A., Smith, S., Stehfest, E., Bosetti, V., Eom, J., Gernaat, D., Masui, T., Rogelj, J., Strefler, J., Drouet, L., Krey, V., Luderer, G., Harmsen, M., Takahashi, K., Baumstark, L., Doelman, J. C., Kainuma, M., Klimont, Z., Marangoni, G., Lotze-Campen, H., Obersteiner, M., Tabeau, A. and Tavoni, M. (2017). The Shared Socioeconomic Pathways and their energy, land use, and greenhouse gas emissions implications: An overview, *Global Environmental Change* **42**: 153–168.

Roelfsema, M., van Soest, H. L., Harmsen, M., van Vuuren, D. P., Bertram, C., den Elzen, M., Höhne, N., Iacobuta, G., Krey, V., Kriegler, E. et al. (2020). Taking stock of national climate policies to evaluate implementation of the paris agreement, *Nature communications* **11**(1): 2096.

Smith, P., Davis, S. J., Creutzig, F., Fuss, S., Minx, J., Gabrielle, B., Kato, E., Jackson, R. B., Cowie, A., Kriegler, E. et al. (2016). Biophysical and economic limits to negative co 2 emissions, *Nature climate change* **6**(1): 42–50.

Stern, N. (2016). Economics: Current climate models are grossly misleading, *Nature* **530**(7591): 407–409.

Tol, R. S. (1997). On the optimal control of carbon dioxide emissions: an application of fund, *Environmental Modeling & Assessment* **2**: 151–163.

Trutnevyte, E. (2016). Does cost optimization approximate the real-world energy transition?, *Energy* **106**: 182–193.

van der Wijst, K.-I., Hof, A. F. and van Vuuren, D. P. (2021). On the optimality of 2° c targets and a decomposition of uncertainty, *Nature communications* **12**(1): 2575.

Van Vuuren, D. P., Hoogwijk, M., Barker, T., Riahi, K., Boeters, S., Chateau, J., Scrieciu, S., van Vliet, J., Masui, T., Blok, K. et al. (2009). Comparison of top-down and bottom-up estimates of sectoral and regional greenhouse gas emission reduction potentials, *Energy policy* **37**(12): 5125–5139.

Weyant, J. (2017). Some contributions of integrated assessment models of global climate change, *Review of Environmental Economics and Policy* .

4.2 . Near-optimal and Paris-compliant pathways robust to physical uncertainty, economic paradigms, and intergenerational equity

Abstract: Integrated Assessment Models (IAMs) play a crucial role in examining the potential impacts of various policy options and socio-economic developments on outcomes such as greenhouse gas emissions, climate change, and human well-being. However, there is limited understanding of how the conceptual choices in these models, such as the form of cost functions or minimization criteria, influence the identification of mitigation pathways. Here, we address this gap by analyzing a large set of CO_2 emission pathways that are compatible with the 2°C temperature target, generated using a reduced-form climate model with a thousand different representations of Earth system physics for a comprehensive representation of climate uncertainty. We estimate and compare the costs of these CO_2 emission pathways according to a variety of conceptual choices for both the minimization criterion and the cost function. Given the size and scope of our ensemble, we consider the least-cost pathways are near optimal. We find that about half of the near-optimal pathways are common to all conceptual choices (six cost functions and two minimization criteria) and can therefore be described as economically robust. To deal with the physical uncertainty represented by the thousand physical states of the world of our ensemble, we calculate the proportions of robust pathways in each of them and summarize the results by reporting the median value. If we choose net present value (NPV) as the minimization criterion, about 80% of the near-optimal pathways are robust to the choice of the cost function. The shape of the cost function becomes more discriminatory when a minimax approach is chosen as the minimization criterion. We establish that the most important distinguishing factor is whether or not inertia is considered in the costs. To consider generational cost repartition, we propose a third minimization criterion with the difference in costs between the current generation (2021-2060) and the future generation (2061-2100). 24% of the near-optimal pathways are robust to this minimization criterion across all the cost functions and are described as generationally robust. Hence, it is more difficult to be generationally robust than economically robust. About half of these generationally robust pathways are also economically robust to conceptual choices regarding the cost function and the minimization criterion. Accounting for physical uncertainty appears to be critical for 4% of the explored physical states of the world that do not find generationally and economically robust pathways. However, when they exist, these pathways are characterized by early onset of mitigation and net negative emissions at a reasonable scale, similar to or slightly more optimistic than comparable IPCC scenarios. Overall, our results highlight the importance of understanding conceptual choices when IAMs are used to develop mitigation policies and can the modelling community to take more informed decisions about the climate change mitigation strategies to select for in-depth modelling.

Near-optimal and Paris-compliant pathways robust to physical uncertainty, economic paradigms, and intergenerational equity

Thomas Bossy, Thomas Gasser, Franck Lecocq

Introduction

Climate change mitigation is a complex challenge that requires careful planning and strategic decision-making. Integrated Assessment Models (IAMs) have emerged as a crucial tool for informing these decisions, providing insights into the potential costs and benefits of different mitigation strategies [1]. However, the use of aggregated IAMs is not without limitations and uncertainties. These models often rely on simplified representations of complex economic and climatic processes, leading to significant structural uncertainties in their projections [2, 3].

While previous studies [4-6] have acknowledged and explored these limitations and uncertainties, there remains a significant gap in our understanding of how they interact with - and influence - the identification of cost-optimal or near-optimal pathways. In particular, the impact of various conceptual choices on mitigation costs calculation and optimization remains under-studied [7]. In light of these considerations, the objective of this study is to explore how different cost function paradigms and minimization criteria impact the identification of near-optimal pathways for climate change mitigation.

We use a backward approach to back-calculate global CO_2 emission scenarios based on temperature and atmospheric CO_2 concentration pathways that correspond to the Paris Agreement goals: staying below +2°C and asymptotically reaching +1.5°C in the very long term. To do this, we use Pathfinder, a reduced complexity climate model calibrated using observations and climate projections from the sixth Assessment Report (AR6) of the Intergovernmental Panel on Climate Change (IPCC) [8]. Pathfinder provides about 2500 CO_2 ex-ante emission scenarios, all of which remain below 2°C. The model is run under 1000 different configurations where the parameters are drawn from the posterior probability distribution obtained after Bayesian calibration[8] and represent equally likely physical states of the world. Combining this probabilistic evaluation with the thousands of semi-randomly generated pathways yields several million possible futures.

With this very large ensemble of pathways, which comprehensively explores the space of physically compatible emission pathways that remain below 2°C, we search for economically near-optimal pathways in terms of abatement costs. To address the uncertainty of the abatement cost function [3, 9] and the different minimization criterion [10, 11], we explore variations of these two key choices and look for robust pathways defined as the pathways identified as “least cost” in at least two of these variations. We test six different forms of the abatement cost function and two minimization criteria for comparing costs: a net present value (NPV) approach (discounting at 4%) and an alternative minimax approach that minimizes the maximum relative cost (as a percentage of GDP) across pathways, without discounting. While physical uncertainty is addressed by the thousand physical configurations of Pathfinder, we add a final dimension to the analysis with intergenerational cost sharing to identify robust and equitable set of CO_2 emission pathways consistent with the 2°C temperature target.

Methods

Generation of pathways meeting Paris Agreement

Unlike most aggregated IAMs[2], we do not look for one cost-optimal pathway, but for a set of near-optimal pathways derived from a much larger ensemble of possible emission pathways. We back-calculate CO_2 emission and non-CO_2 radiative forcing (non-CO_2 RF) pathways that correspond to temperature pathways that stay below 2°C and asymptotically reach 1.5°C in the long term (Figure 1, step 2). If CO_2 emissions fall below the lower limit of the AR6 scenarios envelope [12], we attribute the gap to carbon dioxide removal (CDR). This model is known as Pathfinder v1.0.1 [8], a reduced-complexity carbon-climate model. The model parameters are based on CMIP6 models and were calibrated by Bayesian inference [13] using observations and assessed values from the latest IPCC report. To account for physical uncertainty, the model is run under 1000 different configurations (i.e. a set of model parameters representing the physics of the Earth system), with parameters drawn from the posterior probability distributions resulting from the Bayesian calibration (Figure 1, step 2).

Our ex-ante method for generating temperature and CO_2 atmospheric concentration input trajectories cannot include socioeconomic constraints by construction (Supplementary Materials). Therefore, the output of Pathfinder is a large ensemble of emissions pathways, some of which explore implausible values of CO_2 emissions or non-CO_2 RF. To eliminate these unrealistic pathways, we add two conditions : i) limit CDR to a maximum of 37 $GtCO_2\ yr^{-1}$ and ii) impose that non-CO_2 RF cannot fall below the lower limit of the AR6 scenarios envelope [12]. In other words, all our pathways are consistent with mitigation of non-CO_2 forcers in AR6 and do not rely on speculative technology such as solar radiation management or direct CH_4 removal. To avoid retaining pathways being realistic only because of a particular Earth system physics in Pathfinder, we ensure that the two conditions above are met in at least 80% of the 1000 configurations.

Definition of abatement cost functions

Aggregated IAMs do not represent all the mitigation technologies and their costs. They necessitate the use of stylized cost functions that are defined by each modeling team. The choice of a cost function results in a wide range of projections for the optimal carbon tax [14]. A common debate about this choice regards the most effective approach to incorporate dynamic realism, i.e. the consideration of prior abatements in the cost function [7]. Historically, most IAMs have overlooked dynamic realism, but in recent years, an increasing number of models have integrated it into their abatement cost functions through induced innovation or inertia. Yet, there is no consensus on the specific form of the term that represents emission reduction. While many models employ a power law, others propose the inclusion of a linear term.

To address the various conceptual possibilities, we developed six abatement cost functions derived from five aggregated models: ACC2 [15], DICE [16], PAGE [17], RESPONSE [18] and DICE-PACE [7]. Based on insights from the literature, we determined that the abatement costs (denoted as $c\left(a, \frac{da}{dt}, \sum a\,, t\right)$ and measured in $10^9\$\ yr^{-1}$) can be derived from the abatement relative to a baseline (a in $GtCO_2\ yr^{-1}$), the abatement rate ($\frac{da}{dt}$ in $GtCO_2\ yr^{-2}$), the absolute cumulative abated emissions ($\sum a$ in $GtCO_2$) and the time (t). Specifically, we decompose the cost into the product of two functions: $Tech(t, \sum a)$ which represents technological change and $S(a, \frac{da}{dt})$ which indicates the form of the cost function. We can write $c\left(a, \frac{da}{dt}, \sum a\,, t\right) = Tech(t, \sum a)\ S(a, \frac{da}{dt})$. One can note that this cost does not consider non-CO_2 RF pathways.

Technological change can manifest as either endogenous or exogenous. In the case of exogenous technological change, referred to as autonomous technological change, it follows the form

$Tech(t) = \tau^t$, where τ represents a discount factor resulting in an annual decrease in abatement costs by (1 - □)*100% due to external innovation.

If we assume endogenous technological change, we utilize the expression $Tech(\sum a) = (1 + \sigma \sum a)^{\mu}$, which captures induced innovation through the process of learning by doing (LBD). Past abated emissions ($\sum a$) are considered an experiential gain that reduces future costs. To account for the initial experience stock (IES) of avoided emissions, which serves as a reference, we define $\sigma = \frac{1}{IES}$ as the reciprocal of IES.

In total, three terms can be combined to form $S\left(a, \frac{da}{dt}\right)$. Firstly, to model the initial behavior of abatement costs, we introduce a linear term (βa). Setting β = 0 represents a pathway where the initial abatement is free.

Secondly, all examined models incorporate a non-linear cost function, such as $(\alpha - \beta)\frac{a^{\theta}}{\theta E^{\theta-1}}$ derived from DICE [16] and employed in RESPONSE [18] and DICE-PACE [7]. Here, α represents the marginal cost for maximum mitigation (a = E), which essentially represents the current price of the backstop technology. The cost elasticity, denoted as θ, remains constant.

Finally, we define an inertia term that penalises the speed of decarbonisation, expressed as $\frac{GDP}{E^{\varphi}}\left(\delta \frac{da}{dt}\right)^{\varphi}$, where □ represents a scaling factor reflecting the transition timescale measured in years. The cost parameter φ, greater than 1, shapes the inertia term.

The non-linear and inertia terms incorporate E and GDP as multipliers to maintain the homogeneity of the cost function. These terms show the dependency of calculated costs on the chosen baselines. To evaluate the impact of conceptual choices on abatement costs, not all combinations of these terms are explored. We calculate the costs for each CO_2 emission pathway using six distinct cost functions that are chosen for their relevance (Supplementary Materials; Figure 1, step 3).

The non-linear term is present under various forms in most of the functions from aggregated IAMs. Therefore, we build all the cost functions around this term. First, we take the most common function used in DICE [16].

- *DICE*: $c(a,t) = \tau^t \left[\alpha \frac{a^{\theta}}{\theta E^{\theta-1}}\right]$

(1)

Since autonomous technical change and LBD have the same discounting role, it is near impossible to calibrate both terms simultaneously, so we choose either one or the other. Therefore, the second functional form is the same as *DICE*, but autonomous technical change is replaced by LBD.

- *DICE_LBD*: $c(a, \sum a) = (1 + \sigma \sum a)^{\mu}\left[\alpha \frac{a^{\theta}}{\theta E^{\theta-1}}\right]$

(2)

This conceptual approach takes into account the dynamic realism of emitting systems through induced innovation. It is also possible to maintain an exogenous innovation and introduce an inertia term to the *DICE* form.

- *DICE_inertia*: $c\left(a, \frac{da}{dt}, t\right) = \tau^t \left[\alpha \frac{a^{\theta}}{\theta E^{\theta-1}} + \frac{GDP}{E^2}\left(\delta \frac{da}{dt}\right)^{\varphi}\right]$

(3)

Instead of inertia, we can add a linear term that artificially determines the costs in the first years.

- *DICE_linear*: $c(a,t) = \tau^t \left[\beta\, a + (\alpha - \beta)\frac{a^\theta}{\theta E^{\theta-1}}\right]$

(4)

DICE_inertia and *DICE_linear* have a new term not represented in other models to study its influence when combined only with the mainstream cost function (*DICE*). Each of the first four functions allows each conceptual choice to be studied separately. We added two more complex functions to examine how abatement costs behave when we combine several of these conceptual terms, while keeping the distinction between exogenous and endogenous technological innovation.

- *Full*: $c\left(a, \frac{da}{dt}, t\right) = \tau^t \left[\beta\, a + (\alpha - \beta)\frac{a^\theta}{\theta E^{\theta-1}} + \frac{GDP}{E^2}\left(\delta \frac{da}{dt}\right)^\varphi\right]$

(5)

- *Full_LBD*: $c\left(a, \sum a, \frac{da}{dt}\right) = (1+\sigma \sum a)^\mu [\beta\, a + (\alpha - \beta)\frac{a^\theta}{\theta E^{\theta-1}} + \frac{GDP}{E^2}\left(\delta \frac{da}{dt}\right)^\varphi]$

(6)

Overall, we chose the *DICE* function because it is widely used in the literature and provides a baseline for comparison. The *DICE_LBD*, *DICE_inertia* and *DICE_linear* functions were chosen to explore the impact of including inertia and linear terms, which have been suggested as important factors in previous studies [7, 18]. The *Full* and *Full_LBD* functions were chosen to examine the combined effect of these terms.

Calibration method

To calibrate the parameters of the six cost functions in equations (1) to (6), we employ data from the AR6 Scenario Explorer database [12]. Process-based integrated assessment models (IAMs) utilize numerous metrics to derive abatement costs [19]. These metrics encompass GDP loss, consumption loss, marginal costs of the energy system, marginal energy investments, or carbon price, serving as proxies for abatement costs. Consequently, directly comparing abatement costs with the IAM database outputs [12] poses challenges, as the reference or baseline values used to estimate costs are not always explicitly provided for each metric, and complete metric values are not available for all scenarios.

Therefore, for scenarios that can be mapped to a consistent "baseline" scenario, we calculate the GDP loss and assume it to be equivalent to the abatement cost. However, the six cost functions aim to represent several processes that may not have been explicitly considered in IAM scenarios. Furthermore, the functional forms contain numerous terms and parameters without sufficient constraints to effectively replicate costs from complex models. Thus, instead of striving for exact replication of each model's behavior, we opt for a rough calibration approach utilizing three target years in 2030, 2050, and 2100. These years were chosen because they are commonly used reference years in IPCC reports [20, 21] and they allow to constrain our functions on the short-, mid- and long-term. Our primary objective is to obtain estimates that provide a realistic order of magnitude compared to the AR6 models' ensemble rather than a precise model replication. Consequently, we calibrate the functional forms simultaneously for all models and scenarios.

In total, there are eight unknown parameters ($\varphi, \theta, \mu, \sigma, \alpha, \beta, \delta, \tau$), with up to seven parameters within the same cost function. To maintain a low degree of freedom in the calibration, we fix all parameters except the two that are common to all cost functions: α and θ. In the Supplementary Materials, we

present the examination of an alternative calibration method that offers greater degrees of freedom, highlighting its limitations through comprehensive testing. Based on literature, we select $\mu = -2$ and $\varphi = 2$ as the shape parameters [7, 17, 18]. For the sensitivity parameters, based on existing models and literature [16-18], we set $\sigma = 1.4\ 10^{-4}\ GtCO_2^{-1}$, $\beta = \$136\ tCO_2^{-1}$, $\delta = 5$ years and $\tau = 0.995$ (Supplementary Materials).

Choice of GDP and CO_2 emissions baseline

Central to our methodology is the requirement for a baseline for both Gross Domestic Product (GDP) and anthropogenic CO_2 emissions. Such baselines are crucial to facilitate the application of our selected cost functions to these scenarios.

The trajectory of our scenarios extends to the year 2500, a horizon that poses significant challenges to forecasting GDP or CO_2 emissions. For example, the AR6 scenarios only extend to the year 2100 [12]. Relying on these scenarios alone has a potential pitfall, as it could lead to an artificial shift of associated costs beyond 2100.

To overcome this challenge, we incorporated the projections proposed by Rennert and colleagues [22], which leveraged expert assessments to project long-term GDP and CO_2 emissions until 2300. We adopted the median values of these projections to define our baseline. Upon comparison with the AR6 scenarios until 2100 [12], we observe that GDP projections remain consistent. However, our baseline emissions are found to reside at the lower end of the AR6 baseline range (Figure S1). To ensure that abatement always starts at 0 $GtCO_2\ yr^{-1}$, we apply a scaling factor to the baseline so that CO_2 emissions in the first year of the projections (2021) correspond to the initial value of Pathfinder's scenarios in each configuration of the model.

Definition of near-optimal and robust pathways

The substantial scale of our ensemble, encompassing mitigation trajectories that maintain consistency with the 2°C threshold, enables us to assume that the subset of pathways which are minimizing abatement costs, are close to optimal. In this study, we define a pathway as near-optimal within each functional form of the cost function and in each of the 1000 configurations if it falls within the 10% least expensive trajectories in the ensemble produced by Pathfinder (Figure 1, Step 4, the choice of 10% is discussed in the Supplementary Materials). The determination of near-optimal pathways depends on the choice of the minimization criterion. Therefore, we used two criteria. First, we apply the net present value (NPV) approach for the period from 2021 to 2300, using a discount rate of 4% in agreement with existing literature [16]. Second, we examine a minimax approach by comparing the maximum relative cost (as a percentage of GDP) across pathways, without discounting. The NPV method is widely used for cost optimization [16, 17]. Our definition of minimax is different from the minimax regret method used in IAMs to account for parameter uncertainty and minimize regret in the presence of multiple uncertain futures [23].

Given the two minimization criteria and our six cost functions, there is twelve combinations resulting into different subsets of near-optimal pathways. These subsets can be intersected altogether (all twelve combinations) or through a more selective number of combinations. Pathways remaining present within the chosen intersection are defined as 'robust'. To quantify the degree of robustness, we count the number of robust pathways and provide it as a percentage. This robustness score is computed as the ratio of the robust pathways to the size of a subset of near-optimal pathways (10% of the ensemble's size).

In this manuscript, the term "economically robust" is used for a pathway that exhibits near-optimality regardless of the employed cost function and/or minimization criteria. We designate as "robust to NPV" a pathway that demonstrates robustness across all cost functions when NPV is utilized as the criterion for minimization. Similarly, a pathway that withstands robustness assessments across all cost functions using minimax as the minimization criterion is labeled as "robust to minimax."

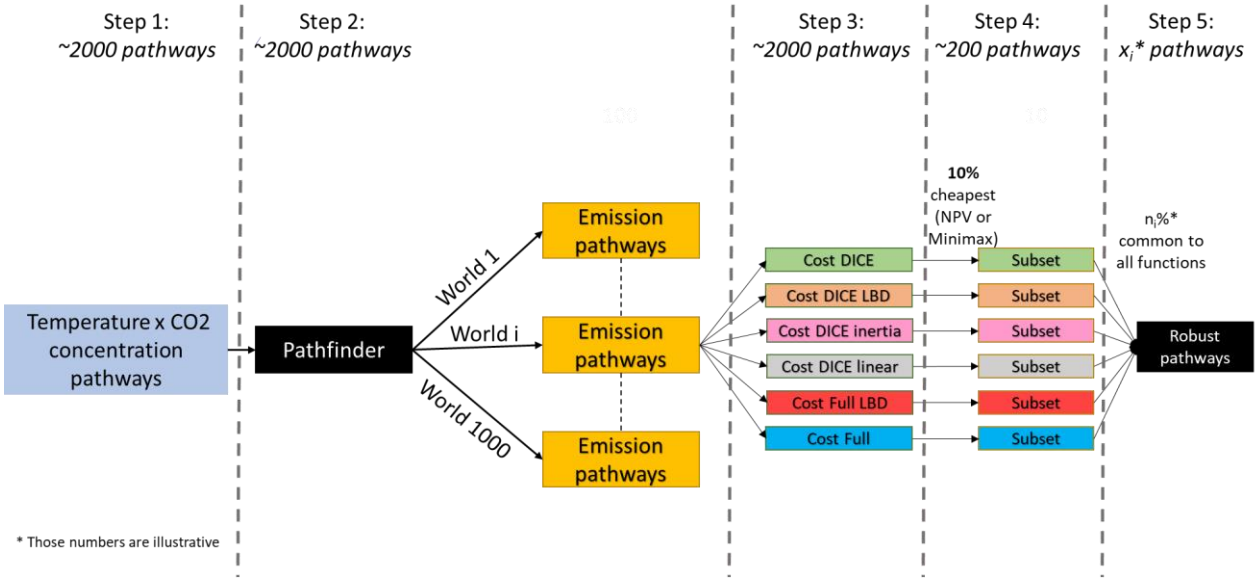

Figure 1 Global framework for defining robust pathways. In step 1, we analytically generate 2°C-compliant temperature and CO_2 concentration pathways. In Step 2, we use Pathfinder to back-calculate CO_2 emissions and non-CO_2 RF pathways that are compatible with our inputs. In Step 3, we estimate abatement costs for all our pathways using six different cost functions. In Step 4, we select only the 10% least expensive pathways (according to a chosen minimization criterion). In Step 5, we compare all subsets of least expensive pathways to define robust near-optimal pathways. This process is applied to 1000 physical worlds, each yielding a different percentage of robust pathways.

Consideration of intergenerational cost repartition

Embedded within the question of the minimization criterion is the intergenerational distribution of costs. The selection of the discount rate is pivotal and has been a topic of considerable debate within the sphere of environmental economics [10, 11, 24].

The minimax strategy seeks to circumvent the complexities associated with the discount rate and expressly avoids signaling a preference for the present. It endeavors to minimize the maximum cost (relative to GDP) throughout the entire temporal span. While this may result in a higher total cost, it ensures that no single generation bears disproportionately high costs for the sake of benefiting others. This methodology should not be conflated with the minimax-regret approach from previous studies, which minimized NPV using an integrated assessment model with extreme parameters for climate sensitivity, damage estimates, and mitigation costs [23].

In order to evaluate the impact of the minimization criterion on the distribution of costs across generations, we partition two generational periods for comparison: an existing generation spanning the years 2021-2060, and a future generation encompassing the years 2061-2100. This partition follows previous work [25] and provides a simple framework to assess intergenerational distribution of global costs. Specifically, we calculate the difference of the NPV estimated for these periods separately (NPV1 for 2021-2060 and NPV2 for 2061-2100). Following [25] we normalize the difference using NPV2. The term "generationally robust" is assigned to a pathway that exhibits near-optimality regardless of the employed cost function and with $NPV_{Diff} = \frac{NPV1-NPV2}{NPV2}$ as the minimization criterion.

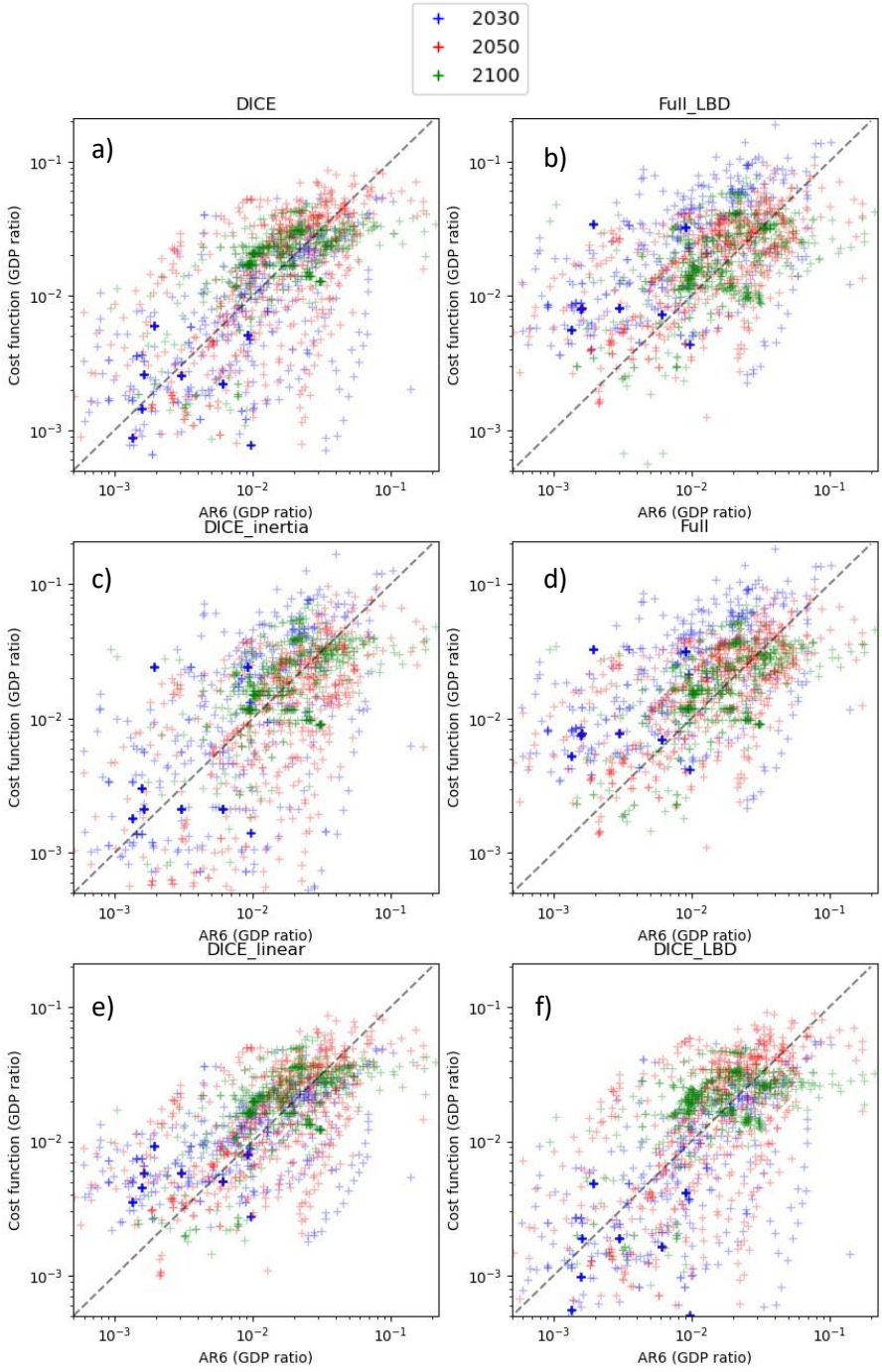

Figure 2 Comparison of abatement costs in AR6 with calibrated costs estimated from the six cost functions: DICE (panel a.), Full_LBD (panel b.), DICE_inertia (panel c.), Full (panel d.), DICE_linear (panel e.), and DICE_LBD (panel f.). The colors represent the three target years we focus on: 2030 (blue), 2050 (red), 2100 (green). This figure is zoomed in and shows most of the points. Figure S2 shows the same panels with all the points.

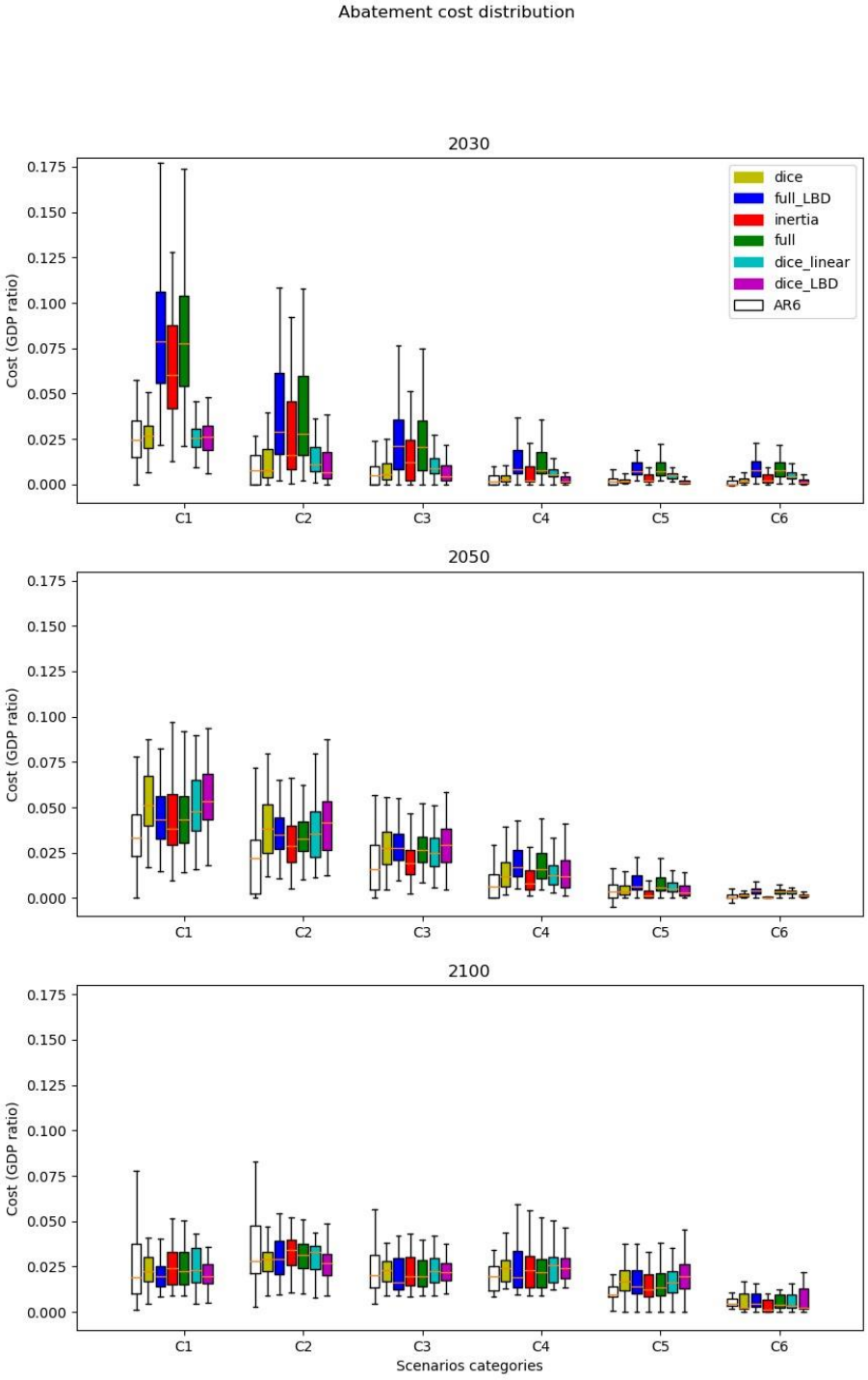

Figure 3 Distribution of mitigation costs from AR6 (white boxes) compared to the six calibrated cost functions (colored boxes) for scenarios across six categories ranked from high to low mitigation scenarios (C1 to C6). Costs are calculated and calibrated on three crossing points in 2030 (panel a.), 2050 (panel b.), and 2100 (panel c.)

Results

Calibration results

The success of the calibration process is assessed for the three target years in 2030, 2050, and 2100. In Figure 2, the costs obtained from six different calibrated cost functions are compared against the AR6 IAMs costs. The results in 2050 and 2100 demonstrate that all six functions yield similar projections reasonably aligned with the AR6. However, the calibrated functions tend to underestimate costs when they are high, i.e. approaching 10% of GDP, while overestimating costs when they are low (Figure S2). Figure 3 presents the cost distribution in the target years and differentiates scenarios into categories from C1 (high mitigation) to C6 (low mitigation) defined in the IPCC's working group III report [26] (Figure S3). In 2050 and 2100, all functional forms of cost estimation remain within the uncertainty range of the IPCC AR6 costs [12]. Nevertheless, in 2050, there is a slight tendency for all functional forms to overestimate costs associated with the high mitigation scenarios (C1 and C2 scenarios). In 2100, regardless of the scenario classification (C1 to C6), all functional forms yield similar cost estimates, with a slight overestimation observed for the C5 scenarios.

Turning our attention to the costs in 2030, the cost estimates associated with the functions incorporating inertia (*DICE_inertia*, *Full*, *Full_LBD*) exhibit significantly higher overestimation (Figure S1, Figure 2). Figure 3 provides further evidence that functions incorporating inertia consistently yield cost estimates well above the range provided by the IPCC for all scenarios, whereas the functions without inertia (*DICE*, *DICE_LBD*, *DICE_linear*) align more closely with the IPCC estimates. This discrepancy is particularly pronounced for the scenarios demanding more stringent mitigation measures, namely C1, C2, and C3. The introduction of the inertia term with a transition time scale (δ) of 5 years, which is more optimistic than what is typically found in the literature, leads to a short-term overestimation of costs. This outcome is expected due to the absence of explicit consideration of inertia in the process-based IAMs employed in the AR6 database [7]. Interestingly, in the presence of the inertia term, the inclusion of the linear term in the cost functions (*Full* and *Full_LBD*) further overestimates the costs compared to the functions without this linear term (*DICE_inertia*). Conversely, the linear term alone (*DICE_linear*) does not contribute to higher cost estimates.

	α	θ
DICE	\$636 / tCO_2	1.93
DICE_LBD	\$792 / tCO_2	2.17
Full	\$661 / tCO_2	5.46
Full_LBD	\$807 / tCO_2	5.74
DICE_inertia	\$881 / tCO_2	3.84
DICE_linear	\$742 / tCO_2	3.35

Table 1: Calibration of the parameters of the abatement cost functions. α represents the marginal cost for maximum mitigation, which essentially represents the current price of the backstop technology. The cost elasticity is denoted as θ.

The calibrated values of the parameters in Table 1 demonstrate that θ, the shape parameter of the power law, is independent of the function used to estimate technological change (endogenous or exogenous). Regardless of whether LBD is included, the same functional forms yield very similar calibrated values for θ. It is observed that the number of terms included in the cost function determines the value of θ. When only the power law is considered, θ is approximately 2 (*DICE* and *DICE_LBD*). Introducing the power law alongside another term increases θ to approximately 3.5

(*DICE_inertia* and *DICE_linear*). Finally, incorporating all three terms (*Full* and *Full_LBD*) in the cost function yields a value of θ around 5.5. The value of α, the sensitivity parameter of the power law, remains stable between \$640/tCO_2 to \$880/tCO_2.. It is in agreement with other similar model's parametrisation (Supplementary Materials).

Selection of economically robust pathways

As previously explained, our investigation incorporates two minimization criteria via NPV and minimax optimization methodologies. We apply these criteria on the large ensemble of Pathfinder's CO_2 emission scenarios to estimate near-optimal pathways for each conceptual cost function. When applying the NPV approach, the choice of the cost function seems to exert minimal influence, as a substantial 78% of the near-optimal pathways are common across all cost functions. However, if the minimax approach is used, the robustness of the near-optimal pathways falls to 55%. This is insightful to identify economically robust near-optimal pathways that are universally shared by both NPV and minimax approaches. These economically pathways robust to the choice of both the cost function and minimization criterion, constitute 54% of all near-optimal pathways. Therefore, a vast majority of pathways demonstrating robustness under the minimax approach also exhibit similar robustness under the NPV approach, as depicted in Figure 4.a.

Minimax	*DICE*	*Full_LBD*	*DICE_inertia*	*Full*	*DICE_linear*	*DICE_LBD*
DICE	100%	62	61%	61%	93%	93%
Full_LBD		100%	98%	98%	57%	57%
DICE_inertia			100%	100%	55%	56%
Full				100%	55%	56%
DICE_linear					100%	96%
DICE_LBD						100%

Table 2.a Percentage of near-optimal pathways robust for minimax$_f$ and two cost functions. The minimax criterion minimizes the maximum relative cost (as a percentage of GDP) across pathways, without discounting.

NPV	*DICE*	*Full_LBD*	*DICE_inertia*	*Full*	*DICE_linear*	*DICE_LBD*
DICE	100%	83%	83%	83%	91%	93%
Full_LBD		100%	98%	98%	81%	83%
DICE_inertia			100%	100%	81%	83%
Full				100%	81%	83%
DICE_linear					100%	96%
DICE_LBD						100%

Table 2.b Percentage of near-optimal pathways robust for NPV and two cost functions. The NPV criterion minimizes the net present value on the period 2021-2300.

NPV$_{Diff}$	*DICE*	*Full_LBD*	*DICE_inertia*	*Full*	*DICE_linear*	*DICE_LBD*
DICE	100%	47%	47%	47%	68%	84%
Full_LBD		100%	99%	99%	38%	33%
DICE_inertia			100%	100%	38%	33%
Full				100%	38%	33%
DICE_linear					100%	58%
DICE_LBD						100%

Table 2.c Percentage of near-optimal pathways robust for NPV$_{Diff}$ and two cost functions. The NPV$_{Diff}$ criterion minimizes the difference of net present value between two generations spanning on the periods 2021-2060 and 2061-2100.

The main discriminatory factor explaining why only 55% of near-optimal pathways are robust to minimax is whether inertia is included in the cost function. On Figure 4.c we divide the cost functions between the ones with inertia (*DICE_inertia*, *Full*, *Full_LBD*) and the ones without (*DICE*, *DICE_LBD*, *DICE_linear*). Both robustness scores to minimax are 98% (with inertia) and 92% (without inertia). This result puts the debates on the linear or technological terms into perspective and would argue for a comparison only between *DICE* and *DICE_inertia*.

Impact of the minimization criterion on inter-generational equity

Following previous studies [27], we evaluate the cost distribution by calculating the NPV difference (NPV_{Diff}) over two generation spans. We find that 24% of the near-optimal pathways are robust to the NPV difference (i.e. generationally robust). We find that the choice of the cost function has a large impact and the key distinguishing feature is inertia. On Figure 4.d we divide the cost functions between the ones with inertia and the ones without. We find a generational robustness scores of 99% for functions with inertia meaning that near-optimal pathways are almost identical for the three functions. Conversely, the generational robustness is only 57% for functions without inertia.

Figure 4.a shows that there is overlap between pathways robust to NPV, minimax and NPV_{Diff}. Indeed, 12% of the near-optimal pathways show robustness to NPV and NPV_{Diff}. 11% of the near-optimal pathways show robustness to NPV, minimax, and NPV_{Diff} and can be qualified as economically and generationally robust.

Generationally robust pathways minimize the difference of NPV between the present and future generations. Yet, it does not say anything about the value of NPV_{Diff} (defined as $NPV_{Diff} = \frac{NPV1-NPV2}{NPV2}$). On Figure S4, we show the distribution of NPV_{Diff} values for generationally robust near-optimal pathways. On one hand, cost functions without inertia are centered on zero and NPV_{Diff} spreads between -0.3 and 0.3. On the other hand, cost functions with inertia shifts costs significantly toward the first generation as NPV_{Diff} is centered on 60.

The role of physical parameters on defining near-optimal pathways.

The determination of robust pathways was repeated for each potential physical world. The physical uncertainties have been accounted for as we have reported so far the median robustness scores across our 1000 potential worlds. However, a comprehensive exploration of the uncertainty range engendered by the 1000 configurations proves informative. The distribution across configurations of four critical robustness scores is shown in Figure 5.Figure 5.a focuses on pathways robust to minimax, Figure 5.b on pathways economically robust, Figure 5.c on pathways generationally robust and Figure 5.d on pathways generationally and economically robust. These distributions underscore that the six cost functions are able to lead to near-optimal pathways robust to various minimization criteria in the vast majority of the configurations. In Figure 5, there are about 1% of the configurations that do not find near-optimal pathways generationally robust (Figure 5.c) and about 4% not finding economically and generationally robust pathways (Figure 5.d). The distributions do not exhibit significant skewness, justifying the use of the median.

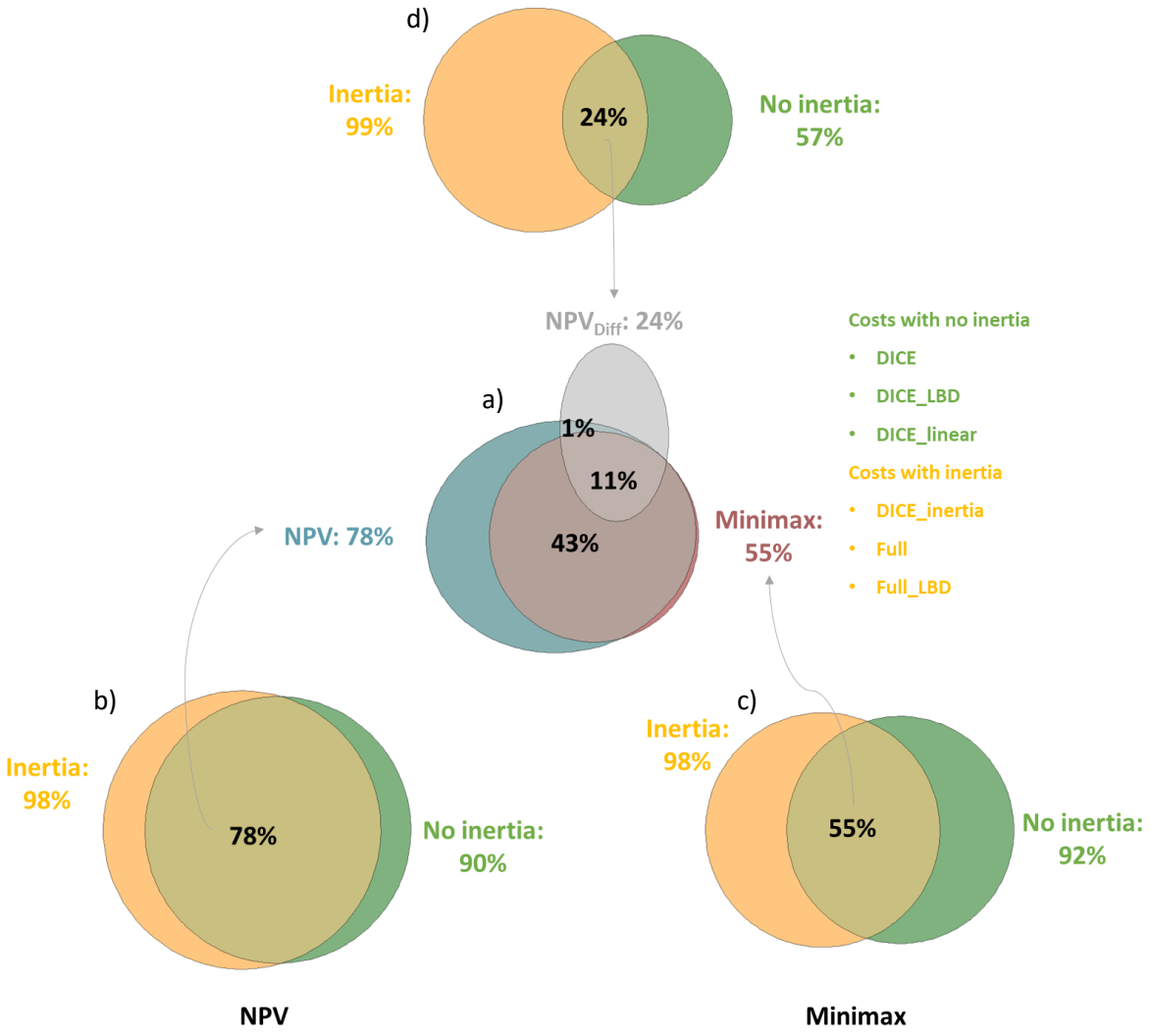

Figure 4 Venn diagrams showing the robustness score for near-optimal pathways that are robust to minimax, NPV and NPV$_{Diff}$ (panel a). Panels b, c and d decompose the robustness score for these robust pathways among cost functions that do or do not account for inertia. The intersection spaces of the circles in panels b, c and d correspond to the size of ellipses in panel a. All robustness scores correspond to the median value across all Pathfinder's configurations.

For enhanced understanding of these distributions, their correlation with certain diagnostic metrics on the model's climate and carbon cycle are considered (Figure 6). Notably, a correlation emerges between the Equilibrium Climate Sensitivity (ECS [28]]) or the Transient Climate Response to Emissions (TCRE [29]) and the robustness score of near-optimal pathways that are economically robust. High TCRE or ECS means that the Earth system is more sensitive to anthropogenic emissions and stronger mitigation is needed to remain below 2°C. The negative correlation signifies that a heightened ECS or TCRE in the model corresponds with lower agreement between the cost functions used to define near-optimal pathways. Therefore, a configuration featuring a lower TCRE or ECS permits smoother mitigation scenarios, attenuating the impact of inertia on costs. Since inertia is the decisive factor when evaluating the robustness score of near-optimal pathways economically robust or only robust to a minimax minimization criterion, a diminished inertia impact logically fosters greater consensus among cost functions and thus a larger robustness score.

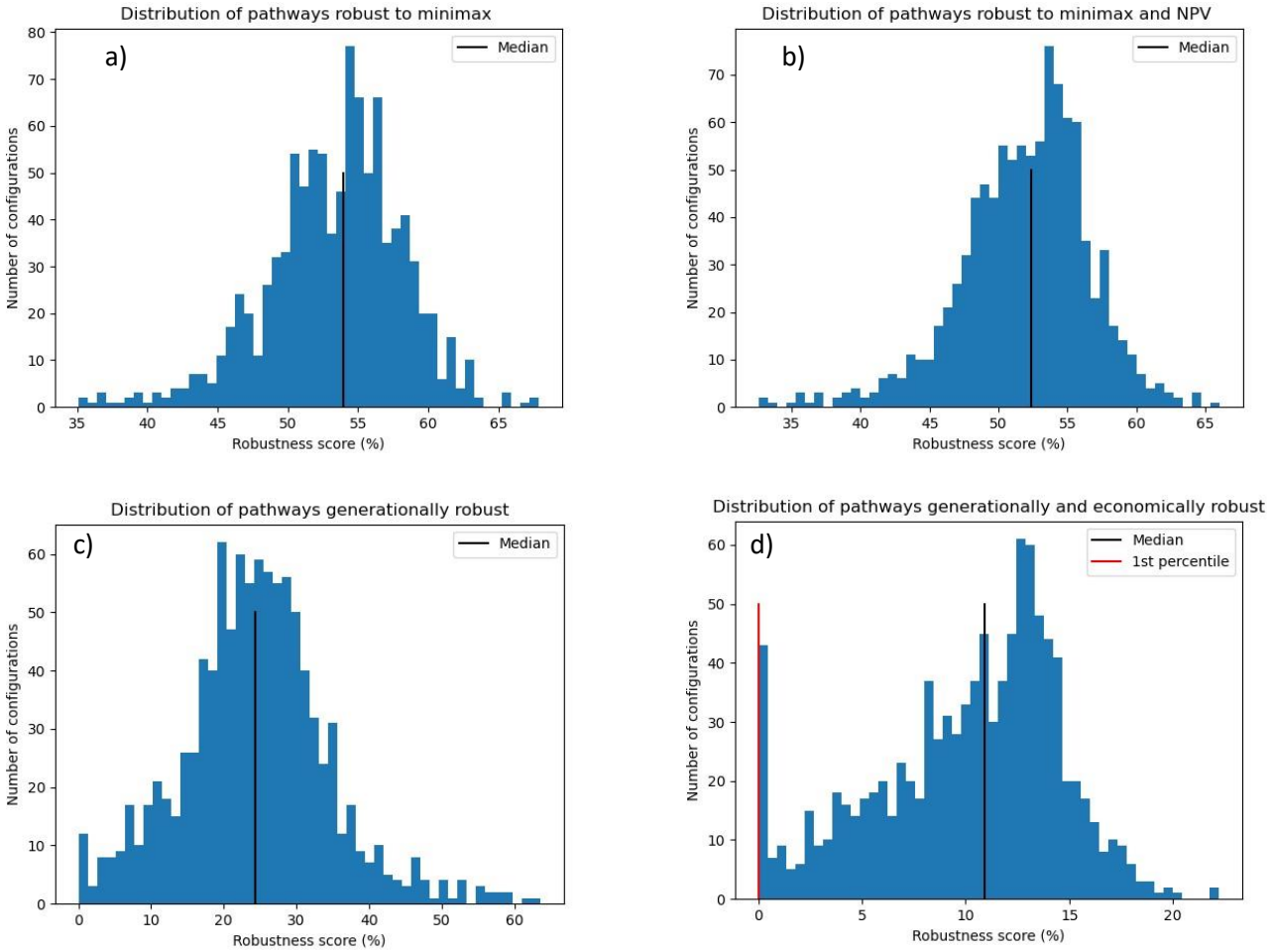

Figure 5 Distribution of the robustness score for near-optimal pathways robust to minimax (panel a), minimax and NPV (panel b), NPV_{Diff} (panel c), and NPV_{Diff}, NPV and minimax (panel d). The black line gives the median value of these distributions. In panel d., the red line gives the 1st percentile of the configuration with the least economically and generationally robust pathways.

There is no significant correlation between physical parameters of the model and the robustness score for generationally or economically and generationally robust pathways.

Influence of robustness criteria on the envelope of near-optimal pathways

We set thresholds for the capacity of physical configurations to identify economically and generationally robust pathways. Suitable thresholds may diverge based on stakeholder groups and risk attitudes [30]. We propose a focus on two: the median (i.e. the 50th percentile), that we have already extensively used, and the 1st percentile of configurations that locate the smallest robustness score of economically and generationally robust pathways. Looking at the 1st percentile is our equivalent of the 'worst possible physical world' aligning with robust decision-making strategies that aim to identify resilience and adaptability amidst uncertainty [31].

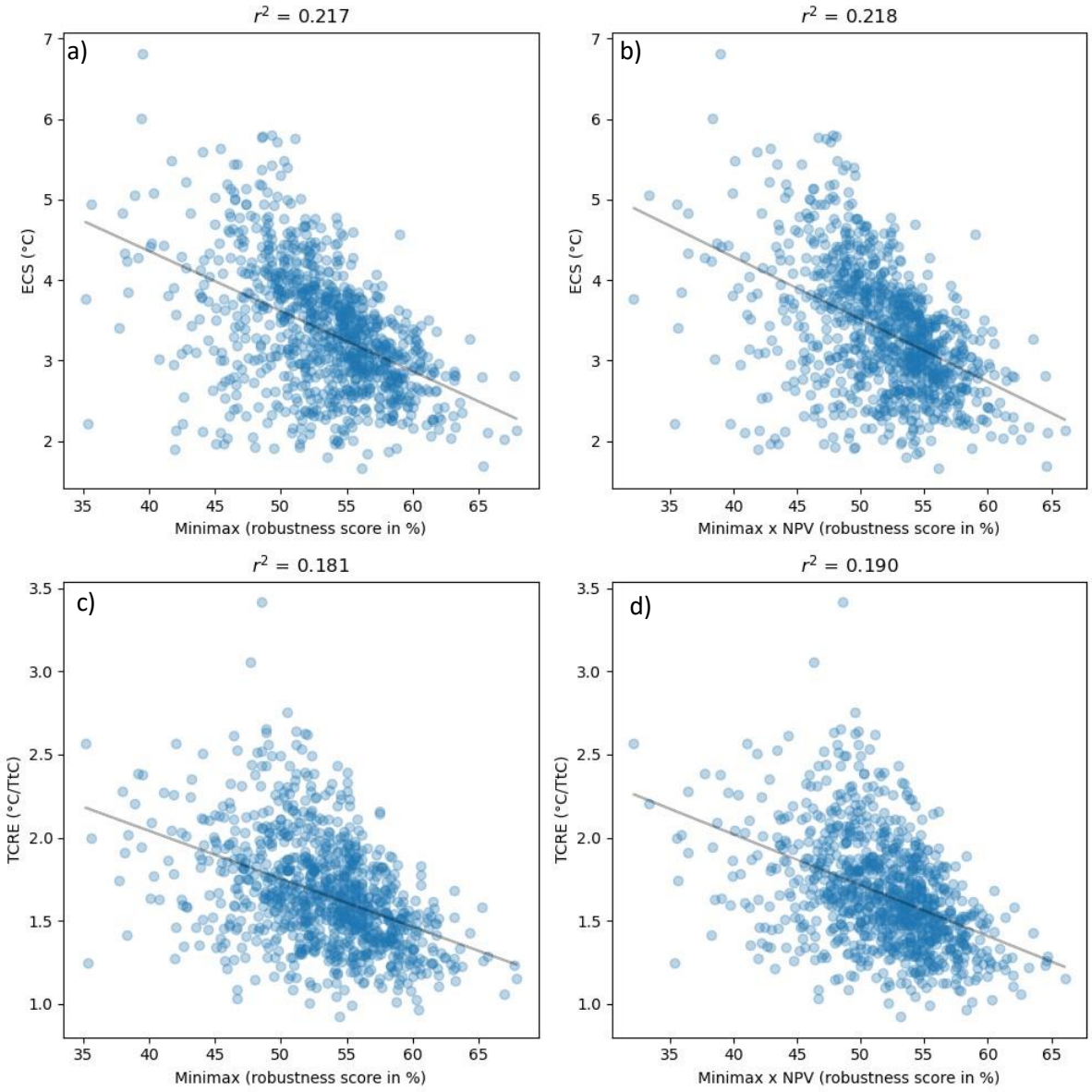

Figure 6 Scatter plots representing the robustness of near-optimal pathways robust to minimax (panels a, c) or economically robust, i.e robust to minimax and NPV (panels b, d) in function of the ECS (panels a, b) or the TCRE (panels c, d).

To explore how the different definitions of robustness influence the selection of pathways, we juxtapose the envelopes of near-optimal pathways generated by different definitions of robustness. Figure 7 illustrate how the envelope of near-optimal pathways reduces when adding conditions for robustness and for the 50th (Figure 7.a) and 1st percentiles (Figure 7.b) of the least robust configurations. On both panels, the widest envelope corresponds to all the 2°C compatible pathways. In this non-optimized case, certain pathways deploy up to 37 $GtCO_2$ yr^{-1} of CDR prior to 2050 and other pathways remain below 2°C with late emission peak and mitigation. The second widest envelope correspond to near-optimal pathways employing only NPV as the minimization criterion and *DICE* as the cost function (denominated as *DICE*-NPV). Pathways from this envelope use up to 33 $GtCO_2$ yr^{-1} from CDR, albeit not prior to 2100. The third envelope encompass economically robust near-optimal pathways. The most extreme of these scenarios requires around 11 $GtCO_2$ yr^{-1} from CDR slightly before 2100. Ultimately, the most restrictive envelope in Figure 7.a ensures both generational and economic

robustness. It covers the lower end of the envelope of economically robust pathways. It implies that earlier net-zero emissions with the use of CDR in the second part of the 21st century is more generationally equitable than pathways aiming for net-zero at the end of the century. As shown in Figure 5.d, there are no near-optimal pathways economically and generationally robust for the 1st percentile of configurations. Therefore, the last envelope disappears in Figure 7.b. Overall, irrespective of the physical configuration, extreme pathways featuring early and severe, or delayed mitigation vanish when economic robustness is incorporated. Conversely, economically and generationally near-optimal pathways, when they exist, appear to advocate a significant early mitigation allowing to delay the deployment of 11 $GtCO_2$ yr^{-1} of negative emissions after 2100. Further analysis in Supplementary Materials demonstrates the consistency of these pathways with comparable IPCC's AR6 scenarios.

Discussion

Our approach to mitigation costs is conceptual and systematic rather than practical. In fact, process-based IAMs behave very differently depending on the model and the SSP scenario chosen. Some very simple mathematical representations [32] reproduce the marginal abatement costs of particular models and scenarios at the expense of generalization and economic interpretation of the emulator. We prefer to use functions that we can interpret economically at the expense of accuracy. However, our functions remain simplified and global representations. In particular, our aggregate approach does not separate the costs of negative emissions technologies from those of conventional emissions reductions.

To calibrate the six cost functions, we decided to fix all parameters save for two (α and θ) that are universally applied across all functions. We also propose an alternative route featuring free calibration, where the two shape parameters were fixed, but with sensitivity parameters calibrated (Supplementary Materials). This permits up to four free parameters simultaneously, leading to the negation of some of the terms of the cost functions. Therefore, such an alternate calibration unveils the most suitable terms for representing process-based costs, providing insights into the dynamics modelled by process-based IAMs, at the cost of eliminating some of the conceptual terms we investigated in our study. For instance, we found that inertia is unnecessary to emulate these costs, indicating that complex IAMs might not adequately model it.

Minimization criterion forms the second choice for calculating mitigation costs that we analyzed. We made deliberate choices in setting the discount rate, a topic extensively debated with well-documented implications of these decisions [23, 24]. A discount rate of 4% is generally acceptable, mirroring the value used in most IAMs, although it generates a strong preference for the present. The minimax approach does not necessitate a discount rate but is different from an NPV without discounting. To substantiate this distinction, we executed a recalculation of cost estimations and optimizations using a 0% discount rate. In this case, 59% of the near-optimal pathways for the NPV devoid of discounting are robust. Interestingly, this percentage is more aligned with the minimax approach than with the NPV that incorporates a 4% discounting. Yet, it is worth noting that the NPV with 0% discounting generates fewer economically robust pathways as compared to an NPV with a 4% discount. Thus, it can be effectively inferred that 54% of near-optimal pathways display robustness under both the minimax and NPV paradigms incorporating a discount rate. Contrarily, a mere 38% of pathways manifest robustness under both the NPV bereft of any discounting and the minimax approach (Figure S5).

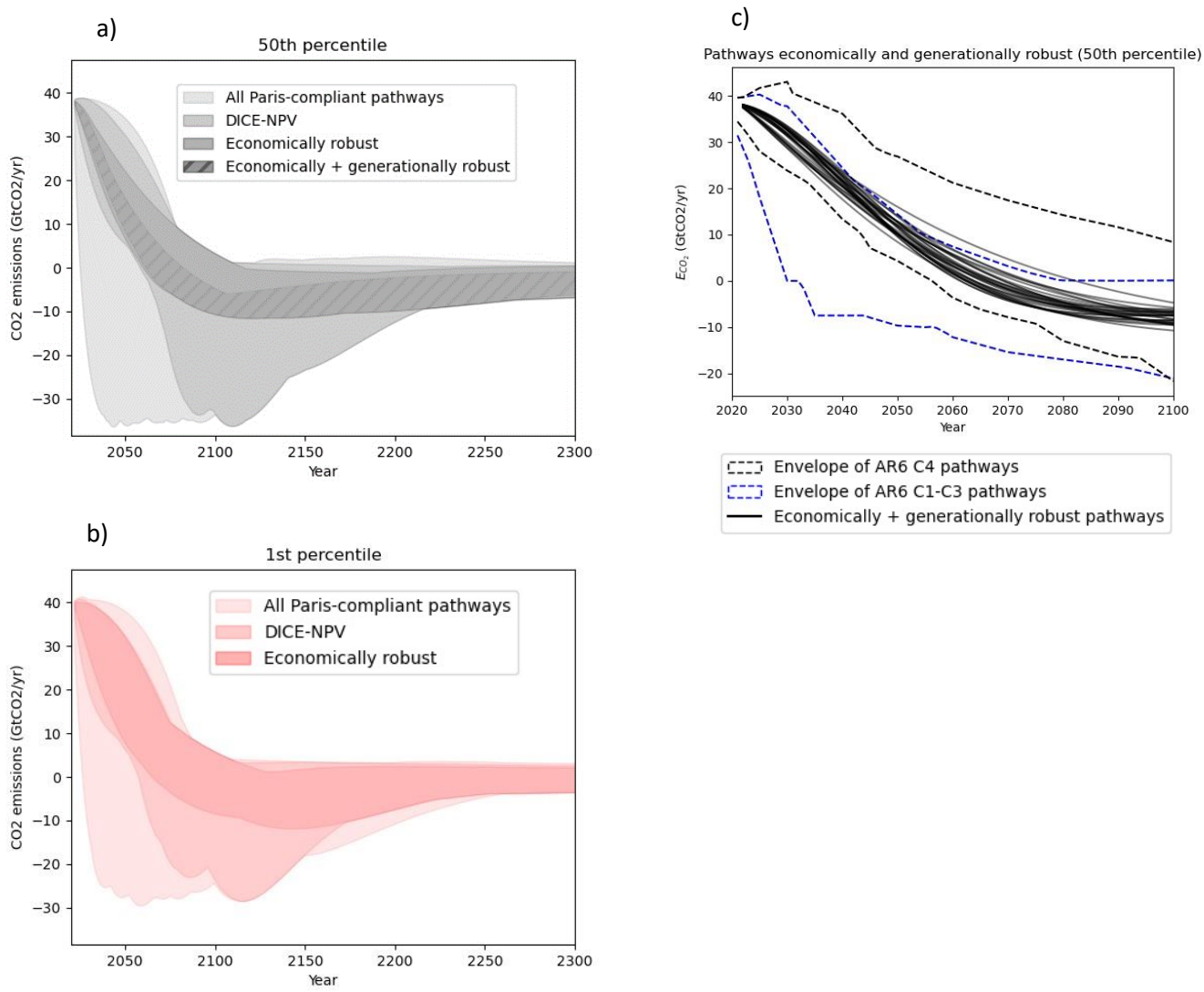

Figure 7 Economically and generationally robust pathways for two Pathfinder configurations corresponding to the 50th (gray) and the 1st (red) percentiles of the distributions of ratios of near-optimal pathways robust to minimax, NPV and NPV$_{Diff}$. Shaded areas give the envelopes (from lighter to darker) of 1) all the Paris-compliant pathways calculated by Pathfinder, 2) the near-optimal pathways for DICE as a cost function and NPV as a minimization paradigm, 3) the near-optimal pathways economically robust, and 4) the near optimal pathways economically and generationally robust. The envelopes are represented for the 50th percentile on panel a), and for the 1st percentile on panel b). Envelope 4) only appears on panel a) and is hatched. Panel c) zooms on the period 2020-2100 and shows all economically and generationally robust pathways for both 1st and 50th percentile configurations. Black and blue dashed lines represent the envelope of C4 and C1-C3 AR6 scenarios. Non-CO$_2$ RF coupled to the CO$_2$ emission trajectories of panel c) are shown in Figure S6.

We opted for a cost-effective approach under a constraint of limiting the temperature to below 2°C to comply with the Paris Agreement. In doing so, we compare pathways that peak at 2°C in 2100 and tend towards 1.5°C in 2500 with pathways that asymptotically reach 1.5°C in 2100. Our cost-effective approach assumes that damages are the same across all emission scenarios meeting that target. This constitutes a potent assumption, especially if we intend to tackle intergenerational equity issues. One could argue that a 2°C limit is adequate to prevent the most disastrous damages, but the impacts of a

1.5°C and a 2°C scenario diverge significantly in terms of costs, population vulnerability, or biodiversity loss [33, 34]. However, our methodology could be applied to any temperature target and hence, remains an insightful tool for identifying and exploring near-optimal scenarios. Further consideration of potential damages and their distribution across generations would be a natural follow-up paper.

Conclusion

This study has built a comprehensive ensemble of 2°C-compatible CO_2 emission scenarios with 1000 different physical representations of the Earth system. This approach allows us to identify pathways near-optimal in terms of mitigation costs according to various perspectives, facilitating a comparative analysis. We have calibrated and analyzed six unique abatement cost functions, each representing a different paradigm for modeling abatement costs in aggregated IAMs. Additionally, we questioned the optimization paradigm by testing two minimization criteria to define near-optimal pathways.

We have found that most near-optimal pathways remain consistent regardless of the calculation method. However, significant differences between cost paradigms emerge when employing the minimax criterion. The primary differentiating factor is inertia, which resonates with the ongoing debate regarding the inclusion of more dynamic realism in the models [7].

Further analysis indicates that some of these economically robust, near-optimal pathways are also among the pathways that distribute costs most evenly between the current and future generations. These economically and generationally robust, near-optimal pathways are within the range of comparable AR6 scenarios. Accounting for physical uncertainties shows that there are worst-case scenarios where it is no longer possible to optimize the intergenerational distribution of mitigation costs while remaining economically robust. When Earth system physics permit them, economically and generationally robust, near-optimal pathways suggest early mitigation efforts and deployment of a measured amount of negative emissions. However, because each CO_2 emissions pathway is associated with a decorrelated mitigation scenario for non-CO_2 GHGs, this paper encourages further detailed research on robust pathways.

[1] (!!! INVALID CITATION !!! {van Beek, 2022 #128;Weyant, 2017 #131;Metcalf, 2017 #126;Riahi, 2022 #73}).
[2] C. Guivarch, E. Kriegler, J. Portugal Pereira, V. Bosetti, J. Edmonds, M. Fischedick, P. Havlik, P. Jaramillo, V. Krey, F. Lecocq, A. Lucena, M. Meinshausen, S. Mirasgedis, B. O'Neill, G. Peters, J. Rogelj, S. Rose, Y. Saheb, G. Strbac, A.H. Stromman, D.P. Van Vuuren, N. Zhou, Annex III: Scenarios and Modelling method, *Climate change 2022: Mitigation of Climate Change. Contribution of Working Group III to the Sixth Assessment Report of the Intergovernmental Panel on Climate Change*, (2022).
[3] K.-I. van der Wijst, A.F. Hof, D.P. van Vuuren, On the optimality of 2° C targets and a decomposition of uncertainty, *Nature communications*, **12** (2021) 2575.
[4] I. Keppo, I. Butnar, N. Bauer, M. Caspani, O. Edelenbosch, J. Emmerling, P. Fragkos, C. Guivarch, M. Harmsen, J. Lefevre, Exploring the possibility space: taking stock of the diverse capabilities and gaps in integrated assessment models, *Environmental Research Letters*, **16** (2021) 053006.
[5] R.S. Pindyck, The use and misuse of models for climate policy, *Review of Environmental Economics and Policy*, (2017).
[6] G. Heal, The economics of the climate, *Journal of Economic Literature*, **55** (2017) 1046-1063.
[7] M. Grubb, C. Wieners, P. Yang, Modeling myths: On DICE and dynamic realism in integrated assessment models of climate change mitigation, *Wiley Interdisciplinary Reviews: Climate Change*, **12** (2021) e698.
[8] T. Bossy, T. Gasser, P. Ciais, Pathfinder v1. 0.1: a Bayesian-inferred simple carbon–climate model to explore climate change scenarios, *Geoscientific Model Development*, **15** (2022) 8831-8868.
[9] D.P. van Vuuren, K.-I. van der Wijst, S. Marsman, M. van den Berg, A.F. Hof, C.D. Jones, The costs of achieving climate targets and the sources of uncertainty, *Nature Climate Change*, **10** (2020) 329-334.
[10] N. Stern, Stern Review: The economics of climate change, (2006).
[11] W.D. Nordhaus, A review of the Stern review on the economics of climate change, *Journal of economic literature*, **45** (2007) 686-702.
[12] E. Byers, V. Krey, E. Kriegler, K. Riahi, R. Schaeffer, J. Kikstra, R. Lamboll, Z. Nicholls, M. Sanstad, C. Smith, AR6 Scenarios Database hosted by IIASA, in, International Institute for Applied Systems Analysis, 2022.
[13] D.M. Ricciuto, K.J. Davis, K. Keller, A Bayesian calibration of a simple carbon cycle model: The role of observations in estimating and reducing uncertainty, *Global biogeochemical cycles*, **22** (2008).
[14] J. Weyant, Some contributions of integrated assessment models of global climate change, *Review of Environmental Economics and Policy*, (2017).
[15] K. Tanaka, O. Boucher, P. Ciais, D.J. Johansson, J. Morfeldt, Cost-effective implementation of the Paris Agreement using flexible greenhouse gas metrics, *Science advances*, **7** (2021) eabf9020.
[16] W. Nordhaus, P. Sztorc, DICE 2013R: Introduction and user's manual, *Yale University and the National Bureau of Economic Research, USA*, (2013).
[17] C. Hope, Critical issues for the calculation of the social cost of CO 2: why the estimates from PAGE09 are higher than those from PAGE2002, *Climatic Change*, **117** (2013) 531-543.
[18] A. Pottier, E. Espagne, B. Perrissin Fabert, P. Dumas, The comparative impact of integrated assessment models' structures on optimal mitigation policies, *Environmental Modeling & Assessment*, **20** (2015) 453-473.
[19] V. Krey, Global energy-climate scenarios and models: a review, *Wiley Interdisciplinary Reviews: Energy and Environment*, **3** (2014) 363-383.
[20] P.-R. Shukla, J. Skea, R. Slade, A. Al Khourdajie, R. van Diemen, D. McCollum, M. Pathak, S. Some, P. Vyas, R. Fradera, M. Belkacemi, A. Hasija, G. Lisboa, S. Luz, J. Malley, Mitigation of Climate Change. Contribution of Working Group III to the Sixth Assessment Report of the Intergovernmental Panel on Climate Change, *IPCC Sixth Assessment Report*, (2022).

[21] V. Masson-Delmotte, P. Zhai, A. Pirani, S.L. Connors, C. Péan, S. Berger, N. Caud, Y. Chen, L. Goldfarb, M. Gomis, Climate change 2021: the physical science basis, *Contribution of working group I to the sixth assessment report of the intergovernmental panel on climate change*, **2** (2021).

[22] K. Rennert, B.C. Prest, W.A. Pizer, R.G. Newell, D. Anthoff, C. Kingdon, L. Rennels, R. Cooke, A.E. Raftery, H. Ševčíková, The social cost of carbon: advances in long-term probabilistic projections of population, GDP, emissions, and discount rates, *Brookings Papers on Economic Activity*, **2021** (2022) 223-305.
[23] A.F. Hof, D.P. Van Vuuren, M.G. Den Elzen, A quantitative minimax regret approach to climate change: Does discounting still matter?, *Ecological Economics*, **70** (2010) 43-51.
[24] J. Emmerling, L. Drouet, K.-I. van der Wijst, D. Van Vuuren, V. Bosetti, M. Tavoni, The role of the discount rate for emission pathways and negative emissions, *Environmental Research Letters*, **14** (2019) 104008.
[25] J.-Y. Liu, S. Fujimori, T. Masui, Temporal and spatial distribution of global mitigation cost: INDCs and equity, *Environmental Research Letters*, **11** (2016) 114004.
[26] K. Riahi, R. Schaeffer, J. Arango, K. Calvin, C. Guivarch, T. Hasegawa, K. Jiang, E. Kriegler, R. Matthews, G. Peters, Mitigation pathways compatible with long-term goals, *Climate change*, (2022).
[27] Z. Liu, Z. Deng, B. Zhu, P. Ciais, S.J. Davis, J. Tan, R.M. Andrew, O. Boucher, S.B. Arous, J.G. Canadell, Global patterns of daily CO2 emissions reductions in the first year of COVID-19, *Nature Geoscience*, **15** (2022) 615-620.
[28] S. Sherwood, M.J. Webb, J.D. Annan, K.C. Armour, P.M. Forster, J.C. Hargreaves, G. Hegerl, S.A. Klein, K.D. Marvel, E.J. Rohling, An assessment of Earth's climate sensitivity using multiple lines of evidence, *Reviews of Geophysics*, **58** (2020) e2019RG000678.
[29] P. Goodwin, R.G. Williams, A. Ridgwell, Sensitivity of climate to cumulative carbon emissions due to compensation of ocean heat and carbon uptake, *Nature Geoscience*, **8** (2015) 29-34.
[30] D. Hadka, J. Herman, P. Reed, K. Keller, An open source framework for many-objective robust decision making, *Environmental Modelling & Software*, **74** (2015) 114-129.
[31] C.P. Weaver, R.J. Lempert, C. Brown, J.A. Hall, D. Revell, D. Sarewitz, Improving the contribution of climate model information to decision making: the value and demands of robust decision frameworks, *Wiley Interdisciplinary Reviews: Climate Change*, **4** (2013) 39-60.
[32] W. Xiong, K. Tanaka, P. Ciais, D.J. Johansson, M. Lehtveer, emIAM v1. 0: an emulator for Integrated Assessment Models using marginal abatement cost curves, *EGUsphere*, **2023** (2023) 1-39.
[33] D.I. Armstrong McKay, A. Staal, J.F. Abrams, R. Winkelmann, B. Sakschewski, S. Loriani, I. Fetzer, S.E. Cornell, J. Rockström, T.M. Lenton, Exceeding 1.5 C global warming could trigger multiple climate tipping points, *Science*, **377** (2022) eabn7950.
[34] O. Hoegh-Guldberg, D. Jacob, M. Bindi, S. Brown, I. Camilloni, A. Diedhiou, R. Djalante, K. Ebi, F. Engelbrecht, J. Guiot, Y. Hijioka, S. Mehrotra, A.J. Payne, S.I. Seneviratne, A. Thomas, R. Warren, G. Zhou, Impacts of 1.5 C global warming on natural and human systems. , *Global warming of 1.5° C. An IPCC Special Report on the impacts of global warming of 1.5°C above pre-industrial levels and related globabl greenhouse has emission pathways, in the context of strengthening the global response to the threat of climate change, sustainable development, and efforts to eradicate poverty* (2018) 175-312.

4.3 . Discussion

4.4 . Downscaling of global CO_2 emission pathways

Many caveats and perspectives of our approach to defining near-optimal robust pathways are discussed in the paper *Near-optimal and Paris-compliant pathways robust to physical uncertainty, economic paradigms, and intergenerational equity* or its appendix. However, to ground this paper in the global framework of my doctoral research, this section will discuss what the next step would be if we were able to identify a selection of global CO_2 emission pathways. Keeping in mind the idea of facilitating the proposal and exploration of new scenarios, we find that process-based IAMs are more likely to be used to deal with a carbon budget constraint at the global level than with time series. Since most process-based IAMs are regionalized, it may be interesting to propose a downscaling of global CO_2 emission pathways to the country level. To do this, we draw inspiration from the literature on carbon budget quotas (Gignac and Matthews; 2015; Raupach et al.; 2014; Van den Berg et al.; 2020), but adapt it to apply this quota to each time step of the emissions pathway. The choice of downscaling method is difficult because there are many different approaches to allocating effort that represent different visions of fairness and equity. Grandfathering assumes that the quota should remain proportional to current emissions; per capita convergence assumes that the emissions allocation should be proportional to the country's population; historical emissions can be added to the equation through a carbon debt; ability to pay determines the budget, taking into account countries' GDP per capita. Here we will consider different nuances between grandfathering and overall per capita convergence to share emissions until 2100. The assumption that an abrupt transition to annual emissions proportional to population is not realistic. Therefore, we define downscaling for the end-of-century budget and propose a smooth transition from historical emissions. We define a country's budget in 2100 as

$$b(r) = s_{final}(r, \omega) \cdot B \tag{4.1}$$

where the budget sharing quota defined as

$$s_{final}(r, \omega) = ((1 - \omega) \cdot \frac{e(y_0, r)}{E(y_0)} + \omega \cdot \frac{pop(y_0, r)}{POP(y_0)}) \tag{4.2}$$

where B is the global carbon budget in 2100, r is the country or region, $\frac{e(y_0,r)}{E(y_0)}$ is the current ratio of regional emissions to global CO_2 emissions, $\frac{pop(y_0,r)}{POP(y_0)}$ is the current ratio of current regional population to global population, and ω is a factor representing the preference between grandfathering ($\omega = 0$) and per capita convergence ($\omega = 1$).
We note that $B = \sum_{t=y_0}^{2100} E(t)$ with $E(y)$ the annual global emissions, y the year, and y_0 the initial year of our projections. We translate the quota for the budget into an annual factor, so we have expressed annual regional emissions $e(y, r)$ as

$$e(y, r, \omega) = \sigma(y, r, \omega) \cdot E(y) \tag{4.3}$$

$\sigma(y, r, \omega)$ is iteratively defined as

$$\sigma(y, r, \omega) = \frac{\alpha(y) \cdot s(y, r, \omega) - \gamma(y - 1, r, \omega) + a_{sum}(y - 1) \cdot s(y, r, \omega)}{\alpha(y)} \tag{4.4}$$

with

$$s(y,r,\omega) = \frac{(2100-y)\cdot\frac{e(y_0,r)}{E(y_0)} + y\cdot s_{final}(r,\omega)}{2100-y_0} \tag{4.5}$$

$$\alpha(y) = \frac{E(y)}{B} \tag{4.6}$$

$$\gamma(y-1,r,\omega) = \sum_{t=y_0}^{y-1}\alpha(t)\cdot\sigma(t,r,\omega) \tag{4.7}$$

$$a_{sum}(y-1) = \sum_{t=y_0}^{y-1}\alpha(t) \tag{4.8}$$

$$\tag{4.9}$$

Therefore, $s(y,r,\omega)$ is the temporary budget sharing quota in year y, $\alpha(y)$ is the share of annual emissions in the total budget, $a_{sum}(y)$ is the cumulative share of past emissions in the total budget, and $\gamma(y,r,\omega)$ is the cumulative share of past emission sharing quotas weighted by the share of each annual emission in the total budget. The initialization is given by

$$\sigma(r,y_0) = \frac{e(y_0,r)}{E(y_0)} \tag{4.10}$$

$$\gamma(y_0,r) = \alpha(y_0)\cdot\sigma(y_0,r) \tag{4.11}$$

$$a_{sum}(y_0) = \alpha(y_0) \tag{4.12}$$

A major advantage of this approach is that the political or ethical decision for the effort- sharing approach is only included in the final budget sharing quotas $s_{final}(r,\omega)$. Therefore, we can easily reproduce this method with other vision of effort- sharing.

In summary, downscaling global CO_2 emissions to the regional level would allow us to close the loop with regionally defined impacts, which was quickly discussed in section 3.4 of Chapter 3. Because this downscaling method is simple to implement and computationally easy, we believe it is a promising development for improving our integrated backward-looking approach.

Bibliography

Gignac, R. and Matthews, H. D. (2015). Allocating a 2 c cumulative carbon budget to countries, *Environmental Research Letters* **10**(7): 075004.

Raupach, M. R., Davis, S. J., Peters, G. P., Andrew, R. M., Canadell, J. G., Ciais, P., Friedlingstein, P., Jotzo, F., Van Vuuren, D. P. and Le Quéré, C. (2014). Sharing a quota on cumulative carbon emissions, *Nature Climate Change* **4**(10): 873–879.

Van den Berg, N. J., van Soest, H. L., Hof, A. F., den Elzen, M. G., van Vuuren, D. P., Chen, W., Drouet, L., Emmerling, J., Fujimori, S., Höhne, N. et al. (2020). Implications of various effort-sharing approaches for national carbon budgets and emission pathways, *Climatic Change* **162**: 1805–1822.

5 - Conclusion

5.1 . Key contributions of this thesis

The common thread of this thesis revolves around the question we posed in section 1.5: Can we propose a methodological framework that allows the construction of scenarios that reverse the causal chain from the definition of impact exposure to the socioeconomic constraints of mitigation scenarios consistent with the previously defined impacts?
In a first step, we introduced Pathfinder, a new, simple model that meets the key requirements we identified to apply our methodological framework. In particular, Pathfinder is invertible, so it can be run backwards. Once we developed and diagnosed our main tool, the second step was to develop a backward approach that allows us to back-calculate CO_2 emissions from ex-ante temperature and atmospheric CO_2 concentration pathways. Thanks to this approach, we have proposed a new framework that finds a comprehensive ensemble of emission scenarios compatible with the chosen targets for the physical impacts of climate change such as sea level rise, global warming and ocean acidification. Finally, the last step developed in this thesis provides an initial assessment of the economic robustness of the previously defined scenarios. The following subsections detail the main contribution of my work to these three steps, highlighting the reversal of the cause-effect chain.

5.1.1 . Introducing Pathfinder

Chapter 2 introduces the Pathfinder model, a new and innovative global carbon climate model. This model was developed to balance simplicity and accuracy, with an emphasis on representing CO_2-related physical processes. The Pathfinder model is calibrated using Bayesian inference so that it can integrate the latest observations. Its simplicity facilitates coupling with integrated assessment models and exploration of a wide range of climate scenarios. The model is open source and is described comprehensively for the first time in this chapter, detailing the calibration process and parameter estimation.
The performance of the Pathfinder model is evaluated using key diagnostic metrics. We show that the model performs very well in the historical period. We also provide diagnostics for idealized simulations that demonstrate the interest of Bayesian calibration in providing “middle of the road” estimates between complex models and observations. Finally, we validate the model against the forecast scenarios used in IPCC AR6. Pathfinder’s projections agree very well with the scenarios evaluated by the IPCC in AR6, especially for low-warming scenarios, which we have explored extensively in our various studies.
The Pathfinder model fills a gap in the literature by providing a simple but effective model for climate scenarios. Despite its simplicity, the Pathfinder model accurately reproduces the behavior and results of more complex models. This is particularly useful for integrated assessment models. We also identify opportunities to further improve the model, including reducing complexity where possible, developing an alternative formulation of ocean carbon dynamics, integrating land use and land cover change, extending the Bayesian approach, and potentially including non-CO_2 climate forcers into Pathfinder. Our approach to addressing these potential improvements underscores their commitment to improving the utility and effectiveness of the model in climate modeling.
Thomas Gasser already developed the model before the start of my PhD. Personally, I helped to the development of the sea level module, I ran all the diagnostic tests and made the analysis on the representation of the ocean in Pathfinder.

5.1.2 . Proposing a new framework for scenario development

As a first application of Pathfinder, we estimate the chances of limiting warming to 1.5°C by conducting a comprehensive analysis of the physical requirements needed to limit global warming to 1.5°C, based on the most recent data through 2022. We argue that a 50 percent probability of keeping global warming below 1.5°C this century requires a linear decrease in CO_2 emissions from fossil fuels and industry of about 5 percent per year, a decarbonization rate that must be sustained annually. Interestingly, this rate is only slightly below the unprecedented near-term emissions reductions seen during the COVID -19 pandemic. Our study also highlights the critical role of assumed CO_2 emissions from land use and non-CO_2 forcing in determining the likelihood of staying below the 1.5°C global warming threshold.

To further advance the exploration of scenarios, we proposed a new backward approach that includes not only the temperature target but also impacts such as ocean acidification and sea level rise. Specifically, we consider thousands of pathways in 1500 different physical states of the world to provide a comprehensive estimate of the range of possible pathways, all of which remain below the +2°C global warming limit by design. We consider different planetary boundaries independently and in combination with each other, and examine the nonlinear effects of these combinations on compatible space by comparing the envelope of all pathways that remain within a given boundary.

We express the compatible space in terms of key characteristics on anthropogenic activities and associate them with a probability that this space is safe, which we call the safety level. We analyze these compatible spaces to understand and quantify the tradeoffs between different options and mitigation strategies. Overall, this results in an innovative framework that determines what is and is not physically possible to stay within a set of planetary boundaries.

About my personal contribution to the creation of this framework, I took an active role in the conceptualization of both studies. I did all the data representation and analysis presented in the papers.

5.1.3 . Assessing the economic robustness of scenarios

In Chapter 4, our work begins with pathways generated in Chapter 3. We focus only on the 2°C global warming boundary and add a socioeconomic dimension to reduce the physically relevant compatible space to an economically robust set of pathways. To do this, we adopt a cost-effective approach based only on mitigation costs.

Our goal is to provide a comprehensive analysis of mechanisms that determine near-optimal costs. The costs of the CO_2 emission pathways calculated by Pathfinder are estimated and compared using a series of conceptual choices for the minimization criterion and the cost function chosen to estimate the mitigation costs. The least-cost pathways are defined as near-optimal, and we introduce the concept of robust pathways to denote pathways that are common to all of the conceptual approaches we examine. In addition to the economic uncertainty arising from the conceptual choices, we also consider physical uncertainty by calculating the proportions of robust pathways in each physical state of the world. We also consider intergenerational equity by attempting to minimize the difference between a current generation (2021-2060) and a future generation (2061-2100).

Finally, we illustrate economically and generationally robust pathways for different configurations

and provide a visual representation of the analysis to help policymakers make more informed decisions about climate change mitigation strategies. We show that the range of near-optimal pathways is reduced when conditions for robustness are added. Pathways with late emission peaks or that require the use of a large amount of CDR are not among the most robust pathways. The most restrictive envelope of pathways ensures both generational and economic robustness. This suggests that achieving net-zero emissions early by using CDR in the second half of the 21st century is more intergenerationally equitable than economically robust pathways that target net-zero emissions at the end of the century.

For this part, I was very active in the proposition and conceptualization of the study. I also made all the data representation and analysis.

5.2 . Limitations and new frontiers

In the previous section, we recalled the main achievements of this thesis, demonstrating that we, at least partly, succeeded to propose a framework that reverses the causal chain to estimate ensembles of pathways of CO_2 emissions compatible to impact-defined climate targets. However, we also faced many challenges with some of them remaining unsolved. This section presents first limitations of our approach and the development they would require (5.2.1,5.2.2). Then, we discuss new frontiers that would gain to be developed in future works (5.2.3,5.2.4).

5.2.1 . Development of the representation of non-CO_2 gases in Pathfinder

In Chapters 3 and 4, reference is made to the difficulty of interpreting non-CO_2 radiative forcing because it is an aggregate variable that is independent of CO_2 emissions and is difficult to disaggregate. Because of this aggregate variable, we cannot include the methane pledge to estimate the chances to stay below 1.5°C in Chapter 3, although it would be help reducing uncertainty about the non-CO_2 contribution by having a separate estimation of methane forcing. In mapping compatible spaces, a more detailed decomposition of non-CO_2 forcers would also allow a more precise determination of the lower bound below which we consider SRM to be deployed. This could also open up new analytical perspectives, e.g., with respect to trade-offs between methane mitigation and deployment of CDR. In Chapter 4, a more detailed decomposition of non-CO_2 forcers would allow us to allocate the costs of mitigating some non-CO_2 GHGs and more concretely interpret the policy implications of our near-optimal pathways. To improve the decomposition of non-CO_2 forcers in Pathfinder, one solution would be to add the methane cycle or even the nitrogen cycle. If the methane cycle already exists in other SCMs, emulating the nitrogen cycle might be more challenging. In either case, this would result in additional computational costs to consider, since one of the goals of Pathfinder is to keep computational costs low. Another solution would be to attribute some of the non-CO_2 radiative forcing to GHGs that are co-emitted with CO_2. However, these co-emissions (mainly CH4) are sector dependent and would therefore require a decomposition of CO_2 emissions, which is also non-trivial and would require strong assumptions. Therefore, I do not really believe in this second possibility in the context of a backward-looking use of Pathfinder.

5.2.2 . Exploring optimization as an alternative to brute force in Pathfinder

The brute force methodology employed by Pathfinder in Chapters 3 and 4 – which generates thousands of trajectories in an attempt to encompass the entirety of possible pathways – is not without its drawbacks. Firstly, there's no absolute guarantee that the method captures every potential scenario, and secondly, formulating continuous, differentiable pathways for temperature and CO_2 concentration, which in turn yield credible CO_2 emissions and non-CO_2 radiative forcing, is a challenging task. A potential solution to these constraints could be the implementation of an optimization-based approach. This approach would allow us to explore the space of potential trajectories systematically, ensuring all possibilities are captured and generating plausible pathways with greater efficiency. An additional advantage lies in the existing GAMS version of Pathfinder, which has previously been utilized in a DICE study as a replacement for the climate module, thereby simplifying the adoption of this optimization technique. However, rather than a single cost optimization, a series of optimizations might be more suited to outlining the boundaries of

compatible spaces. The process would involve the use of impact objectives and constraints for all pathway characteristics (excluding one, as detailed in Section 3.3), with the output being the pathway that presents the least restrictive constraint for the unconstrained pathway characteristic. Through this, we could gain a more efficient, thorough exploration of potential climate change scenarios. To increase efficiency further, we could execute the optimization iteratively, gradually introducing constraints on key characteristics or impact objectives until the process yields no viable solution. This would result in a smaller set of pathways compared to the brute force approach. However, it's important to note that optimization is more computationally demanding. Furthermore, the feasibility of implementing all constraints is still uncertain, as we have not yet attempted to do so. Hence, while promising, the success of this approach will depend on its practical implementation.

5.2.3 . Improvement of the ocean module of Pathfinder

Chapter 2 discussion scrutinizes the "Ocean Heat-Carbon Nexus" and its depiction in simplistic climate models, including Pathfinder. However, a noteworthy divergence is observed in the representation of this nexus in Pathfinder when compared to the latest Earth System Models (ESMs) employed in recent IPCC assessments. This discrepancy is attributed to the physical inconsistency in SCMs that crudely account for the coupling between the ocean thermal and carbon cycle modules. The discussion further identifies a regime shift in the ocean heat-carbon nexus, driven by three factors: the unrestricted ability of the surface ocean temperature to equilibrate with the atmospheric temperature, the ocean's differing capacities to retain heat and absorb CO_2, and the accumulation of heat which intensifies the stratification of the surface ocean. An in-depth examination of the representation of the ocean heat-carbon nexus in Pathfinder reveals that the response of the ocean heat and carbon uptake as simulated by Pathfinder does not exhibit the saturation of the ocean carbon uptake observed in the ESMs and corroborated by theory. The modelling framework of Pathfinder treats the thermal response of the ocean to radiative forcing and that of the ocean carbon cycle in two distinct modules, leading to physically inconsistent structures and parameters. The development of an alternative formulation of the ocean carbon dynamic, calibrated on state-of-the-art ocean models and properly connected to ocean pH and the ocean of the climate module, would be a significant advancement for the SCM community. This finding is a relevant example of the interest in constantly thinking about how to improve or add to the representation of processes in SCMs.

5.2.4 . Addition of impacts of climate change on human activities

Chapter 3 proposes a reversal of system causality by defining planetary boundaries and identifying human activities that stay within these limits. As discussed in section 3.4, Pathfinder, coupled with spatially-resolved emulators, could be used to set local climate targets based on land area or population exposure. Initial applications could use existing crop yield emulators to predict crop yields based on various factors. This, combined with population projections, would estimate human exposure to changes in crop yields. Additionally, linking global SLR to local extreme sea level could allow to estimate exposure to coastal flooding. Furthermore, the ISIMIP dataset provides a framework for linking exposure to various impacts with global temperature change. Ultimately, Pathfinder can estimate anthropogenic emission pathways consistent with climate targets, aiding

policy makers in scenario design.

The evaluation of impacts in terms of exposure necessitates a critical examination of adaptation strategies and population projections. While the SSPs narratives offer some guidance, the integration of expertise from impact specialists would greatly enhance the articulation of population or land area exposure in the most pertinent manner. In addition, while quantifying exposure is of considerable interest, describing target-based pathways requires establishing acceptance thresholds for exposure. From a research standpoint, the simplest solution might be to arbitrarily select thresholds for sensitivity analysis, but this raises questions about the appropriateness of using Pathfinder for scenario development. It raises ethical considerations about the authority of researchers or policy makers to consider the exposure of several million people to climate change impacts as acceptable. Even more critical is the question of how we should deal with impacts that cannot be quantified in terms of human exposure, such as loss of biodiversity. It is an inescapable truth that we will never be able to comprehensively model all the impacts of climate change, especially not with emulators. As we move forward, it is important to keep in mind that while we are developing a powerful tool to suggest a novel and complementary approach to building future scenarios, such modeling tools should not be misconstrued as definitive predictions for policy decisions.

5.3 . Reflecting on the challenges and drivers in Climate Change research

5.3.1 . Simple climate models can help to build integrated framework between all climate change disciplines

The advantage of a simple climate model, such as Pathfinder, is its simplicity and computational efficiency. Such a model can readily encapsulate fundamental aspects of climate science, which can be easily understood and manipulated by stakeholders from a variety of backgrounds. This accessibility can foster productive discussions and scenario-building exercises among all IPCC WGs and decision-makers, bridging the gap that currently exists between these disparate but interconnected fields of study. The streamlined nature of simple climate models does not detract from their utility. They efficiently capture key aspects of the Earth's climate system, acting as powerful tools for testing different scenarios. By focusing on core climate dynamics, these models allow the exploration of a wide array of potential futures, each of which has varying climate, biodiversity, and socio-economic implications. This broad range of scenarios forms a rich tapestry from which decision-makers can weave climate policy. In the context of the global framework this thesis proposed, Pathfinder serves as the backbone. It offers the geophysical basis upon which socio-economic considerations and impact analyses can be integrated. The possibility to couple other emulators further enhances the potential of this platform by replicating the outcomes of complex models with a significantly lower computational cost. This capability not only broadens the scope of potential scenario investigations but also makes the entire process more feasible and time-efficient. In essence, by placing a simple climate model at the core of our framework, we aim to create a platform that encourages multi-disciplinary dialogue and holistic scenario development. This integrative approach provides a more comprehensive outlook on the intricacies of climate change and its impacts, facilitating more informed, robust, and forward-thinking decision-making.

Our hope is that such framework can catalyze an era of enhanced collaboration and integrative thinking in addressing one of the most pressing challenges of our time – climate change.

5.3.2 . The challenge of visualizing the results

The appeal of simple climate models primarily lies in their low computational cost, enabling a broader exploration of scenarios compared to complex models. This ability facilitates an in-depth analysis across two primary dimensions: a diverse range of scenario timeseries and the inherent physical uncertainty. The expansion of our analysis dimensions was accomplished through multiple methods. In Chapter 3, scenarios were categorized based on key characteristics such as CO_2 emissions peak, CO_2 net zero dates or the volume of CDR. Also a combination of different impacts or planetary boundaries was considered for a more comprehensive view of possible climate change outcomes adding a dimension to the framework. In Chapter 4, we introduced economic aspects into our analysis by calculating and comparing costs across different cost functions and minimization criteria. The challenge, then, arises when dealing with this multitude of dimensions. Crafting visualizations that not only illustrate but accurately represent the results becomes an intricate task. In Chapter 3, we managed to circumvent this issue by introducing the concept of 'compatible spaces,' which effectively bypasses the temporal dimension. However, in Chapter 4, we initially sidestepped this problem by focusing on the ratio of overlapping sub-ensembles to define near-optimal robs. Still, subsequent discussions highlighted the need to portray actual emission scenarios as timeseries. The idea of presenting a median or average across configurations was dismissed due to the unique and non-comparable nature of each scenario. This brought forth the need to select a "representative" configuration, thereby defining what "representative" means in this context, but at the cost of losing some information. Collectively, these experiences underline the complexity of applying intricate analytic grids to multidimensional climate data. On the contrary, simpler approaches, like the study on the chances of staying below 1.5°C, often deliver more impactful and straightforward results. As we continue to advance climate modeling, finding the balance between these intricate, multi-dimensional explorations and the communication of clear, concise findings will remain a key challenge and learning experience.

5.3.3 . About the drivers of research

Throughout the course of my PhD, I've grappled with the concept of political relevance in the context of climate change research. Climate science, in its essence, straddles the realm of pure scientific inquiry and its societal implications, including policy-making and strategic planning. Our research efforts invariably raise the question - how do our results contribute to a broader understanding of climate impacts, and how can they inform mitigation strategies, estimate feedback loops, and more? In the climate research community, there is an understandable tendency to align our work with the latest findings of esteemed bodies like the IPCC or initiatives like CMIP. These entities provide crucial comparative frameworks that, while not entirely identical to our methodologies, offer some common ground for interpretation and analysis. However, the question arises - should these comparison frameworks be the drivers of our research? Undoubtedly, aligning with these recognized frameworks can enhance a study's visibility and acceptance within the scientific community. It also facilitates inclusion in important global reports. However, this alignment may inadvertently encourage researchers to fit their work into predefined molds to gain

recognition. It might also lead to skepticism when the results diverge from these reference frameworks, despite the potentially distinct methods and incomparable nature of these findings. This dynamic can result in a circular pattern, where the same scenarios are studied over and over again, and discussions tend to orbit around popular topics while sidelining alternative approaches or less-explored areas. The answer to the question of what should drive our scientific pursuit remains elusive. Nevertheless, one key insight that I have derived from my doctoral journey is the importance of maintaining an open mind. Regardless of the prevailing trends, alternative approaches and original results can offer invaluable perspectives, stimulate intellectual growth, and propel our collective understanding forward. As researchers in a field as vital and urgent as climate change, it is our responsibility to promote and welcome diversity in thought, methodologies, and conclusions.

A - Appendix

A.1 . Supplementary from Bossy et al. (2022)

Appendix A: Additional information on the model

A1 Technical requirements

Pathfinder has been developed and run in Python (v3.7.6) (Van Rossum and Drake, 2009), preferentially using IPython (v7.19.0) (Pérez and Granger, 2007). Currently, packages required to run it are NumPy (v1.19.2) (Harris et al., 2020), SciPy (v1.5.2) (Virtanen et al., 2020) and Xarray (v0.16.0) (Hoyer and Hamman, 2017), and it has hard-coded dependencies on PyMC3 (v3.8) (Salvatier et al., 2016) and Theano (v1.0.4) (Theano Development Team, 2016) that are in fact used only for calibration. Other versions of Python or these packages were not tested.

The calibration procedure takes about 9 hours to run on a desktop computer (with a base speed of 3.4 GHz). Simple use of the model is much faster: the idealized experiments and SSP scenarios for this description paper, which represent 2984 simulated years, were run in about 20 minutes for all 2000 configurations and on a single core. A single simulated year takes a few tenth of a second, although a number of options in the model can drastically alter this performance. Note also that this scales sub-linearly with the amount of configurations or scenarios because of the internal workings of the Xarray package, albeit at the cost of increased demand in random-access memory.

A2 Known issues

Two relatively benign issues that have been identified during development remain unsolved. First, the model requires a high number of sub-time steps (i.e. high n_t) to remain stable under high CO2, because of the ocean carbon cycle. Second, the version of the model that is driven by T and R_x time series is extremely sensitive to its inputs, because mathematically it requires the first two derivatives of T and the first derivative of R_x.

A3 Changelog

Brief description of the successive versions of Pathfinder:

v1.0.1. Exact same physical equations and numerical values as v1.0. Added best-guess parameters calculated as the average of the posterior distribution, and corresponding historical outputs, for single-configuration runs. Improved README and MANUAL files.

v1.0. First release. Exact model described in the preprint version of this very paper (Bossy et al., 2022).

Appendix B: Additional figures and tables

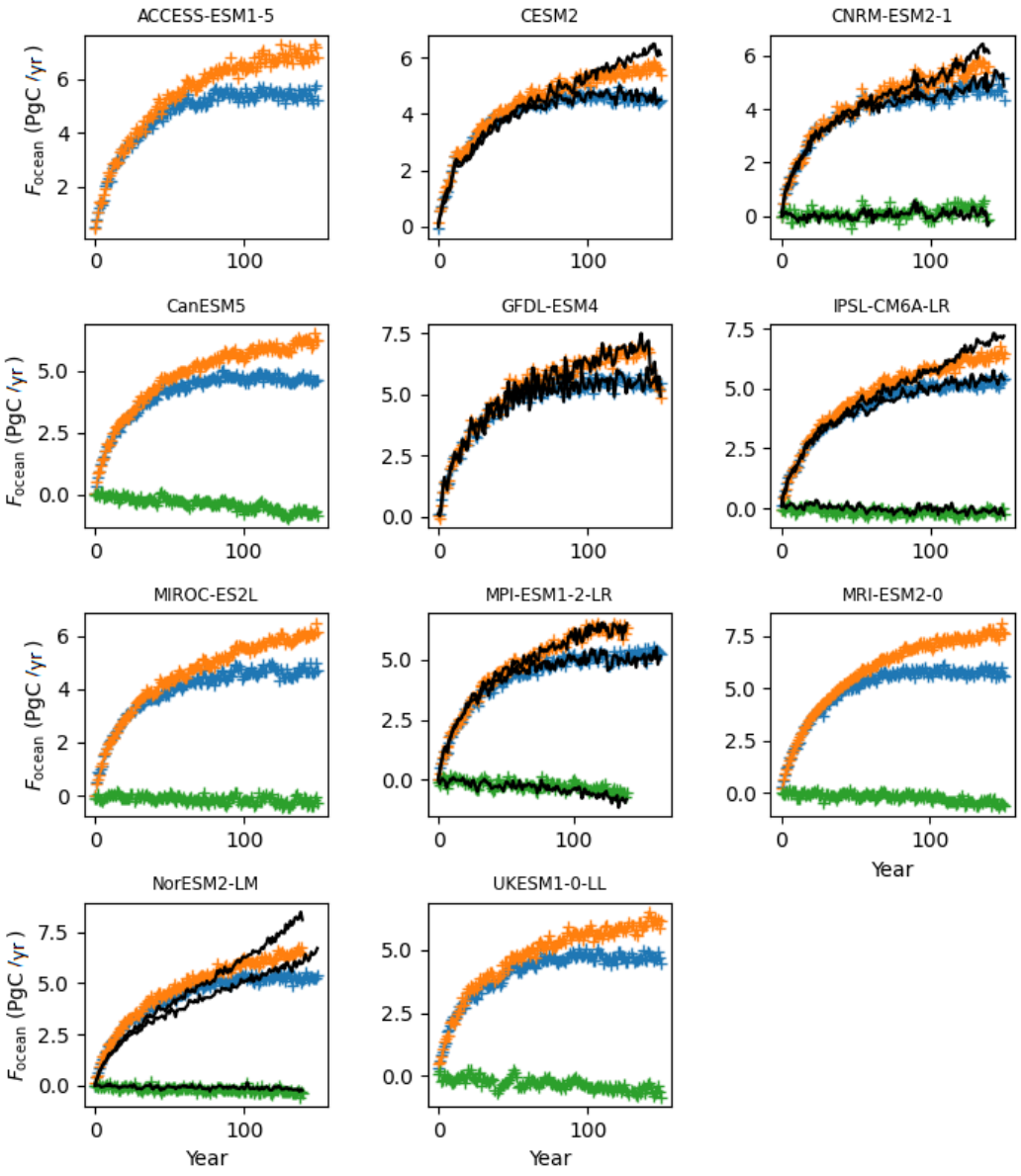

Figure B1. Calibration to estimate prior ν_{gx} and γ_{gx} from CMIP6 time series of F_{ocean}. We fit our equation on the results of the +1% CO_2 (*1pctCO2*) experiment (in blue) and its variants *1pctCO2-rad* (in green) and *1pctCO2-bgc* (in orange). Coloured markers are CMIP6 models data while the solid black lines show the fit from Pathfinder. Panels without black line indicate that at least one of the required variables was not reported by the complex model.

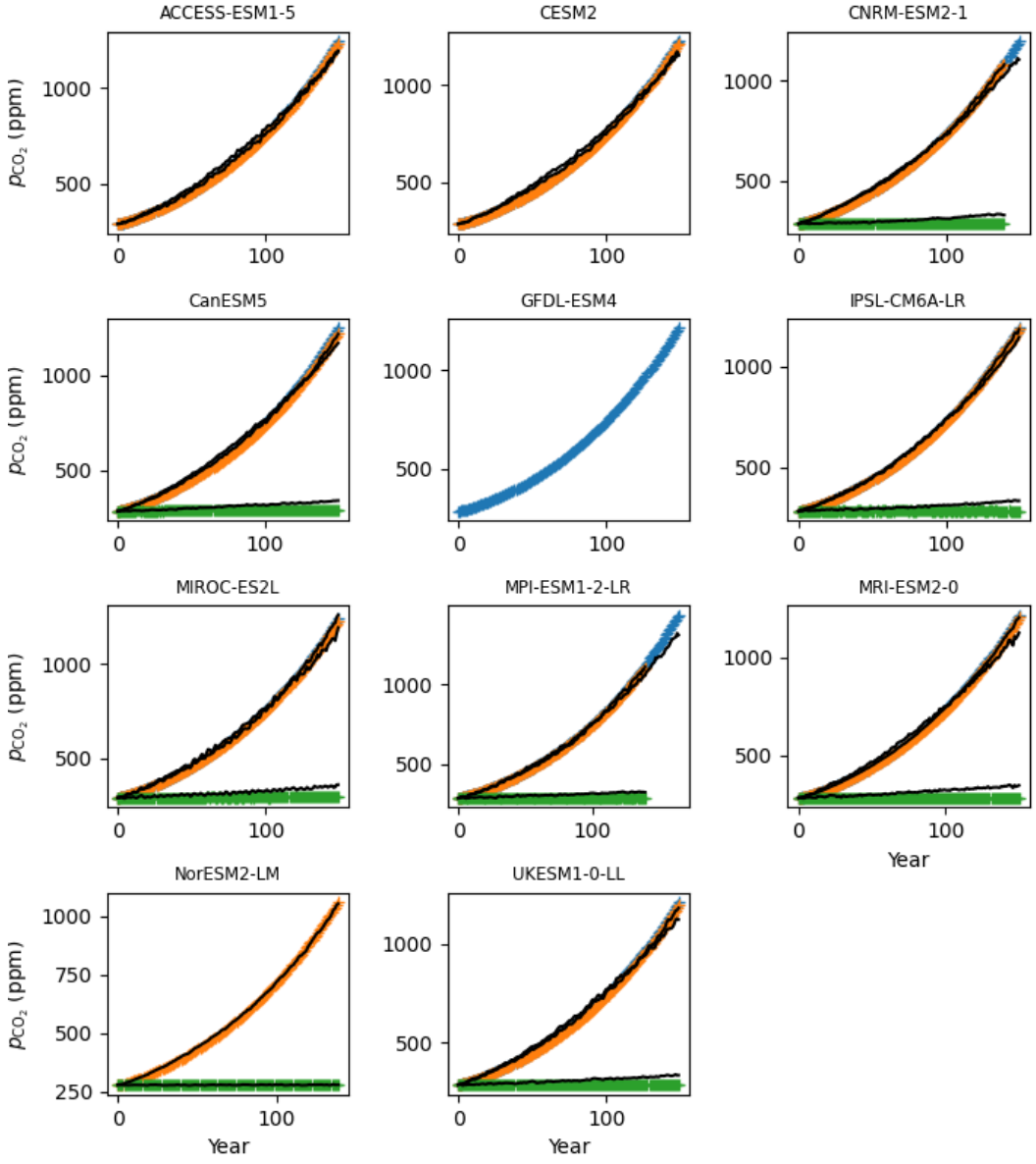

Figure B2. Calibration to estimate prior β_{dic} and γ_{dic} from CMIP6 time series of p_{CO_2}. We fit our equation on the results of the +1% CO_2 (*1pctCO2*) experiment (in blue) and its variants *1pctCO2-rad* (in green) and *1pctCO2-bgc* (in orange). Coloured markers are CMIP6 models data while the solid black lines show the fit from Pathfinder. Panels without black line indicate that at least one of the required variables was not reported by the complex model.

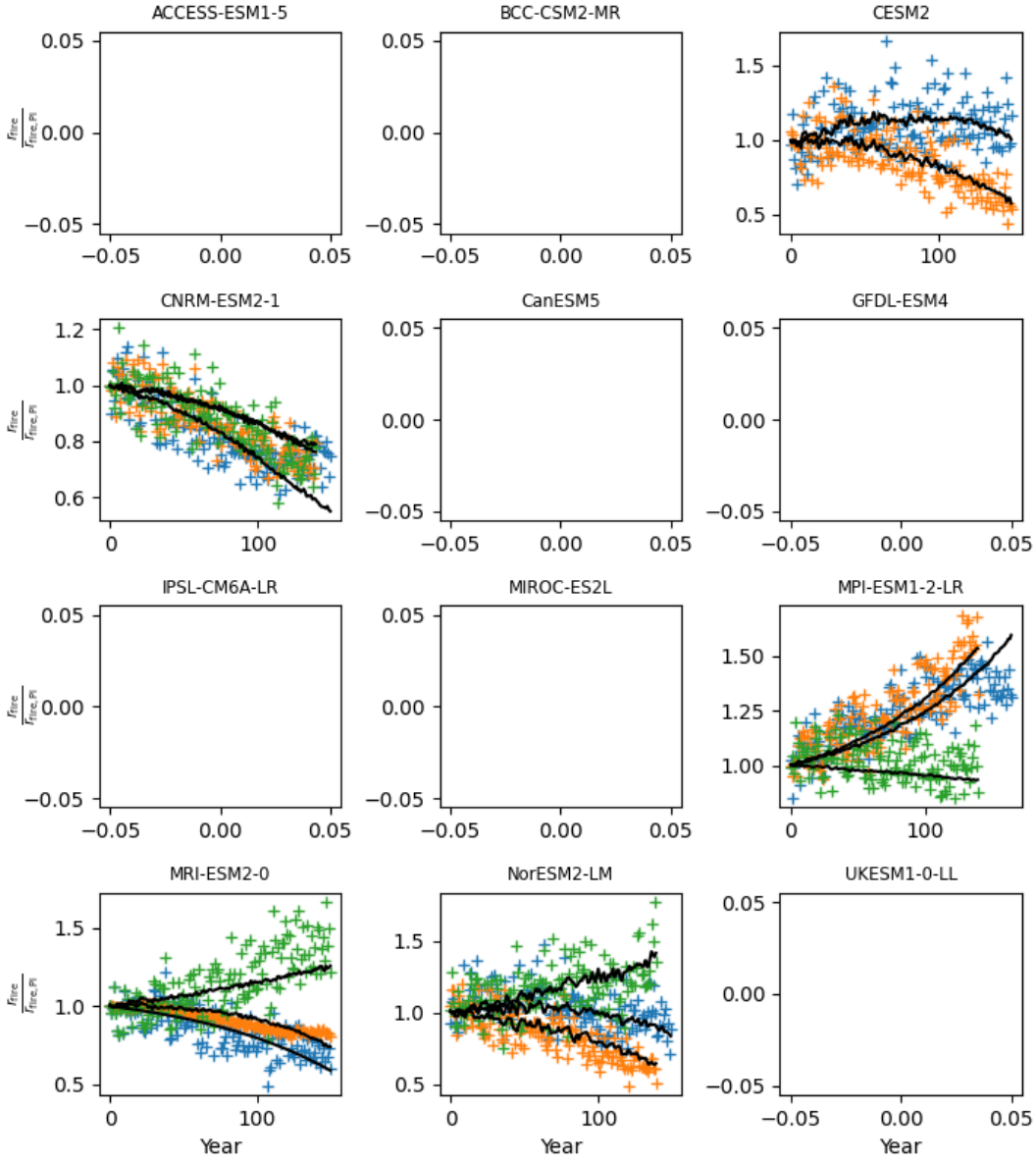

Figure B3. Calibration to estimate prior β_{ef} and γ_{ef} from CMIP6 time series of r_{fire}, shown as a ratio over its preindustrial value. We fit our equation on the results of the +1% CO_2 (*1pctCO2*) experiment (in blue) and its variants *1pctCO2-rad* (in green) and *1pctCO2-bgc* (in orange). Coloured markers are CMIP6 models data while the solid black lines show the fit from Pathfinder. Panels without black line indicate that at least one of the required variables was not reported by the complex model.

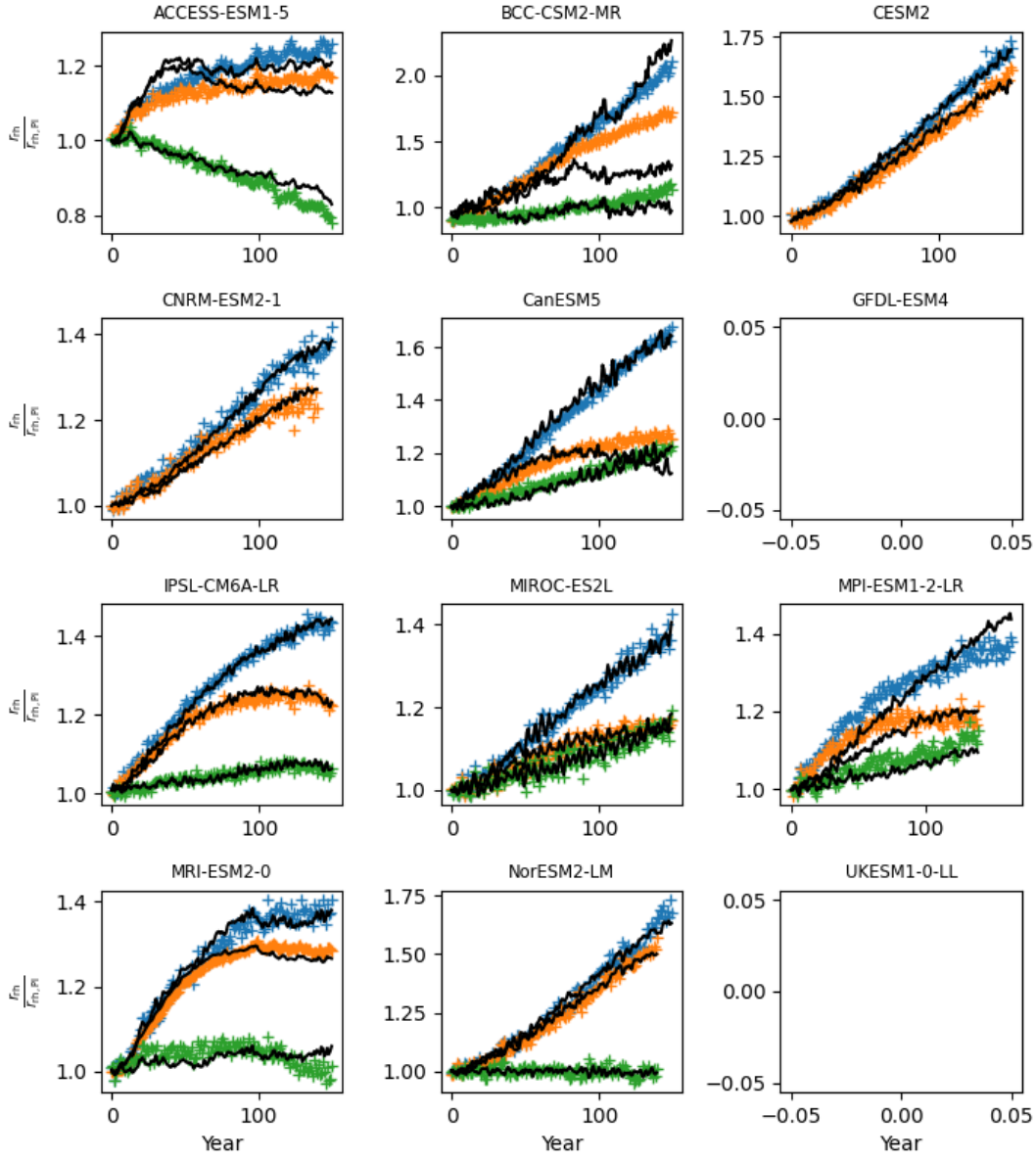

Figure B4. Calibration to estimate prior β_{rh} and γ_{rh} from CMIP6 time series of r_{rh}, shown as a ratio over its preindustrial value. We fit our equation on the results of the +1% CO_2 (*1pctCO2*) experiment (in blue) and its variants *1pctCO2-rad* (in green) and *1pctCO2-bgc* (in orange). Coloured markers are CMIP6 models data while the solid black lines show the fit from Pathfinder. Panels without black line indicate that at least one of the required variables was not reported by the complex model.

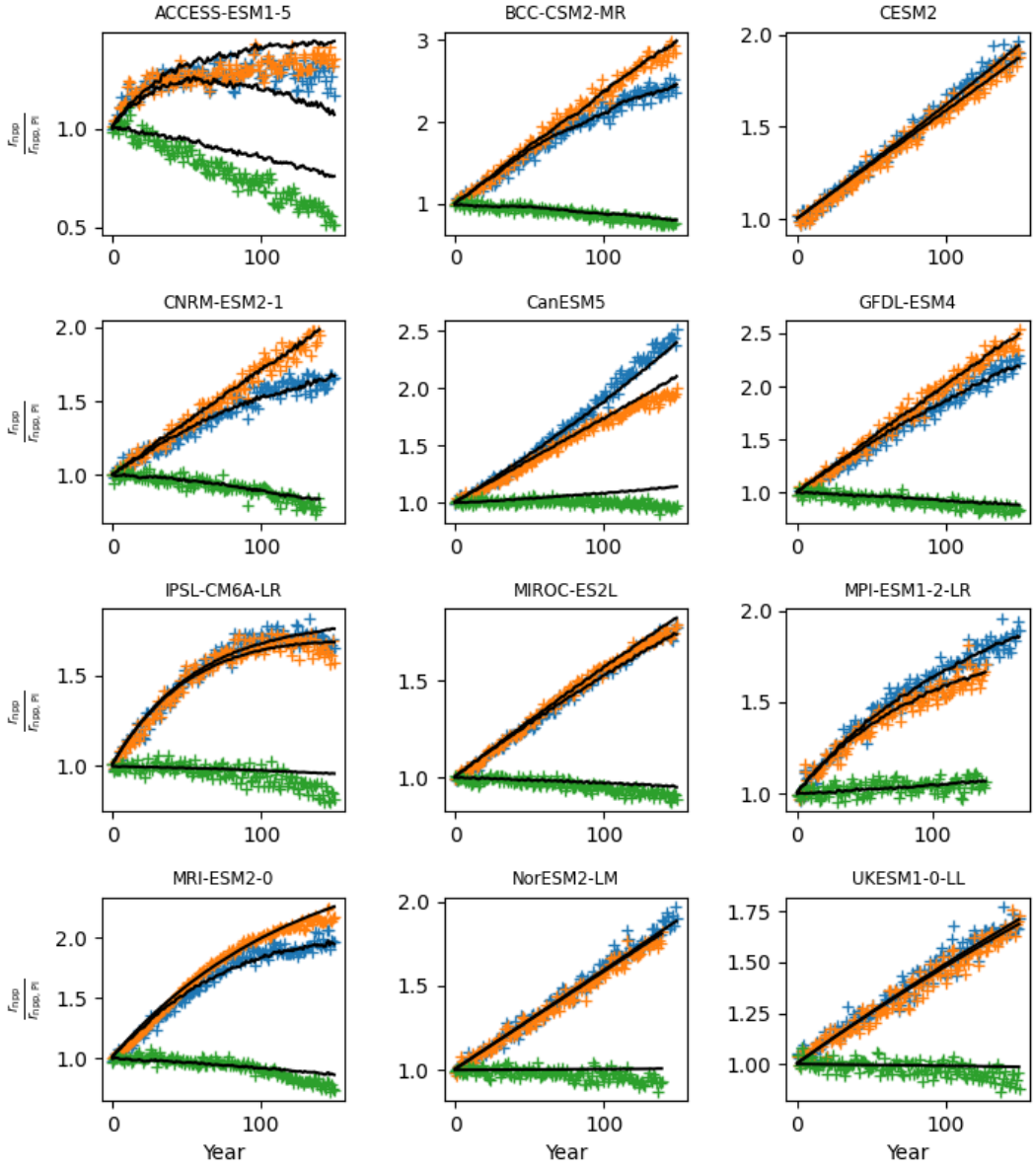

Figure B5. Calibration to estimate prior β_{npp}, α_{npp} and γ_{npp} from CMIP6 time series of r_{npp}, shown as a ratio over its preindustrial value. We fit our equation on the results of the +1% CO_2 (*1pctCO2*) experiment (in blue) and its variants *1pctCO2-rad* (in green) and *1pctCO2-bgc* (in orange). Coloured markers are CMIP6 models data while the solid black lines show the fit from Pathfinder. Panels without black line indicate that at least one of the required variables was not reported by the complex model.

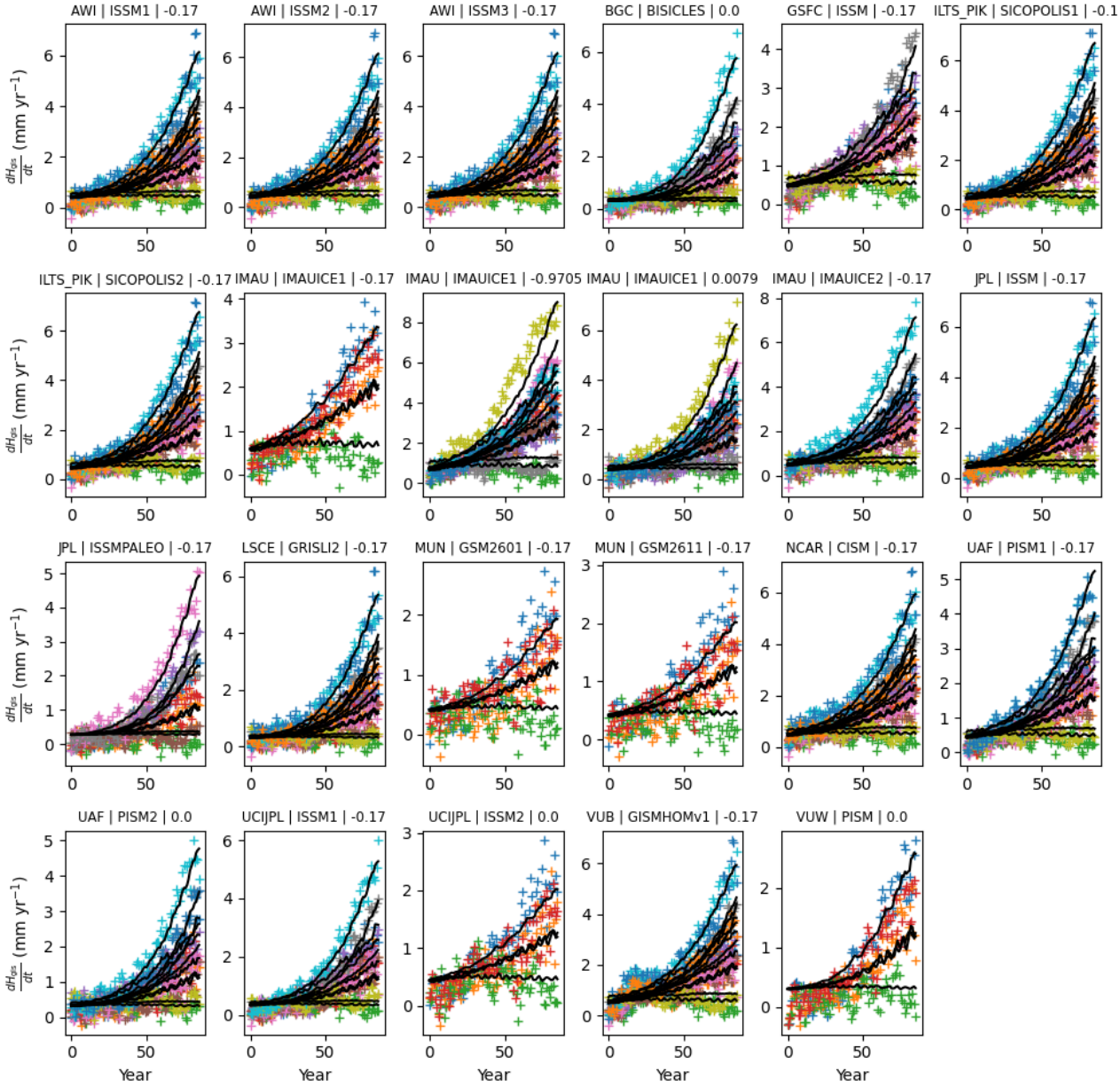

Figure B6. Calibration to estimate the prior of GIS SLR module parameters (Λ_{gis1}, Λ_{gis3} and λ_{gis0}). We fit our equation on the compiled outputs from Edwards et al. (2021) for which there is more than one scenario available. Each panel's title displays the name of the institute, model and configuration used. Coloured markers are the models data while the solid black lines show the fit from Pathfinder.

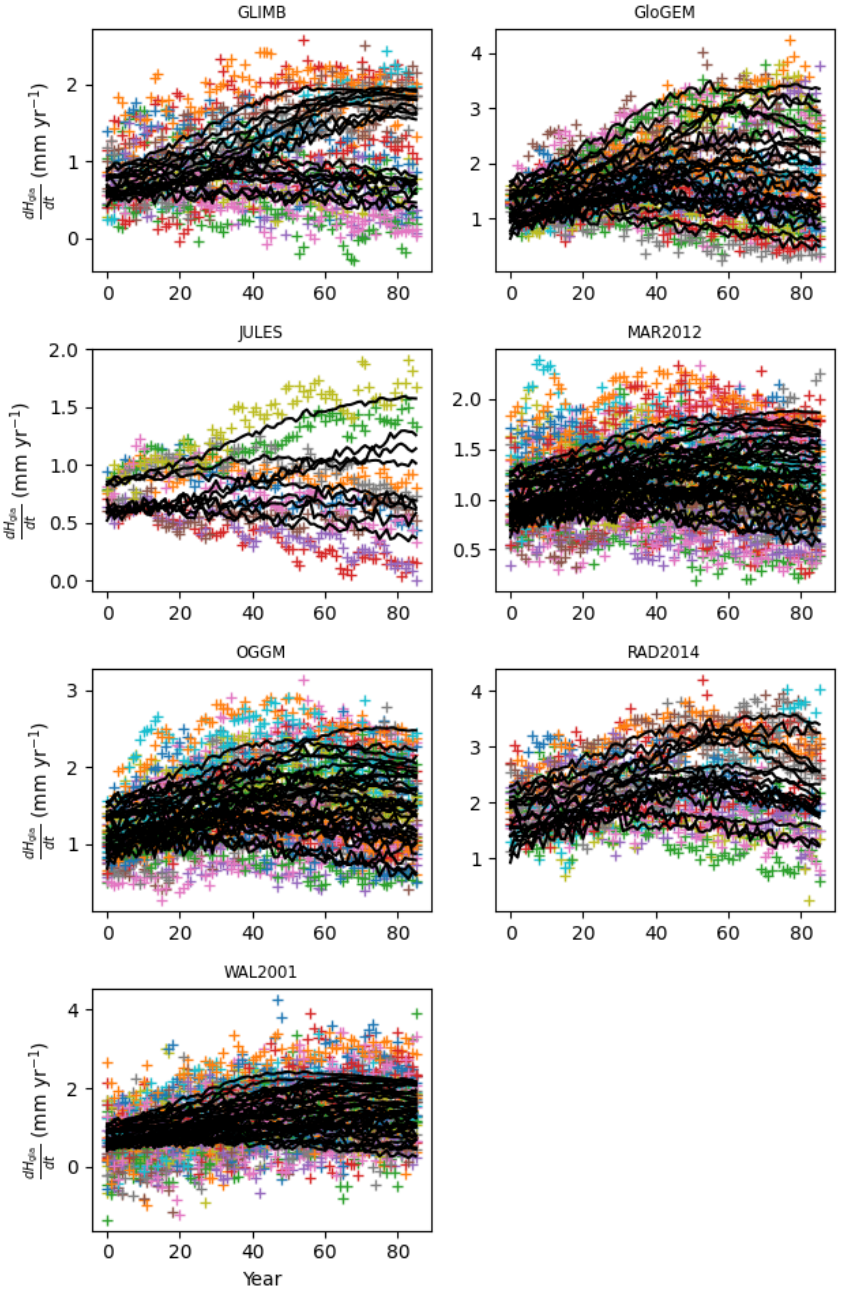

Figure B7. Calibration to estimate the prior of Glaciers SLR module parameters (Γ_{gla1}, Γ_{gla3}, γ_{gla} and λ_{gla0}). We fit our equation on the compiled outputs from Edwards et al. (2021) for which there is more than one scenario available. Each panel's title displays the name of the model or study used. Coloured markers are the models data while the solid black lines show the fit from Pathfinder.

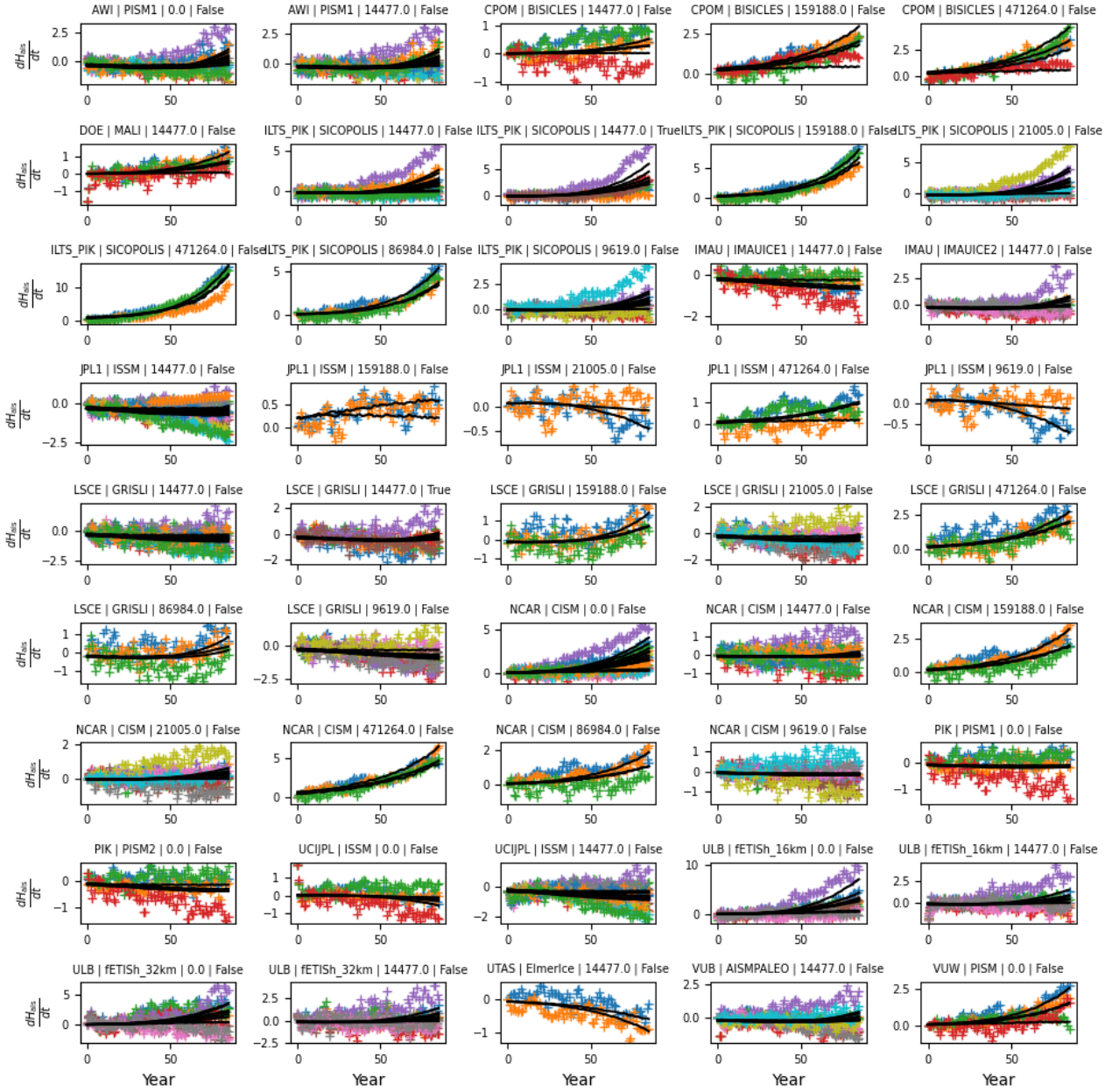

Figure B8. Calibration to estimate the prior of AIS SLR module parameters ($\Lambda_{\mathrm{ais,smb}}$, α_{ais} and λ_{ais0}). We fit our equation on the compiled outputs from Edwards et al. (2021) for which there is more than one scenario available. Each panel's title displays the name of the institute, model and configuration used. Coloured markers are the models data while the solid black lines show the fit from Pathfinder.

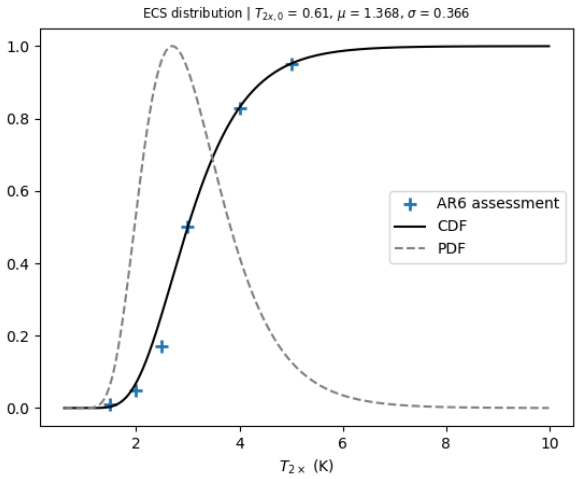

Figure B9. Distribution of the logit of the ECS ($T_{2\times}$) inferred from AR6. Blue points are the assessments from AR6, the plain line is the CDF fitted on those assessment and the dashed line is the PDF associated with the CDF (arbitrary scale). The value of the fitted parameters is given above the plot.

In manual	In code	Description	Units	
R_c	RFco2	CO2 (effective) radiative forcing	W m^{-2}	
R_x	ERFx	Non-CO2 effective radiative forcing	W m^{-2}	
R	ERF	Effective radiative forcing	W m^{-2}	
T	T	Global surface temperature anomaly	K	
T_d	Td	Deep ocean temperature anomaly	K	
$\mathrm{logit(ff)}$	logit_ff	Logit of the climate feedback factor (for calib.)	1	
U_{ohc}	OHC	Ocean heat content (anomaly)	W yr m^{-2}	
H_{thx}	Hthx	Thermosteric sea level rise	mm	
H_{gla}	Hgla	Glaciers' contribution to sea level rise	mm	
H_{gis}	Hgis	Grenland ice sheet's contribution to sea level rise	mm	
$H_{\mathrm{ais,smb}}$	Hais_smb	Surface mass balance component of Hais	mm	
H_{ais}	Hais	Antartica ice sheet's contribution to sea level rise	mm	
H_{tot}	Htot	Total sea level rise	mm	
H_{lia}	Hlia	Sea level rise from relaxation after LIA between 1900 and 2005 (for calib.)	mm	
$C_{o,j}$	Co_j	Change in surface ocean carbon subpools	PgC	$j \in [\![1,5]\!]$
C_o	Co	Change in surface ocean carbon pool	PgC	
C_d	Cd	Change in deep ocean carbon pool		
c_{dic}	dic	Change in surface DIC	μmol kg^{-1}	
p_{dic}	pdic	Subcomponent of pCO2	ppm	
p_{CO2}	pCO2	CO2 partial pressure at the ocean surface	ppm	
F_{ocean}	Focean	Ocean carbon sink	PgC yr^{-1}	

Table B1. Summary of PathFinder's equation variables in climate, sea level and ocean carbon modules.

In manual	In code	Description	Units	
r_{npp}	r_npp	Relative change in NPP	1	
r_{fire}	r_fire	Relative change in wildfire intensity	1	
r_{rh}	r_rh	Relative change in heterotrophic respiration rate	1	
F_{npp}	NPP	Net primary productivity	PgC yr^{-1}	
E_{fire}	Efire	Emissions from wildfire	PgC yr^{-1}	
E_{harv}	Eharv	Emissions from harvest and grazing	PgC yr^{-1}	
F_{mort}	Fmort	Mortality flux	PgC yr^{-1}	
E_{rh1}	RH1	Litter heterotrophic respiration	PgC yr^{-1}	
F_{stab}	Fstab	Stabilization flux	PgC yr^{-1}	
E_{rh2}	RH2	Active soil heterotrophic respiration	PgC yr^{-1}	
F_{pass}	Fpass	Passivization flux	PgC yr^{-1}	
E_{rh3}	RH3	Passive soil heterotrophic respiration	PgC yr^{-1}	
F_{land}	Fland	Land carbon sink	PgC yr^{-1}	
E_{rh}	RH	Heterotrophic respiration	PgC yr^{-1}	
C_v	Cv	Vegetation carbon pool	PgC	
C_{s1}	Cs1	Litter carbon pool	PgC	
C_{s2}	Cs2	Active soil carbon pool	PgC	
C_{s3}	Cs3	Passive soil carbon pool	PgC	
C_s	Cs	Total soil carbon pool	PgC	
r_{rt}	r_rt	Relative change in permafrost respiration rate	1	
$\bar{a}$	abar	Theoretical thawed fraction	1	
a	a	Actual thawed fraction	1	
E_{pf}	Epf	Emissions from permafrost	PgC yr^{-1}	
$C_{\mathrm{th},j}$	Cth_j	Thawed permafrost carbon subpools	PgC	$j \in [\![1,3]\!]$
C_{fr}	Cfr	Frozen permafrost carbon pool	PgC	
E_{CO2}	Eco2	Anthropogenic CO2 emissions	PgC yr^{-1}	
C	CO2	Atmospheric CO2 concentration	ppm	
pH	pH	Surface ocean pH	1	

Table B2. Summary of PathFinder's equation variables for land carbon, permafrost and atmospheric modules.

In manual	In code	Description	Units
ϕ	phi	Radiative parameter of CO2	W m^{-2}
$T_{2\times}$	T2x	Equilibrium climate sensitivity	K
Θ_s	THs	Heat capacity of the surface	W yr m^{-2} K^{-1}
Θ_d	THd	Heat capacity of the deep ocean	W yr m^{-2} K^{-1}
θ	th	Heat exchange coefficient	W m^{-2} K^{-1}
ϵ_{heat}	eheat	Deep ocean heat uptake efficacy	1
$T^*_{2\times}$	T2x0	Minimal value of the ECS distribution (for calib.)	K
α_{ohc}	aOHC	Fraction of energy warming the ocean	1
Λ_{thx}	Lthx	Proportionality factor of thermosteric SLR	mm m^2 W^{-1} yr^{-1}
λ_{gla}	lgla0	Initial imbalance in SLR from Glaciers	mm yr^{-1}
Λ_{gla}	Lgla	Maximum contribution to SLR from Glaciers	mm
Γ_{gla1}	Ggla1	Linear sensitivity of steady-state Glaciers SLR to climate	K^{-1}
Γ_{gla3}	Ggla3	Cubic sensitivity of steady-state Glaciers SLR to climate	K^{-3}
τ_{gla}	tgla	Timescale of Glaciers' contribution to SLR	yr
γ_{gla}	ggla	Sensitivity of Glaciers' timescale to climate	K^{-1}
λ_{gis}	lgis0	Initial imbalance in SLR from GIS	mm yr^{-1}
Λ_{gis1}	Lgis1	Linear sensitivity of steady-state GIS SLR to climate	mm K^{-1}
Λ_{gis3}	Lgis3	Cubic sensitivity of steady-state GIS SLR to climate	mm K^{-3}
τ_{gis}	tgis	Timescale of GIS contribution to SLR	yr
$\Lambda_{\text{ais,smb}}$	Lais_smb	Sensitivity of AIS SMB increase due to climate	mm yr^{-1} K^{-1}
λ_{ais}	lais	Initial imbalance in SLR from AIS	mm yr^{-1}
Λ_{ais}	Lais	Sensitivity of steady-state AIS SLR to climate	mm K^{-1}
τ_{ais}	tais	Timescale of AIS contribution to SLR	yr
α_{ais}	aais	Sensitivity of AIS timescale to AIS SLR	mm^{-1}
α_{dic}	adic	Conversion factor for DIC	μmol kg^{-1} PgC^{-1}
β_{dic}	bdic	Inverse-scaling factor for DIC	1
γ_{dic}	gdic	Sensitivity of pCO2 to climate	K^{-1}
T_o	To	Preindustrial surface ocean temperature	°C
ν_{gx}	vgx	Surface ocean gas exchange rate	yr^{-1}
γ_{gx}	ggx	Sensitivity of gas exchange to climate	K^{-1}
$\alpha_{o,j}$	aoc_j	Surface ocean subpools fractions	1 $j \in [\![1,5]\!]$
$\tau_{o,j}$	toc_j	Timescales of surface ocean subpools	yr $j \in [\![1,5]\!]$
κ_{τ_o}	k_toc	Scaling factor for timescales of surface ocean subpools	1

Table B3. Parameters used in the climate, ocean carbon and sea level modules.

In manual	In code	Description	Units
β_{npp}	bnpp	Sensitivity of NPP to CO2 (= fertilization effect)	1
α_{npp}	anpp	Shape parameter for fertilization effect	1
γ_{npp}	gnpp	Sensitivity of NPP to climate	K^{-1}
β_{fire}	bfire	Sensitivity of wildfire intensity to CO2	1
γ_{fire}	gfire	Sensitivity of wildfire intensity to climate	K^{-1}
β_{rh}	brh	Sensitivity of heterotrophic respiration to fresh organic matter	1
γ_{rh}	grh	Sensitivity of heterotrophic respiration to climate	K^{-1}
$F_{\mathrm{npp},0}$	npp0	Preindustrial NPP	PgC yr^{-1}
ν_{fire}	vfire	Wildfire intensity	yr^{-1}
ν_{harv}	vharv	Harvest and grazing rate	yr^{-1}
ν_{mort}	vmort	Mortality rate	yr^{-1}
ν_{stab}	vstab	Stabilization rate	yr^{-1}
ν_{rh1}	vrh1	Litter heterotrophic respiration rate	yr^{-1}
ν_{rh23}	vrh23	Soil (active and passive) respiration rate	yr^{-1}
ν_{rh3}	vrh3	Passive soil respiration rate	yr^{-1}
α_{pass}	apass	Fraction of passive soil	1
α_{lst}	aLST	Climate scaling factor over permafrost regions	1
γ_{rt1}	grt1	Sensitivity of (boreal) heterotrophic respiration to climate	K^{-1}
γ_{rt2}	grt2	Sensitivity of (boreal) heterotrophic respiration to climate (quadratic)	K^{-2}
κ_{rt}	krt	Scaling factor for sensitivity of permafrost respiration to climate	1
a_{min}	amin	Minimal thawed fraction	1
κ_a	ka	Shape parameter for theoretical thawed fraction	1
γ_a	ga	Sensitivity of theoretical thawed fraction to climate	K^{-1}
ν_{thaw}	vthaw	Thawing rate	yr^{-1}
ν_{froz}	vfroz	Freezing rate	yr^{-1}
$\alpha_{\mathrm{th},j}$	ath_j	Thawed permafrost carbon subpools fractions	1 $j \in [\![1,3]\!]$
$\tau_{\mathrm{th},j}$	tth_j	Timescales of thawed permafrost carbon subpools	yr $j \in [\![1,3]\!]$
$\kappa_{\tau_{\mathrm{th}}}$	k_tth	Scaling factor for timescales of surface ocean subpools	1
$C_{\mathrm{fr},0}$	Cfr0	Preindustrial frozen permafrost carbon pool	PgC
α_C	aCO2	Conversion factor for atmospheric CO2	PgC ppm^{-1}
C_{pi}	CO2pi	Preindustrial CO2 concentration	ppm
κ_{pH}	k_pH	Scaling factor for surface ocean pH	1
$\tilde{\sigma}_C$	std_CO2	Relative standard deviation of the historical CO2 time series (for calib.)	1
ϵ_C	ampl_CO2	Noise amplitude of the historical CO2 time series (for calib.)	ppm
ρ_C	corr_CO2	Autocorrelation of the historical CO2 time series (for calib.)	1
$\tilde{\sigma}_T$	std_T	Relative standard deviation of the historical T time series (for calib.)	1
ϵ_T	ampl_T	Noise amplitude of the historical T time series (for calib.)	K
ρ_T	corr_T	Autocorrelation of the historical T time series (for calib.)	1

Table B4. Parameters used in the permafrost, land carbon modules and for calibration.

Parameters	Prior	Unit
Lgla	380	mm
Lais	1200	mm
tgla	190	yr
tgis	481	yr
tais	2093	yr
T2x0	0.61	K
adic	4.49	μmol kg^{-1} PgC^{-1}
aoc_1	0.87	1
aoc_2	0.06	1
aoc_3	0.04	1
aoc_4	0.02	1
aoc_5	0.01	1
toc_1	1.3	yr
toc_2	16.7	yr
toc_3	65	yr
toc_4	348	yr
toc_5	10^9	yr
vrh3	8.27 10^{-5}	yr^{-1}
aLST	1.87	1
grt1	0.12	K^{-1}
grt2	0.0029	K^{-2}
krt	1.34	1
amin	0.98	1
vthaw	0.14	yr^{-1}
vfroz	0.011	yr^{-1}
ath_1	0.05	1
ath_2	0.12	1
ath_3	0.83	1
tth_1	18.2	yr
tth_2	252	yr
tth_3	3490	yr
aCO2	2.12	PgC ppm^{-1}
k_pH	1	1

Table B5. Structural parameters values. Parameters are noted under their code notation, and Tables B3 and B4 provide the corresponding notation in text.

Parameters	Prior	Posterior	Unit	Parameters	Prior	Posterior	Unit
phi	5.35 ± 0.54	5.29 ± 0.54	W m^{-2}	T2x	4.13 ± 1.37	3.37 ± 0.77	K
THs	8.14 ± 0.99	8.21 ± 1.06	W yr m^{-2} K^{-1}	THd	108.6 ± 61.8	123.8 ± 57.8	W yr m^{-2} K^{-1}
th	0.61 ± 0.13	0.67 ± 0.12	W m^{-2} K^{-1}	eheat	1.35 ± 0.40	1.41 ± 0.43	1
aOHC	0.91 ± 0.02	0.91 ± 0.02	1	Lthx	1.82 ± 0.21	1.85 ± 0.23	mm m^2 W^{-1} yr^{-1}
lgla0	0.59 ± 0.24	0.40 ± 0.21	mm yr^{-1}	Ggla1	0.34 ± 0.18	0.34 ± 0.05	mm K^{-1}
Ggla3	0.022 ± 0.013	0.022 ± 0.013	mm K^{-3}	ggla	0.12 ± 0.09	0.11 ± 0.07	K^{-1}
Lgis1	82 ± 45	189 ± 55	mm K^{-1}	Lgis3	5.7 ± 1.4	5.8 ± 1.5	mm K^{-3}
Lais_smb	0.61 ± 0.19	0.40 ± 0.10	mm K^{-1} yr^{-1}	lais0	0.00 ± 0.11	0.07 ± 0.08	mm yr^{-1}
aais	0.002 ± 0.003	0.004 ± 0.003	mm^{-1}	lgis0	0.33 ± 0.14	0.35 ± 0.14	mm yr^{-1}
k_toc	1.00 ± 0.20	0.91 ± 0.18	1	vgx	0.19 ± 0.06	0.20 ± 0.07	PgC ppm^{-1} yr^{-1}
ggx	0.018 ± 0.029	0.019 ± 0.033	K^{-1}	To	18.0 ± 0.5	18.0 ± 0.5	K
bdic	0.87 ± 0.08	0.90 ± 0.09	1	gdic	0.04 ± 0.02	0.04 ± 0.02	K^{-1}
npp0	48.2 ± 5.1	46.5 ± 3.3	PgC yr^{-1}	vfire	0.006 ± 0.003	0.006 ± 0.002	yr^{-1}
vharv	0.003 ± 0.003	0.003 ± 0.002	yr^{-1}	vmort	0.11 ± 0.01	0.11 ± 0.01	yr^{-1}
vstab	0.32 ± 0.28	0.30 ± 0.22	yr^{-1}	vrh1	0.33 ± 0.29	0.27 ± 0.20	yr^{-1}
vrh23	0.024 ± 0.009	0.024 ± 0.008	yr^{-1}	bnpp	0.93 ± 0.37	1.09 ± 0.25	1
anpp	0.48 ± 0.57	0.36 ± 0.38	1	gnpp	-0.014 ± 0.023	-0.005 ± 0.024	K^{-1}
bfire	-0.05 ± 0.12	-0.06 ± 0.14	1	gfire	0.052 ± 0.072	0.044 ± 0.088	K^{-1}
brh	1.06 ± 0.43	1.01 ± 0.41	1	grh	0.056 ± 0.053	0.042 ± 0.035	K^{-1}
apass	0.69 ± 0.19	0.63 ± 0.20	1	ga	0.13 ± 0.04	0.13 ± 0.04	K^{-1}
ka	2.6 ± 2.0	2.4 ± 1.8	1	k_tth	0.96 ± 0.93	1.00 ± 0.87	1
Cfr0	546 ± 120	538 ± 122	PgC	CO2pi	278 ± 3	279 ± 3	ppm

Table B6. Calibrated parameters values before and after Bayesian calibration. Parameters are noted under their code notation, and Tables B3 and B4 provide the corresponding notation in text. The uncertainty correspond to the 1 σ uncertainty range.

A.2 . Supplementary Figure for section 2.3

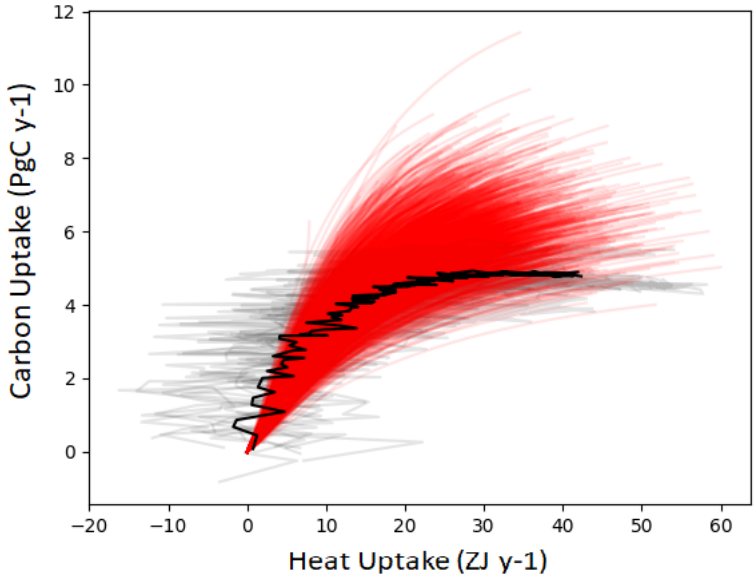

Figure A.1: Perturbed parameter ensemble from Pathfinder under an idealized set-up. Individual realization of Pathfinder are given in colored solid lines, individual ESMs in thin grey lines and ESM multi-model mean in black lines.

A.3 . Supplementary from Bossy, Gasser, Ciais, Tanaka, Lecocq and Bousquet (2023)

Supplementary text

Coverage of AR6 scenarios

As explicated in the primary textual content, our Pathfinder scenarios encompass the entirety of comparable AR6 scenarios in 100% of the configurations. This signifies that the estimated limits of the compatible spaces we explore are consistently less restrictive than those of the AR6 scenario ensemble, thereby affirming our exploration of a broader range of potential future scenarios (Figure S1 for illustration). Figure S10 provides a comparative analysis of the limits of the compatible space between AR6 scenarios and the scenarios generated by Pathfinder. The considered ensembles employ a consistent year of peak CO_2 emissions in 2022, assuming net-zero achievable in 2050, prohibiting SRM, and permitting the deployment of CDR up to 10 PgC yr^{-1}. Each subplot of Figure S10 represents a limit for a distinct key characteristic while the other pathway characteristics adhere to their default constraints. It is noteworthy that both AR6 and Pathfinder scenarios identify pathways that do not require the implementation of CDR (Figure S10.a). From a logical standpoint, if CDR is unnecessary, the specific year of achieving net-zero emissions or the commencement of significant CDR becomes irrelevant. Figure S10.b, focusing on the year of peak CO_2 emissions, reveals that Pathfinder identifies pathways capable of peaking between 2030 and 2040, irrespective of the safety level or boundary considered. In contrast, the AR6 scenarios indicate a peak in 2030 at latest or even 2025 for the Arctic sea ice boundary associated to a 90% safety level. Moreover, Figure S10.c demonstrates that Pathfinder scenarios exhibit peak CO_2 emissions surpassing those depicted in AR6 scenarios across all boundaries and safety levels.

Interpretation of the limits of compatible spaces

We look at thousands of pathways in every state of the world. Although our sampling is extensive enough to provide a comprehensive estimation of the range of possibilities, it does not encompass every conceivable pathway. Consequently, situations arise in which, under identical constraints on all pathway characteristics except for one (e.g., 10 PgC yr^{-1} of CDR, absence SRM, net zero emissions by 2100), we may not identify a compatible pathway for all values of the variable pathway characteristic below the limit of the compatible space in a given state of the world. For instance, we might establish a limit of the compatible space in 2037 for the peak date but fail to discover a pathway with a peak in 2035. For the sake of simplicity in interpreting the results, we assume that this pathway would be viable but was not generated by Pathfinder. To illustrate the advantages of this simplification, let us consider the result in which the limit of the compatible space for all boundaries combined is determined to be 2033 at a 67% safety level, with net-zero emissions achieved by 2050, CDR limited to 10 PgC yr^{-1}, and no SRM. In practice, this outcome indicates that 67% of Pathfinder's configurations identify at least one pathway meeting these conditions with a peak date in 2033 or later. Consequently, it is plausible that a configuration exists with a pathway peaking in 2035 but no pathways peaking in 2033. By virtue of our assumption, we can confidently assert that 67% of Pathfinder's configurations discover at least one pathway with a peak date in 2033.

Supplementary Figures

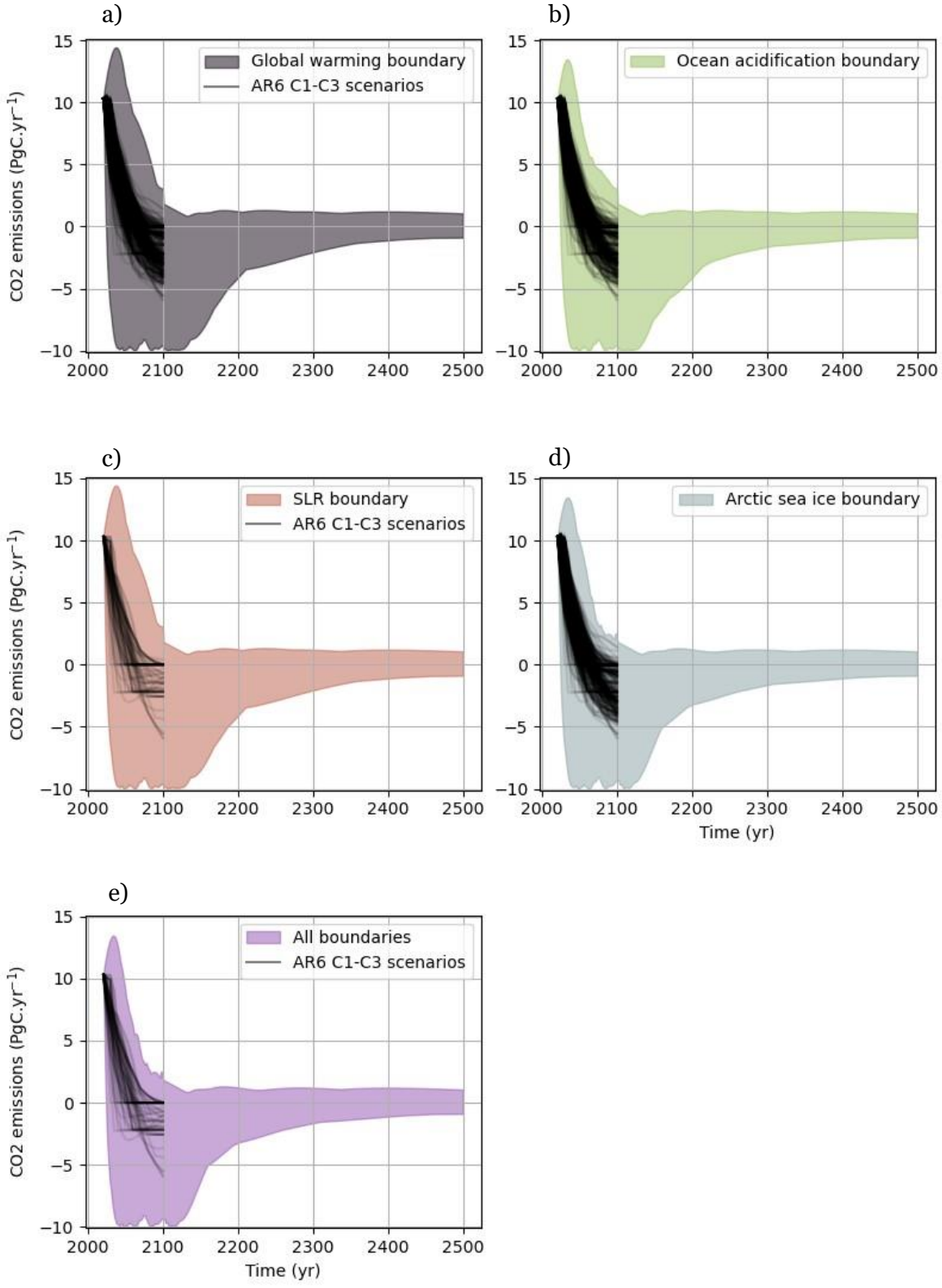

Figure S1: Illustration with the “best guess” configuration of Pathfinder. It is a configuration where we apply the mean value to all parameters. In this specific configuration, AR6 C1-C3 scenarios that are Paris-compliant (black lines) are covered by scenarios calculated by Pathfinder in our framework (colored envelope**s**) under comparable conditions on pathways characteristics: no SRM and up to 10 $PgC.yr^{-1}$ of CDR. All pathways remain below 2°C. Pathfinder pathways tend to 1.5°C in the long term. Our results show that this coverage is similar in all 1500 configurations of Pathfinder used in this study. Panel a) shows the pathways compatible with the global warming boundary. Panel b) shows pathways compatible with the ocean acidification boundary. Panel c) shows pathways compatible with the SLR boundary. Panel d) shows pathways compatible with the Arctic sea ice boundary. Panel e) shows pathways compatible with all boundaries together**.**

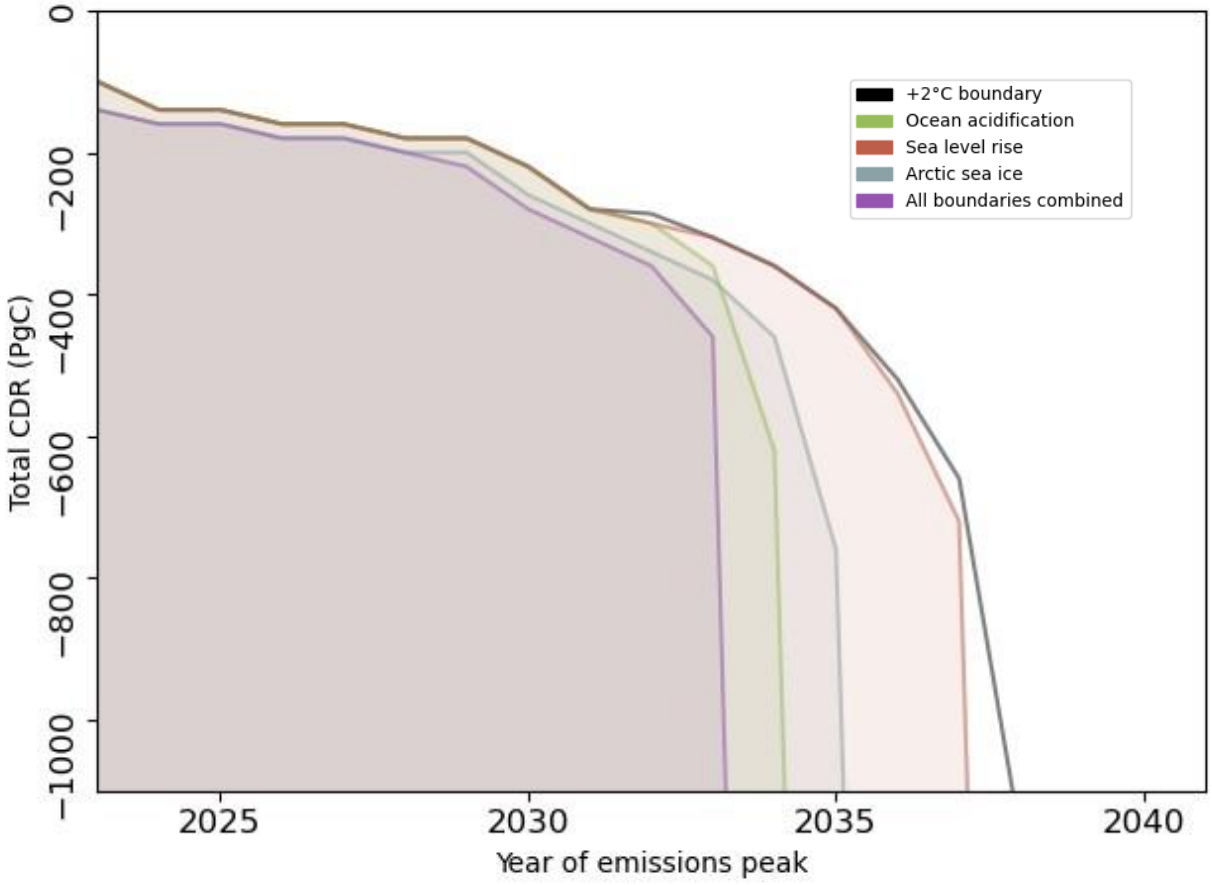

Figure S2: Trade-offs between the date of emissions peak and the total amount of CDR needed before 2100, for a 67% safety level. Shaded areas represent the spaces compatible with one planetary boundaries. Plain lines give the frontier of the compatible space. Black is for the global warming boundary, green for the ocean acidification boundary, red for the SLR boundary, blue for the Arctic sea ice boundary, and purple for the combination all boundaries.

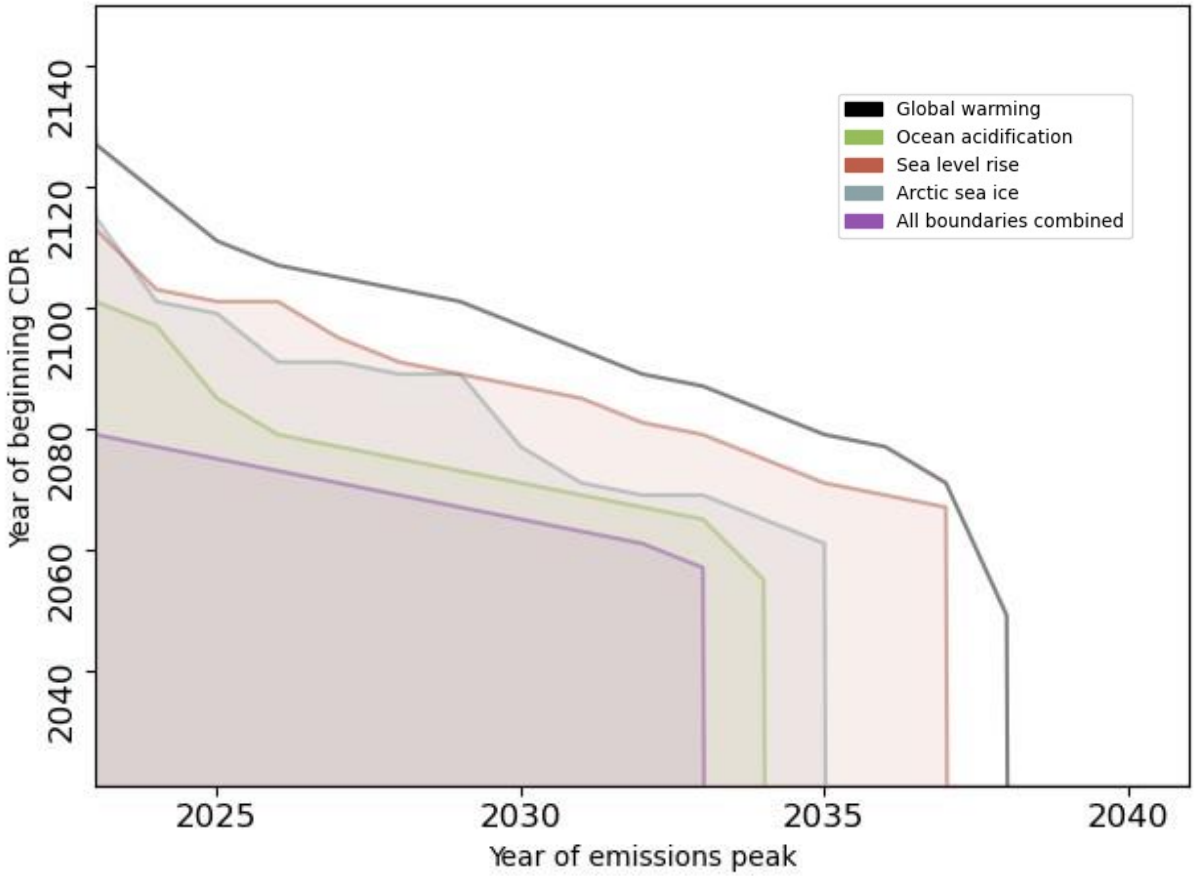

Figure S3: Trade-offs interaction between the year when CDR is significantly deployed (more than 0.5 $PgC.yr^{-1}$) and the year of peak emission for a 67% safety level. Shaded areas represent the spaces compatible with one planetary boundary. Plain lines give the frontier of the compatible space. Black is for the global warming boundary, green for the ocean acidification boundary, red for the SLR boundary, blue for the Arctic sea ice boundary, and purple for the combination all boundaries.

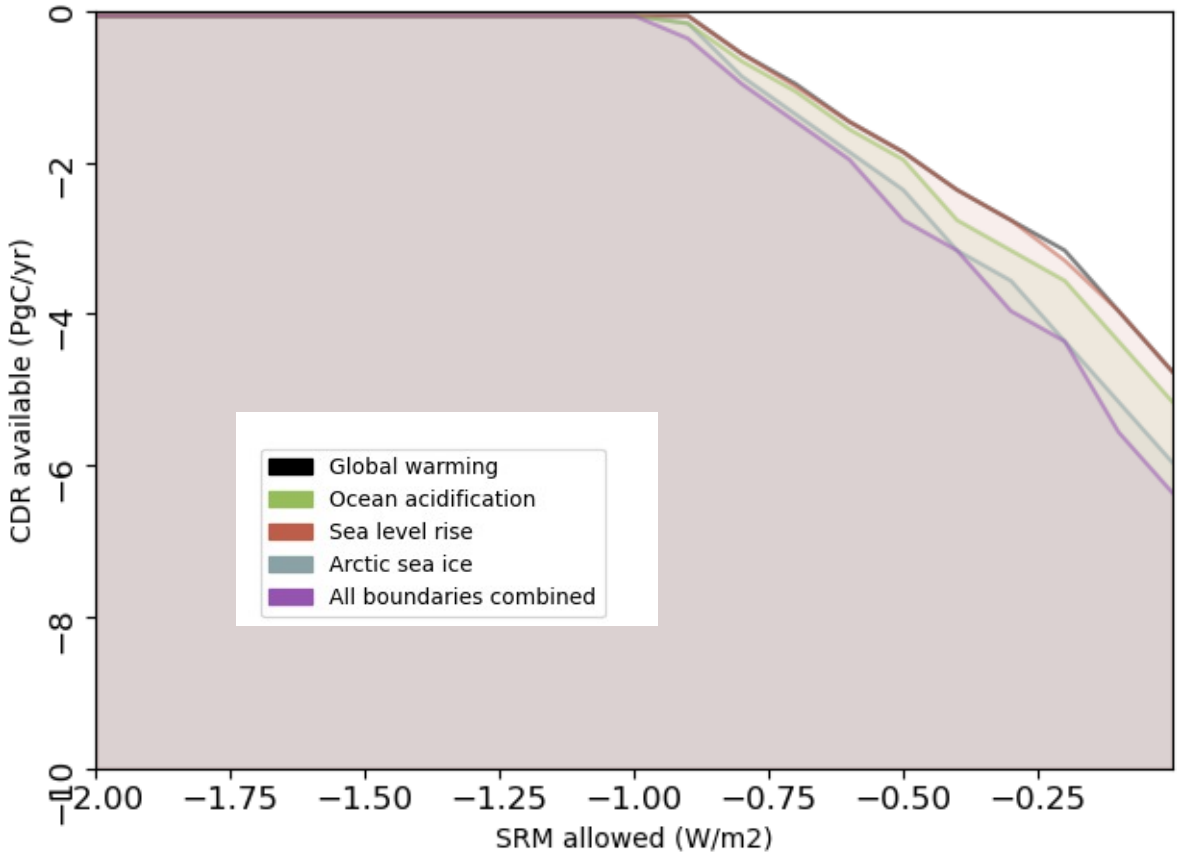

Figure S4: Trade-offs between CDR available and how much SRM is allowed in the case of a peak of CO_2 emission in 2030 for a 67% safety level. Shaded areas represent the spaces compatible with one planetary boundary. Plain lines give the frontier of the compatible space. Black is for the global warming boundary, green for the ocean acidification boundary, red for the SLR boundary, blue for the Arctic sea ice boundary, and purple for the combination all boundaries.

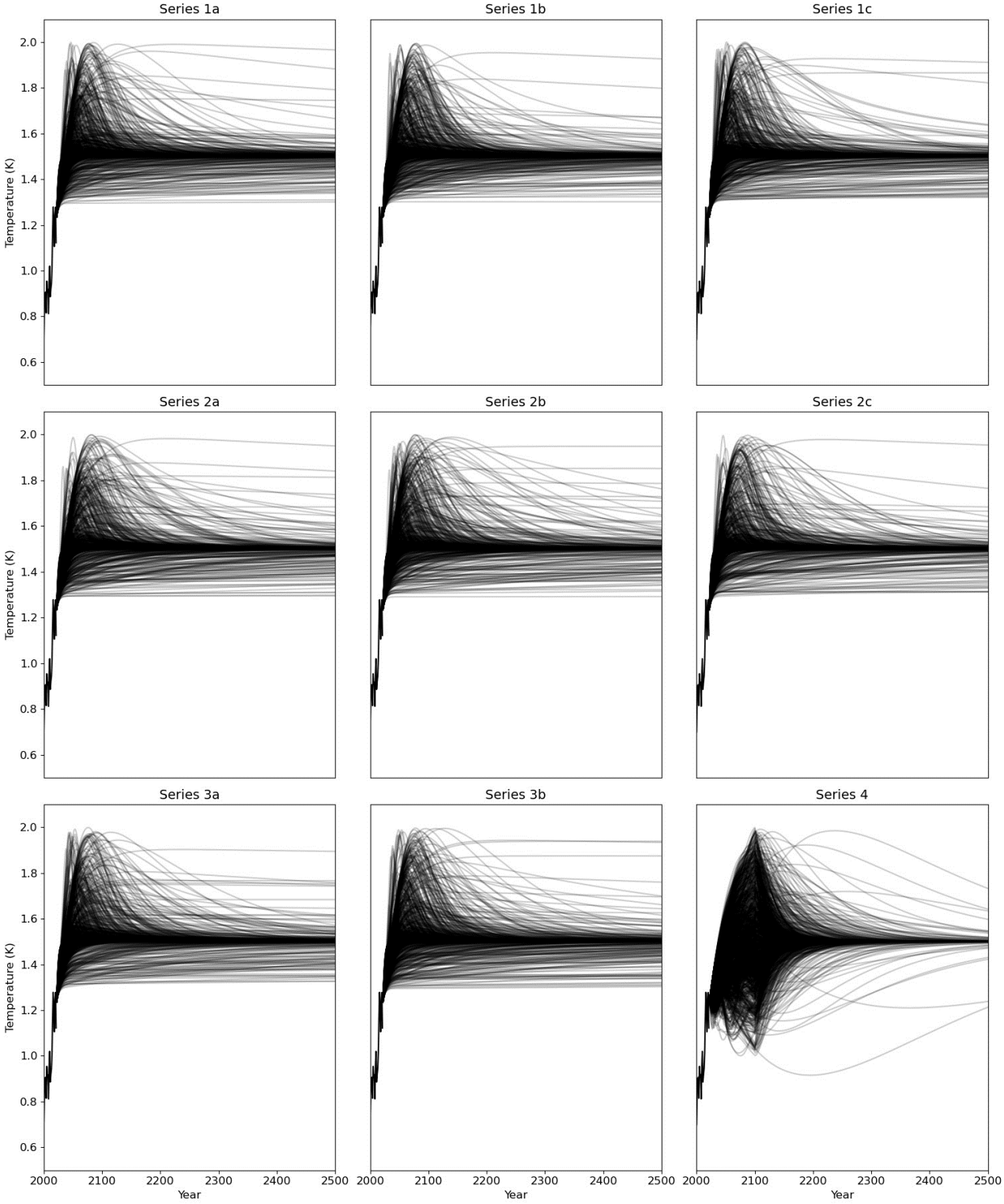

Figure S5: Temperature trajectories classified by series for one configuration of Pathfinder

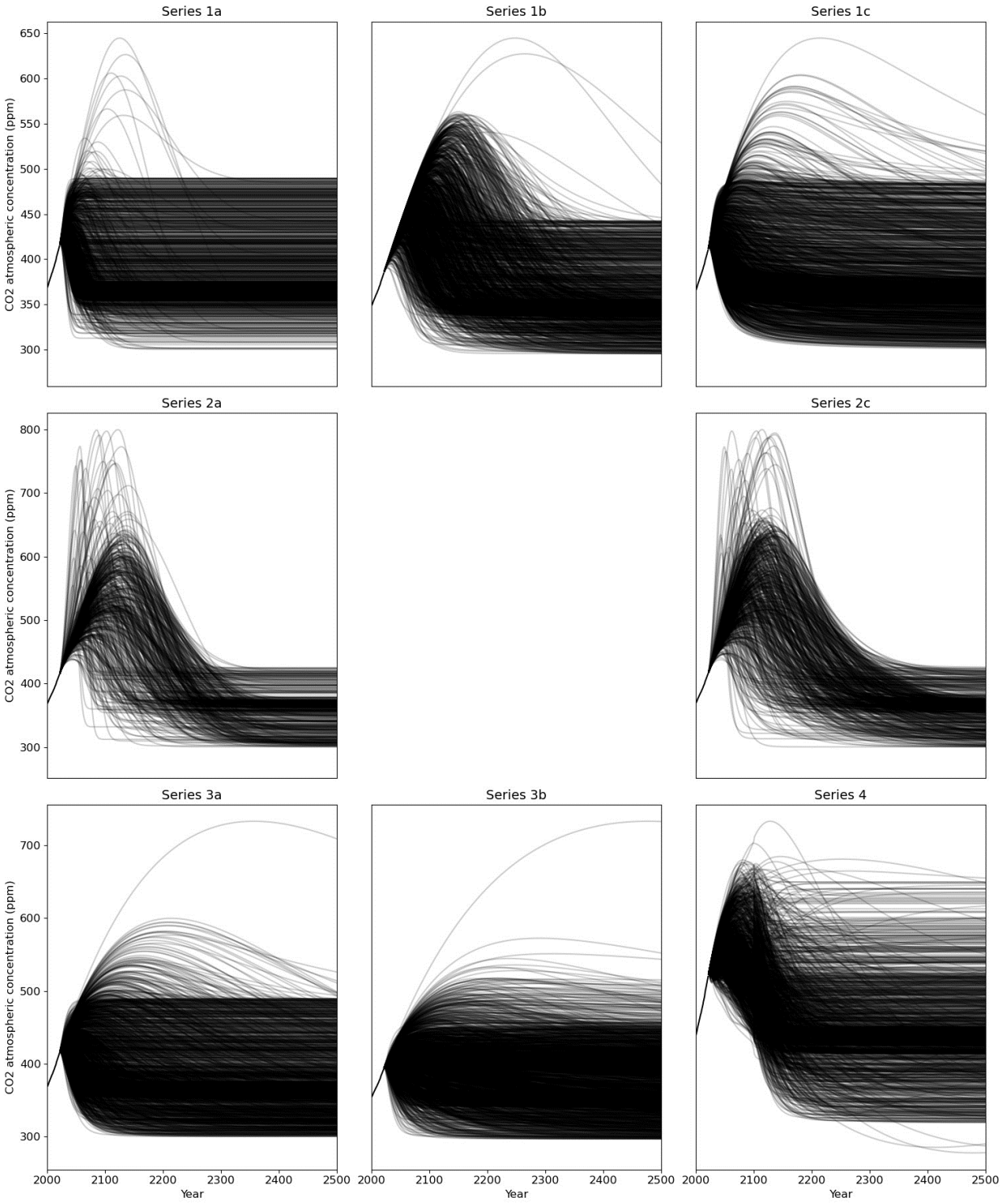

Figure S6: Atmospheric CO_2 concentration classified by series for one configuration of Pathfinder

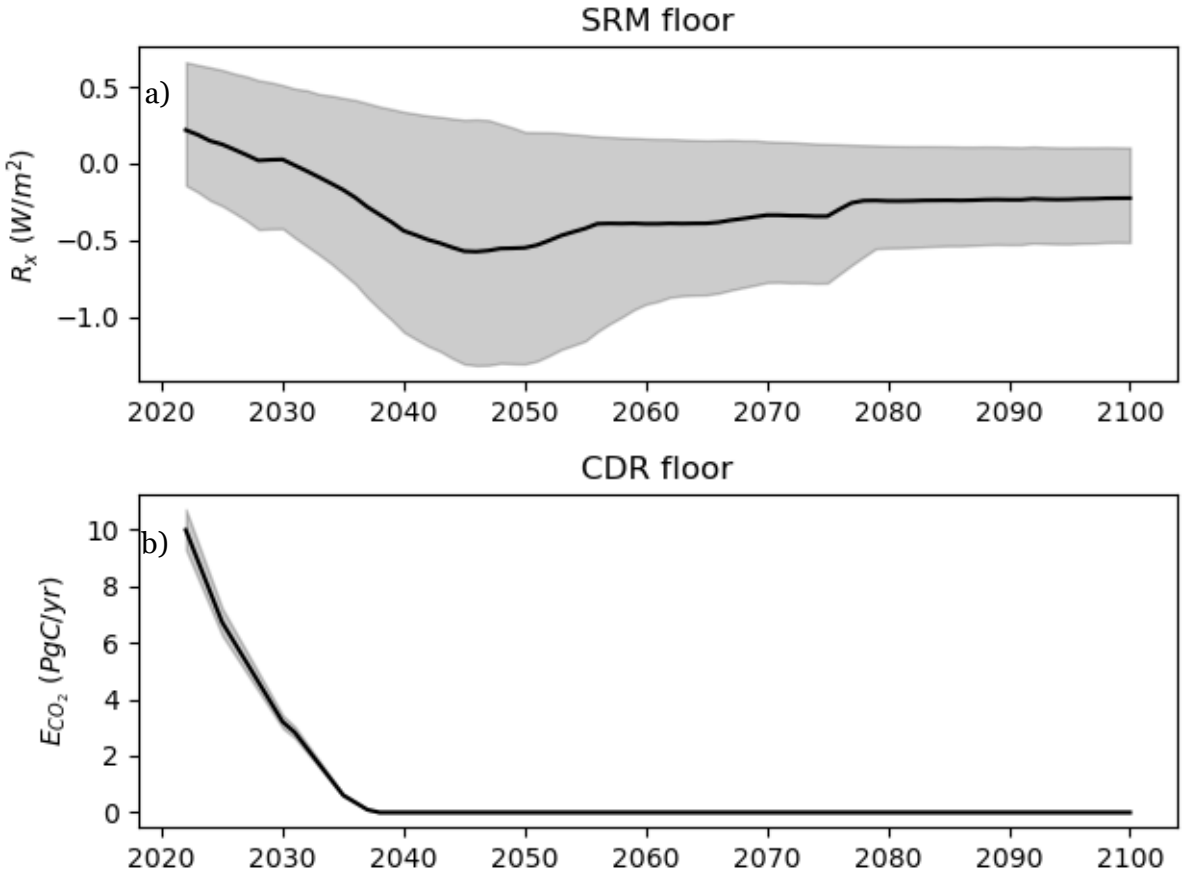

Figure S7: SRM (Panel a) and CDR (Panel b) floors in Pathfinder. Shaded areas show the 1-sigma uncertainty range.

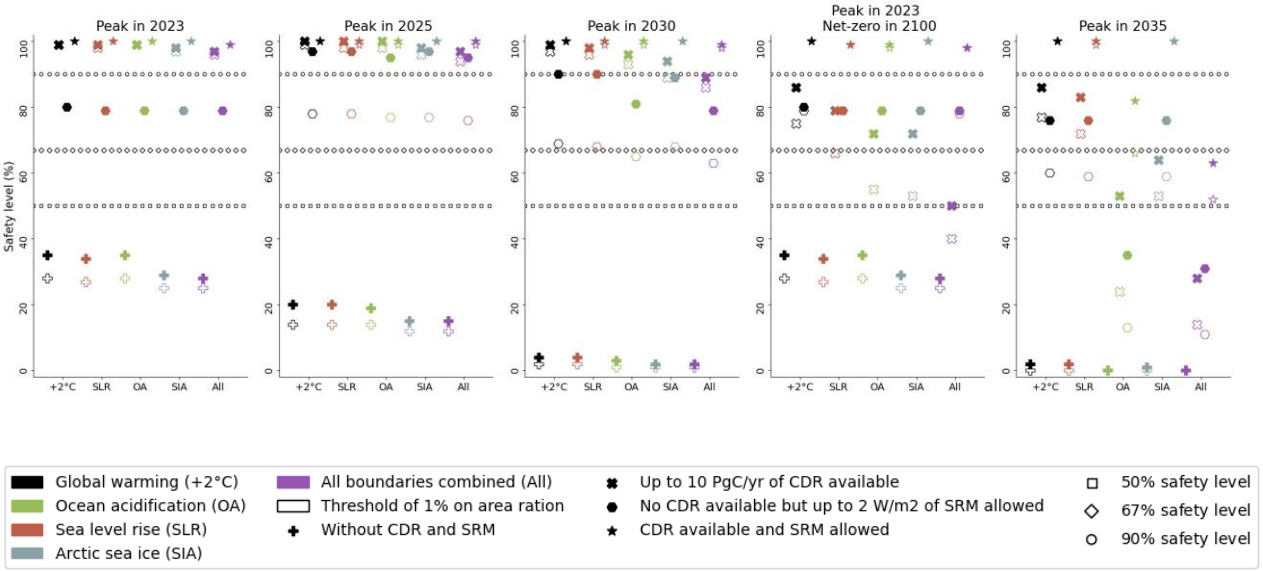

Figure S8: Safety levels of compatible spaces defined by various combinations of conditions on pathway characteristics and for two different definitions of the compatible space. Plain markers reproduce results from Figure 2 by defining a space compatible when there remains at least one pathway. Empty markers give the same values for a space considered compatible only if the relative size of the remaining compatible pathways envelope is kept above a 1% area ratio (Methods). Subplots distinguish conditions on the date of CO_2 emissions peak and of net-zero. *Net-zero in 2100* means that CO_2 net-zero is reached in 2100 or later. No information on net-zero means that this pathways characteristic is not constrained. *Peak in 2023, 2025, 2030 and 2035* means that the compatible CO_2 pathways reaches their peak in 2023, 2025, 2030, or 2035. Markers distinguish conditions on speculative technologies, *Up to 10 PgC yr^{-1} of CDR* assumes that SRM will never be available while CDR will be available, possibly up to 10 PgC yr^{-1}. *No technologies* assumes that neither SRM nor CDR will be available. *CDR available and SRM allowed* assumes SRM being possibly used up to 2 W m^{-2} in addition to CDR. Finally, the *SRM replaces CDR* case assumes that CDR will never be available but SRM can be used up to 2 W m^{-2}. Marker lines show the 90% safety level, 67% safety level and 50% safety level.

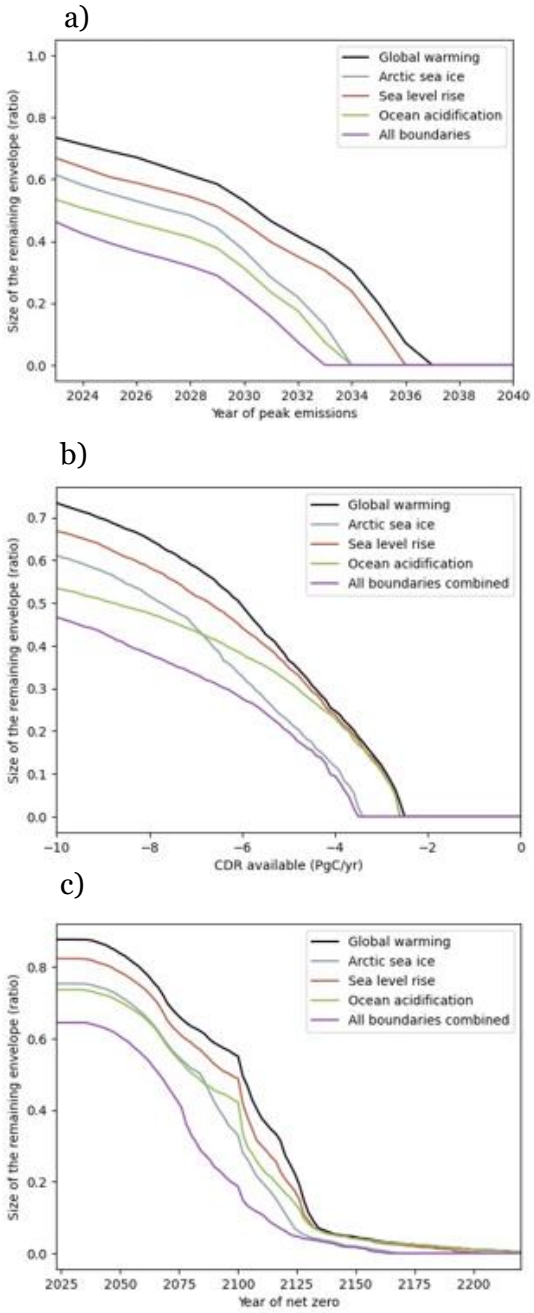

Figure S9: Size of the remaining envelope for different planetary boundaries for a 67% safety level. Panel a shows the evolution of the size under different year of CO_2 emission peak with up to 10PgC yr^{-1} of CDR, no SRM and net-zero CO_2 emissions reachable in 2050. Panel b shows the evolution of the size under different amount of CDR available at peak deployment with no SRM, CO_2 emissions peak in 2023 and net-zero CO_2 emissions reachable in 2050. Panel c shows the evolution of the size under different year of net-zero CO_2 emission with up to 10PgC yr^{-1} of CDR, no SRM and CO_2 emissions peak in 2023.

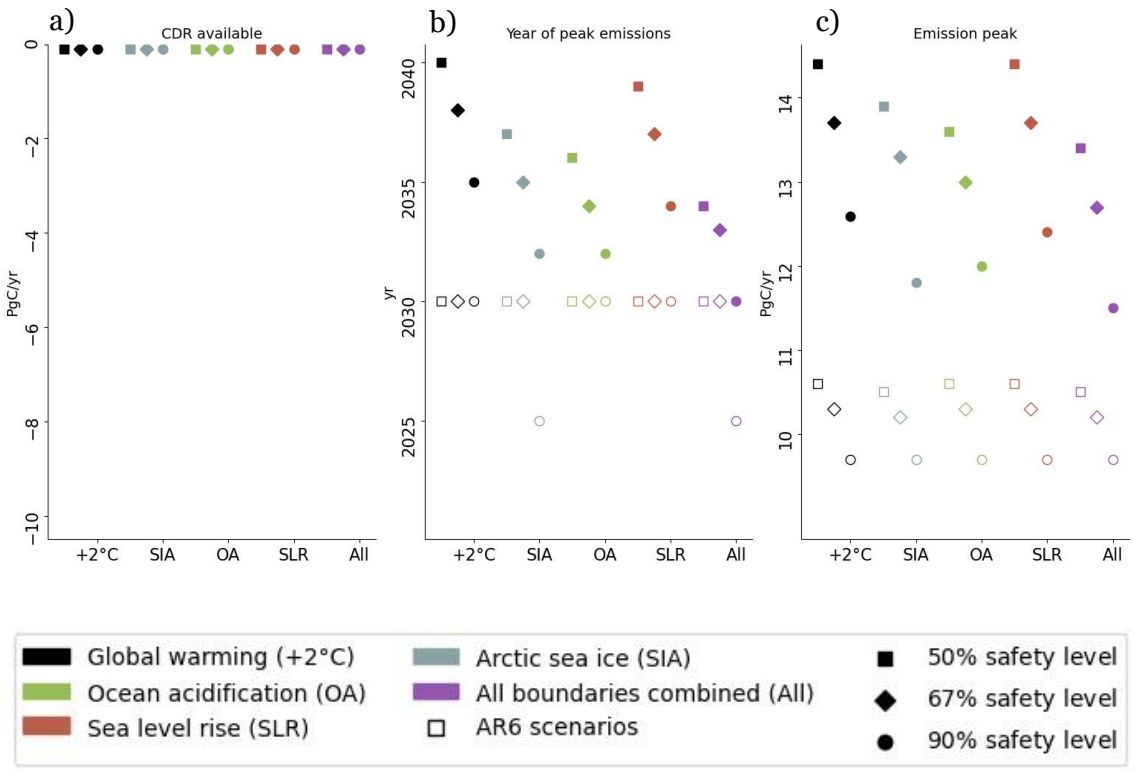

Figure S10: Limits of the compatible space for one key characteristic if the other pathway characteristics are not constrained and for three safety levels: 50% (squares), 67% (diamonds) and 90% (circles). Panel a focus on the amount of CDR available at peak deployment, panel b on the year of CO_2 peak emissions and panel c focus on the level of CO_2 emission peak. Black is for the global warming boundary, green for the ocean acidification boundary, red for the SLR boundary, blue for the Arctic sea ice boundary, and purple for the combination all boundaries. We compare those limits given by the ensemble of scenarios from Pathfinder (plain markers) to the same limits given by the ensemble of scenarios C1, C2 and C3 from the AR6 database run through Pathfinder (empty markers). If the limit is the same for both scenarios ensemble, we only show plain markers.

A.4 . Supplementary from Bossy, Gasser, Ciais, Tanaka and Lecocq (2023)

SUPPLEMENTARY MATERIALS

Supplementary texts

Input trajectories: Temperature and Atmospheric CO_2 concentration.

We randomly and independently draw temperature (*T*) and atmospheric CO_2 concentration (*C*) trajectories using 4 different approaches grouped into "series" and "sub-series". Series 1, 2 and 3 correspond to different analytical expressions while series 4 is derived from AR6 scenarios[1]. All series have some common characteristics:

- T, $\frac{d}{dt}T$ and C are defined and differentiable.
- We impose an upper boundary so that $T \leq 2^{\circ}C$.
- We also impose $\lim_{t\to\infty} T = 1.5^{\circ}C$.
- We randomly choose an asymptotic value for *C* which is determined by the share $k_{x,final}$ of non-CO_2 components in the global radiative forcing. $k_{x,final}$ is uniformly drawn within one of three equiprobable ensembles (i.e. 1/3 chance of being in each):
  - $k_{x,final} \in]-1; -0.1[$
  - $k_{x,final} \in [-0.1; 0.1]$
  - $k_{x,final} \in]0.1; 0.66[$

In Series 1, for *X* being *T* or *C*, we choose *X* of the form $X(t) = X_0 + (X_{lim} - X_0) \cdot \omega(t - t_0) + \alpha \cdot t \cdot (1 - \omega(t - t_0))$, with $X_0 = X(t{=}t_0)$ the initial value of *X* given by the historical calibration, with t_0=2021, and X_{lim} the asymptotic value. We determine α so that $\left.\frac{dX}{dt}\right|_{t=t_0} = \left.\frac{dX}{dt}\right|_0$, where $\left.\frac{dX}{dt}\right|_0$ is the differentiated variable given by the historical calibration in 2021.

$\omega(t)$ is the function we use to distinguish the sub-series. This function must tend towards 0 for $t = 0$ and towards 1 for $t \to \infty$. To keep the continuity and differentiability for *X* and $\frac{dX}{dt}$, ω must be continuously differentiable at least once. In series 1a, $\omega(t) = 1 - e^{-\mu_0 t - \mu_1^2 t^2}$ [2], in series 1b, $\omega(t) = \frac{t}{t + \mu_1 e^{-\mu_0 t}}$, and in series 1c, $\omega(t) = \frac{\mu_0 t^2 + \mu_1 t}{1 + \mu_0 t^2}$. Parameter distributions are given in Table S1.

Series 2 follows the probability density function of a Kumaraswamy distribution[3] until it peaks (i.e. for $t < t_{peak}$), $\mathrm{X}(t < t_{peak}) = \mathrm{X}_0 + [X_{peak} - \mathrm{X}_0] \cdot [1 - (1 - (\tau_o / (\tau_o - t_{peak}))^{\alpha})^{-\beta} \cdot (1 - ((\tau_o - t) / (\tau_o - t_{peak}))^{\alpha})^{\beta}]$. Peaking dates ($t_{peak}$) and peaking values ($X_{peak}$) are chosen randomly in ensembles that are compatible with our constraints and for which we can maintain continuity and differentiability of *X* and $\frac{dX}{dt}$. τ_o is defined such as $f(\tau_o) = -t_{peak}$ with $f(t) = -t \cdot ((1 - \frac{t_{peak}}{t})^{\alpha} - 1) - \alpha \cdot \beta \cdot \frac{X_{peak} - \mathrm{X}_0}{\left.\frac{dX}{dt}\right|_0}$. Sub-series have different functional forms after the peak ($t > t_{peak}$) to converge to the asymptotic value X_{lim}. Series 2a follows the probability density function of a normal distribution such as $\mathrm{X}(t \geq t_{peak}) = X_{lim} + (X_{peak} - X_{lim}) \cdot e^{-\frac{(t - t_{peak})^2}{\tau^2}}$. With $\tau = \frac{\sqrt{X_{peak} - X_{lim}}}{\sqrt{X_{peak} - X_0}} \cdot (t_{peak} - \tau_o) \cdot \left(1 - \left(-\frac{\tau_o}{t_{peak} - \tau_o}\right)^{\alpha}\right)^{\beta/2} \cdot \sqrt{\frac{2}{\alpha^2 \cdot \beta \cdot (\beta - 1)}}$. Series

2b follows the probability function of a log-normal distribution so $X(t \geq t_{peak}) = X_{lim} + (X_{peak} - X_{lim}) \cdot e^{-0.5\frac{log(t/t_{peak})^2}{\sigma^2}}$. With $\sigma = \frac{\sqrt{X_{peak} - X_{lim}}}{\sqrt{X_{peak} - X_0}} \cdot \left(1 - \frac{\tau_o}{t_{peak}}\right) \cdot \left(1 - \left(-\frac{\tau_o}{t_{peak} - \tau_o}\right)^{\alpha}\right)^{\beta/2} \cdot \sqrt{\frac{2}{\alpha^2 \cdot \beta \cdot (\beta - 1)}}$. Series 2c follows the probability function of a Gompertz distribution[4]: $X(t \geq t_{peak}) = X_{lim} + (X_{peak} - X_{lim}) \cdot \eta^{1 - t/t_{peak}} e^{1 - \eta^{1 - t/t_{peak}}}$. With $\eta = exp\left(\frac{\sqrt{X_{peak} - X_{lim}}}{\sqrt{X_{peak} - X_0}} \cdot \left(1 - \frac{\tau_o}{t_{peak}}\right) \cdot \left(1 - \left(-\frac{\tau_o}{t_{peak} - \tau_o}\right)^{\alpha}\right)^{-\beta/2} \cdot \sqrt{\frac{2}{\alpha^2 \cdot \beta \cdot (\beta - 1)}}\right)$. We apply all three sub-series to the temperature but only series 2a and 2c to the atmospheric CO_2 concentration. Parameter distributions are given in Table S1.

Series 3 follows the solution of a damped harmonic oscillator differential system with non-zero initial positions and velocities. Depending on sub-series, it is either in a critical regime (series 3a) under the form $X(t) = X_{lim} + (X_0 - X_{lim} + (\kappa \cdot (X_0 - X_{lim}) + \left.\frac{dX}{dt}\right|_0) \cdot t) \cdot e^{-\kappa t}$, or in an over-critical regime (aperiodic) for series 3b, $X(t) = X_{lim} + [(X_0 - X_{lim}) \cdot cosh(\sqrt{\kappa^2 - \Omega^2} \cdot t) + \frac{\kappa \cdot (X_0 - X_{lim}) + \left.\frac{dX}{dt}\right|_0}{\sqrt{\kappa^2 - \Omega^2}} \cdot sinh(\sqrt{\kappa^2 - \Omega^2} \cdot t)] \cdot e^{-\kappa t}$. Parameter distributions are given in Table S1.

Series 4 is derived from the AR6 scenarios. Initially, we simulate all AR6 scenarios[1] using Pathfinder (as detailed in the subsequent section), and select only those scenarios where the maximum temperature remains below 2°C. To these T and C time series, we introduce noise generated through an AR(1) process[5]. We then apply an 11-year moving average to smoothen the trajectories affected by noise. We infer the lost 11 values by following the trend observed in the original T or C time series. To ensure the generated pathways are continuously differentiable, we fit the resulting trajectories with spline functions. These functions are defined piecewise by polynomials and allow for differentiation. Similar to other series, we impose constraints on the initial values of *X* and $\frac{dX}{dt}$ to maintain continuity with the historical trajectory. Additionally, to prevent splines with excessively steep or rapid trends at 2100, we also constrain the derivative at that point with the original value of the AR6 scenario before the noise.

Since Series 4 are derived from AR6 scenarios, the processed trajectories are limited to the year 2100. However, for our purposes, we require pathways that span up to 2500. To address this, we employ the analytical form of Series 3a to extend the trajectories from 2100 to 2500, ensuring continuity and differentiability are maintained throughout the extended period.

Series	Parameters	Values	Distribution
1a	μ_0	[-0.05, 0, 0.10]	Triangular
	μ_1	[0, 0.05, 0.10]	Triangular
1b	μ_0	[0.001, 0.01, 0.10]	Triangular
	μ_1	[1,100,1000]	Triangular
1c	μ_0	[2.5E-5, 3E-5, 1E-1]	Triangular
	μ_1	0	
2	α	[1.001, 1.0015, 20]	Triangular
	β	2	
	t_{peak}	[10, 70, 120]	Triangular
3a - 3b	κ	[0, 0.05, 0.15]	Triangular
3b	Ω	[0, κ]	Uniform

Table S1 Characteristics of the parameters for the T and CO_2 time series. Values for triangular distributions give the minimum, the peak and the maximum of the distribution. Values for uniform distribution give the minimum and the maximum.

Implementation of AR6 scenarios in Pathfinder

The AR6 database[1] hosts scenarios explored by different IAM and assessed by the working group 3 of the IPCC. However, these projections are inconsistent with the historical values of Pathfinder, making it infeasible to directly incorporate the raw data into our model.

To utilize CO_2 emissions and non-CO_2 radiative forcing (R_x) as inputs to Pathfinder, we perform linear interpolation to convert the pentadal or decadal data into annual data. Then, we rescale both drivers to align with the historical trajectories of Pathfinder. Due to the inherent natural variability present in Pathfinder's historical runs, it is not possible to directly utilize the year 2021 as a reference for rescaling. Instead, we compute the mean value of the historical Pathfinder's pathways between 2011 and 2021. We extend the mean values calculated in Pathfinder for 2016 by incorporating the trend in observational values until 2021. This approach ensures consistency with Pathfinder's configurations, as the 2016 value is specific to each configuration, while also aligning with the most recently observed trend. The rescaling factor is determined by comparing the reconstructed value for 2021 with the corresponding value in the AR6 scenario.

For observed CO_2 emissions, we employ the most recent estimates available until 2022[6] , while for R_x, we utilize estimates from 2019[7] . To establish the starting point of our simulations in 2021, we rely on the available trend for R_x over the last 10 years to infer the values for 2020 and 2021. (while CO_2 emissions were taken from the latest Global Carbon Budget[6]).

Similarly, for R_x, we reconstruct the historical value in 2021 by extending the mean value calculated in Pathfinder for 2016 and incorporating the trend in observational values until 2021. However, the treatment of R_x differs from that of CO_2 emissions due to its nature as a radiative forcing resulting from a combination of various GHGs (positive) and aerosols (mostly negative). Consequently, depending on the model's parameterization, the reconstructed historical R_x value in 2021 can be either negative or positive. Rescaling R_x without accounting for this decomposition could potentially lead to an artificial reversal of the sign of R_x in the scenarios. To address this, we first decompose R_x and rescale each component separately: $R_x^{AR6} = R_{x,ghgs}^{AR6} + R_{x,aerosols}^{AR6}$, where R_x^{AR6} is the radiative forcing due to non-CO_2 forcers in AR6 scenarios, $R_{x,ghgs}^{AR6}$ is the

radiative forcing due to a combination of different GHGs in AR6 scenarios, and $\mathrm{R}_{\mathrm{x,aerosols}}^{\mathrm{AR6}}$ is the radiative forcing due to aerosols in AR6 scenarios. As Pathfinder lacks such a decomposition, we use the IPCC AR6 extrapolated value of $R_{x,ghgs}^{hist} = 1.18 \pm 0.14\ W\ m^{-2}$ in 2021[7]. Assuming a normal distribution we randomly draw one value of the GHG component of R_x for each configuration of Pathfinder. Finally, the rescaling factor for GHGs is $\frac{R_{x,ghgs}^{hist}}{R_{x,ghgs}^{AR6,2021}}$, and the rescaling factor for aerosols is $\frac{R_x^{hist} - R_{x,ghgs}^{hist}}{R_{x,aerosols}^{AR6,2021}}$, where R_x^{hist} is the reconstructed historical value in Pathfinder in 2021 and $R_{x,aerosols}^{AR6,2021}$.and $R_{x,ghgs}^{AR6,2021}$ are the respective AR6 radiative forcing due to a combination of aerosols and different GHGs in 2021.

Cost functions and parameters values in the existing models

To derive our six cost functions, we conducted a comprehensive literature review, and isolated five models. These were selected based on factors such as data availability, prominence in the literature, and their aggregate form. All the terms we introduce in the six functions appear in at least one of these models. They therefore provide a starting point to choose a value for our ad hoc parameters or simply to assess the credibility of our calibrated parameters. We explain the values of these parameters below.

All models except ACC2 [8] have a term in their cost functions that represents autonomous technical change. □ is estimated between 0.95 (low estimate of RESPONSE [9]) and 0.998 (PAGE [10]), while DICE [11] estimates of 0.995 are widely used. For this reason, we chose □=0.995 in this paper.

Induced technical change is introduced in this form only in PAGE. Their model estimate the IES to be 150 $GtCO_2$ and □=ln(0.2). Calibration of our functions fails at such values. We fix σ=1.4.10^{-4} $GtCO_2^{-1}$, which corresponds to IES = 7333 $GtCO_2$ and □=-2.

The linear term was introduced by the RESPONSE model as a term that sets the price of the first mitigation option. The assumption □ =0 for no initial abatement cost is adopted by all other stylized IAMs we examined. RESPONSE examines four scenarios with marginal costs for initial abatement estimated between \$0 and \$229/tCO_2. On this basis, and given the free calibration of the sensitivity parameters (see next section), we set □ =\$136/tCO_2.

The non-linear term serves as the baseline value since it is widely used in all aggregated abatement cost functions. Therefore, this is the only term common to all cost functions studied. The two parameters of this non-linear term are calibrated. □ ranges between \$ 636/tCO_2 and \$ 881/tCO_2 and □ varies between 1.93 and 5.74. In the literature, the models estimate □ between \$400 (PAGE) and \$1200 (High estimate of RESPONSE) per tCO_2. The elasticity □ varies between 2 (ACC2) and 3.5 (RESPONSE).

Finally, the inertia term has been a source of discussion in the community. Two models (RESPONSE and DICE-PACE) use this term in a similar form in their function. RESPONSE estimates the transition time □ to be about 5 years, while DICE-PACE [12] uses previous diffusion rates of technologies such as nuclear, wind, or coal power to provide an estimate between 20 and 40 years. Following RESPONSE, we set □ = 5 years. The cost parameter □ is greater than 1 and shapes the inertia term, as with □, we decide to give this parameter a fixed value of □=2.

Free calibration of the sensitivity parameters of the cost function

Instead of having only two free parameters, an alternative calibration method is to calibrate all sensitivity parameters. In total, there are 8 unknown parameters (□, θ, μ, σ, α, β, δ, τ) and up to 7 in the same functional form. Since it is impossible to leave all parameters free for calibration, we set all shape parameters similarly as in the previous section: μ = -2, θ = 2.5, and □ = 2.

The distribution of costs in Figure S7 shows that, in 2050 and 2100, all cost functions estimate similar costs, regardless of the classification of the scenario (C1 to C6). In 2030, *DICE* and *DICE_LBD* are slightly lower than the other functions in all classifications, although the distribution of *DICE* is slightly larger. We also compare these distributions to the original distribution from the AR6 data [1]. With the exception of C1 and C2 in 2050, where the estimates of the cost functions are slightly too high, the median of the estimates of the functions is always within the uncertainty range of the AR6 data.

	α	θ	τ	β	δ	σ	ϕ	μ
DICE	3223 $/tC	2.5	0.994					
DICE_LBD	2372 $/tC	2.5				3.00 10^{-5} PgC^{-1}		-2
Full	1752 $/tC	2.5	0.9997	346 $/tC	1.48 yr		2	
Full_LBD	1711 $/tC	2.5		348 $/tC	1.5 yr	7.00 10^{-19} PgC^{-1}	2	-2
DICE_inertia	2500 $/tC	2.5	0.9973		2.5 yr		2	
DICE_linear	1771 $/tC	2.5	0.9992	417 $/tC				

Table S2: Calibration of the parameters of the abatement cost functions

A disadvantage of this calibration is that some terms of the cost function all but disappear, since the LBD sensitivity parameter (σ) in *Full_LBD* is very close to 0. For the inertia term, δ is between 1.5 and 2.5 years, which does not cancel the term but significantly reduces its role. Moreover, this value is quite small for the economic interpretation we have given to this term: a transition period for a new technology between invention and generalization of its use. Finally, τ can also be very close to 1 (e.g., 0.9997 in *Full*), again minimizing the impact of this discounting term.

Consequently, due to this "cancelation" of some parameters by the calibration, comparing all six cost functions would not be relevant anymore. It also appears that some cost functions seem to be more efficient in fitting data from more complex models. Typically, an LBD term based on the accumulation of experience does not help to predict abatement costs from processed-based IAMs.

Discussion of "10% cheapest" as a threshold for near-optimality

When defining near-optimal pathways, we chose to select all pathways that are among the 10% least expensive trajectories in the ensemble produced by Pathfinder. The choice of 10% relates to other studies that impose a tolerance threshold relative to the optimal pathways [13, 14]. However, our method differs from theirs, as they explore near-optimal spaces that differ from the cost-optimal path while staying in a 10% range around the optimized cost. In our work, the cost function is a tool to compare different conceptual approaches and the calibration only ensures that the modelled costs remain in the right order of magnitude for three target years.

Results for NPV with 0% discounting

Here, we follow the same analysis as before, except that we do not apply discounting to NPV (4% discount rate in the main text). This new minimization criterion does not favor the present and still differs from the minimax.

Selecting near-optimal pathways that are robust to all cost functions

In the NPV approach without discounting (NPV-*nodisc*), the conceptual choice of cost function is more discriminating, as we find 59% of near-optimal pathways are robust to NPV-*nodisc*. As with minimax, the discriminating factor is inertia. Indeed, Figure S5 illustrates that when the minimax approach is used, the costs calculated with or without accounting for inertia match respectively 99% and 93% of near optimal pathways.

Overall, it is particularly interesting to look for economically robust near-optimal pathways that apply to both the NPV-*nodisc* and minimax approaches. These pathways, which are economically robust to two minimization criteria with no preference for the present, account for 38% of the near-optimal pathways. This result demonstrates the difference between the two approaches.

It is also possible to apply this no discounting approach to NPV_{Diff} (NPV_{Diff}-*nodisc*). When using NPV_{Diff}-*nodisc* to define generational robustness, we find that there are no near-optimal pathways that are generationally robust, while robustness is 99% for cost functions with inertia (*DICE_inertia, Full, Full_LBD*) and 48% for those without (*DICE, DICE_linear, DICE_LBD*).

NPV-*nodisc*

	DICE	*Full_LBD*	*DICE_inertia*	*Full*	*DICE_linear*	*DICE_LBD*
DICE	100%	67%	67%	67%	94%	94%
Full_LBD		100%	99%	99%	63%	63%
DICE_inertia			100%	100%	62%	62%
Full				100%	62%	62%
DICE_linear					100%	98%
DICE_LBD						100%

Table S3 Matrix of ratios of robust pathways for NPV and two forms of cost functions

Consistency of robust near-optimal pathways with AR6 scenarios

It is important to remember that it is the size of the ensemble of 2°C-compliant pathways computed by Pathfinder that allows us to define near-optimal pathways. While our main results give median values, Pathfinder computes these pathways in 1000 configurations representing as many plausible physical states of the world. However, because of how the pathways are generated (see above), the studied trajectories also depend on these independent physical worlds.

Since pathways are uniquely tied to each individual configuration, it is impossible to derive a median trajectory across all configurations. Hence, representing a median trajectory for CO_2 emissions is challenging as it requires to mix pathways from all configurations that are not comparable. However, we can examine a 'best guess' configuration where parameters are closest to their median distribution value suggesting that this is the physical state of world that is the most likely to happen. By replicating the selection process of robust pathways delineated in Figure 1, we are able to present pathways that are both economically and generationally robust in this 'best guess' configuration.

The scenarios under this configuration, as plotted in Figure 7.c, are comparable to scenarios that carry 'at least a 50% chance' in the AR6 categorisation framework. Consequently, our economically and generationally robust near-optimal pathways are aligned with C4 scenarios, which represent a 50% or greater likelihood of staying below a 2°C increase [1].

Supplementary Figures

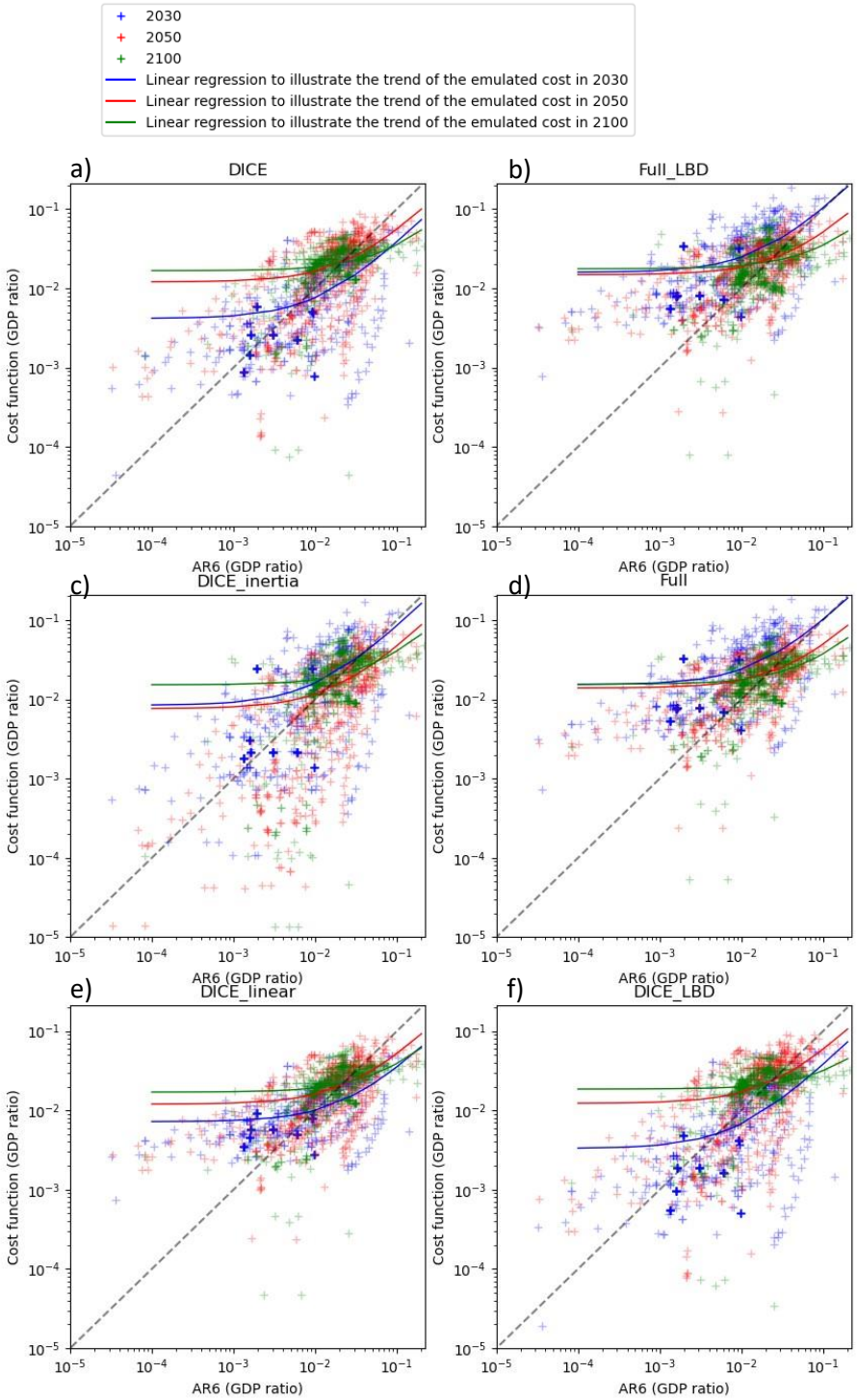

Figure S1 Comparison of abatement costs in AR6 with calibrated costs estimated using the 6 cost functions: *DICE* (panel a.), *Full_LBD* (panel b.), *DICE_inertia* (panel c.), Full (panel d.), *DICE_linear* (panel e.), and *DICE_LBD* (panel f.). The colors represent the 3 crossing points we focus on: 2030 (blue), 2050 (red), 2100 (green). The plain lines show the linear regression illustrating the trend of the calibrated costs for all 3 crossing points.

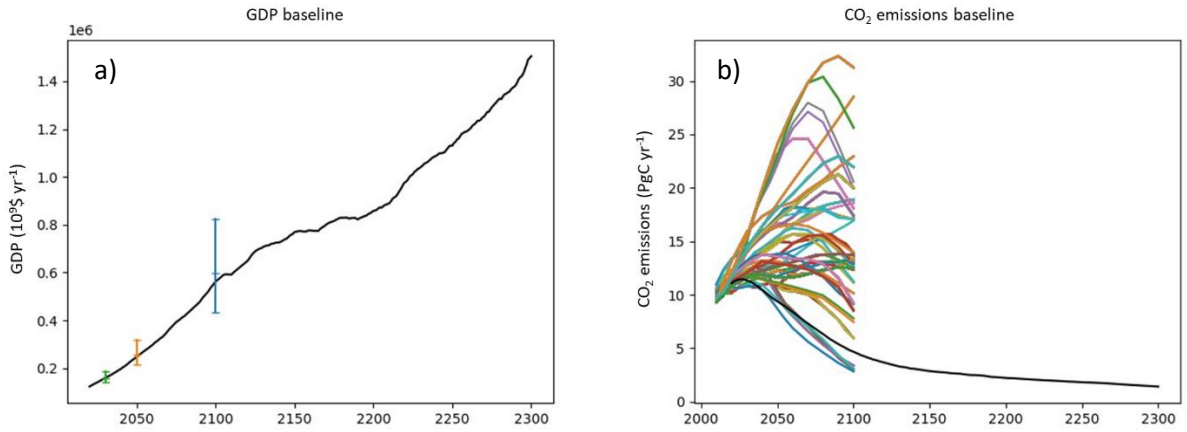

Figure S2 GDP (panel a) and CO2 emissions (panel b) baselines. The black lines show the baselines used in this study, i.e., the median value of the Rennert et al. [15] projections. The colored bar in panel a shows the range of baseline GDP from the AR6 scenarios at the three crossing points (2030, 2050, 2100). The colored lines in panel b show the baselines of CO2 emissions from the AR6 scenarios through 2100.

Category	Description
C1: Limit warming to 1.5°C (>50%) with no or limited overshoot	Reach or exceed 1.5°C during the 21st century with a likelihood of ≤67%, and limit warming to 1.5°C in 2100 with a likelihood >50%. Limited overshoot refers to exceeding 1.5°C by up to about 0.1°C and for up to several decades.
C2: Return warming to 1.5°C (>50%) after a high overshoot	Exceed warming of 1.5°C during the 21st century with a likelihood of >67%, and limit warming to 1.5°C in 2100 with a likelihood of >50%. High overshoot refers to temporarily exceeding 1.5°C global warming by 0.1°C–0.3°C for up to several decades.
C3: *Limit warming to 2°C (>67%)*	Limit peak warming to 2°C throughout the 21st century with a likelihood of >67%.
C4: Limit warming to 2°C (>50%)	Limit peak warming to 2°C throughout the 21st century with a likelihood of >50%.
C5: Limit warming to 2.5°C (>50%)	Limit peak warming to 2.5°C throughout the 21st century with a likelihood of >50%.
C6: Limit warming to 3°C (>50%)	Limit peak warming to 3°C throughout the 21st century with a likelihood of >50%.
C7: Limit warming to 4°C (>50%)	Limit peak warming to 4°C throughout the 21st century with a likelihood of >50%.
C8: Exceed warming of 4°C (≥50%)	Exceed warming of 4°C during the 21st century with a likelihood of ≥50%.
C1, C2, C3: limit warming to 2°C (>67%) or lower	All scenarios in Categories C1, C2 and C3

Figure S3: Scenarios classification in IPCC's WGIII AR6 report [16]. This figure is taken from Chapter 3, section 3.2 [17].

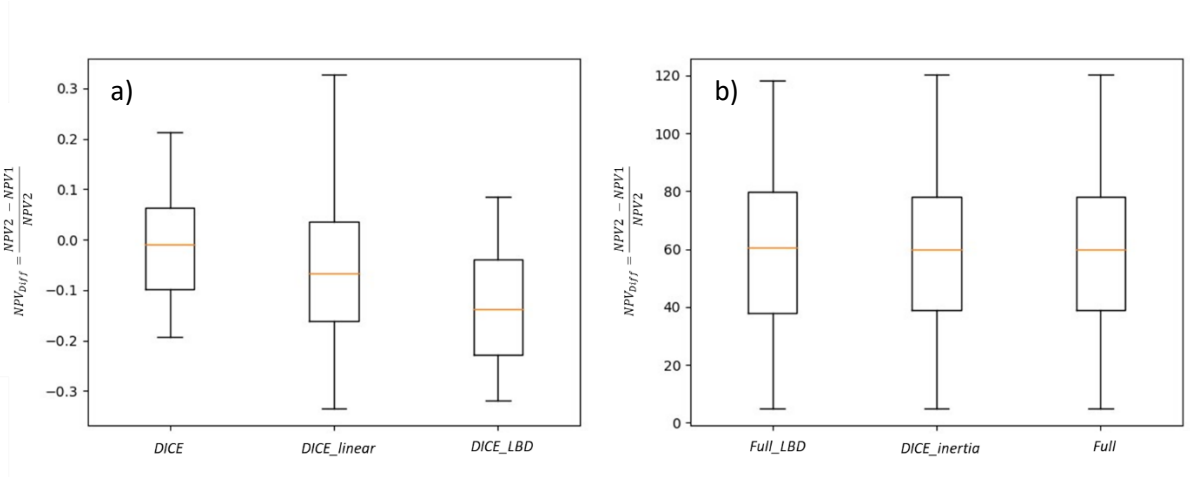

Figure S4 Distribution of NPV_{Diff} for generationally robust near-optimal pathways in the configuration corresponding to the 50th percentile of least robust pathways (as in Figures 7.a and 7.b). Panel a shows NPV_{Diff} for cost functions without inertia and panel b for cost functions with inertia.

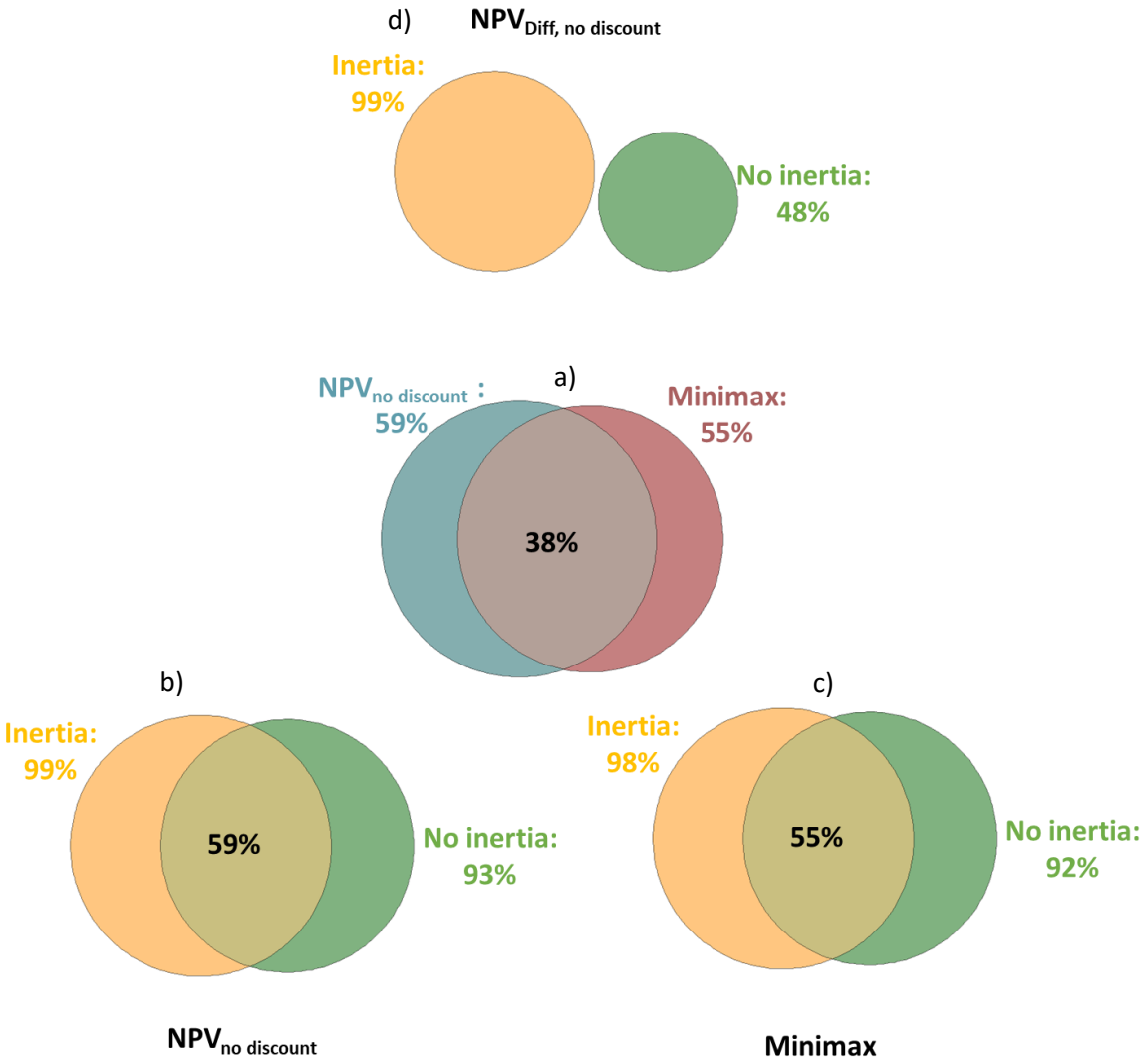

Figure S5 Venn diagrams showing the proportion of near-optimal pathways that are robust to minimax, NPV-*nodisc* and NPV_{Diff} (panel a). Panels b, c and d decompose the proportion of these robust pathways among cost functions that do or do not account for inertia. The intersection spaces of the circles in panels b, c and d correspond to the size of ellipses in panel a.

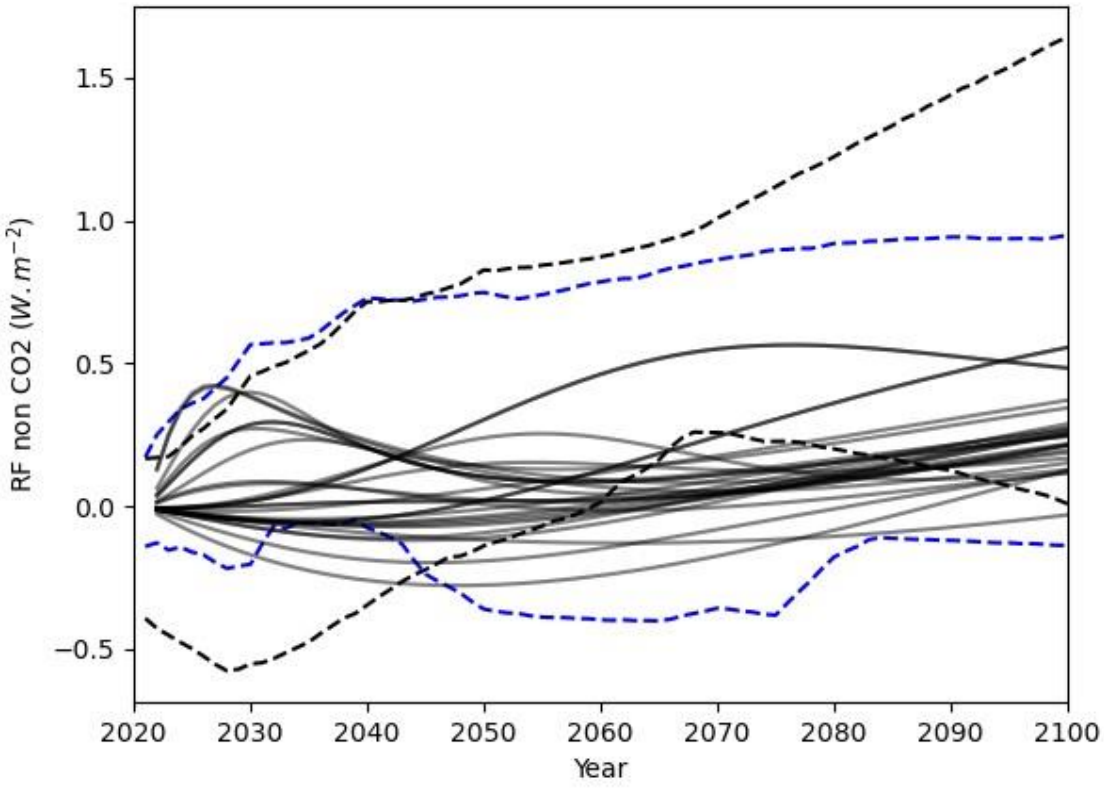

Figure S6: Non CO_2 RF corresponding to economically and generationally robust pathways for a median configuration of Pathfinder (Figure 7.c). Black pathways remain below 2°C and are similar to C4 scenarios from AR6 (envelope represented with black dashed lines). Blue dashed lines represent the envelope of C1-C3 scenarios from AR6

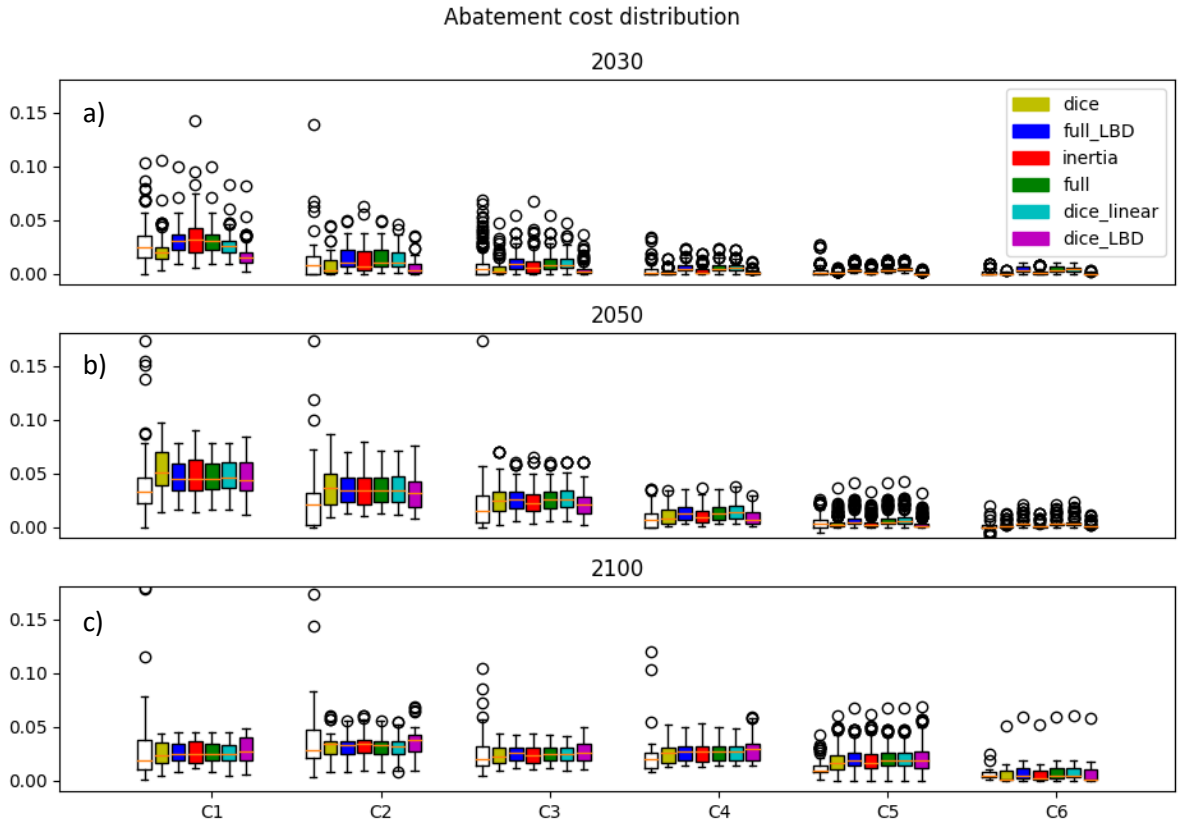

Figure S7 Distribution of mitigation costs from AR6 (white boxes) compared to the six calibrated cost functions (colored boxes) for scenarios across 6 categories (C1 to C6) for the “free calibration”. Costs are calculated and calibrated on three crossing points in 2030 (panel a.), 2050 (panel b.), and 2100 (panel c.)

[1] E. Byers, V. Krey, E. Kriegler, K. Riahi, R. Schaeffer, J. Kikstra, R. Lamboll, Z. Nicholls, M. Sanstad, C. Smith, AR6 Scenarios Database hosted by IIASA, in, International Institute for Applied Systems Analysis, 2022.
[2] C. Huntingford, H. Yang, A. Harper, P.M. Cox, N. Gedney, E.J. Burke, J.A. Lowe, G. Hayman, W.J. Collins, S.M. Smith, Flexible parameter-sparse global temperature time profiles that stabilise at 1.5 and 2.0° C, *Earth System Dynamics*, **8** (2017) 617-626.
[3] P. Kumaraswamy, A generalized probability density function for double-bounded random processes, *Journal of hydrology*, **46** (1980) 79-88.
[4] B. Gompertz, XXIV. On the nature of the function expressive of the law of human mortality, and on a new mode of determining the value of life contingencies. In a letter to Francis Baily, Esq. FRS &c, *Philosophical transactions of the Royal Society of London*, (1825) 513-583.
[5] J. Salvatier, T.V. Wiecki, C. Fonnesbeck, Probabilistic programming in Python using PyMC3, *PeerJ Computer Science*, **2** (2016) e55.
[6] P. Friedlingstein, M. O'Sullivan, M.W. Jones, R.M. Andrew, L. Gregor, J. Hauck, C. Le Quéré, I.T. Luijkx, A. Olsen, G.P. Peters, Global carbon budget 2022, *Earth System Science Data*, **14** (2022) 4811-4900.
[7] C. Smith, Nicholls, Z. R. J., Armour, K., Collins, W., Forster, P., M. M., Palmer, M. D., and Watanabe, M., The Earth's Energy Budget, Climate Feedbacks, and Climate Sensitivity Supplementary Material, in: Climate Change 2021: The Physical Science Basis, Contribution of Working Group I to the Sixth Assessment Report of the Intergovernmental Panel on Climate Change, 2021.
[8] K. Tanaka, O. Boucher, P. Ciais, D.J. Johansson, J. Morfeldt, Cost-effective implementation of the Paris Agreement using flexible greenhouse gas metrics, *Science advances*, **7** (2021) eabf9020.
[9] A. Pottier, E. Espagne, B. Perrissin Fabert, P. Dumas, The comparative impact of integrated assessment models' structures on optimal mitigation policies, *Environmental Modeling & Assessment*, **20** (2015) 453-473.
[10] C. Hope, Critical issues for the calculation of the social cost of CO 2: why the estimates from PAGE09 are higher than those from PAGE2002, *Climatic Change*, **117** (2013) 531-543.
[11] W. Nordhaus, P. Sztorc, DICE 2013R: Introduction and user's manual, *Yale University and the National Bureau of Economic Research, USA*, (2013).
[12] M. Grubb, C. Wieners, P. Yang, Modeling myths: On DICE and dynamic realism in integrated assessment models of climate change mitigation, *Wiley Interdisciplinary Reviews: Climate Change*, **12** (2021) e698.
[13] J. DeCarolis, H. Daly, P. Dodds, I. Keppo, F. Li, W. McDowall, S. Pye, N. Strachan, E. Trutnevyte, W. Usher, Formalizing best practice for energy system optimization modelling, *Applied energy*, **194** (2017) 184-198.
[14] F.G. Li, E. Trutnevyte, Investment appraisal of cost-optimal and near-optimal pathways for the UK electricity sector transition to 2050, *Applied energy*, **189** (2017) 89-109.
[15] K. Rennert, B.C. Prest, W.A. Pizer, R.G. Newell, D. Anthoff, C. Kingdon, L. Rennels, R. Cooke, A.E. Raftery, H. Ševčíková, The social cost of carbon: advances in long-term probabilistic projections of population, GDP, emissions, and discount rates, *Brookings Papers on Economic Activity*, **2021** (2022) 223-305.
[16] P.-R. Shukla, J. Skea, R. Slade, A. Al Khourdajie, R. van Diemen, D. McCollum, M. Pathak, S. Some, P. Vyas, R. Fradera, M. Belkacemi, A. Hasija, G. Lisboa, S. Luz, J. Malley, Mitigation of Climate Change. Contribution of Working Group III to the Sixth Assessment Report of the Intergovernmental Panel on Climate Change, *IPCC Sixth Assessment Report*, (2022).

[17] K. Riahi, R. Schaeffer, J. Arango, K. Calvin, C. Guivarch, T. Hasegawa, K. Jiang, E. Kriegler, R. Matthews, G. Peters, Mitigation pathways compatible with long-term goals, *Climate change*, (2022).